CORA Cork Open Research Archive
Cartlann Taighde Oscailte Chorcaí

Title	Design, development and characterization of nanostructured electrochemical sensors
Authors	Juska, Vuslat B.
Publication date	2020
Original Citation	Juska, V. B. 2020. Design, development and characterization of nanostructured electrochemical sensors. PhD Thesis, University College Cork.
Type of publication	Doctoral thesis
Rights	© 2020, Vuslat B. Juska. - https://creativecommons.org/licenses/by-nc-nd/4.0/
Download date	2026-10-30 03:19:42
Item downloaded from	https://hdl.handle.net/10468/10021



UCC
University College Cork, Ireland
Coláiste na hOllscoile Corcaigh

Ollscoil na hÉireann, Corcaigh
National University of Ireland, Cork



ucc
Coláiste na hOllscoile Corcaigh, Éire
University College Cork, Ireland

DESIGN, DEVELOPMENT AND CHARACTERIZATION OF NANOSTRUCTURED ELECTROCHEMICAL SENSORS

Thesis presented by

Vuslat B. Juska

https://orcid.org/0000-0001-7727-6249

for the degree of
Doctor of Philosophy

University College Cork
School of Chemistry
Head of School: Dr. Humphrey Moynihan
Supervisor: Prof. Martyn E. Pemble

2020

Contents

Acknowledgments 7
Abstract 9
CHAPTER 1 11
1. Introduction 12
1.1 A Brief history of glucose biosensors 12
1.2 Nanomaterial-based electrochemical enzymatic glucose biosensors 18
1.2.1 Gold nanostructures and their use in hybrid glucose biosensors 20
1.2.2 Carbon nanotubes (CNTs) and their hybrid-based glucose biosensors 25
1.2.3 Chitosan based glucose biosensors 29
1.2.4 Carbon/Graphene quantum dots (CQDs, GQDs)-based glucose biosensors 32
1.3 Non-enzymatic detection of glucose; direct glucose electro oxidation 33
1.4 Microfabrication and miniaturization in the development of electrochemical biosensors 37
1.4.1 Microfabricated neural sensor probes 38
1.4.2 Miniaturized electrochemical biosensors 40
1.4.3 Microfabricated biosensor integrated fluidic devices 44
1.5 Conclusion and Future perspectives 49
1.6 References: 49
CHAPTER 2 62
2. Cu Nanodendrite Foams on Integrated Band Array Electrodes for the Nonenzymatic Detection of Glucose 63
2.1 Abstract 63
2.2 Introduction 64
2.3 Results and discussion 67
2.3.1 Fabrication and investigation of gold micro band array electrodes 67
2.3.2 Electrodeposition of CuFoam and electrocatalytic behavior of CuFoam deposited band array electrodes 69
2.3.3 Chronoamperometric detection of glucose and analytical parameters of the CuFoam deposited array electrodes 78
2.4 Conclusions 83
2.5 Methods 84
2.5.1 Chemicals and instrumentation 84
2.5.2 Microfabrication of electrodes 85
2.5.3 Electrochemical measurements and CuFoam electrode preparation 85
2.6 Acknowledgments 86
2.7 References 87
2.8 Supporting Information 92
CHAPTER 3 99
3. Fabrication and evaluation of a carbon quantum dot/gold nanoparticle nanohybrid material integrated onto planar micro gold electrodes for potential bioelectrochemical sensing applications 100

3.1 Abstract 100
3.2 Introduction 101
3.3 Materials and methods 104
3.3.1 Chemicals and instrumentation 104
3.3.2 Preparation of CQDs/AuNPs nanohybrid material 104
3.3.3 Preparation of the CQD/AuNP-GOx modified electrodes 105
3.4 Results and discussions 106
3.4.1 Characterization of CQDs, AuNPs and CQDs/AuNPs nanohybrid material 106
3.4.2 Optimization of the CQDS/AuNPs-GOx biosensor and electrochemical impedance spectroscopy 110
3.4.3 Direct electrochemistry of the CQD/AuNP-GOx modified gold surfaces 112
3.4.4 Chronoamperometric detection of glucose 115
3.4.5 Interference effect, reproducibility and reusability of the CQD/AuNP-GOx biosensor 117
3.4.6 Real sample analysis 118
3.5 Conclusions 119
3.6 Acknowledgments 120
3.7 References 120
3.8 Supporting Information 126
CHAPTER 4 129
4. A highly sensitive glucose biosensor based on a micro disk array electrode design modified with carbon quantum dots and gold nanoparticles 130
4.1 Abstract 130
4.2 Introduction: 131
4.3 Materials and Methods 133
4.3.1 Materials 133
4.3.2 Instrumentation and Methods 133
4.3.3 Preparation of CQDs/AuNPs-GOx biosensor 134
4.4 Results and discussion 135
4.4.1 Characterisation of fabricated micro disk array electrodes 135
4.4.2 Fabrication process of the biosensor 138
4.4.3 Chronoamperometric detection of glucose 140
4.5 Acknowledgments 145
4.6 References 145
4.7 Supporting information 148
CHAPTER 5 153
5. A dual-enzyme, micro-band array biosensor based on the electrodeposition of carbon nanotubes embedded in chitosan and nanostructured Au-foams on microfabricated gold band electrodes 154
5.1 Abstract 154
5.2 Introduction: 155
5.3 Materials and methods 157
5.3.1 Chemicals and Instrumentation 157

5.3.2 Au-foam/CS-MWCNT/GOx-HRP micro band array biosensor preparation 158
5.4 Results and Discussions 159
5.4.1 Micro band array electrode characterisation 159
5.4.2 Au-foam and CS-MWCNT electrodeposition, characterisation and the construction of the biosensor 161
5.4.3 Chronoamperometric detection of glucose by Au-foam/CS-MWCNT/GOx-HRP micro band array biosensor 169
5.4.4 Interference effect, Stability and Reproducibility 171
5.4.5 A real-world application 172
5.5 Acknowledgements 173
5.6 References 174
5.7 Supporting Information 179
CHAPTER 6 181
6. Summary and future perspectives 182
7. APPENDIX A 186
7.1 GRANTS 186
7.2 PUBLICATIONS 186
7.3 ACADEMIC HONORS AND AWARDS 186
7.4 CONFERENCES, SEMINARS 187

I, Vuslat Buk Juska, hereby certify that this thesis is my own work and I have not obtained a degree in University College Cork or elsewhere on the basis of the work submitted in this thesis. All external references and sources are acknowledged within the contents. I have read and understood the regulations of University College Cork concerning plagiarism

Vuslat Buk Juska

Dedicated to Fatma Nejla and Mustafa Buk

Acknowledgments

I started my PhD with a clear focus on several ambitious goals which included publishing high impact research work, attendance at prestigious conferences, and development of professional skills. I must admit I have happily and successfully achieved many of these aims during the progress of my thesis, largely thanks to the support of my supervisor Prof. Martyn Pemble. His scientific intuition, professionalism and knowledge have no doubt had a great impact on my research experience. This thesis would not have been completed without the freedom he allowed me, while at the same time being always available to guide or discuss. Likewise, I am very grateful for his time, encouragement and support on my postdoctoral grant applications.

I would like to acknowledge my thesis committee members Prof. Colin Hill and Dr. Brendan O'Flynn for their support and guidance to improve my research skills. I would like to thank Dan O'Connell from the Compound Semiconductor Laboratory for helping me with the microfabrication aspects of my electrodes. Similarly, I would like to acknowledge the former and current members of LSI group.

Overall, I would like to acknowledge the Department of Agriculture, Food and the Marine for funding my research and Tyndall National Institute, University College Cork, for access to the relevant facilities and trainings, which allowed me to grow professionally, improve the skills and increase the impact of my research. I always felt confident and encouraged in Tyndall as an early stage career researcher.

A special thanks to Gediminas Juska – colleague, best friend and husband – for his greatest support in science and in personal life. He is one of the researchers I admire and I am proud of. He is the biggest help and motivation in keeping me on the track of my scientific route. I am very thankful to him for bringing me a lot of love, laughter and new life experiences. "Let the SwampaSensors come true!"

Finally, the deepest thanks to my family. Their love and support is priceless. Without them I simply would not have been able to complete this thesis. For that and so much more I am eternally grateful.

Abstract

This is a publication-based thesis which focuses on the study of electrochemical microbiosensors for glucose detection. It investigates applications of a series of microfabricated gold electrodes based on several nanostructures in electrochemical biosensing technologies, embracing three major methodologies: direct electro-catalytic detection, enzymatic detection and dual-enzyme cascade detection. The study is described over five main chapters with a sixth providing a summary of the material presented and perspectives for the future.

Chapter 1 provides an introduction to the field of the electrochemical biosensors with a specific focus on the chosen nanostructures and miniaturized systems, as well as a brief history of the biosensor.

Chapter 2 presents results published in *ACS Applied Nanomaterials, 2019, 2, 9, 5878-5889.* It demonstrates the enzyme free detection of glucose *via* a direct electro-catalytic reaction. The miniaturized band array electrodes with specific width, length and inter-electrode-distance were integrated with homogeneously distributed copper foam nano dendrites. Such foam deposits presented for the first time at the micro scale were achieved using the *in-situ* hydrogen bubble template method. The resulting very high electroactive surface area of the porous foam deposits was one of the major advantages in terms of achieving superior performance from each micro band foam electrode towards glucose detection. Moreover, both sensors also showed a strong resistance to the poisoning effects of chloride ions and displayed excellent stability over a period of three months.

Chapter 3 presents the first of two sets of results for the enzymatic detection of glucose, results published in *Elsevier Electrochimica Acta, 2019, 293, 307-317.*

Chapter 4 then presents the second set of results on this topic which is published in and *Elsevier Electrochimica Acta, 2019, 298, 97-105.* The aim of these two chapters is to discuss the effect of

miniaturization on the enzymatic biosensor performance which was studied in the presence of a carbon quantum dot (CQD) and gold nanoparticle nanohybrid system. CQDs, are a new class of carbon-based materials and have been used here for the first time as a matrix component integrated onto microfabricated gold electrode surfaces for enzyme immobilization and further miniaturization. The biosensors developed were studied by electrochemistry to investigate the analytical performance of each device. By scaling down the surface area of the biosensor, a 13-times increase in sensitivity was achieved towards glucose. Moreover both sensors-planar, micro disk array- exhibited excellent reproducibility, reusability and operational stability in terms of the performance of biosensors.

Chapter 5 presents results published in *RSC Analyst, 2020 (DOI: 10.1039/C9AN01664C).* It demonstrates the operation of a dual-enzyme cascade which was constructed onto a micro band array electrode based on glucose oxidase and horseradish peroxidase enzymes. To achieve a very high surface area, a porous gold-foam was electrodeposited onto surface and then a second electrodeposition layer of chitosan and multi walled carbon nanotube nano-bio-composite. The micro band cascade scheme developed exhibited the highest sensitivity towards glucose detection in comparison to other systems reported in the literature.

Chapter 6 provides an insight into the field of electrochemical biosensing with the support of the achievements presented in this thesis. Thus, by taking advantage of the available system, this chapter discusses the possible future applications of the electrochemical biosensors.

The thesis then ends with section 7 which presents some Appendices.

CHAPTER 1

Introduction

1. Introduction

This introduction aims to provide context relevant to this doctoral study in the form of a brief history of electrochemical glucose biosensors, the evolution of sensor technology towards miniaturized systems and a discussion of recent trends and state-of-the-art results available in the literature. It starts with the history of biosensors showing the recent progress made in this interdisciplinary research field, highlighting the most influential studies which have opened up a new era within the field. The literature examples of enzymatic glucose biosensors based on gold nanostructures, carbon nanotubes, carbon quantum dots and chitosan are described in detail. The systems which do not require an enzyme but successfully catalyze the glucose –so called "non-enzymatic" or "enzyme-free" sensors– are also highlighted by some very recent research examples. Finally the miniaturized systems based on microfabrication technologies are introduced paying particular attention to the neural sensor probes, miniaturized electrochemical biosensors and microbiosensor integrated devices.

1.1 A Brief history of glucose biosensors

The first enzyme-based electrode was reported by Clark and Lyons in 1962[1]. This device was based on glucose oxidase entrapped within a semipermeable dialysis membrane which was constructed on an oxygen electrode. Following this, Clark's patent in 1970 demonstrated the use of enzymes to convert electroinactive substrates to electroactive substances (Fig. 1.1). This system relied on two different electrode systems. The first electrode system, which consisted of at least one enzyme in a capillary thin layer between the electrode and the membrane, was responsible for the conversion of the substrate to electroactive material in the presence of interfering species. The second electrode system was sensitive to the interfering species available in the sample. By subtracting the measured current from the second electrode system from the measured current from the first electrode system, Clark's device was able to monitor the glucose.

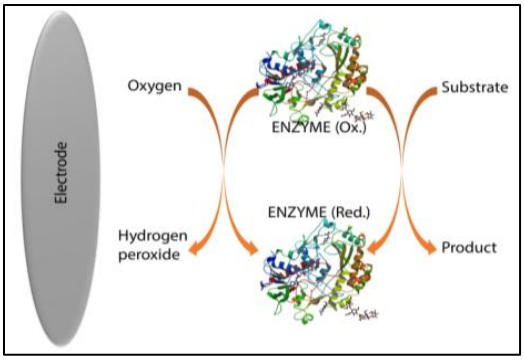


Figure 1.1. The schematic representation of first generation glucose biosensor based on oxygen electrode or peroxide electrode (redrawn from A.P.F. Turner, Home blood glucose biosensors: a commercial perspective[2], first generation biosensors

First Generation Biosensors. Clark's technology was transferred to the Yellow Springs Instrument Company (Ohio, USA) and became commercial in 1975 with the successful launch of the first glucose analyzer based on the amperometric detection of hydrogen peroxide from 25 µL samples of whole blood, so called model 23A YSI analyzer, Fig.1.2.

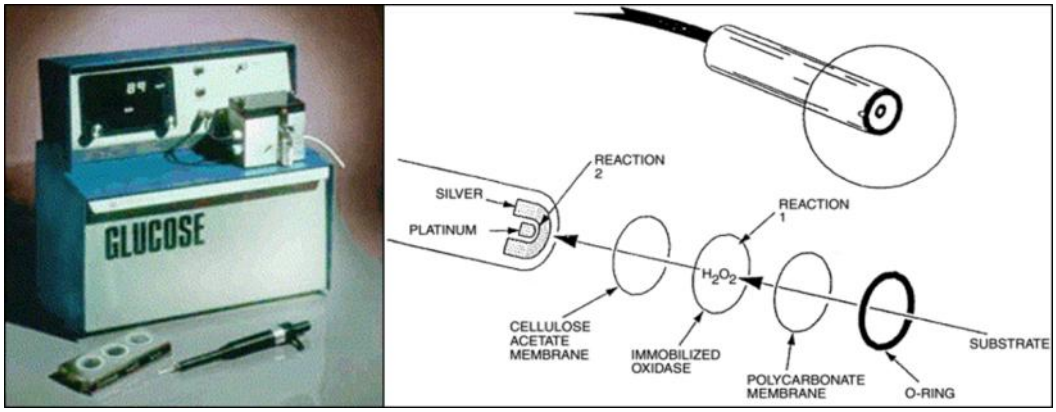


Figure 1.2, YSI 23A glucose biosensor[2] and sensor probe with immobilized enzyme membrane for the Yellow Springs Instruments[3], 1975

Clark's electrode scheme (Fig.1.1) also shows the possibility of glucose monitoring *via* the oxidation of hydrogen peroxide produced by the enzymatic reaction which is proportional to the glucose concentration. Thus for the construction of the biosensor of 23A YSI analyzer, glucose oxidase was immobilized between two membrane layers. The first layer was a polycarbonate membrane which was used to permit only glucose molecules to move towards

the enzyme layer by blocking the many other larger substances including enzymes and proteins available in whole blood; thus decreasing the interference effect. Therefore, only glucose reached the enzyme layer where it was oxidized. The product hydrogen peroxide from this reaction passed through a cellulose acetate membrane which also acted as a barrier for the larger molecules. Finally hydrogen peroxide was amperometrically detected at the platinum electrode surface. The associated reactions are shown below:

Reaction 1: $\text{Glucose} + O_2 \xrightarrow{Glucose\ oxidase} \text{Gluconic acid} + H_2O_2$ (1)

Reaction 2: $H_2O_2 \xrightarrow{+0.7\ V\ vs.\ Ag/AgCl} O_2 + 2H^+ + 2e^-$ (2)

The first generation biosensor of the "23A sensor probe" was relatively expensive due to the presence of a platinum electrode. Even though it was robust, it was not suitable for miniaturization since it was not based on a simple detection method. Moreover the high applied voltage for hydrogen peroxide detection made the system prone to interference in the absence of the utilized barrier membranes[2].

Consideration of such issues in relation to the first commercial biosensor have led to fierce competition in the market which in turn has established the highly interdisciplinary research area of biosensors (and in particular electrochemical biosensors), which aims to improve the characteristics and performance of the biosensors and further miniaturize the overall systems.

Second Generation Biosensors. With this latter consideration in mind, the maturation of the fields of surface chemistry, screen-printing technologies and semiconductor integration technologies combined with the use of synthetic electron acceptors has resulted in major advances in the development of commercial electrochemical glucose biosensors. Synthetic electron acceptors in the form of redox couples or mediators are able to shuttle electrons between the redox center of the enzyme and the surface of the electrode. Thus, many inorganic redox couples and organic dyes have been successfully deployed in order to shuttle electrons for the reaction of glucose catalysis by glucose oxidase. In the early 1980s, it was

realized that this method allowed the devices to operate at lower potentials, decreasing interference effects. In addition it was found that the reaction did not depend on the concentration of dissolved oxygen in the electrolyte. This was reported in 1984 as the first mediated amperometric biosensor toward glucose, which was the result of collaboration between Oxford University and Cranfield University[4]. Meanwhile, screen printing technologies were adapted for the production of disposable, small or miniaturized, robust and cheap electrodes for amperometric biosensors. These two innovative research initiatives gave rise to the first very successful home-use blood glucose biosensor based on mediators and screen printed electrodes. In 1987, these biosensors were launched under the brand name of ExacTech by the MediSense Company (whose original name was Genetics International) which was a company founded between the universities of Cranfield and Oxford. Fig. 1.3 shows the first home-use glucose biosensor and illustrates its working principle.

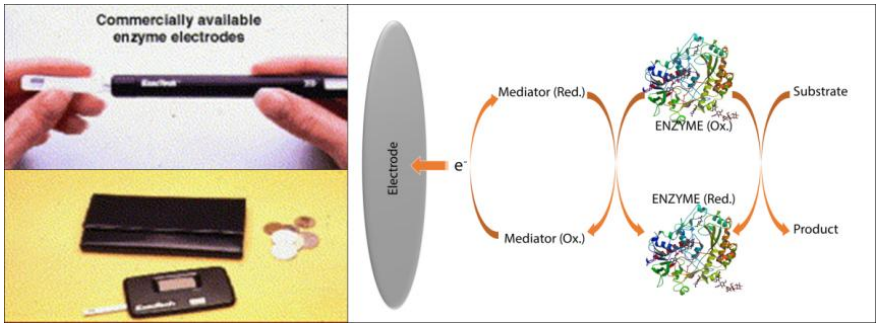


Figure 1.3, The MediSense ExacTech home-use glucose biosensors[2], 1984 and the schematic image of the mediated biosensor working principle, second generation biosensors

To date, all subsequent MediSense (now owned by Abbott) glucose biosensors have applied essentially similar technology in the form of an amperometric biosensor. Briefly, this biosensor involves the use of the enzyme glucose oxidase and mediators deployed on a disposable strip. Several improvements have been implemented since the launch of the first device in 1987, however the concept of the biosensor has remained mostly the same. The market for glucose biosensors has grown rapidly. The lion's share of this market is currently dispersed between Roche Diagnostics, LifeScan, Abbott and Bayer. Arguably the application of mediators and

screen printed electrodes was a great step-forward for the development of amperometric biosensors and commercial products for home-use.

The "wiring" or "modification" of enzymes; toward third generation glucose biosensors: Even with the enormous success of the commercial, mediated glucose biosensors, the nature of the biochemical structure of the glucose oxidase enzyme, the relative solubility and toxicity of the mediators and the overall poor stability of these mediated systems towards extended continuous operation lead researchers to concentrate on sensors based on the direct electron transfer between the enzyme redox center and the electrode. The Flavin redox center of the enzyme (co-factor), which is deeply buried in an electrically insulated thick protein shell, is incapable of achieving an electrical connection with the electrode surface[5-6]. Thus, minimization of the electron-transfer distance is vital in order to ensure the performance of the sensor. Heller's group reported one of the first smart routes to establishing this communication between the glucose oxidase active sites and the electrode using a long, flexible poly(4-vinlypyridine) (PVP) or poly(vinylimidazole) polymer backbone which had a dense array of linked osmium-complex electron relays[7].

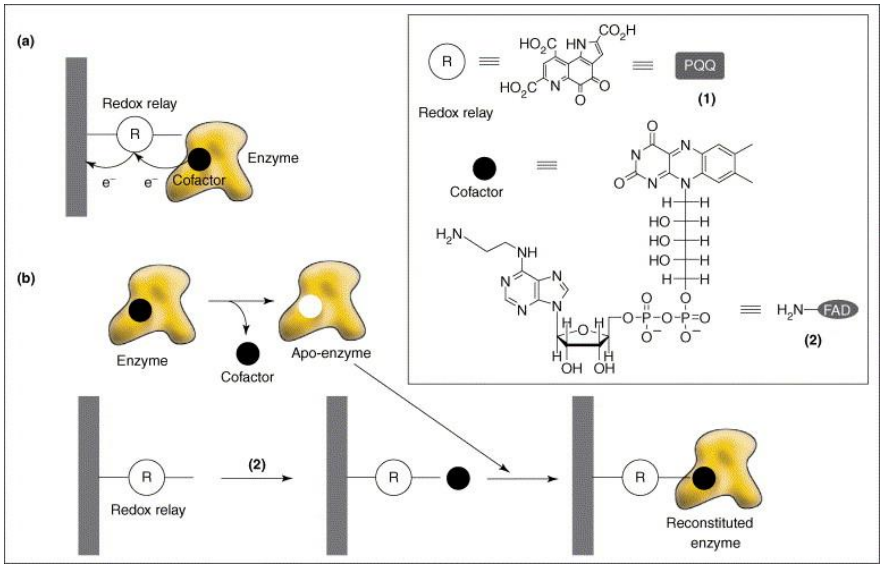


Figure 1.4, Electrical wiring of redox enzymes (a) construction of the electrical contact of the redox enzyme with the electrode, (b) reconstruction of the apo-enzyme on a relay-cofactor complex[8] (inset; molecular structure of redox relay PQQ and co-factor amino-FAD)

In this way, the redox polymer penetrates and binds the enzyme which results in a three dimensional network. Such an immobilization technique – wiring the enzyme to the surface – dramatically decreases the distance between the redox center of the polymer matrix and the redox center of the enzyme. Since the polymer structure on the electrode surface is permeable to glucose and the product of the reaction, the electrons originating from the redox center of glucose oxidase are transferred through the matrix to electrode. Another attractive route to facilitate electron transfer between the glucose oxidase redox center and the electrode surface is the chemical modification of the enzyme itself. In 1987, Degani and Heller[9] demonstrated the covalent attachment of ferrocenecarboxylic acid to the glucose oxidase via carbodiimide chemistry. When a sufficient amount of ferrocenecarboxylic acid molecules was covalently attached to the enzyme, it was found that an enhanced electrical communication was established between the redox center of the enzyme and gold, platinum or carbon electrodes. In 1995, Willner's group reported a highly elegant approach to improve the electrical contact by treating the glucose oxidase with electron relays[10]. In this study, the redox center of the glucose oxidase – Flavin adenine dinucleotide (FAD) – was removed and modified with ferrocene. This was followed the reconstruction of the apo-enzyme with the ferrocene modified FAD. Fig. 1.4 summarizes schematically both of these approaches: namely, the enzyme immobilization in the presence of redox polymers (Fig.1.4a) and enzyme-modification-reconstitution in the presence of the redox relays (Fig.1.4b).

These various initiatives had a great influence on the development of the third generation biosensors which are based on direct electron transfer in the absence of any kind of redox mediator. Such biosensors are able to operate at low operating potentials; thereby greatly reducing interference effects. However, as mentioned earlier, part of the challenge with these systems arises from the molecular structure of the enzyme itself. Many attempts have been made to try to create a successful matrix for the transfer of electrons between the FAD and the electrode by integration of conductive polymers and emerging nanomaterials such as carbon-based nanomaterials (carbon nanotubes[11-15], graphene[16-18], carbon/graphene quantum dots[19-21], etc.), metal nanoparticles[22-26] (gold, silver, copper, etc.), dendrimers[27-28], and many more.

Furthermore, the developments in the silicon technologies provide excellent opportunities to construct micro/nano patterned miniaturized electrodes which are highly reproducibility, scalable, design-flexible and with multiplexed features[29-31]. The resulting three dimensional micro/nano structured electrodes serve as exceptional platforms for many research fields such as neuroscience[32-33], microbiology[34], food-marine-agriculture[20, 35-36], chemistry[24, 37] and many more. Such advanced developments have lead to a new class of sensing technologies so called miniaturized systems.

Clearly, research in the field of electrochemical biosensors has encompassed many research fields including biochemistry, nanotechnology, materials, printing technologies, microtechnologies, etc. However, in the context of this thesis this present review focuses mainly on the most recent achievements of electrochemical glucose sensors from the perspectives of firstly the use of nanomaterials and secondly miniaturization of biosensors via the application of semiconductor microfabrication technologies.

1.2 Nanomaterial-based electrochemical enzymatic glucose biosensors

The enormous progress in the field of nanotechnology that has taken place over the past decade or so has been transferred to biosensors and bioelectronics in order to take advantage of some of the highly desirable features of nanomaterials. For example, in the context of biosensors, several methods have been developed for the synthesis of nanomaterials with different shapes and dimensions such as spherical particles[20-21], rods[38-39], cubes[40], *etc*. In particular, carbon-based nanomaterials such as carbon nanotubes and graphene have given rise to major advances in the field[41-46]. The structural, electrical, chemical and mechanical properties of such nanostructures have made them an essential component of many detection technologies. In particular, due to the similar size and dimensions of nanomaterials such as gold nanoparticles and carbon nanotubes to the redox enzymes, such nano structures might be used to establish a bridge between the electrode and the redox center as electrical connectors which might enable an improved electron transfer [8, 47-49]. An excellent example of this type of approach may be found by considering the work of the Willner group, Figure 1.5:

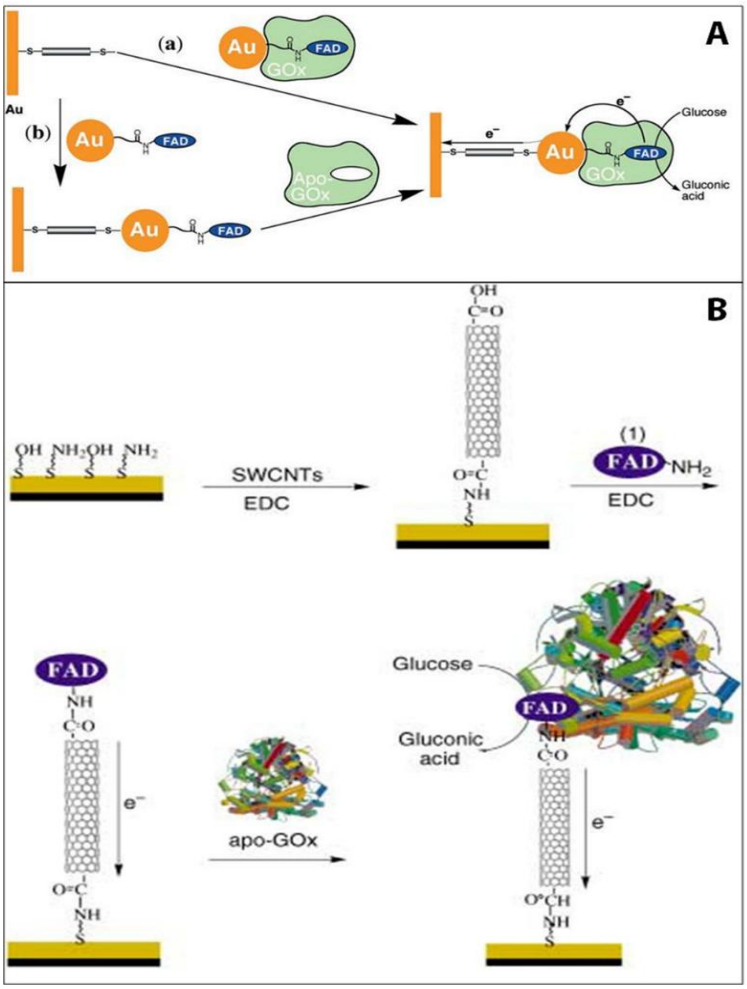


Figure 1.5, (A) Schematic image of the assembly of a AuNP-reconstituted GOx electrode via (a) the immobilization of AuNP-reconstituted GOx onto electrode surface[50], (b) immobilization of a AuNP-FAD complex onto surface followed by reconstitution of apo-GOx, (B) Assembly of glucose oxidase electrode via the use of single-walled carbon nanotubes (SWCNTs) as a direct electrical contact[51]

Willner's group consecutively reported two interesting approaches for nanowiring of redox enzymes which have been accepted as seminal approaches by researchers in the field of biosensors and bioelectronics (Fig 1.5A)[50-51]. The first study was published in 2003, used 1.4 nm diameter gold nanoparticles (carboxylic acid functionalized) to modify the electrode surface[50]. Then, a cofactor, aminoethyl-modified FAD, was immobilized onto the gold nanoparticles followed by the reconstitution of the apo-enzyme on the cofactor-functionalized gold nanoparticles. This study showed the ability of gold nanoparticles to act as relay units facilitating electron transport from the FAD to the electrode surface, thus activating the catalytic function of the enzyme (Fig.1.5A)[50]. Subsequently, in 2004 the same group published a

second report which was based on the use of carbon nanotubes as molecular wires ('nanoconnectors')[51]. In this study, the aligned, reconstituted glucose oxidase on the edge of a single walled carbon nanotube was successfully linked to the surface thus 'plugging' the electrode into the enzyme. Electrons could then be transferred along the length of the carbon nanotubes (Fig.1.5B). Such an enhanced direct connection between an enzyme and an electrode via aligned carbon nanotubes arrays was also reported by Gooding's group in 2005[52]. These pioneering studies from the Willner and Gooding groups encouraged researchers to further consider using nanostructures as the components of biosensors[50-52]. As a consequence growth of research in the field of glucose biosensors and nanomaterials based biosensors has been phenomenal, Fig. 1.6. It is noteworthy that the vast majority of glucose biosensors in recent times are based on what might be termed 'emerging' nanomaterials:

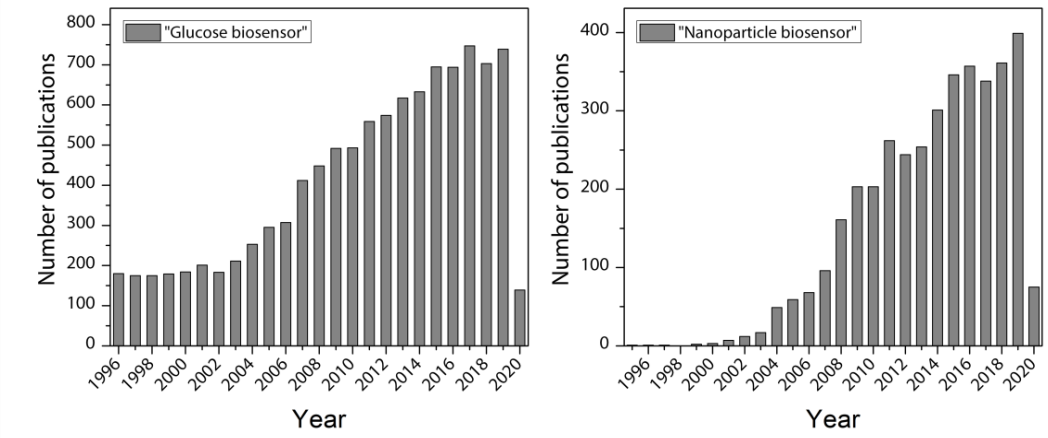


Figure 1.6 Graphs on the search terms "glucose biosensor" and "nanoparticle biosensor" during the period 1996 to 2020, using Web of Knowledge (20 March 2020)

1.2.1 Gold nanostructures and their use in hybrid glucose biosensors

Gold nanostructures alone or in combination with other nanomaterials have been extensively studied in order to develop excellent matrixes for biomolecules and in particular those used for glucose oxidase immobilization[53-54]. For instance, nanoporous gold (NPG) has attracted significant interest in the field of electrochemical biosensors due to its large surface area and porosity. In 2015, Wang *et al*. reported a glucose biosensor based on a porous gold/enzyme combination[55]. Briefly, in this work NPG was prepared by de-alloying 12-carat white gold leaves in concentrated HNO_3. The resulting freshly-made NPG was immediately transferred onto a

clean glassy carbon electrode surface and kept under vacuum. The NPG surface was later immersed into glucose oxidase solution for enzyme immobilization. The resulting GOx/NPG/GCE bio-electrode showed a sensitivity of 12.1 μA mM^{-1} cm^{-2} and a detection limit of 1.02 μM towards glucose detection. The success of this biosensor was attributed to the three dimensional structure of the porous-gold matrix, which provided a good interface between the active sites of the enzyme and the electrode.

Rivas's group demonstrated the use of globular gold nanoparticles as components of a nanohybrid structure by applying a series of chemical modifications to establish a highly efficient immobilization matrix for glucose oxidase, Fig.1.7[56]. For this purpose, gold nanoparticles were functionalized with 3-mercaptophenyl boronic acid (AuNPSs-$B(OH)_2$). A clean glassy carbon electrode was drop-cast by bamboo-like multi walled carbon nanotubes (bMWCNTs) dispersion in polyethylene imine. Then the GCE/bMWCNTs-PEI electrode was treated with AuNPs-$B(OH)_2$ and the resulting hybrid surface was used for GOx immobilization. This biosensor exhibited a sensitivity of 28.6 mA M^{-1} cm^{-2} and showed reasonable levels of stability and reproducibility such that the sensitivity was measured to be some 86.1% of the original value after 14 days of storage. The goal of such work was to design a novel hybrid nanomaterial integrating the inherent advantages of the chosen components, namely gold nanoparticles and carbon nanotubes. Thus, the presence of boronic acid residues allowed the easy immobilization of the enzyme while the bMWCNTs-PEI dispersion provided the best platform for the transduction of the electrochemical response.

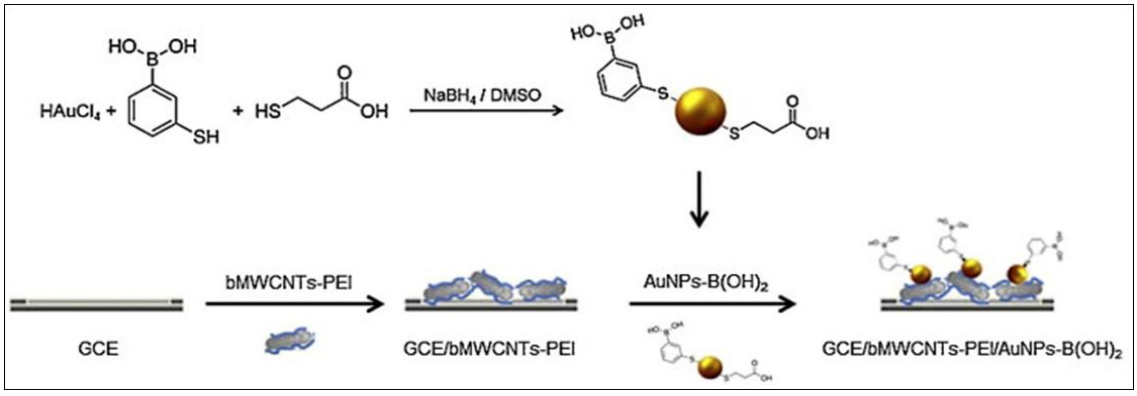


Figure 1.7 Schematic image of the GCE/bMWCNTs-PEI/AuNPs-$B(OH)_2$/GOx biosensor preparation[56]

Turner's group have shown the structuring of gold nanoparticles on two-dimensional molybdenum disulfide (MoS_2) nanosheets which has gained attention very recently in the field of electrochemical biosensors as an ideal candidate for matrix development, Fig.1.8[57]. Briefly, a dispersion of MoS_2 nanosheets in PBS was prepared by ultrasonic treatment and then the dispersion of MoS_2 was mixed with a commercial 5 nm diameter gold nanoparticles solution. By incubating the mixture at room temperature for 3 h, MoS_2/AuNPs self-assembled nanosheets were prepared. The resulting MoS_2/AuNPs were mixed with glucose oxidase enzyme and incubated overnight. The MoS_2/AuNPs/GOx hybrid structure was assembled onto a gold electrode surface by drop-casting. The biosensor showed a sensitivity of 13.80 μA mM^{-1} cm^{-2}. This novel bio-catalytic interface based on two-dimensional MoS_2 and gold nanoparticles has the potential to be used for the immobilization of other biomolecules[58-61].

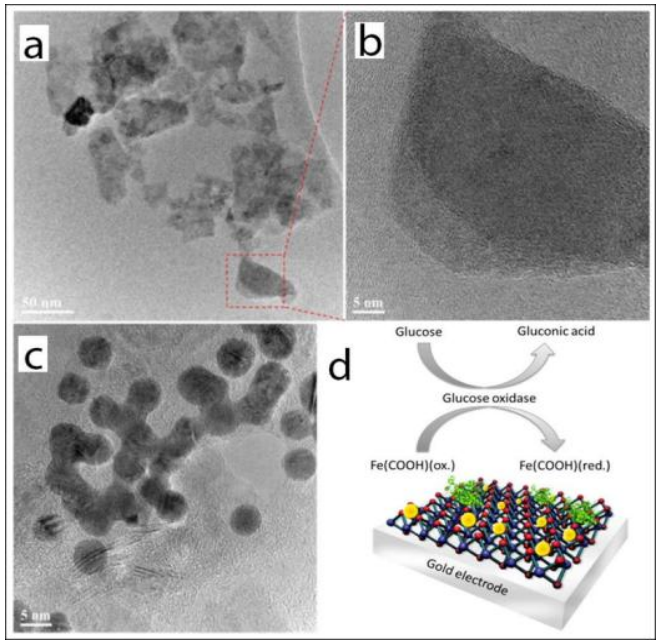


Figure 1.8 TEM images of MoS_2 nanosheets at (a) low and (b) high magnifications, (c) AuNPs structured MoS_2 nanosheets, and (d) schematic display of Au nanoparticle-structuring on a MoS_2 interface and mediated electron transfer process of the hybrid biostructure on the gold electrode surface[57]

Huang *et al*.[62] described the controlled preparation of a layered superstructure of gold nano-octahedra and their application as a host matrix for glucose oxidase immobilization (Fig. 1.9). In this study, gold nanoparticles were synthesized in a PEG solution via a polyol process. The pre-

synthesized Au nano-octahedra were attached onto the gold surface via a 1,8-octadithiol-mediated assembly process which was repeated five times in order to obtain 5 layers of nanoparticles. Finally, glucose oxidase was immobilized onto the five-layer gold structures. This bio-electrode exhibited a sensitivity of 0.349 μA mM^{-1} over a wide concentration range of 0.125 to 12 mM.

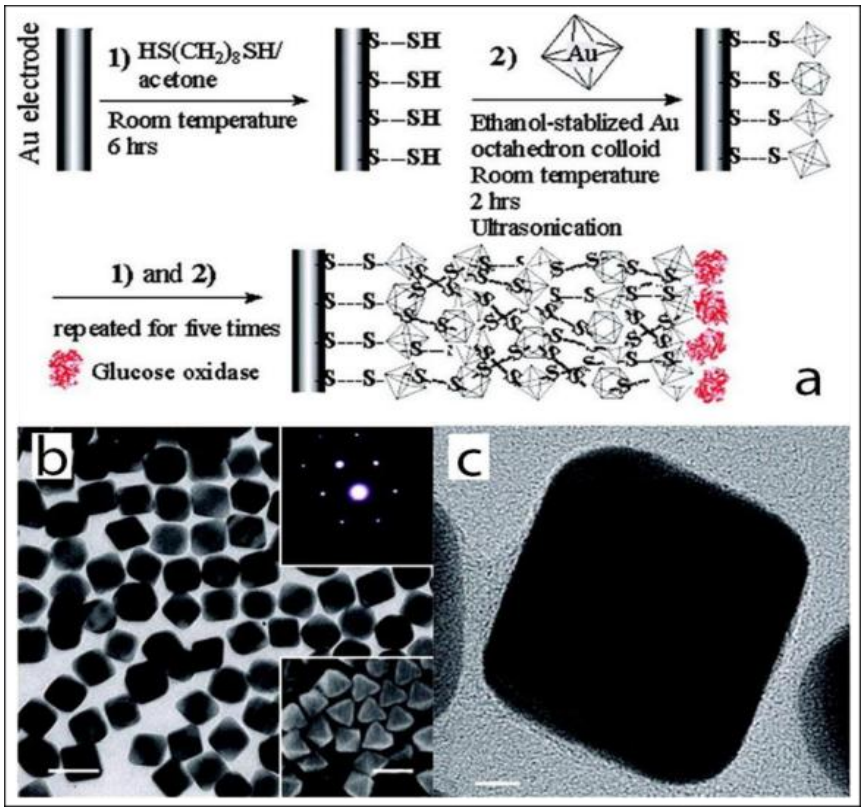


Figure 1.9 (a) Schematic representation of the stepwise construction of the gold nananooctahedra and glucose oxidase base biosensor, TEM images of gold nanooctahedra particles at (b) low and (c) high magnifications[62]

A new method has been developed for the encapsulation of gold nanoparticles and glucose oxidase together into the cavity of a zeolitic imidazole framework (ZIF-8), Fig.1.10[63]. This study shows that the ZIF-8 is stable and provides a very large surface area with a unique cavity which can accommodate both AuNPs and GOx. Furthermore, the AuNPs were found to promote the electron transfer efficiency of the system due to their high conductivity and for this reason the authors claim that the incorporation of AuNPs improved the sensitivity of the system by up to 10-fold.

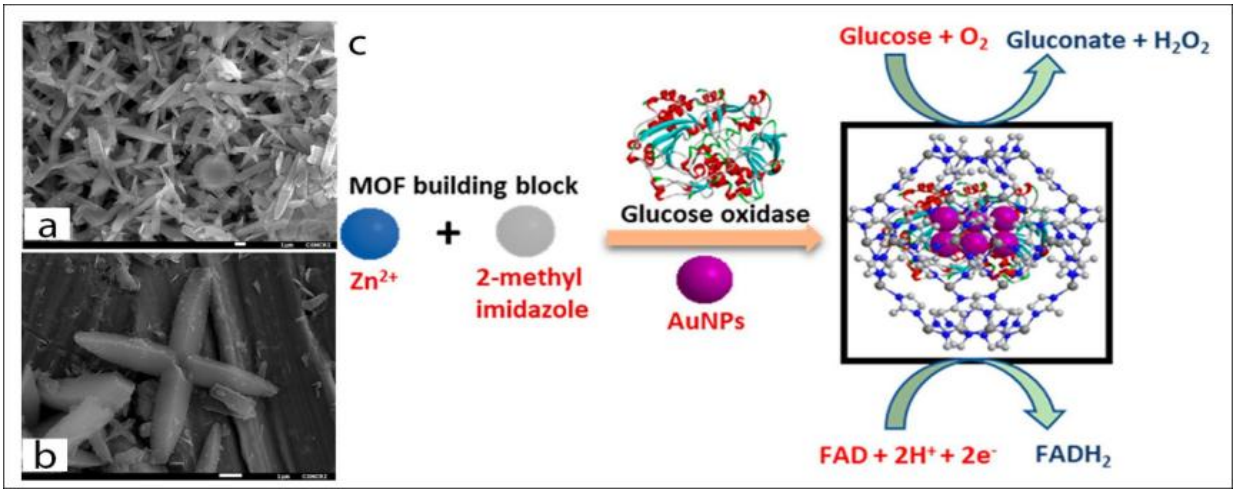


Figure 1.10 FESEM images of (a) 5 nm gold coated GOx@ZIF8(AuNPs) and (b) crystalline growth of a single particle showing a large surface area, and (c) Schematic image of the biosensor construction[63]

A study of gold nanoparticles, graphene oxide and copper nanostructures incorporated into a glucose biosensor has been reported recently, Fig.1.11[17]. The biosensor matrix was established on a gold chip. A solution of poly(vinyl alcohol) (PVA) was prepared and mixed with graphene oxide (GO) under constant stirring conditions. The mixture prepared was then spin-coated on the surface of the gold chip to obtain GO/PVA nanofibre. This was followed the attachment of cysteamine-modified gold nanoparticles onto the surface of the fibres. Meanwhile, Cu-nanoflowers were synthesized using a mixture of glucose oxidase, horse radish peroxidase and $CuSO_4$ in PBS which was incubated at room temperature for 72 hours and then washed with PBS several times. The mechanism of nanoflower formation was explained in terms of both nucleation and growth processes. Basically, the formation of the Cu-protein complex acts as a seed for the nanoflower and these nuclei grow over the reaction time and form the petals of the flower. The as-prepared nanoflowers were dropped onto the AuNPs-GO/PVA electrode surface. This biosensor exhibited the best activity at pH 5 with very good associated analytical performance. Furthermore, our group has very recently reported a highly sensitive glucose biosensor platform based on gold nanoparticles and carbon quantum dots[20-21]. These results are presented in Chapter 3 and 4.

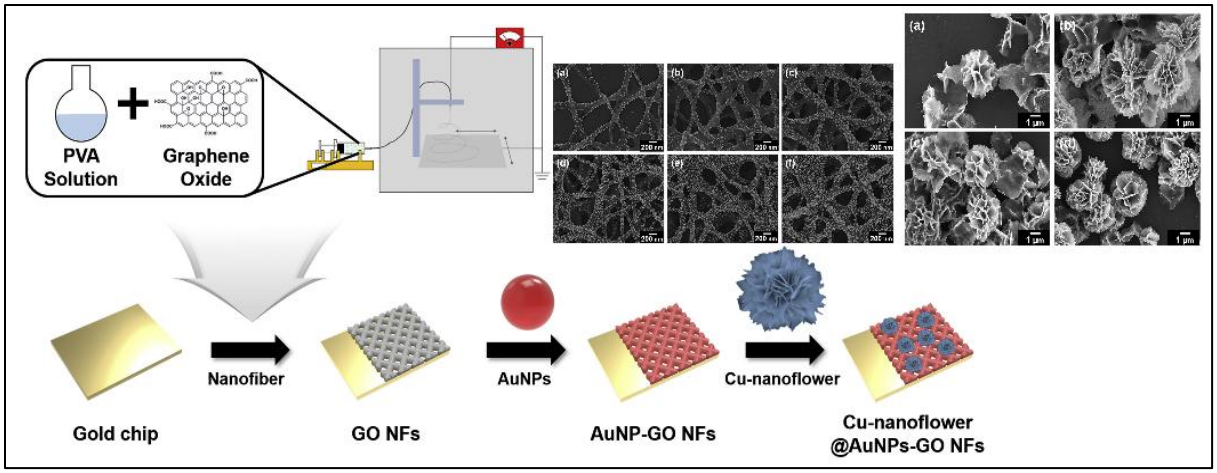


Figure 1.11 Schematic display of the fabrication of Cu-nanoflower@AuNPs-GO NFs-based electrochemical glucose nano-biosensor[17]

1.2.2 Carbon nanotubes (CNTs) and their hybrid-based glucose biosensors

Since their early discovery in 1991[64], carbon nanotubes have attracted enormous interest from researchers studying many different fields[65-69]. A considerable amount of work has been performed in which CNTs have been incorporated into electrochemical sensors and biosensors; thus in this review some of the most promising examples of CNT-glucose biosensors are described.

Yu *et al*.[14] have reported the preparation of poly (diallyldimethylammonium chloride) (PDDA)-capped gold nanoparticles (AuNPs) which were then combined with functionalized graphene (G)/multi-walled carbon nanotubes (MWCNTs) to form a nanocomposite which was then used as an immobilization matrix for GOx enzyme. This biosensor exhibited a sensitivity of 29.72 mA M^{-1} cm^{-2} and satisfactory associated analytical performance towards glucose since the graphene-nanotube and gold nanoparticle composite hierarchical structure provided a conductive network for efficient electron transfer as well as providing more binding sites for the enzyme.

Turner's group[70] have reported a highly sensitive glucose biosensor fabricated by the immobilization of glucose oxidase onto a poly(2,6-diaminopyridine)/multi-walled carbon nanotube/glassy carbon electrode (poly(2,6-DP)/MWNT/GCE), Fig. 1.12. The authors claim that

the synergistic effect of the high surface area of the poly-(2,6-DP) and the MWCNTs provided a remarkable improvement in the electrocatalytic performance of the developed biosensor. This biosensor demonstrated a sensitivity of 52.0 µA mM^{-1} cm^{-2}, repeatability of 1.6% and long-term stability, which could make it a promising bio-electrode for the precise detection of glucose in the biological samples.

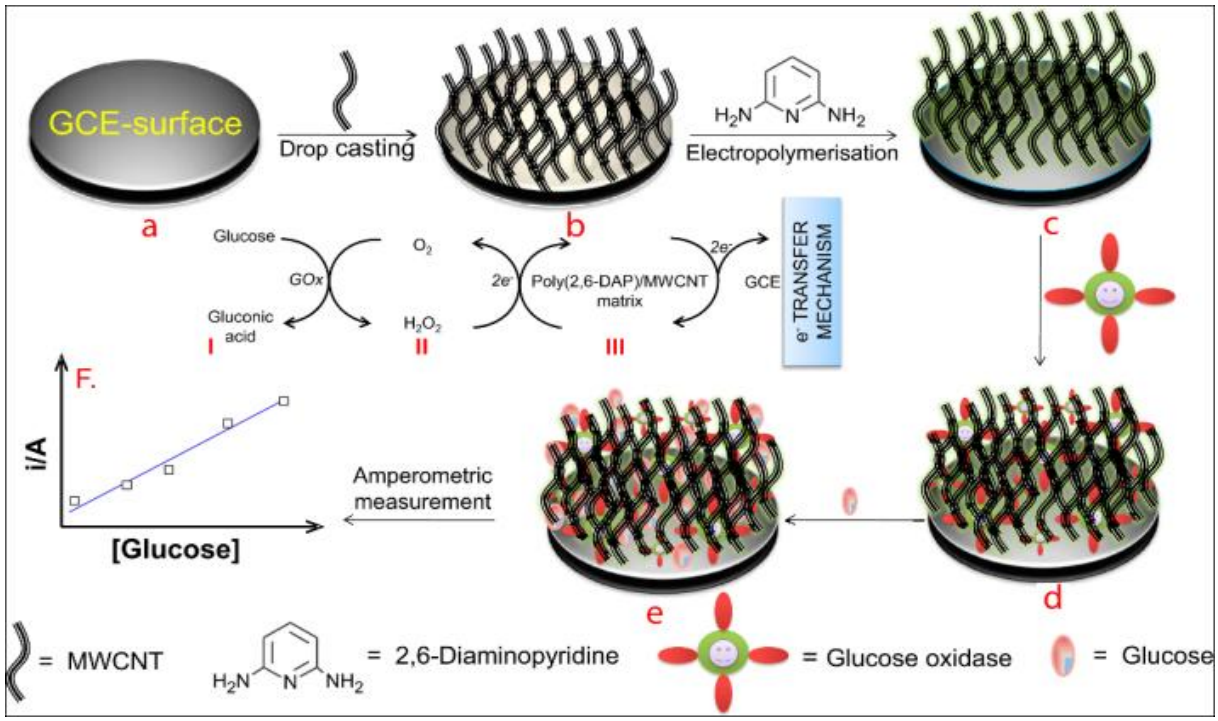


Figure 1.12 Schematic illustrations of fabrication, biosensing and electron transfer mechanism of an ultra-sensitive glucose biosensor (a-f). (a-b) treatment and casting of MWNT on a GC electrode; (c) electrodeposition of poly(2,6-DAP) on MWNT/GC electrode; (d) covalent-immobilization of GOx on a poly(2,6-DAP)/MWNT/GC electrode using gluteraldehyde as a linker and (e-f) amperometric glucose biosensing through direct electron transfer mechanism from I to III onto a GOx/poly(2,6-DAP)/MWNT/GC bioelectrode at physiological pH[70]

Lin *et al.*[12] have reported an interesting approach to the development of a carbon nanotube-based glucose oxidase biosensor (Fig.1.13A). Briefly, a Cr-coated Si wafer substrate of 1 cm^2 area was covered by Ni nanoparticles via an electrodeposition technique. Then, aligned CNT arrays were grown from those Ni nanoparticles by plasma enhanced chemical vapor deposition. An epoxy based polymer was spin-coated on the substrate to cover half the length of the CNTs. The protruding parts of the CNTs were removed by polishing. The glucose oxidase enzyme was later immobilized onto the tips of the CNTs via carbodiimide chemistry based on 1-ethyl-3-(3-

dimethylaminopropyl) carbodiimide (EDC) and using N-hydroxysulfo-succinimide (sulfo-NHS) to obtain covalent binding. This resulting biosensor was shown to be capable of performing the selective electrochemical analysis of glucose in the presence of common interfering species.

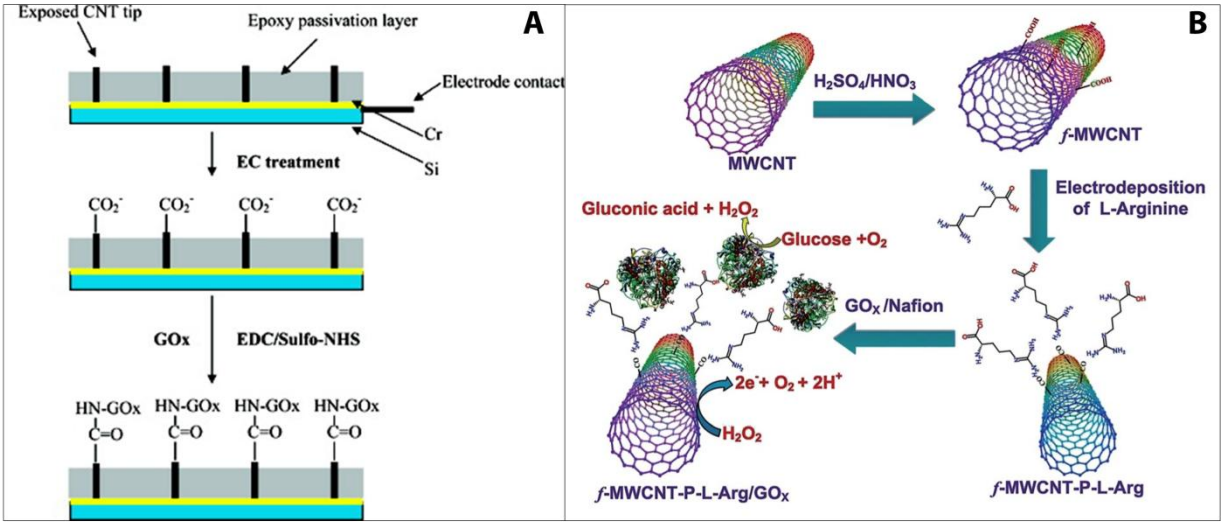


Figure 1.13 (A) Fabrication of a glucose biosensor based on CNT nanoelectrode ensembles[12], (B) Schematic diagram of the preparation of the GOx/P-L-Arg/ f-MWCNTs/GCE modified electrode for use in glucose biosensors[71]

Vilian and Chen[71] developed a glucose oxide biosensor based on multiwalled carbon nanotubes which was modified with the biopolymer L-arginine (Fig.1.13B). MWCNTs were treated with strong acids to produce surface carboxyl groups and then the functionalized MWCNTs (f-MWCNTs) were drop-cast onto a clean glassy carbon electrode. Following this a poly(L-arginine) film was formed on the f-MWCNTs-modified GCE via electro-polymerization. The as-prepared P-L-Arg/f-MWCNT/GCE electrode was then treated with GOx solution in order to immobilize the enzyme. The sensitivity of this biosensor was found to be 48.86 µA mM^{-1} cm^{-2} with a good storage stability of 25 days.

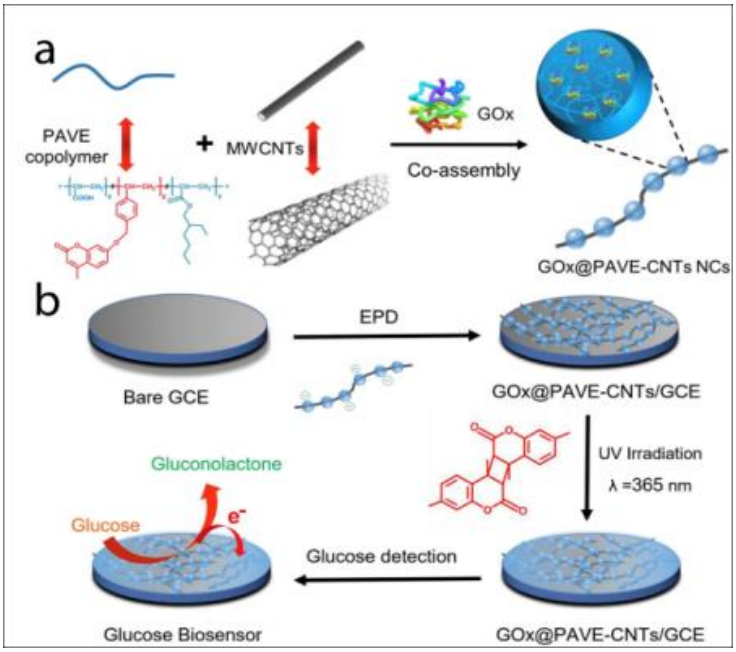


Figure 1.14 Schematic illustration of the enzymatic glucose biosensor fabrication; (a) Preparation of the long conducting enzyme-loading hybrid nanocomposite GOx@PAVE-CNTs via one-step co-assembly. (b) Preparation process of glucose biosensor via direct electrophoretic deposition (EPD) of GOx@PAVE-CNTs onto glassy carbon electrode (GCE) surface and subsequent photo-cross-linking13

Xu et al.[13] developed a highly interesting nanocomposite, a so-called "necklace-like" material, by the facile one-step co-assembly of the GOx, a copolymer and MWCNTs (Fig. 1.14). For this purpose, the copolymer poly(acrylic acid-r-(7-(4-vinylbenzyloxy)-4-methyl coumarin)-r-ethylhexyl acrylate) (PAVE) which contains photo-cross-linkable coumarin segments and carboxylic groups was co-assembled with MWCNTs, while simultaneously encapsulating the GOx. This preparation process generated enzyme-loaded polymeric nano beads attached along the length of the MWCNTs. Then, the resulting GOx@PAVE-CNTs bio-nanocomposites were electrodeposited onto a glassy carbon electrode surface followed by a photo-cross-linking process induced by UV irradiation. In this way a robust, complex, biosensing film having a porous network was achieved. The resulting biosensor exhibited highly satisfactory analytical performance towards glucose in terms of linear range (0.001-1.0 mM and 1.0-5.0 mM), stability (35 days) and reproducibility (RSD 3.27%, n= 5).

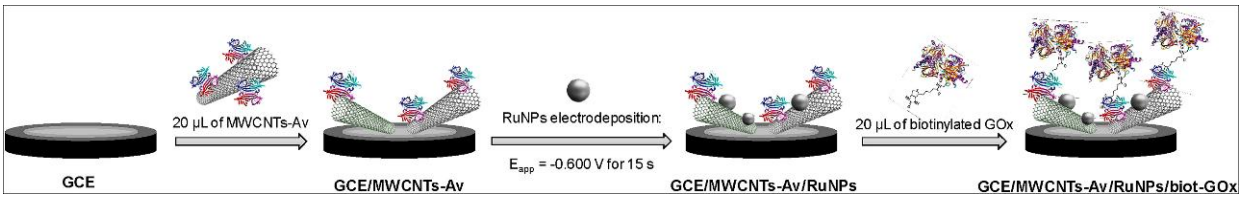


Figure 1.15 Schematic display of the steps involved in the preparation of the GCE/MWCNTs-Av/RuNPs/biot-GOx biosensor[72]

Recently, Rivas's group[72] have demonstrated an original supramolecular architecture based on a rationally-designed nanohybrid combination of MWCNTs and ruthenium nanoparticles (Fig. 1.15). For this construction they took advantage of avidin which is a biotin-binding protein. Briefly, MWCNTs were functionalized by avidin creating MWCNTs-Av which then served as a platform for the immobilization of a biotinylated glucose oxidase enzyme. The clean glassy carbon electrode was drop-cast with as-prepared MWCNT-Av complex and this was followed by electrodeposition of Ru nanoparticles. This GCE/MWCNTs-Av/RuNPs electrode with avidin terminals was found to be highly suitable for the attachment of the biotinylated enzyme complex which was achieved by incubating the electrode with biot-GOx solution. It was shown that the resulting developed surface was highly sensitive towards hydrogen peroxide. Then it was proven that the final GCE/MWCNTs/Av/RuNPs/biot-GOx biosensor) showed a sensitivity of 2.60 µA mM^{-1} cm^{-2} towards glucose. The authors claims that their platform acts as a pseudo-bienzymatic glucose biosensor where glucose was first oxidized by GOx and the resulting hydrogen peroxide was then reduced by the MWCNTs-Av/RuNPs complex.

1.2.3 Chitosan based glucose biosensors

Chitin and chitosan are natural polyaminosaccharides. Chitosan is obtained by controlled N-deacetylation of chitin. Chitosan is insoluble in water; however the amino groups render it soluble in acidic solution below pH 6.5. Most importantly it has an ability to form hydrogels and it is possible to produce thin hydrogel films of chitosan on solid electrode surfaces via a controlled electrodeposition process which makes it particular applicable to the fabrication of miniaturized biosensors. Moreover, the abundant amine groups of the chemical structure makes it a useful candidate for applications where various surface chemical methods are

required in order to achieve immobilization of a particular biomolecule As a result of these benefits together with its biocompatibility and lack of toxicity, chitosan has been widely used not only in the field of electrochemical biosensors[73] but also in controlled release systems[74-75], drug delivery applications[76-78], wound dressing[79] and tissue engineering[80-82].

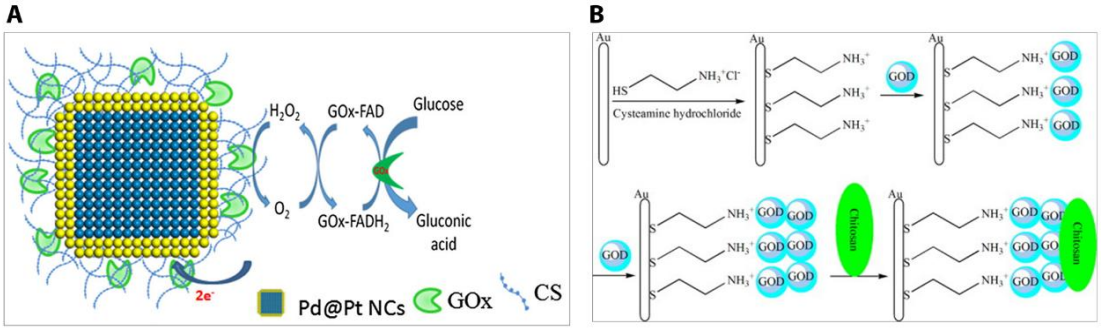


Figure 1.16 (A) Schematic Displaying the Surface Modification of Pd@Pt NCs Using CS Biopolymer and the Covalent Immobilization of GOx to the CS by Reacting with GA to Cross-Link the Amino Group of CS and the FAD Site of GOx[40], (B) Stepwise assembly of cysteamine, two layers of GOD, chitosan on an Au electrode[83]

Here, we focus on the fabrication and characterization of glucose oxidase immobilized chitosan matrixes. For example, Krishnan *et al.* utilized chitosan as an immobilization matrix for glucose oxidase enzym[40]. Briefly, Pd nanocubes were synthesized with an average edge length of 13 nm and then a shell of Pt was deposited on their surfaces. The as-prepared nanocubes of Pd-Pt were then incubated with a chitosan solution to achieve the chitosan coating (Fig. 1.16A). The covalent immobilization of glucose oxidase on the surface of chitosan coated nanocubes was accomplished by reacting with gluteraldehyde followed by addition of the glucose oxidase enzyme. The GOx-immobilized chitosan-coated nanocubes were then deposited on a glassy carbon electrode surface. The sensitivity of the resulting biosensor was determined to be 6.82 $\mu A\ mM^{-1}\ cm^{-2}$.

In another study chitosan was used as a protection barrier for the immobilized enzyme to ensure the stability and biocompatibility of the biosensor, Fig. 1. 16B[83]. For this purpose, a gold electrode was modified with cysteamine to obtain an amine-functionalized surface and then a solution of glucose oxidase enzyme was drop-cast onto the electrode which was then allowed

to dry. This process was repeated several times. Then, chitosan solution was coated onto the glucose oxidase layer. It was found that the response of the resulting biosensor response remained almost constant over a 30 day period, with the RSD range from 1.3% to 7.2%. The stability of the biosensor was attributed to the chitosan protection layer.

Anusha et al.[84] developed a glucose oxidase biosensor based on the use of chitosan nanoparticles taken from a squid (Fig. 1.17A). Briefly, the squid was dried at room temperature after removal of debris and then powdered to extract the chitin by deprotenization and demineralization processes. The chitin obtained was then treated to prepare the chitosan by a deacetylation process and the resulting chitosan was used to prepare chitosan nanoparticles. To construct the biosensor, electrodes were first covered with gold nanostructures to increase the surface area, and then these electrodes were immersed into a solution of chitosan nanoparticles. The resulting surfaces were then used to immobilize glucose oxidase enzyme. The resulting biosensor exhibited a high sensitivity of 156.27 µA mM^{-1} cm^{-2} with good associated analytical performance. The results were attributed to the presence of a chitosan nanoparticles matrix over the gold nanostructures which created a friendly environment for enzymes and enhanced the catalytic activity towards glucose.

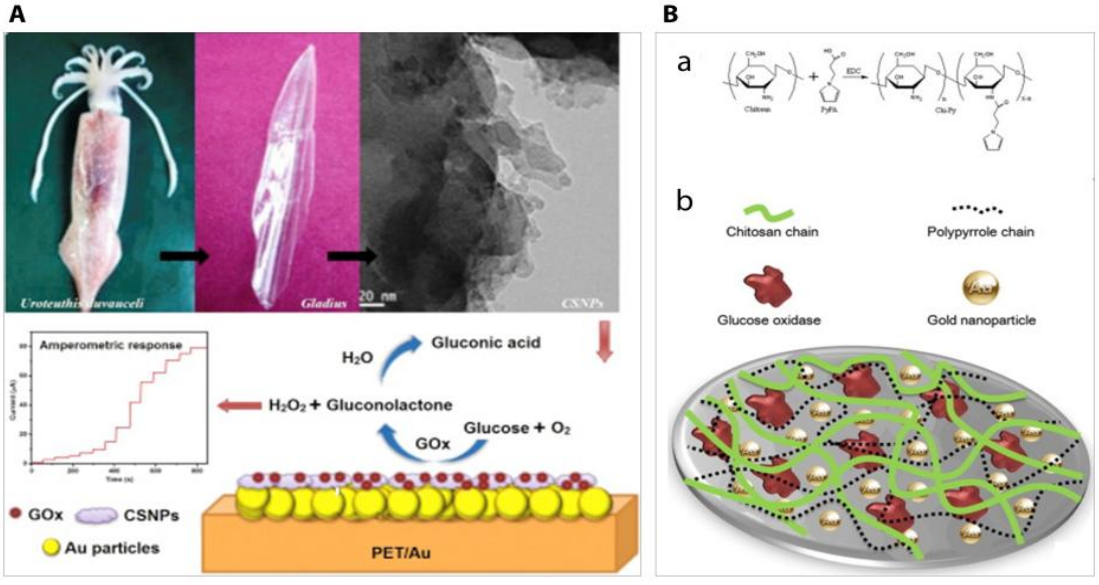


Figure 1.17 (A) Schematic illustration of electrochemical glucose biosensor fabricated over PET/Au electrode by immobilization of glucose oxidase on chitosan nanoparticles synthesized from gladius of squid, Uroteuthis duvauceli

and glucose determination of developed Au/CSNPs/GOx biosensor by electrochemical method[84], and (B) Synthesis of pyrrole branched-chitosan (a), schematization of the surface of GOx immobilized gold electrode (b)[85]

Another approach utilizing chitosan as a matrix component for glucose biosensor development was reported based on a pyrrole-branched-chitosan (Fig. 1.17B)[85]. This polymer composite structure was prepared via carbodiimide chemistry. The carboxylated pyrrole was attached to the amine groups of chitosan via amide binding. A chitosan-pyrrole-gold-GOx nano-biocomposite was then prepared by mixing and incubating on the electrode surface. It was found that the chitosan-pyrrole (hydrogel-conductive polymer) composite was a useful host for the immobilization of biomolecules as well as acting as an *in situ* reducing agent for the formation of gold nanoparticles on the electrode surface.

The electrodeposition of chitosan films is one of the common methods now used in biosensor development[86-88]. For example, Che et al.[89] reported a simple one-step deposition of chitosan in the presence of MWCNTs, hollow PtCo nanochains and the dye, Prussian blue. The electrodeposited hybrid film was deployed as a glucose oxidase immobilization matrix and then coated with nafion film. Encapsulation of MWCNTs and Prussian blue in the chitosan gel layer was found to improve the electron transfer ability of the three dimensional matrix in comparison to the Prussian Blue-encapsulated chitosan matrix alone. The authors attributed these enhanced electrical characteristics to the interactions between the MWCNTs, the hollow PtCo nanochains and the Prussian blue molecules.

1.2.4 Carbon/Graphene quantum dots (CQDs, GQDs)-based glucose biosensors

Carbon or graphene quantum dots are a relatively new class of carbon-based nanomaterials. Since their discovery in 2004, they have attracted considerable attention from researchers due primarily to their highly interesting photoluminescence (PL) behavior. At the time of writing the use of such tiny nanostructures in the field of electrochemical biosensors is limited. Apart from their PL properties, carbon/graphene quantum dots have several other interesting properties associated with their very small size, their ability to be readily functionalized, their relatively cheap, easy methods of preparation and their ability to disperse readily in water[20-21, 90-91]. These

benefits combined with the fact that they are essentially non-toxic make them highly promising candidates as components of a biosensing matrix. For instance it has been reported that the graphene quantum dots are highly suitable for use as substrates for the glucose oxidase immobilization process[19]. In this report, the graphene quantum dots were prepared by a hydrothermal method from graphite powder. The as-prepared graphene quantum dot solution was drop-cast onto a ceramic carbon electrode surface and dried at room temperature. The resulting GQDs electrode was then activated at a potential of 1.7 V (vs. SCE) and followed by glucose oxidase immobilization. The sensitivity of this relatively simple biosensor based on GQDs was reported to be 0.085 μA μM^{-1} cm^{-2}, while it showed reasonable stability over a two week period. Recently, our group has also reported the use of carbon quantum dots integrated with gold nanoparticles for glucose oxidase attachment as part of the development of an electrochemical biosensor development at both the bulk, planar and micro scales [20-21]. These results are presented in Chapter 3 and 4.

1.3 Non-enzymatic detection of glucose; direct glucose electro oxidation

Glucose oxidase based biosensors have been studied extensively (as discussed above); however the possible decrease in catalytic activity of the enzyme arising from the immobilization process is still a great challenge for researchers in terms of the performance of the sensor as well as the long-term stability of the desired biosensor[92-93]. Direct electro-oxidation of glucose in the absence of the enzyme may bring a solution to some of the problems of enzymatic systems. However, the selectivity of the catalysts developed towards glucose should be investigated in detail if the biosensor is to be used in a highly complex matrix. It is noteworthy that at the time of writing most enzyme-free biosensors for glucose detection exhibit sensitivities at the highest end of the scale in comparison to the enzyme based glucose sensors[24, 94-96].

For example, a biosensor based on a simple nanohybrid composition of ZnO nanorods and CuO nanoparticles was reported in 2017 which showed excellent analytical performance, yielding a sensitivity of 2961.7 μA mM^{-1} cm^{-2}, Fig. 1.18A[97]. In this study, vertically-aligned ZnO nanorods were grown on fluorine doped tin oxide (FTO) electrodes. The hydrothermally-grown ZnO

nanorods on the electrode surface were then modified with CuO nanostructures through a dip-coating and annealing process. The resulting hybrid CuO-ZnO material was coated with nafion to reduce possible fouling and to help limit possible interference effects. The resulting hybrid sensor exhibited a sensitivity of 2961.7 µA mM^{-1} cm^{-2} with excellent reproducibility, repeatability, stability and selectivity. Furthermore, the sensor was also used to determine the glucose concentration in real human serum samples. The high performance of the sensor was attributed to the efficient electrocatalyst behavior of the CuO-ZnO hybrid material for glucose oxidation.

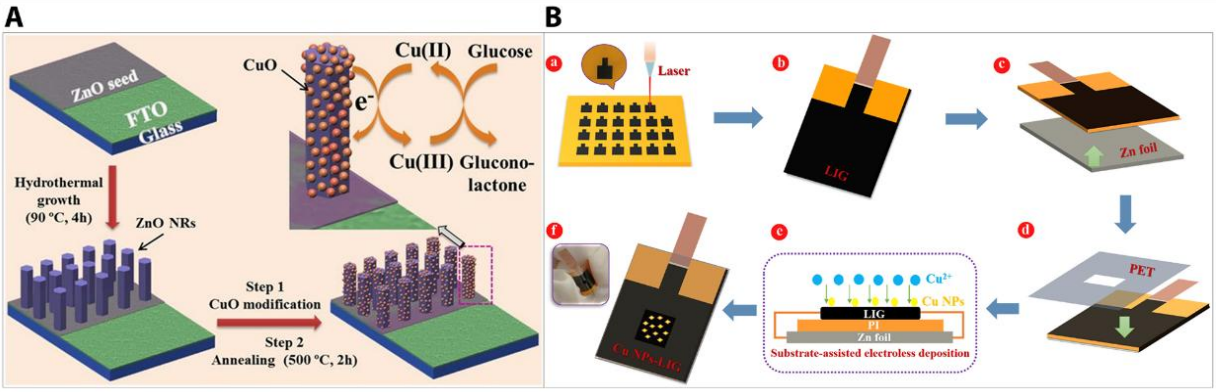


Figure 1.18 (A) Schematic illustration of non-enzymatic glucose sensor electrode fabrication and its application in glucose detection[97], (B) schematic illustration of fabrication process of the flexible Cu NPs-LIG sensor[98]

Recently, a flexible non-enzymatic glucose biosensor based on a laser-induced graphene electrode modified with copper nanoparticles has been reported (Fig. 1.18B)[98]. The flexible graphene electrodes were prepared by laser irradiation of the surface of a sample of polyimide. Since high-intensity laser radiation is applied, the polyimide is essentially depolymerized, which leads to subsequent carbonization and eventual graphitization. The resulting three-dimensional porous graphene electrodes (LIG) obtained were modified with Cu nanoparticles (Cu NPs). The as-prepared Cu NPs-LIG sensor demonstrated a glucose sensitivity of 495 µA mM^{-1} cm^{-2}. The authors refer to the use of such a 'simple method' for the fabrication of a sensor device and suggest that their approach could be attractive in terms of the fabrication of next-generation flexible diagnostic devices, although the need for high intensity laser irradiation rather calls this presumption into question.

Another recent study based on the use of a novel uniform composite of an Au nanostructured honeycomb coated with a layer of Co_3O_4 nanoneedles appeared to be a highly promising catalyst for glucose oxidation, Fig. 1.19[99]. These authors achieved the deposition of the highly porous honeycomb-like gold nanostructures onto the electrode surface via electrodeposition in acidic environment. The synthesis of Co_3O_4 nanoneedles on the surface of the honeycomb-like gold was then achieved by a hydrothermal synthesis process in an autoclave and subsequent annealing at 450 °C. The resulting hybrid electrode was studied to determine its performance as a glucose sensor and exhibited a sensitivity of 2013.6 µA mM^{-1} cm^{-2} with a good selectivity towards glucose in alkaline media for both blood and synthetic saliva.

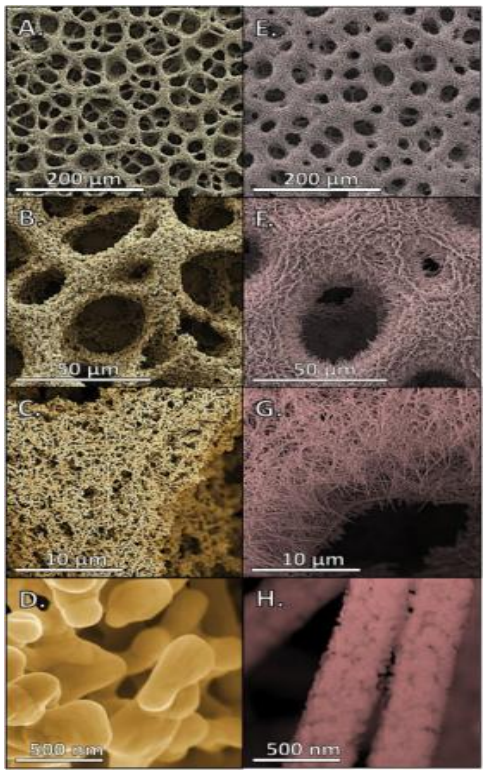


Figure 19 SEM images (false colour) of Au honeycomb (left panel) and Au honeycomb coated with 100 mM $CoCl_2$ (right panel) at different magnifications[99]

Another interesting non-enzymatic approach has been reported which involves the synthesis of Cu-Cu_2O nanoparticles on the surface of TiO_2 nanotubes which act as transducers for the direct electrocatalytic oxidation of glucose (Fig. 1.20)[100]. The TiO_2 nanotubes were prepared by the two-step anodization of Ti foils and then the preformed Cu and Cu_2O particles were coated

onto the TiO_2 nanotubes by an electrodeposition technique. The resulting hybrid electrode was then used for the non-enzymatic electro-oxidation of glucose. The sensitivity of sensor was calculated to be 4895 μA mM^{-1} cm^{-2}. Such a high sensitivity was attributed to the synergistic effect of the small Cu-Cu_2O grain size and the very large surface area of the TiO_2 nanotube arrays as well as to fast electron transfer. Moreover, by evaluating the results obtained from studies of the various deposition parameters used, the authors claim that the Cu_2O helps to provide a broad linear range while the incorporation of the Cu nanoparticles helps to improve the response current and sensitivity.

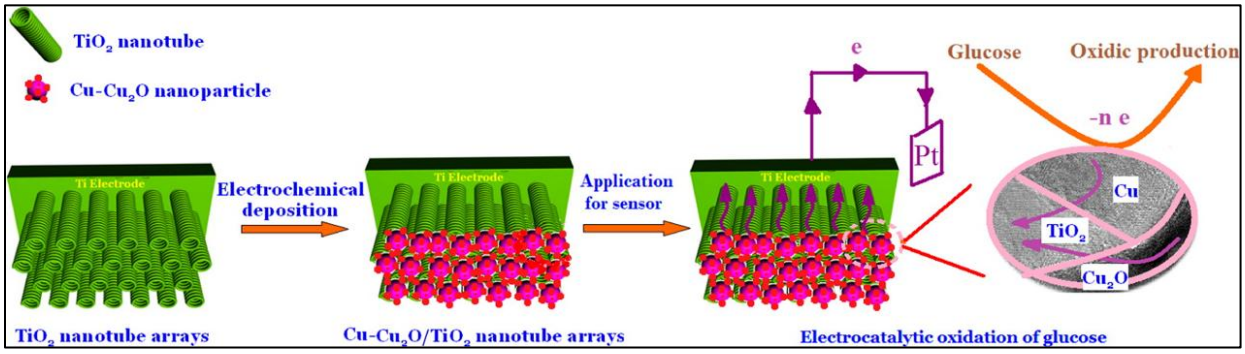


Figure 1.20 Schematic illustration of the preparation of the Cu–Cu_2O/TiO_2 NTA/Ti electrode and the electron transfer through the Cu–Cu_2O/TiO_2 TNA interface for the electrocatalytic oxidation of glucose[100]

Li et al.[101] have reported a novel hybrid non-enzymatic glucose sensor consisting of a freestanding $Cu(OH)_2$ nanograss array on the surface of a nanoporous copper (NPC) substrate, Fig. 1.21. These authors first prepared the nanoporous copper substrate from a CuZrAl glassy precursor *via* a chemical de-alloying process. Then, the $Cu(OH)_2$ nanograss was synthesized on the NPC substrate through an oxidative alkaline method, wherein the morphology of the nanograss was tailored by varying the etching time. The substrate was placed into a solution of $(N_2H_4)_2S_2O_8$ and NaOH until the surface colour turned light blue. This process was explained in terms of four stages; oxidation, self-assembly, germination and growth. The resulting uniform hybrids also grow homogenously. It was found that the nanograss clusters exhibited high performance towards the oxidation of glucose, with a sensitivity of 2.09 mA mM^{-1} cm^{-2} being recorded

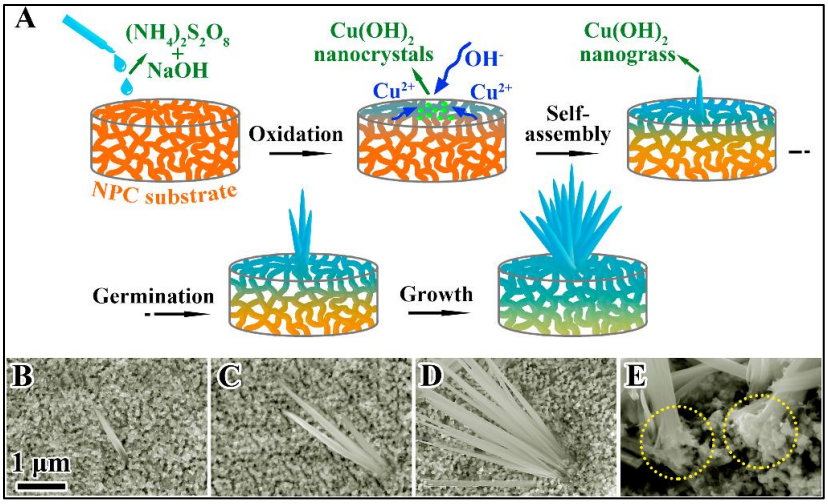


Figure 1.21 Schematic illustration of the growth process of the $Cu(OH)_2$ nanograss structure on a NPC substrate (a), the corresponding surface SEM images at different growth stages (b, c, and d), magnified cross-section of the fabricated nanohybrid (e)[101].

1.4 Microfabrication and miniaturization in the development of electrochemical biosensors

Currently, silicon is the most used material in the semiconductor industry and an entire technology has been developed around the use of silicon in terms of the various approaches needed to fabricate devices. Silicon-based microtechnologies provide excellent opportunities for the construction of micro/nano-scale electrodes to be used as components in biosensors offering a high degree of reproducibility, scalability, design flexibility and multiplexing of operational features. Innovative devices such as microelectrode-integrated fluidics, implantable chips, lab-on-a-chip, organ-on-a-chip, miniaturized diagnostic devices/biosensors and neural probes have been appearing rapidly in prototype forms from various research labs[20-21, 31, 102-106].

In general, the microfabrication of devices is based on the repeated application of unit process steps such as photolithography, deposition and etching. Photolithography is used to transfer a specific pattern onto a substrate by using a designed stencil, the so-called mask. In use, a photo-mask which usually consists of an optically flat glass or a quartz plate substrate with a metal pattern, is placed on a photoresist-coated wafer surface the wafer is exposed to UV radiation. This is followed by the deposition of the metal layers and the use of a so-called lift-off process which removes the excess metal and photoresist. For the etching process, firstly a

passivation layer is applied over the surface of the wafer, and then subsequently either dry or wet etching of the underlying material takes place[29].

When implemented correctly, microfabrication can either significantly improve a device in relation to its conventional counterparts or enable entirely new devices. An interesting example of an improvement to a device is the fabrication of miniaturized micro-nano electrodes for use in neurological recordings and as neurotransmitters for the detection of various chemical agents in the brain. This type of device is described in the following section:

1.4.1 Microfabricated neural sensor probes

The human brain has a highly diverse chemical environment[107]. Approximately two hundred different molecules have been identified as neurotransmitters (NTs). The classification of NTs can be grouped according their chemical structures such as amines (dopamine, serotonin, epinephrine, histamine, acetylcholine, etc.), amino acids (glutamate, γ-aminobutyric acid, glycine, etc.), peptides (vasopressin, somatostatin, neurotensin, etc.) and gaseous NTs (nitric oxide, carbon monoxide and hydrogen sulfide)[108].There is an undisputed need for enhanced monitoring of NTs in brain tissue since such molecules may provide valuable information related to human brain functions. However, the major and currently long-term goal of such a device is to provide a greater understanding of brain function and in particular shed light on the nature and possible cures for several neurological disorders such as Alzheimer's disease and Parkinson's disease.

One of the most successful microprobe arrays fabricated specifically for the field of neurotechnology was reported in 2010 as a result of a collaboration between the Ecole Polytechnique Fédérale de Lausanne and the University of Cambridge, Fig. 1 22[109]. These authors described the development of a brain-implantable microprobe array consisting of several recessed Pt microelectrodes and an integrated reference electrode. The probes were fabricated by applying a standard microfabrication flow process designed for Si-based microtechnologies. Briefly, a silicon wafer with an oxide layer was used as a substrate for the

transfer of the first pattern via wet etching. Subsequently a passivation layer was applied. This was followed by metal deposition of Pt and a lift-off process. Silicon nitride and oxide were used as passivation layers that was opened at the active surface to facilitate the fabrication of the connection pads via etching. The fabricated probes were attached to a custom-made circuit board and embedded in epoxy glue to mechanically protect and electrically insulate the connections. The microelectrodes were coated by an enzyme membrane and a semi-permeable m-phenylenediamine layer for the selective detection of the neurotransmitters choline and l-glutamate at physiologically relevant concentrations. The results showed that the design of the probes and the surface chemistry selected to facilitate biomolecule immobilization were fully compatible with the simultaneous detection of several analytes in different brain target areas. A sensitivity of 132 ± 20 µA mM^{-1} cm^{-2} for choline and 95 ± 20 µA mM^{-1} cm^{-2} for l-glutamate was achieved and the authors noted that their aim was to transfer their sensor technology into a package for use in living animals.

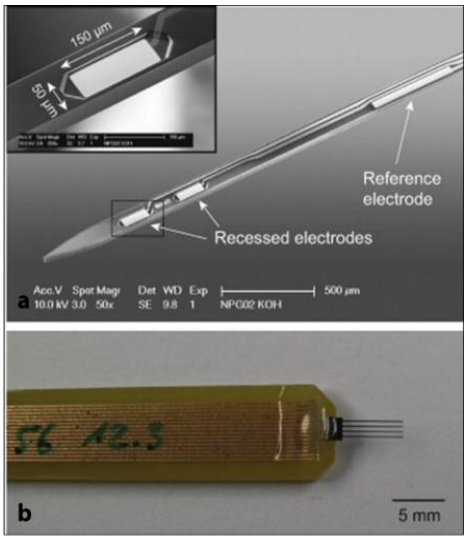


Figure 1.22 SEM micrograph of the front part of the shaft of the fabricated silicon microprobe and close up view of the KOH-recessed Pt microelectrode. The metal interconnection track is laid across the inclined side wall appearing after the KOH etch[109]

Ferreira et al.[110] demonstrated another successful approach for the detection of neurotransmitters based on nanocomposite sensors consisting of carbon fibre microelectrodes and microelectrode biosensor arrays designed to measure ascorbate and glutamate (Fig. 1.23).

Carbon microfibre microelectrodes were modified with nafion and carbon nanotubes and calibrated towards ascorbate. Microbiosensor arrays consisting of two pairs of side-by-side Pt sites on a ceramic substrate were used which were fabricated via photolithography. The Pt surfaces were modified with glutamate oxidase and covered with 1,3-phenylenediamine to improve the selectivity. Both biosensors were coupled to a pulled micropipette and successfully used for simultaneous and real time measurement in the hippocampus of anesthetized rats.

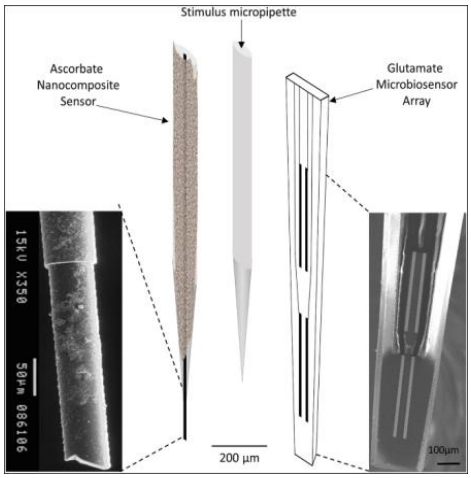


Figure 1.23 Schematic representation of the array composed by the ascorbate nanocomposite microsensor (left), the glutamate microbiosensor (right) and the micropipette (center) used for local application of solutions in the extracellular space of the rat hippocampus[110].

1.4.2 Miniaturized electrochemical biosensors

Arguably, the fabrication of inexpensive but highly sensitive and accurate electrochemical biosensor devices will in the future rely heavily on the enhancements and developments that take place in the area of semiconductor micro (and/or nano) fabrication, particularly in relation to miniaturization or the transition from planar to micro and nano electrodes which may be required in order to achieve improved performance. Scaling down of the systems provides several advantages in terms of analytical performance of the biosensors as well as the decreased sample size and easy packaging.

Wang et al.[111] developed a micro immunosensor to determine the concentration of the TAU proteins which are possible biomarkers for the diagnosis of Alzheimer's disease, Fig.1.24. The

electrode used was a microelectrode array composed of four gold microband electrodes. The fabrication process was again based on standard microfabrication technology applied to a silicon substrate. A gold surface was modified with a self-assembled monolayer of 3,3'-dithiobis (sulfosuccinimidyl propionate) (DTSSP). Protein G and anti-TAU antibodies were immobilized onto the surface, respectively. The performance of the biosensor was investigated by applying electrochemical impedance spectroscopy. The assay developed was both fast and sensitive.

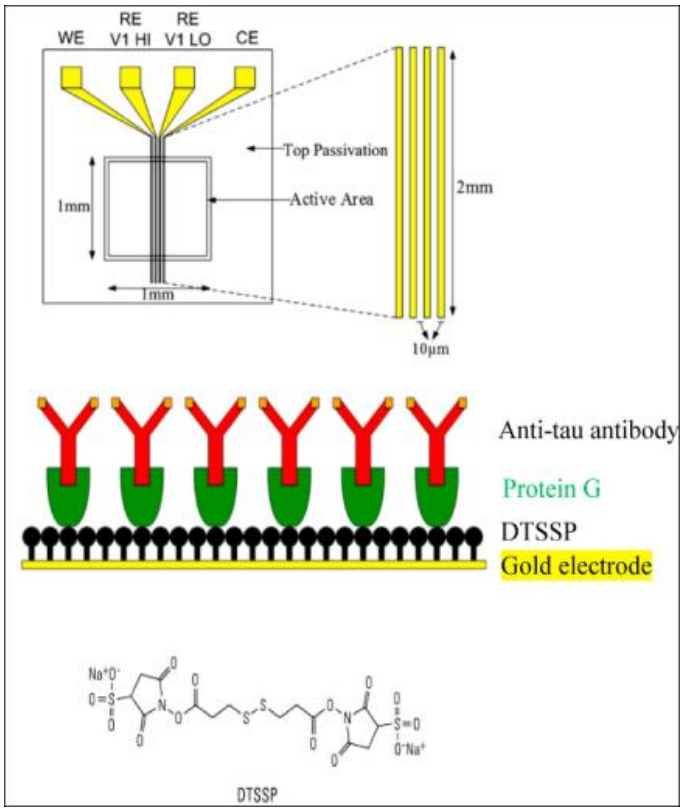


Figure 1.24 Detailed image of gold microband electrodes, schematic side view of the biosensor and chemical structure of DTSSP which contains an amine-reactive N-hydroxysulfosuccinimide (sulfo-NHS) ester at each end and forms the SAM layer. From bottom to top: gold microband electrode, SAM layer, protein G layer and antibodies[111]

Mir et al.[112] reported the use of a method for biomolecule immobilization onto interdigitated electrodes via a biomolecule-friendly lithographic process (Fig. 1.25). For these purposes a photoresist based on a methacrylate copolymer was used, which was highly suitable for processing under mild conditions and thus it was possible to achieve the immobilization of the biomolecules via lithography. The silicon-based interdigitated electrodes consisted of 50

microelectrodes which were fabricated via lithography, deposition and etching. However to complete the process a bio-photoresist was used and in this way the biomolecules were successfully transferred to the surface as part of the fabrication flow. This biocompatible resist was composed of four different monomers which offered the necessary functional groups needed for the lithography process. These monomers were butyl methacrylate (TBMA), hydroxyethyl methacrylate (HEMA), acrylic acid (AA) and isobornyl methacrylate (IBMA). These researchers studied the immobilization of three different biomolecules via the same fabrication process. By doing so, they successfully demonstrated a biocompatible photolithography process. Moreover, using this approach, a gene mutation related to breast and ovarian cancer, has also been detected amperometrically, a patterned device has been made using a combination of two different enzymes GOx and SOx and hormone T4 has been detected by using an interdigitated electrode microarray patterned with biocompatible photolithography.

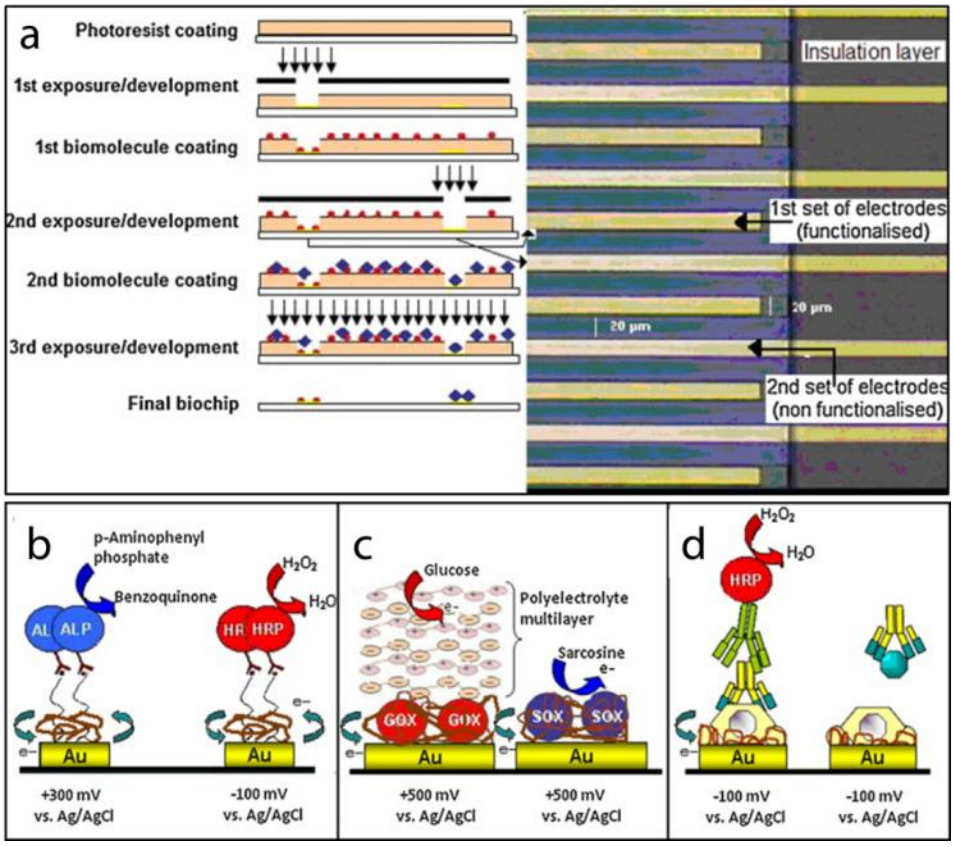


Figure 1.25 (a) Bio-photolithographic process for biomolecules patterning on the electrode array. On the right, gold IDE array detail (b) DNA with different enzyme labels, ALP and HRP immobilized on each electrode, (c) sarcosine

and glucose enzymatic sensors, using a polyelectrolyte multilayers blocking on the first set of electrodes in order to avoid the non-specific adsorption from the second enzyme and (d) competitive immunoassay for T4 detection[112]

Fig.1.26 shows the fabrication and use of a contact lens with an embedded sensor designed to measure glucose concentrations from tears[113]. For the construction of the contact lens, a PET polymer was used as a substrate and spin-coated with a resist. This was followed by metal deposition and lift-off in acetone. The fabricated electrodes were cut into small pieces of 1 cm diameter and heat molded to the shape of the contact lens. To achieve the immobilization of the glucose oxidase enzyme, a solution of enzyme was drop-cast on the electrode surface, and then the surface was suspended vertically above a titanium isopropoxide solution in a sealed dish to create a glucose oxidase/titania sol-gel membrane. After forming the sol-gel membrane, the surface was covered with nafion. This non-invasive glucose monitoring system was studied using amperometry. The simple micro-sized glucose sensor showed a sensitivity of 240 µA cm^{-2} mM^{-1}, however many characteristics of the sensor required improvement including its stability, its biocompatibility for such a 'wearable' device and the methods used to integrate the device with a read-out-communication circuit.

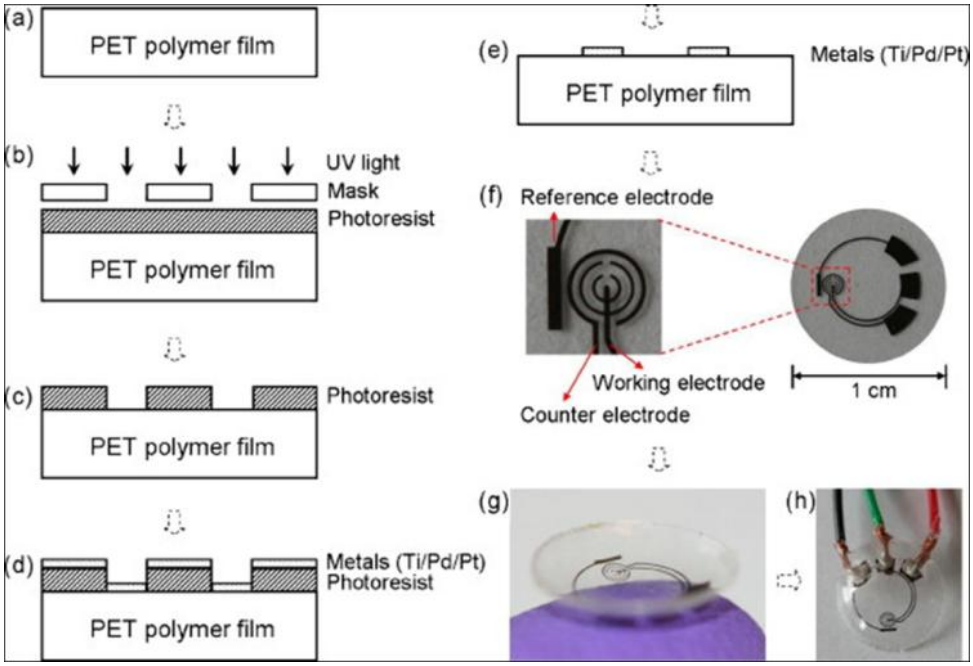


Figure 1.26 The sensor fabrication process (a-e), images of a sensor after it has been cut out of the substrate (f), image of a completed sensor after molding held on a finger (g); the sensor may be hardwired for testing (h)[113]

Rajapaksha et al. described the microfabrication of interdigitated electrodes with 6 µm wide and 4 µm spacing distance, Fig. 1.27[114]. These authors applied photolithography, deposition and etching in their fabrication flow. The electrodes were modified with (3-aminopropyl) triethoxysilane (APTES) for the silanization of the surface SiO_2 layer present between the gold fingers of electrode. The immobilization of probe DNA was achieved via the formation of amide bonding between the carboxyl groups of the pre-labeled DNA and the amine groups of APTES layer. When the DNA hybridized with the complementary target DNA strand, the positive charge associated with the APTES layer increased due to the increased total negative charge of the DNA layer which was studied *via* the *I-V* characteristics of the sensor towards increased concentration of complementary DNA.

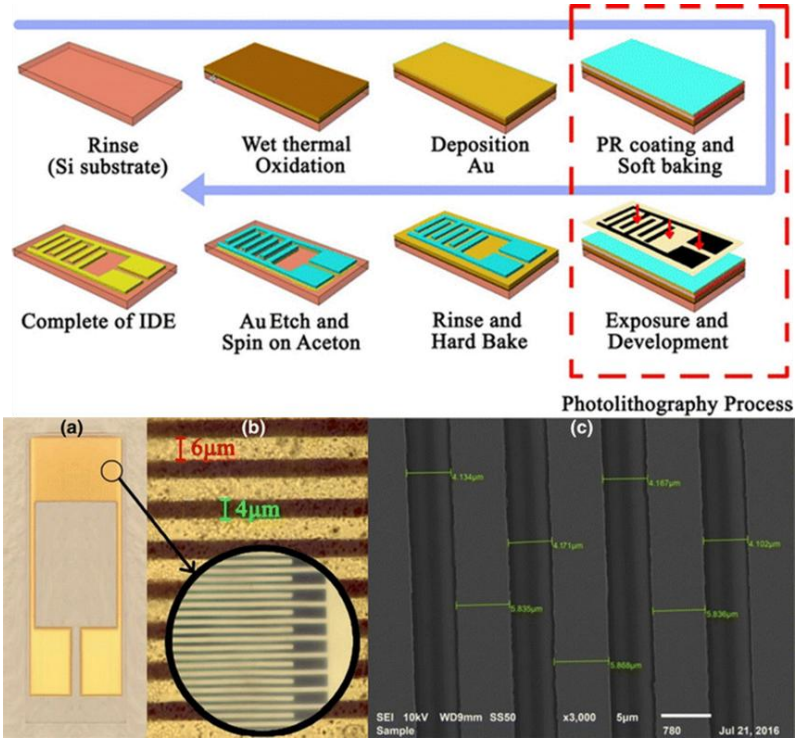


Figure 1.27 Fabrication of the electrode. LPM, HPM and SEM images for Au IDE electrode; (a) LPM image under 4.5× magnification, (b) 15× and 50× magnification was used to scan the Au IDE surface using HPM under ambient temperature (c) SEM image for 3000× magnification114

1.4.3 Microfabricated biosensor integrated fluidic devices

The area of research into microfluidic devices integrated together with electrochemical micro-nano biosensors is currently attracting considerable interest. At present, the most attractive

aspect of this research is considered to be the effects of size and in particular size reduction since a miniaturized, perhaps also portable analysis platform of this type would ideally only require small amounts of reagents and analyte without compromising and perhaps even enhancing sensitivity.

Most of the current generations of microfluidic devices are also packed with separation or sample preparation units as well as a detection section having high resolution and sensitivity. A very recent study reported by Dincer's group successfully demonstrates the integration of CRISPR technology (Clustered Regularly Interspaced Short Palindromic Repeats) with an electrochemical microfluidic biosensor having a cost at the time of writing of €0.838 per biosensor chip, Fig. 1.28[102]. These authors described a CRISPR-on-a-microfluidic electrochemical biosensor which measured the micro RNA levels of the potential brain tumor marker miR-19b in serum samples of patients who had been diagnosed with brain cancer. For the biosensor they used a polyimide substrate subjected to a fabrication process based on deposition, etching and lithography. The resulting microfluidic biosensor channel consisted of an immobilization area and electrochemical cell based on a Pt working electrode, a counter electrode and a reference electrode, separated by a hydrophobic stopping barrier. The surface of the immobilization area was pre-functionalized by applying a streptavidin. For the CRISPR powered process, the enzyme Cas13a was mixed with its target specific crRNA, a biotin and 6-FAM (6-fluorescein amidite) labeled reRNA, and the sample of interest. The mixture was incubated at 37 ^{o}C, where the Cas13a formed a complex with the target specific crRNA. Thus, in the presence of target miRNAs, the Cas13a becomes activated and subsequently a collateral cleavage of the surrounding reRNA is achieved. This solution was then applied directly to the immobilization area which was modified with streptavidin; at this point the biotin and 6-FAM labeled RNA molecules became bound to surface streptavidin. This was followed by the application a GOx enzyme coupled to anti-6FAM antibodies to the immobilization area. The biosensor assay was then treated with glucose solution. Thus GOx enzyme catalyzed reaction produced H_2O_2 which was amperometrically detected in the electrochemical cell of the biosensor. In this way, the interesting combination of CRISPR/Cas13a technology with a microfluidic biosensor was

demonstrated and shown to be a highly promising and unique platform for the detection of miRNAs in small sample volumes efficiently and accurately in a very short time. Subsequently the validation of the system developed with a standard quantitative real-time polymerase chain reaction (qRT-PCR) process has proven the capability of the system for use in miRNAs-related disease diagnostics.

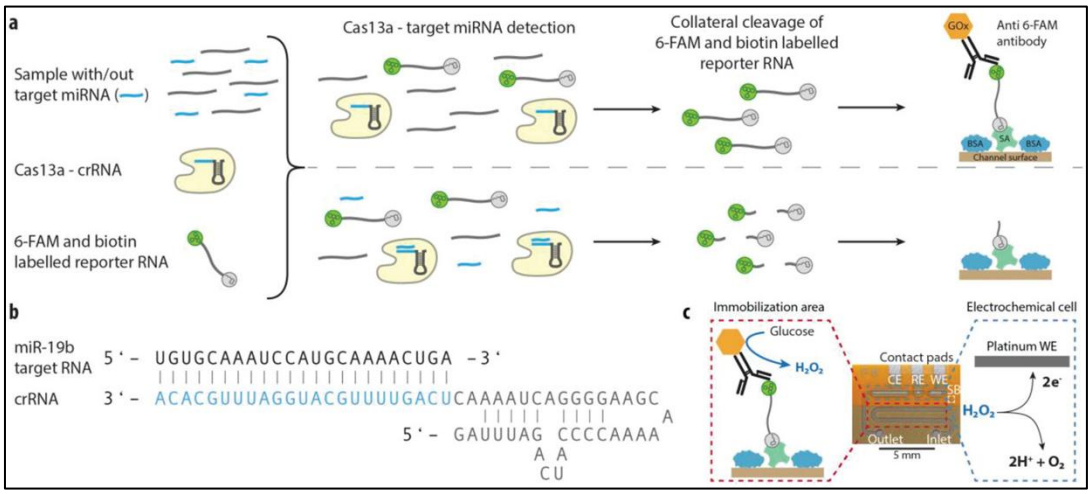


Figure 1.28 Combination of the CRISPR technology along with an electrochemical microfluidic biosensor for miRNA diagnostics. a) Schematic of the off-chip miRNA targeting b) Schematic of the single-stranded target miRNA, miR-19b, and the crRNA, where the complementary sequence is highlighted in blue. c) Working principle and photo of the microfluidic biosensor with its main elements [102]

Another highly promising approach towards the production of a fully on-chip, integrated rolled-up microelectrode for DNA detection has been reported by Schmidt's group, Fig. 1.29[115]. These authors fabricated electrodes via deposition, photolithography and etching on a sacrificial layer. When this layer was dissolved, it led to the rolling-up of the electrode as shown in Fig. 1.29. To improve the mechanical stability, SiO_2 was deposited on top of the tubular electrode. This was followed by the integration of the rolled-up electrode into a microfluidic channel which was fabricated by soft-lithography. The inner part of the rolled-up electrode was modified with 11-mercaptoundecanoic acid (11-MUA) and then the resulting surface carboxyl groups were activated via carbodiimide chemistry. After rinsing the electrode, amino-modified DNA was attached to surface. The resulting rolled-up microelectrode biosensor was used to detect DNA

of avian influenza A virus (AIV), subtype H1N1 without any amplification or labeling in the range 20 aM to 2 pM.

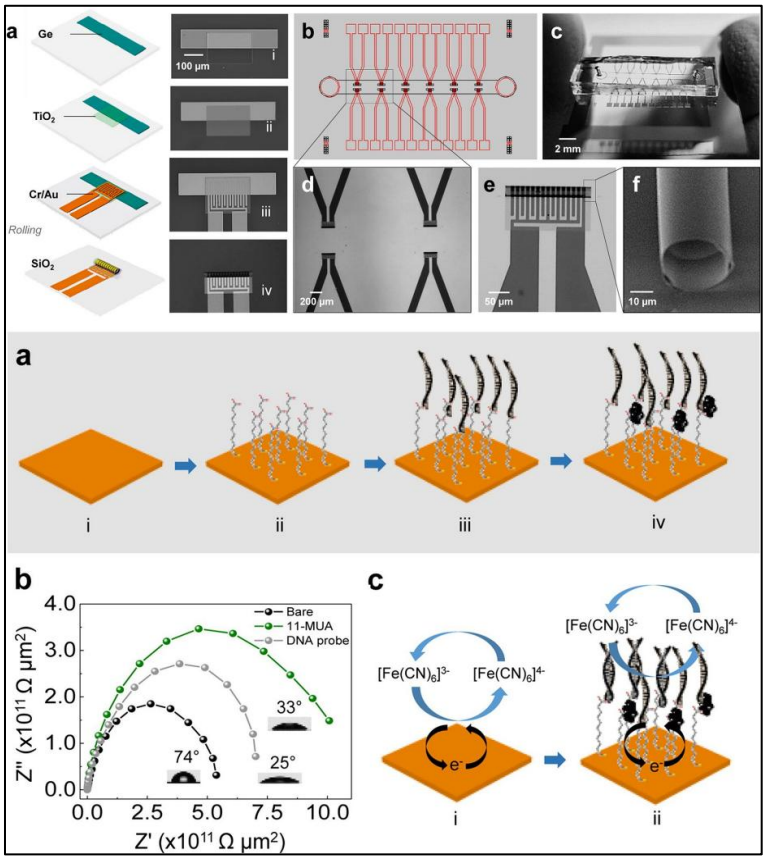


Figure 1.29 (a) Steps for the fabrication of tubular electrodes: (i) Ge, (ii) strained TiO_2 bilayer, (iii) Cr/Au, and (iv) SiO_2 passivation layer. (b) Layout of the electrode and fluidic design. (c) Final fabricated device. (d) View of the tubular electrodes inside the fluidic channel. (e) Single tubular electrode and (f) its scanning electron microscope image[115]

Plaxco's group[116] have reported an integrated microfluidic electrochemical DNA chip which is capable of detecting and discriminating between closely-related *Salmonella* serovars, Fig. 1.13C. For this purpose, they fabricated gold electrodes on a glass wafer which was then bonded to a PDMS microfluidic system which contained an amplification chamber designed to support the loop-mediated isothermal amplification (LAMP) process, as shown in Fig. 1.30. By using the LAMP-on-chip microfluidic device, they were able to demonstrate the detection of salmonella DNA with a detection-limit of less than 10 aM. Then, they successfully applied the sensor to the study of whole blood samples taken from septic mice.

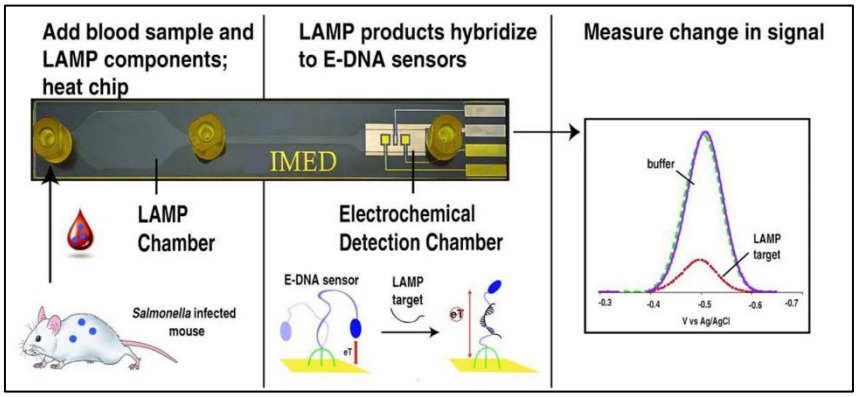


Figure 1.30 A salmonella microfluidic sensor comprising microfluidic sample delivery, LAMP gene amplification, and detection electrodes[116]

Yu et al.[117] developed a perfusion-incubator-liver-chip for 3D cell culture (Fig.1.13D). The device structure consisted of a glass/silicon microfluidic circuit, a cell culture chamber, a bubble trap chamber and a heater as shown in Fig. 1.31. The fabrication of this microfluidic device was based on generic microfabrication technologies including photolithography, deposition and etching. By constraining rat hepotocyte spheroids between the cover glass and a porous – ultra thin Parylene C membrane integrated to the microfluidic chip, these authors were able to maintain cell viability over a period of some 24 days.

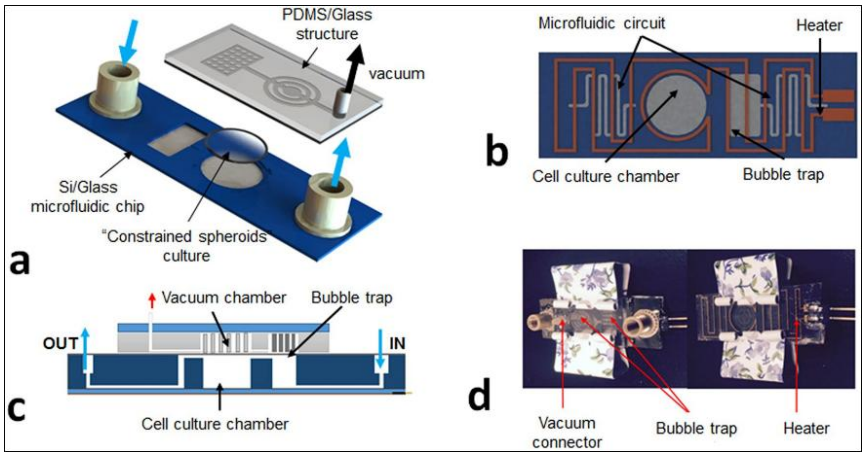


*Figure 1.31 Schematic of the PIC chip. (**a**) 3D view with the PIC, (**b**) bottom view of the chip's layout illustrating the microfluidic circuit, the cell culture chamber, the bubble trap and the heater, (**c**) cross-section of the PIC, (**d**) Top and bottom view of the PIC*[117].

1.5 Conclusion and Future perspectives

Electrochemical biosensors based on advanced nanostructures and/or miniaturized devices offer an important sensing and diagnosis platform having high sensitivity and selectivity towards various target analytes. Since the very first discovery of biosensors many breakthrough innovations have been demonstrated in order to improve the characteristics and performance of the desired sensing devices. First, second and third generation glucose biosensors, the use of nanomaterials or integrated polymers matrixes and highly innovative miniaturized devices based on the use of particular microfabrication technologies have been described in detail for a number of specific applications. Enhanced sensitivities have been achieved for glucose biosensors by applying the use of emerging nanostructures, hybrid materials and micro-nano technologies.

The use of non-enzymatic catalysts towards glucose has also been shown to produce excellent analytical performance. Since many glucose oxidase-based electrochemical biosensors have been used as idealized model systems for the fabrication of diverse sensing platforms, they have opened up the possibility of their use in a new generation of (integrated) electrochemical biosensors for the detection of several analytes. For example, a combination of an electrochemical glucose biosensor with advanced DNA technologies on a small microfluidic device has been developed at low cost in order to detect miRNAs[102]. However, there are many other unexplored strategies. With this in mind, there is still a high demand and expectation for robust, accurate, sensitive, selective and cheap sensing devices particularly for the early-stage detection of biomarkers associated with various cancers and diseases such as Alzheimer's, multiple sclerosis, *etc*. It is also noteworthy that the development of sensors for the reliable, continuous, real-time monitoring of glucose with high selectivity and speed also currently presents a massive challenge in the area of diabetes control.

1.6 References:

1. Clark, L. C., Jr.; Lyons, C., Electrode systems for continuous monitoring in cardiovascular surgery. *Ann N Y Acad Sci* 1962, *102*, 29-45.

2. Newman, J. D.; Turner, A. P. F., Home blood glucose biosensors: a commercial perspective. *Biosensors & Bioelectronics* 2005, *20* (12), 2435-2453.

3. D'Orazio, P., Biosensors in clinical chemistry. *Clinica Chimica Acta* 2003, *334* (1), 41-69.

4. Cass, A. E.; Davis, G.; Francis, G. D.; Hill, H. A.; Aston, W. J.; Higgins, I. J.; Plotkin, E. V.; Scott, L. D.; Turner, A. P., Ferrocene-mediated enzyme electrode for amperometric determination of glucose. *Anal Chem* 1984, *56* (4), 667-71.

5. Wilson, R.; Turner, A. P. F., Glucose oxidase: an ideal enzyme. *Biosensors and Bioelectronics* 1992, *7* (3), 165-185.

6. Christwardana, M.; Chung, Y.; Kim, D.-H.; Kwon, Y., Glucose biofuel cells using the two-step reduction reaction of bienzyme structure as cathodic catalyst. *Journal of Industrial and Engineering Chemistry* 2019, *71*, 435-444.

7. Pishko, M. V.; Katakis, I.; Lindquist, S. E.; Ye, L.; Gregg, B. A.; Heller, A., Direct Electrical Communication between Graphite-Electrodes and Surface Adsorbed Glucose-Oxidase Redox Polymer Complexes. *Angewandte Chemie-International Edition in English* 1990, *29* (1), 82-89.

8. Willner, B.; Katz, E.; Willner, I., Electrical contacting of redox proteins by nanotechnological means. *Current Opinion in Biotechnology* 2006, *17* (6), 589-596.

9. Degani, Y.; Heller, A., Direct Electrical Communication between Chemically Modified Enzymes and Metal-Electrodes .1. Electron-Transfer from Glucose-Oxidase to Metal-Electrodes Via Electron Relays, Bound Covalently to the Enzyme. *Journal of Physical Chemistry* 1987, *91* (6), 1285-1289.

10. Riklin, A.; Katz, E.; Wiliner, I.; Stocker, A.; Bückmann, A. F., Improving enzyme–electrode contacts by redox modification of cofactors. *Nature* 1995, *376* (6542), 672-675.

11. Rizwan, M.; Elma, S.; Lim, S. A.; Ahmed, M. U., AuNPs/CNOs/SWCNTs/chitosan-nanocomposite modified electrochemical sensor for the label-free detection of carcinoembryonic antigen. *Biosensors and Bioelectronics* 2018, *107*, 211-217.

12. Lin, Y.; Lu, F.; Tu, Y.; Ren, Z., Glucose Biosensors Based on Carbon Nanotube Nanoelectrode Ensembles. *Nano Letters* 2004, *4* (2), 191-195.

13. Xu, S.; Zhang, Y.; Zhu, Y.; Wu, J.; Li, K.; Lin, G.; Li, X.; Liu, R.; Liu, X.; Wong, C.-P., Facile one-step fabrication of glucose oxidase loaded polymeric nanoparticles decorating MWCNTs for

constructing glucose biosensing platform: Structure matters. *Biosensors and Bioelectronics* 2019, *135*, 153-159.

14. Yu, Y.; Chen, Z.; He, S.; Zhang, B.; Li, X.; Yao, M., Direct electron transfer of glucose oxidase and biosensing for glucose based on PDDA-capped gold nanoparticle modified graphene/multi-walled carbon nanotubes electrode. *Biosensors and Bioelectronics* 2014, *52*, 147-152.

15. Juska, V. B.; Pemble, M. E., A dual-enzyme, micro-band array biosensor based on the electrodeposition of carbon nanotubes embedded in chitosan and nanostructured Au-foams on microfabricated gold band electrodes. *Analyst* 2019.

16. Feng, X.; Cheng, H.; Pan, Y.; Zheng, H., Development of glucose biosensors based on nanostructured graphene-conducting polyaniline composite. *Biosensors and Bioelectronics* 2015, *70* (Supplement C), 411-417.

17. Baek, S. H.; Roh, J.; Park, C. Y.; Kim, M. W.; Shi, R.; Kailasa, S. K.; Park, T. J., Cu-nanoflower decorated gold nanoparticles-graphene oxide nanofiber as electrochemical biosensor for glucose detection. *Materials Science and Engineering: C* 2020, *107*, 110273.

18. Bharath, G.; Madhu, R.; Chen, S. M.; Veeramani, V.; Balamurugan, A.; Mangalaraj, D.; Viswanathan, C.; Ponpandian, N., Enzymatic electrochemical glucose biosensors by mesoporous 1D hydroxyapatite-on-2D reduced graphene oxide. *Journal of Materials Chemistry B* 2015, *3* (7), 1360-1370.

19. Razmi, H.; Mohammad-Rezaei, R., Graphene quantum dots as a new substrate for immobilization and direct electrochemistry of glucose oxidase: Application to sensitive glucose determination. *Biosensors and Bioelectronics* 2013, *41*, 498-504.

20. Buk, V.; Pemble, M. E., A highly sensitive glucose biosensor based on a micro disk array electrode design modified with carbon quantum dots and gold nanoparticles. *Electrochimica Acta* 2019, *298*, 97-105.

21. Buk, V.; Pemble, M. E.; Twomey, K., Fabrication and evaluation of a carbon quantum dot/gold nanoparticle nanohybrid material integrated onto planar micro gold electrodes for potential bioelectrochemical sensing applications. *Electrochimica Acta* 2019, *293*, 307-317.

22. Buk, V.; Emregul, E.; Emregul, K. C., Alginate copper oxide nano-biocomposite as a novel material for amperometric glucose biosensing. *Materials Science & Engineering C-Materials for Biological Applications* 2017, *74*, 307-314.

23. Shan, C.; Yang, H.; Han, D.; Zhang, Q.; Ivaska, A.; Niu, L., Graphene/AuNPs/chitosan nanocomposites film for glucose biosensing. *Biosensors and Bioelectronics* 2010, *25* (5), 1070-1074.

24. Juska, V. B.; Walcarius, A.; Pemble, M. E., Cu Nanodendrite Foams on Integrated Band Array Electrodes for the Nonenzymatic Detection of Glucose. *ACS Applied Nano Materials* 2019.

25. Yuan, Y.; Wang, Y.; Wang, H.; Hou, S., Gold nanoparticles decorated on single layer graphene applied for electrochemical ultrasensitive glucose biosensor. *Journal of Electroanalytical Chemistry* 2019, *855*, 113495.

26. Lin, J.; He, C.; Zhao, Y.; Zhang, S., One-step synthesis of silver nanoparticles/carbon nanotubes/chitosan film and its application in glucose biosensor. *Sensors and Actuators B: Chemical* 2009, *137* (2), 768-773.

27. Şenel, M.; Nergiz, C.; Çevik, E., Novel reagentless glucose biosensor based on ferrocene cored asymmetric PAMAM dendrimers. *Sensors and Actuators B: Chemical* 2013, *176*, 299-306.

28. Xu, L.; Zhu, Y.; Yang, X.; Li, C., Amperometric biosensor based on carbon nanotubes coated with polyaniline/dendrimer-encapsulated Pt nanoparticles for glucose detection. *Materials Science and Engineering: C* 2009, *29* (4), 1306-1310.

29. Voldman, J.; Gray, M. L.; Schmidt, M. A., Microfabrication in biology and medicine. *Annual Review of Biomedical Engineering* 1999, *1*, 401-425.

30. Sant, S.; Tao, S. L.; Fisher, O. Z.; Xu, Q.; Peppas, N. A.; Khademhosseini, A., Microfabrication technologies for oral drug delivery. *Advanced Drug Delivery Reviews* 2012, *64* (6), 496-507.

31. Huh, D.; Kim, H. J.; Fraser, J. P.; Shea, D. E.; Khan, M.; Bahinski, A.; Hamilton, G. A.; Ingber, D. E., Microfabrication of human organs-on-chips. *Nature Protocols* 2013, *8* (11), 2135-2157.

32. Park, D. W.; Schendel, A. A.; Mikael, S.; Brodnick, S. K.; Richner, T. J.; Ness, J. P.; Hayat, M. R.; Atry, F.; Frye, S. T.; Pashaie, R.; Thongpang, S.; Ma, Z. Q.; Williams, J. C., Graphene-based

carbon-layered electrode array technology for neural imaging and optogenetic applications. *Nature Communications* 2014, *5*.

33. Fekete, Z.; Németh, A.; Márton, G.; Ulbert, I.; Pongrácz, A., Experimental study on the mechanical interaction between silicon neural microprobes and rat dura mater during insertion. *Journal of Materials Science: Materials in Medicine* 2015, *26* (2), 70.

34. Weibel, D. B.; DiLuzio, W. R.; Whitesides, G. M., Microfabrication meets microbiology. *Nat Rev Microbiol* 2007, *5* (3), 209-218.

35. Xuan, X.; Hossain, M. F.; Park, J. Y., A Fully Integrated and Miniaturized Heavy-metal-detection Sensor Based on Micro-patterned Reduced Graphene Oxide. *Scientific Reports* 2016, *6* (1), 33125.

36. Orozco, J.; Fernandez-Sanchez, C.; Jimenez-Jorquera, C., Ultramicroelectrode Array Based Sensors: A Promising Analytical Tool for Environmental Monitoring. *Sensors* 2010, *10* (1), 475-490.

37. Huang, X. J.; O'Mahony, A. M.; Compton, R. G., Microelectrode arrays for electrochemistry: approaches to fabrication. *Small* 2009, *5* (7), 776-88.

38. Yang, X.; Wang, Y.; Liu, Y.; Jiang, X., A sensitive hydrogen peroxide and glucose biosensor based on gold/silver core–shell nanorods. *Electrochimica Acta* 2013, *108*, 39-44.

39. Yang, Z.; Tang, Y.; Li, J.; Zhang, Y.; Hu, X., Facile synthesis of tetragonal columnar-shaped TiO2 nanorods for the construction of sensitive electrochemical glucose biosensor. *Biosensors and Bioelectronics* 2014, *54*, 528-533.

40. Krishnan, S. K.; Prokhorov, E.; Bahena, D.; Esparza, R.; Meyyappan, M., Chitosan-Covered Pd@Pt Core–Shell Nanocubes for Direct Electron Transfer in Electrochemical Enzymatic Glucose Biosensor. *ACS Omega* 2017, *2* (5), 1896-1904.

41. Nikoleli, G.-P.; Nikolelis, D. P.; Siontorou, C.; Karapetis, S.; Bratakou, S.; Tzamtzis, N., Chapter 6 - Nanobiosensors Based on Graphene Electrodes: Recent Trends and Future Applications. In *Applications of Nanomaterials*, Mohan Bhagyaraj, S.; Oluwafemi, O. S.; Kalarikkal, N.; Thomas, S., Eds. Woodhead Publishing: 2018; pp 161-177.

42. Justino, C. I. L.; Gomes, A. R.; Freitas, A. C.; Duarte, A. C.; Rocha-Santos, T. A. P., Graphene based sensors and biosensors. *TrAC Trends in Analytical Chemistry* 2017, *91*, 53-66.

43. Lawal, A. T., Progress in utilisation of graphene for electrochemical biosensors. *Biosensors and Bioelectronics* 2018, *106*, 149-178.

44. Gupta, S.; Murthy, C. N.; Prabha, C. R., Recent advances in carbon nanotube based electrochemical biosensors. *International Journal of Biological Macromolecules* 2018, *108*, 687-703.

45. Alim, S.; Vejayan, J.; Yusoff, M. M.; Kafi, A. K. M., Recent uses of carbon nanotubes & gold nanoparticles in electrochemistry with application in biosensing: A review. *Biosensors and Bioelectronics* 2018, *121*, 125-136.

46. Scognamiglio, V.; Arduini, F., The technology tree in the design of glucose biosensors. *TrAC Trends in Analytical Chemistry* 2019, *120*, 115642.

47. Katz, E.; Willner, I., Integrated nanoparticle-biomolecule hybrid systems: Synthesis, properties, and applications. *Angewandte Chemie-International Edition* 2004, *43* (45), 6042-6108.

48. Katz, E.; Willner, I., Biomolecule-Functionalized Carbon Nanotubes: Applications in Nanobioelectronics. *ChemPhysChem* 2004, *5* (8), 1084-1104.

49. Niemeyer, C. M., Functional Hybrid Devices of Proteins and Inorganic Nanoparticles. *Angewandte Chemie International Edition* 2003, *42* (47), 5796-5800.

50. Xiao, Y.; Patolsky, F.; Katz, E.; Hainfeld, J. F.; Willner, I., "Plugging into enzymes": Nanowiring of redox enzymes by a gold nanoparticle. *Science* 2003, *299* (5614), 1877-1881.

51. Patolsky, F.; Weizmann, Y.; Willner, I., Long-range electrical contacting of redox enzymes by SWCNT connectors. *Angewandte Chemie-International Edition* 2004, *43* (16), 2113-2117.

52. Liu, J. Q.; Chou, A.; Rahmat, W.; Paddon-Row, M. N.; Gooding, J. J., Achieving direct electrical connection to glucose oxidase using aligned single walled carbon nanotube arrays. *Electroanalysis* 2005, *17* (1), 38-46.

53. Chen, C.; Xie, Q. J.; Yang, D. W.; Xiao, H. L.; Fu, Y. C.; Tan, Y. M.; Yao, S. Z., Recent advances in electrochemical glucose biosensors: a review. *Rsc Advances* 2013, *3* (14), 4473-4491.

54. Guo, S.; Wang, E., Synthesis and electrochemical applications of gold nanoparticles. *Analytica Chimica Acta* 2007, *598* (2), 181-192.

55. Wu, C.; Sun, H.; Li, Y.; Liu, X.; Du, X.; Wang, X.; Xu, P., Biosensor based on glucose oxidase-nanoporous gold co-catalysis for glucose detection. *Biosensors and Bioelectronics* 2015, *66*, 350-355.

56. Eguílaz, M.; Villalonga, R.; Pingarrón, J. M.; Ferreyra, N. F.; Rivas, G. A., Functionalization of bamboo-like carbon nanotubes with 3-mercaptophenylboronic acid-modified gold nanoparticles for the development of a hybrid glucose enzyme electrochemical biosensor. *Sensors and Actuators B: Chemical* 2015, *216*, 629-637.

57. Parlak, O.; İncel, A.; Uzun, L.; Turner, A. P. F.; Tiwari, A., Structuring Au nanoparticles on two-dimensional MoS2 nanosheets for electrochemical glucose biosensors. *Biosensors and Bioelectronics* 2017, *89*, 545-550.

58. Ma, E.; Wang, P.; Yang, Q.; Yu, H.; Pei, F.; Li, Y.; Liu, Q.; Dong, Y., Electrochemical immunosensor based on MoS2 NFs/Au@AgPt YNCs as signal amplification label for sensitive detection of CEA. *Biosensors and Bioelectronics* 2019, *142*, 111580.

59. Gao, Z.; Li, Y.; Zhang, X.; Feng, J.; Kong, L.; Wang, P.; Chen, Z.; Dong, Y.; Wei, Q., Ultrasensitive electrochemical immunosensor for quantitative detection of HBeAg using Au@Pd/MoS2@MWCNTs nanocomposite as enzyme-mimetic labels. *Biosensors and Bioelectronics* 2018, *102*, 189-195.

60. Zhang, Y.; Li, X.; Li, D.; Wei, Q., A laccase based biosensor on AuNPs-MoS2 modified glassy carbon electrode for catechol detection. *Colloids and Surfaces B: Biointerfaces* 2020, *186*, 110683.

61. Liu, L.; Zhu, S.; Wei, Y.; Liu, X.; Jiao, S.; Yang, J., Ultrasensitive detection of miRNA-155 based on controlled fabrication of AuNPs@MoS2 nanostructures by atomic layer deposition. *Biosensors and Bioelectronics* 2019, *144*, 111660.

62. Huang, X.-J.; Li, C.-C.; Gu, B.; Kim, J.-h.; Cho, S.-O.; Choi, Y.-K., Controlled Molecularly Mediated Assembly of Gold Nanooctahedra for a Glucose Biosensor. *The Journal of Physical Chemistry C* 2008, *112* (10), 3605-3611.

63. Paul, A.; Vyas, G.; Paul, P.; Srivastava, D. N., Gold-Nanoparticle-Encapsulated ZIF-8 for a Mediator-Free Enzymatic Glucose Sensor by Amperometry. *ACS Applied Nano Materials* 2018, *1* (7), 3600-3607.

64. Iijima, S., Helical microtubules of graphitic carbon. *Nature* 1991, *354* (6348), 56-58.

65. Zhang, X.; Meng, L.; Lu, Q.; Fei, Z.; Dyson, P. J., Targeted delivery and controlled release of doxorubicin to cancer cells using modified single wall carbon nanotubes. *Biomaterials* 2009, *30* (30), 6041-6047.

66. Chernova, T.; Murphy, F. A.; Galavotti, S.; Sun, X.-M.; Powley, I. R.; Grosso, S.; Schinwald, A.; Zacarias-Cabeza, J.; Dudek, K. M.; Dinsdale, D.; Le Quesne, J.; Bennett, J.; Nakas, A.; Greaves, P.; Poland, C. A.; Donaldson, K.; Bushell, M.; Willis, A. E.; MacFarlane, M., Long-Fiber Carbon Nanotubes Replicate Asbestos-Induced Mesothelioma with Disruption of the Tumor Suppressor Gene Cdkn2a (Ink4a/Arf). *Current Biology* 2017, *27* (21), 3302-3314.e6.

67. Kanninen, P.; Eriksson, B.; Davodi, F.; Buan, M. E. M.; Sorsa, O.; Kallio, T.; Lindström, R. W., Carbon corrosion properties and performance of multi-walled carbon nanotube support with and without nitrogen-functionalization in fuel cell electrodes. *Electrochimica Acta* 2020, *332*, 135384.

68. Yan, H.; Tang, X.; Zhu, X.; Zeng, Y.; Lu, X.; Yin, Z.; Lu, Y.; Yang, Y.; Li, L., Sandwich-type electrochemical immunosensor for highly sensitive determination of cardiac troponin I using carboxyl-terminated ionic liquid and helical carbon nanotube composite as platform and ferrocenecarboxylic acid as signal label. *Sensors and Actuators B: Chemical* 2018, *277*, 234-240.

69. Wei, A.; Mu, J.; He, R.; Bai, X.; Liu, Z.; Zhang, L.; Liu, Z.; Wang, Y., Preparation of Li4Ti5O12/carbon nanotubes composites and LiCoO2/Li4Ti5O12 full-cell with enhanced electrochemical performance for high-power lithium-ion batteries. *Journal of Physics and Chemistry of Solids* 2020, *138*, 109303.

70. Ali Kamyabi, M.; Hajari, N.; Turner, A. P. F.; Tiwari, A., A high-performance glucose biosensor using covalently immobilised glucose oxidase on a poly(2,6-diaminopyridine)/carbon nanotube electrode. *Talanta* 2013, *116*, 801-808.

71. Vilian, A. T. E.; Chen, S.-M., Direct electrochemistry and electrocatalysis of glucose oxidase based poly(l-arginine)-multi-walled carbon nanotubes. *RSC Advances* 2014, *4* (92), 50771-50781.

72. Gallay, P.; Eguílaz, M.; Rivas, G., Designing electrochemical interfaces based on nanohybrids of avidin functionalized-carbon nanotubes and ruthenium nanoparticles as

peroxidase-like nanozyme with supramolecular recognition properties for site-specific anchoring of biotinylated residues. *Biosensors and Bioelectronics* 2020, *148*, 111764.

73. Suginta, W.; Khunkaewla, P.; Schulte, A., Electrochemical Biosensor Applications of Polysaccharides Chitin and Chitosan. *Chemical Reviews* 2013, *113* (7), 5458-5479.

74. Patel, M. P.; Patel, R. R.; Patel, J. K., Chitosan Mediated Targeted Drug Delivery System: A Review. *Journal of Pharmacy and Pharmaceutical Sciences* 2010, *13* (4), 536-557.

75. Safdar, R.; Omar, A. A.; Arunagiri, A.; Regupathi, I.; Thanabalan, M., Potential of Chitosan and its derivatives for controlled drug release applications – A review. *Journal of Drug Delivery Science and Technology* 2019, *49*, 642-659.

76. Hamman, J. H., Chitosan based polyelectrolyte complexes as potential carrier materials in drug delivery systems. *Marine drugs* 2010, *8* (4), 1305-1322.

77. Morris, G. A.; Kök, S. M.; Harding, S. E.; Adams, G. G., Polysaccharide drug delivery systems based on pectin and chitosan. *Biotechnology and Genetic Engineering Reviews* 2010, *27* (1), 257-284.

78. Amidi, M.; Mastrobattista, E.; Jiskoot, W.; Hennink, W. E., Chitosan-based delivery systems for protein therapeutics and antigens. *Advanced Drug Delivery Reviews* 2010, *62* (1), 59-82.

79. Jayakumar, R.; Prabaharan, M.; Sudheesh Kumar, P. T.; Nair, S. V.; Tamura, H., Biomaterials based on chitin and chitosan in wound dressing applications. *Biotechnology Advances* 2011, *29* (3), 322-337.

80. Kim, I.-Y.; Seo, S.-J.; Moon, H.-S.; Yoo, M.-K.; Park, I.-Y.; Kim, B.-C.; Cho, C.-S., Chitosan and its derivatives for tissue engineering applications. *Biotechnology Advances* 2008, *26* (1), 1-21.

81. Dang, J. M.; Leong, K. W., Natural polymers for gene delivery and tissue engineering. *Advanced Drug Delivery Reviews* 2006, *58* (4), 487-499.

82. Di Martino, A.; Sittinger, M.; Risbud, M. V., Chitosan: A versatile biopolymer for orthopaedic tissue-engineering. *Biomaterials* 2005, *26* (30), 5983-5990.

83. Zhang, Y.; Li, Y.; Wu, W.; Jiang, Y.; Hu, B., Chitosan coated on the layers' glucose oxidase immobilized on cysteamine/Au electrode for use as glucose biosensor. *Biosensors and Bioelectronics* 2014, *60*, 271-276.

84. Anusha, J. R.; Raj, C. J.; Cho, B.-B.; Fleming, A. T.; Yu, K.-H.; Kim, B. C., Amperometric glucose biosensor based on glucose oxidase immobilized over chitosan nanoparticles from gladius of Uroteuthis duvauceli. *Sensors and Actuators B: Chemical* 2015, *215*, 536-543.

85. Şenel, M., Simple method for preparing glucose biosensor based on in-situ polypyrrole cross-linked chitosan/glucose oxidase/gold bionanocomposite film. *Materials Science and Engineering: C* 2015, *48*, 287-293.

86. Ma, H.; Sun, J.; Zhang, Y.; Bian, C.; Xia, S.; Zhen, T., Label-free immunosensor based on one-step electrodeposition of chitosan-gold nanoparticles biocompatible film on Au microelectrode for determination of aflatoxin B1 in maize. *Biosensors and Bioelectronics* 2016, *80*, 222-229.

87. Zeng, X.; Li, X.; Xing, L.; Liu, X.; Luo, S.; Wei, W.; Kong, B.; Li, Y., Electrodeposition of chitosan–ionic liquid–glucose oxidase biocomposite onto nano-gold electrode for amperometric glucose sensing. *Biosensors and Bioelectronics* 2009, *24* (9), 2898-2903.

88. Safavi, A.; Farjami, F., Electrodeposition of gold–platinum alloy nanoparticles on ionic liquid–chitosan composite film and its application in fabricating an amperometric cholesterol biosensor. *Biosensors and Bioelectronics* 2011, *26* (5), 2547-2552.

89. Che, X.; Yuan, R.; Chai, Y.; Li, J.; Song, Z.; Li, W.; Zhong, X., A glucose biosensor based on chitosan–Prussian blue–multiwall carbon nanotubes–hollow PtCo nanochains formed by one-step electrodeposition. *Colloids and Surfaces B: Biointerfaces* 2011, *84* (2), 454-461.

90. Luo, P. J. G.; Sahu, S.; Yang, S. T.; Sonkar, S. K.; Wang, J. P.; Wang, H. F.; LeCroy, G. E.; Cao, L.; Sun, Y. P., Carbon "quantum" dots for optical bioimaging. *Journal of Materials Chemistry B* 2013, *1* (16), 2116-2127.

91. Lim, S. Y.; Shen, W.; Gao, Z. Q., Carbon quantum dots and their applications. *Chemical Society Reviews* 2015, *44* (1), 362-381.

92. Hwang, D.-W.; Lee, S.; Seo, M.; Chung, T. D., Recent advances in electrochemical non-enzymatic glucose sensors – A review. *Analytica Chimica Acta* 2018, *1033*, 1-34.

93. Zhu, H.; Li, L.; Zhou, W.; Shao, Z. P.; Chen, X. J., Advances in non-enzymatic glucose sensors based on metal oxides. *Journal of Materials Chemistry B* 2016, *4* (46), 7333-7349.

94. Meng, S. J.; Wu, M. Y.; Wang, Q.; Dai, Z. Y.; Si, W. L.; Huang, W.; Dong, X. C., Cobalt oxide nanosheets wrapped onto nickel foam for non-enzymatic detection of glucose. *Nanotechnology* 2016, *27* (34).

95. Long, M.; Tan, L.; Liu, H.; He, Z.; Tang, A., Novel helical TiO2 nanotube arrays modified by Cu2O for enzyme-free glucose oxidation. *Biosensors and Bioelectronics* 2014, *59*, 243-250.

96. Xu, H.; Xia, C.; Wang, S.; Han, F.; Akbari, M. K.; Hai, Z.; Zhuiykov, S., Electrochemical non-enzymatic glucose sensor based on hierarchical 3D Co3O4/Ni heterostructure electrode for pushing sensitivity boundary to a new limit. *Sensors and Actuators B: Chemical* 2018, *267*, 93-103.

97. Ahmad, R.; Tripathy, N.; Ahn, M.-S.; Bhat, K. S.; Mahmoudi, T.; Wang, Y.; Yoo, J.-Y.; Kwon, D.-W.; Yang, H.-Y.; Hahn, Y.-B., Highly Efficient Non-Enzymatic Glucose Sensor Based on CuO Modified Vertically-Grown ZnO Nanorods on Electrode. *Scientific Reports* 2017, *7* (1), 5715.

98. Zhang, Y.; Li, N.; Xiang, Y.; Wang, D.; Zhang, P.; Wang, Y.; Lu, S.; Xu, R.; Zhao, J., A flexible non-enzymatic glucose sensor based on copper nanoparticles anchored on laser-induced graphene. *Carbon* 2020, *156*, 506-513.

99. Coyle, V. E.; Kandjani, A. E.; Field, M. R.; Hartley, P.; Chen, M.; Sabri, Y. M.; Bhargava, S. K., Co3O4 needles on Au honeycomb as a non-invasive electrochemical biosensor for glucose in saliva. *Biosensors and Bioelectronics* 2019, *141*, 111479.

100. Yang, Q.; Long, M.; Tan, L.; Zhang, Y.; Ouyang, J.; Liu, P.; Tang, A., Helical TiO2 Nanotube Arrays Modified by Cu–Cu2O with Ultrahigh Sensitivity for the Nonenzymatic Electro-oxidation of Glucose. *ACS Applied Materials & Interfaces* 2015, *7* (23), 12719-12730.

101. Li, R.; Liu, X.; Wang, H.; Wu, Y.; Lu, Z., High-performance hybrid electrode decorated by well-aligned nanograss arrays for glucose sensing. *Biosensors and Bioelectronics* 2018, *102*, 288-295.

102. Bruch, R.; Baaske, J.; Chatelle, C.; Meirich, M.; Madlener, S.; Weber, W.; Dincer, C.; Urban, G. A., CRISPR/Cas13a-Powered Electrochemical Microfluidic Biosensor for Nucleic Acid Amplification-Free miRNA Diagnostics. *Advanced Materials n/a* (n/a), 1905311.

103. Wise, K. D.; Bhatti, P. T.; Wang, J.; Friedrich, C. R., High-density cochlear implants with position sensing and control. *Hearing Research* 2008, *242* (1), 22-30.

104. Ngernsutivorakul, T.; White, T. S.; Kennedy, R. T., Microfabricated Probes for Studying Brain Chemistry: A Review. *ChemPhysChem* 2018, *19* (10), 1128-1142.

105. Dawson, K.; Baudequin, M.; O'Riordan, A., Single on-chip gold nanowires for electrochemical biosensing of glucose. *Analyst* 2011, *136* (21), 4507-4513.

106. Dawson, K.; Strutwolf, J.; Herzog, G.; Arrigan, D. W. M.; Quinn, A. J.; O'Riordan, A., Nanofabrication of Robust Nanoelectrodes for Electrochemical Applications. *Ecs Transactions* 2010, *28* (34), 29-37.

107. Ou, Y. G.; Buchanan, A. M.; Witt, C. E.; Hashemi, P., Frontiers in electrochemical sensors for neurotransmitter detection: towards measuring neurotransmitters as chemical diagnostics for brain disorders. *Anal Methods-Uk* 2019, *11* (21), 2738-2755.

108. Matys, J.; Gieroba, B.; Jóźwiak, K., Recent developments of bioanalytical methods in determination of neurotransmitters in vivo. *Journal of Pharmaceutical and Biomedical Analysis* 2020, *180*, 113079.

109. Frey, O.; Holtzman, T.; McNamara, R. M.; Theobald, D. E. H.; van der Wal, P. D.; de Rooij, N. F.; Dalley, J. W.; Koudelka-Hep, M., Enzyme-based choline and l-glutamate biosensor electrodes on silicon microprobe arrays. *Biosensors and Bioelectronics* 2010, *26* (2), 477-484.

110. Ferreira, N. R.; Ledo, A.; Laranjinha, J.; Gerhardt, G. A.; Barbosa, R. M., Simultaneous measurements of ascorbate and glutamate in vivo in the rat brain using carbon fiber nanocomposite sensors and microbiosensor arrays. *Bioelectrochemistry* 2018, *121*, 142-150.

111. Wang, S. X.; Acha, D.; Shah, A. J.; Hills, F.; Roitt, I.; Demosthenous, A.; Bayford, R. H., Detection of the tau protein in human serum by a sensitive four-electrode electrochemical biosensor. *Biosensors and Bioelectronics* 2017, *92*, 482-488.

112. Mir, M.; Dondapati, S. K.; Duarte, M. V.; Chatzichristidi, M.; Misiakos, K.; Petrou, P.; Kakabakos, S. E.; Argitis, P.; Katakis, I., Electrochemical biosensor microarray functionalized by means of biomolecule friendly photolithography. *Biosensors and Bioelectronics* 2010, *25* (9), 2115-2121.

113. Yao, H.; Shum, A. J.; Cowan, M.; Lähdesmäki, I.; Parviz, B. A., A contact lens with embedded sensor for monitoring tear glucose level. *Biosensors and Bioelectronics* 2011, *26* (7), 3290-3296.

114. Rajapaksha, R. D. A. A.; Hashim, U.; Afnan Uda, M. N.; Fernando, C. A. N.; De Silva, S. N. T., Target ssDNA detection of E.coli O157:H7 through electrical based DNA biosensor. *Microsystem Technologies* 2017, *23* (12), 5771-5780.

115. Medina-Sánchez, M.; Ibarlucea, B.; Pérez, N.; Karnaushenko, D. D.; Weiz, S. M.; Baraban, L.; Cuniberti, G.; Schmidt, O. G., High-Performance Three-Dimensional Tubular Nanomembrane Sensor for DNA Detection. *Nano Letters* 2016, *16* (7), 4288-4296.

116. Patterson, A. S.; Heithoff, D. M.; Ferguson, B. S.; Soh, H. T.; Mahan, M. J.; Plaxco, K. W., Microfluidic chip-based detection and intraspecies strain discrimination of Salmonella serovars derived from whole blood of septic mice. *Applied and environmental microbiology* 2013, *79* (7), 2302-2311.

117. Yu, F.; Deng, R.; Hao Tong, W.; Huan, L.; Chan Way, N.; IslamBadhan, A.; Iliescu, C.; Yu, H., A perfusion incubator liver chip for 3D cell culture with application on chronic hepatotoxicity testing. *Scientific Reports* 2017, *7* (1), 14528.

CHAPTER 2

Enzyme free detection of glucose

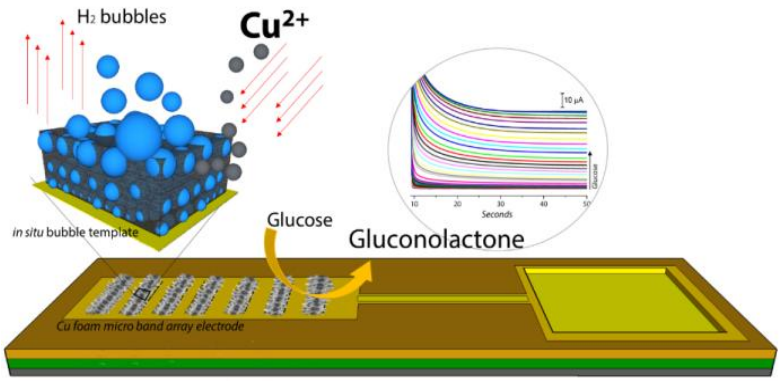
2. Cu Nanodendrite Foams on Integrated Band Array Electrodes for the Nonenzymatic Detection of Glucose

This work has been published in the journal of ACS Applied Nanomaterials, 2019, 2, 9, 5878-5889

2.1 Abstract

We demonstrate the successful electrodeposition of Cu nanodendrite foams (CuFoams) onto a series of lithographically formed gold band electrodes at negative overpotentials in an acidic environment. The nanodendrite foams were deposited onto two different integrated microelectrode arrays fabricated using standard lithographic techniques. Each electrode consisted of 17 gold band electrodes deposited onto a silicon wafer substrate, labelled BA5 (with a width of 5 μm and a length of 250 μm) and BA10 (with a width of 10 μm and a length of 500 μm). Prior to Cu deposition the gold electrodes were characterized by scanning electron microscopy (SEM) in order to evaluate the morphology of each design and by cyclic voltammetry (CV) in order to investigate their diffusion profiles. After Cu deposition the resulting 3D foam structures were studied using SEM, XPS and EDX. The Cu foam/Au microelectrodes were then used for the electrocatalytic detection of glucose via oxidation at a potential of +0.45 V vs. Ag/AgCl in an alkaline medium. It was found that both types of electrode arrays used showed excellent analytical performance in terms of sensitivity, reproducibility and stability in comparison with the best performances reported in the literature. In particular, the BA5-CuFoam electrode exhibited an outstanding sensitivity of 10,630 μA mM^{-1} cm^{-2} towards glucose with a wide linear range up to 22.55 mM, while the BA10-CuFoam electrode showed a sensitivity of 4,437 μA mM^{-1} cm^{-2}. The performance of the proposed electrochemical sensor is attributed to a combination of the use of the very high surface area Cu nanodendrite foam and the enhanced radial distribution profile associated with the use of the smaller band microfabricated electrodes. Additionally, both sensors also showed a strong resistance to the poisoning effects of chlorine ions and excellent stability over a period of three months.

Key words: *microfabrication, band array electrode, electrocatalysis, copper nanodendrites, non-enzymatic sensors*



Graphical abstract, note that the sizes of the components shown are not drawn to scale.

2.2 Introduction

Besides the reproducibility and low variability of silicon-based microelectrodes, their use allows for flexibility in the design and arrangement of the array with numerous shapes, sizes and dimensions available for each electrode on the array[1-2]. Furthermore, precise batch fabrication may provide a cost effective solution for all the fabrication processes. In particular, the use of silicon based micro electrodes as neural probes in the field of neural science for *in vivo* recordings and/or implantable (bio) sensors have been extensively reported since silicon, along with the often applied silicon dioxide and silicon nitride insulator layers, is a biocompatible material[1, 3-6]. For example, the research article by Wei et al.[7] describes an important example of the use of implantable silicon based microelectrode arrays (MEAs) for L-glutamate detection, which is the most common excitatory neurotransmitter for a wide range of neurological diseases. The developed MEA was capable of detecting glutamate with a sensitivity of 56 pA μM^{-1} and a detection limit of 0.5 µM. Furthermore, this study successfully demonstrated the results of monitoring the extracellular glutamate levels, spikes and local field potentials *in vivo*. Micro- or nano-sized silicon based micro fabricated electrodes have also been of great interest for (bio) electrochemical applications[8-9]. From the electrochemistry perspective, the approach

of scaling down of the electrodes has been reported by many researchers[10-13] who have demonstrated the benefits of using these small electrodes in terms of the electro-analytical performance including sensitivity and detection limit.

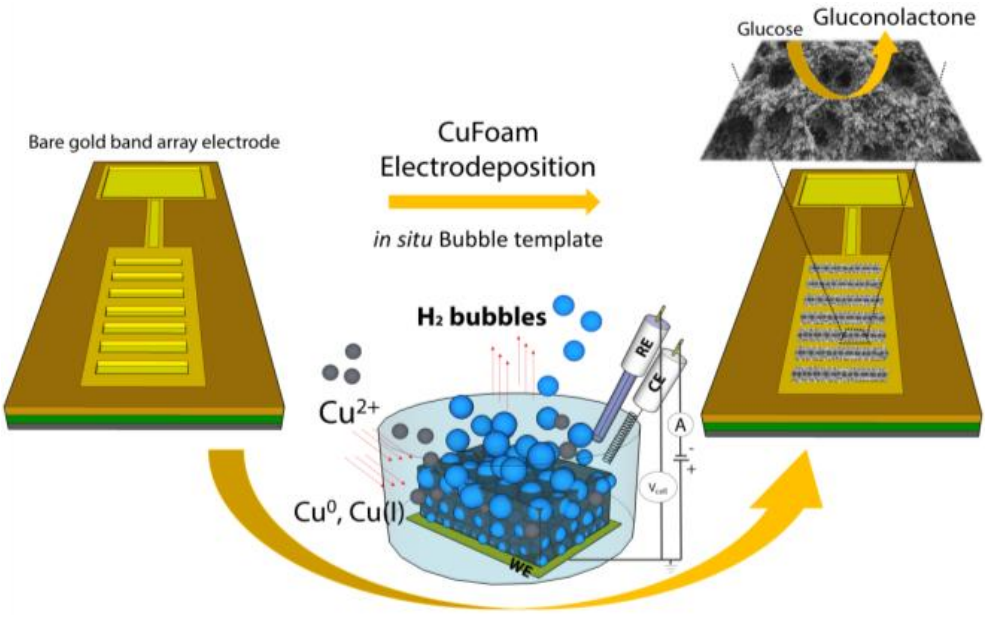
In a previous study, we demonstrated the positive advantage of using micron-sized array electrodes by developing glucose oxidase (GOx) biosensors based on both micro array[8] and planar[9] electrodes with sensitivities of 47.24 and 626.06 μA mM^{-1} cm^{-2}, respectively. The observation of a 13-fold improvement of the sensitivity resulting from the move from planar to micro array electrodes clearly highlighted the advantages of successfully miniaturizing the developed biosensor.

Another potential way to enhance the performance of a glucose sensor is to utilize the electro-oxidation of glucose which requires a catalyst such as nickel[14], gold[15], copper[16] or cobalt[17], instead of employing an enzymatic reaction. Among the possible catalytic metals copper (Cu) - a 3d transition metal - is considered to be a highly promising candidate for many applications in nanotechnology since Cu-based nanomaterials can promote and undergo a variety of reactions due to the presence of two accessible oxidation states which enable reactivity via both one- and two-electron pathways[18].

Cu based nanocrystals have found many applications in electrocatalysis[19], photocatalysis[20], biosensors[21] and electrochemical sensors[22]. The morphology of the Cu-based nanoparticles on the solid electrode surface has a great impact on the catalytic reaction of glucose. The size and shape of these nano structures is highly dependent on the synthesis approach and precursors used. For instance, a variety of copper[23], cupric oxide[24], cuprous oxide[25] nanomaterials with different sizes and shapes, often in combination[26] have been used to prepare non-enzymatic sensors and have demonstrated a high sensitivity towards glucose. The most remarkable advantage of those sensors is the increased stability which has been observed, since stability represents the biggest problem for enzymatic sensors due to the nature of the biomolecule itself, (Table S1; latest enzymatic glucose sensors and their analytical performances). However, until now, CuFoam deposited micro fabricated band array electrodes have not been investigated for glucose electro-oxidation.

In this present work we demonstrate the excellent performance of CuFoam micro band array electrodes for glucose oxidation. We show that CuFoam formed in an acidic environment *via* negative overpotential deposition exhibit well-ordered porous electro-active surfaces for the electrocatalytic detection of glucose. The resulting miniaturized CuFoam sensors showed superior electro-analytical performance as a result of the reduction in geometric surface area of each design combined with the increased electro-active surface area of the porous CuFoam. We successfully demonstrate the impact of the miniaturization of foam electrodeposits and their use as anode materials towards glucose electro-oxidation. The morphologies of the bare and modified electrodes were studied with scanning electron microscopy (SEM). Gold band array electrodes with different widths and lengths were microfabricated on a silicon substrate by applying deposition, lithography and etching and were then characterized electrochemically by applying cyclic voltammetry (CV). CuFoam nanostructures were electrochemically grown on the array electrodes in an acidic environment at high negative overpotentials in order to obtain foam shaped porous deposition layer.

The sensors developed here showed excellent performance even in the presence of the chloride ions and other potentially interfering species. Furthermore, the micro array electrodes exhibited large linear ranges and showed considerably better sensitivities towards glucose than electrocatalytic sensors available in the literature, please see Table 2.



Scheme 2.1. Schematic illustration of in situ bubble template formation and copper foam electrodeposition onto microfabricated band array electrode

2.3 Results and discussion

2.3.1 Fabrication and investigation of gold micro band array electrodes

In this section we describe the lithographic fabrication of two different geometrical types of microelectrode arrays consisting of 17 gold band electrodes placed on top of a silicon wafer substrate. The silicon fabrication process included oxide layer growth on the silicon substrate after a series of cleaning steps of the substrate. Table 1 summarizes the two different band array geometries fabricated and studied here. Electrodes were fabricated in several process steps by lithography, deposition and etching as described previously[9] with a specific mask having been designed for the band array electrodes. This was followed by dicing to separate each electrode. To evaluate the success or otherwise of the fabrication process we performed detailed characterization of clean, bare micro array electrodes, as described below.

The arrangement, size and dimensions of the bare electrodes were analyzed by scanning electron microscopy (SEM). As can be seen in Fig. 2.1A and B, SEM micrographs clearly show the arrangement of the 17 individual band electrodes that are arranged on the Si_3N_4 insulation layer with 100 µm inter electrode distance between electrodes. Fig. 2.1C shows a higher magnification image of electrode array BA5 with a width of 5 µm and a length of 250 µm, placed at 100 µm inter electrode distance. Fig. 2.1D shows a higher magnification image of electrode BA10 had a width of 10 µm and a length of 500 µm, placed at 100 µm inter electrode distance. Each design of the array electrodes consisted of an isolated connection track and an etched large surface area connection pad, as illustrated in Fig. 2.1G.

For the initial electrochemical characterization of the bare gold electrodes cyclic voltammetry (CV) was performed in the presence of the redox probe $Fe(CN)_6^{3-/4-}$ in 0.01 M PBS, containing 0.1 M KCl. As shown in Fig. 2.1E, BA5 exhibits a sigmoidal voltammogram which is characteristic behavior for most microelectrodes. However, in Fig. 2.1 F, BA10 shows a voltammogram which displays the characteristic peaks associated with a conventional reversible redox couple. While each band array design has the same inter electrode distance, the increased (×2) width and length of BA10 may result in an increased diffusion profile diameter which then creates an

overlapping diffusion zone between the adjacent band electrodes. Thus, BA10 shows a characteristic voltammogram shape which is a combination of that expected for both planar electrodes and microelectrodes. Representative diffusion profiles are shown as inset graphs of Fig. 2.1E and F. Moreover, BA10 displays increased current levels in comparison to BA5, which may attributed to increased total surface area with increased number of the electrodes on the array, Table 1. The effect of scan rate on the band array electrodes was investigated. The relationship of scan rate versus anodic and cathodic peak currents were illustrated in Fig. 2.S1 (Supporting Information). The linear relationships of anodic and cathodic peak currents with increased scan rates from 0.05 to 0.9 V s-1 (as shown in Fig. 2.S1, Supporting Information) confirm the excellent redox reaction of electroactive species on the band array electrodes' surfaces as a surface controlled electrochemical process.

***T**able 2.1. Characteristics of the micro band array electrodes*

BAND	Width (µm)	Length (µm)	Inter electrode distance (µm)	Electrodes	Recess depth (nm)	Geometric surface area (cm^2)
BA5	5	250	100	17	200	2.13×10^{-4}
BA10	10	500	100	17	200	8.50×10^{-4}

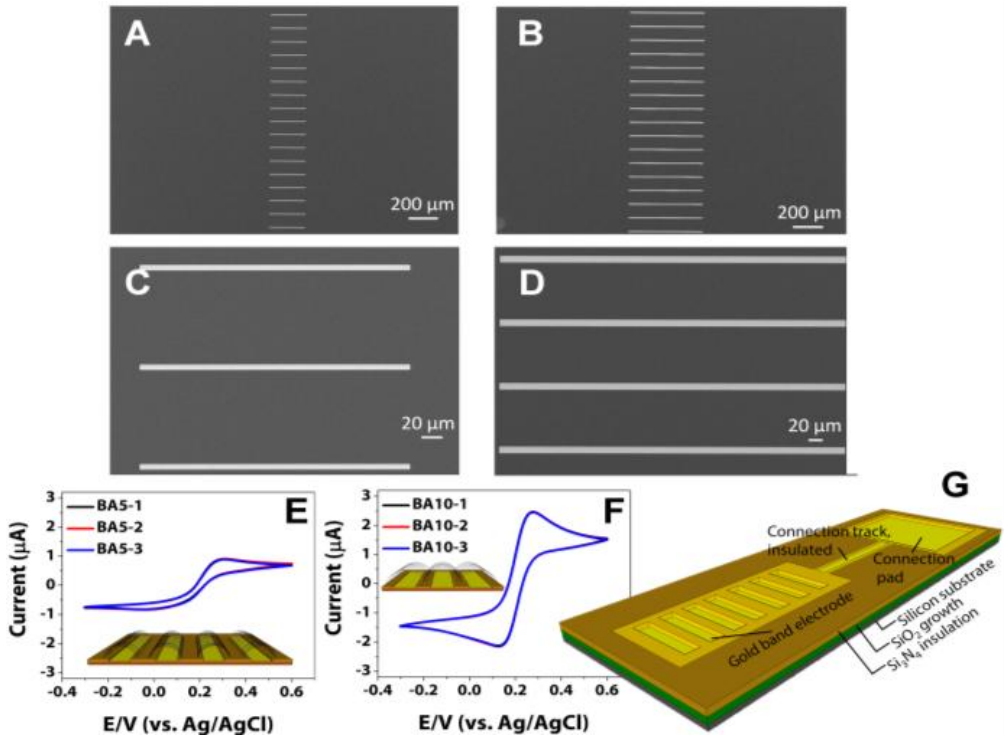


Figure 2.1. SEM images of gold band array electrodes; lower magnification images of BA5 (A) and BA10 (B), higher magnification images of the band electrodes of BA5 (C) and BA10 (D), cyclic voltammograms recorded for BA5 (E) and BA10 (F) at a scan rate of 0.01 V s-1. The solution is 5 mM Fe(CN)63-/4- as a redox probe in 0.01 M PBS (pH 7.4), containing 0.1 M KCl, each design repeated 3 times (inset pictures are the representative images of diffusion profiles of BA5 and BA10, not drawn to scale). Illustration of the band array electrode (not drawn to scale) (G).

2.3.2 Electrodeposition of CuFoam and electrocatalytic behavior of CuFoam deposited band array electrodes

CuFoam modified band arrays were prepared by electrodeposition using a condition that can concurrently reduce water to H_2. The H_2 bubbles formed on gold working electrode served as an *in situ* generated bubble template to deposit porous CuFoam[27-28], as illustrated in Scheme 1. Nikolic et al.[29] studied in detail the effect of the H_2SO_4 concentration over the morphology of Cu deposits by keeping the concentration of Cu^{2+} constant in the solution. In our study, the acidity of the solution also played a crucial role in the formation of well-ordered 3D roll-shaped CuFoam deposits over each gold band electrodes. We studied concentrations of H_2SO_4 of 1 M (Fig. 2.2A), 0.5 M (Fig. 2.2B) and 0.05 M (Fig. 2.2C) to demonstrate the effect of acidity while the Cu^{2+} concentration was kept constant. With decreased acid concentrations, we observed a decrease in the thickness of the Cu dendrites. In the case of the 0.05 M H_2SO_4 concentration, we observed random deposits over the electrode surface with the needle-shaped fragile Cu dendrites which were weakly attached to the surface (Fig. 2.2C). This result shows the acidity of the electrodeposition solution has an important impact on the adhesion of Cu nanodendrites on the gold electrode surface.

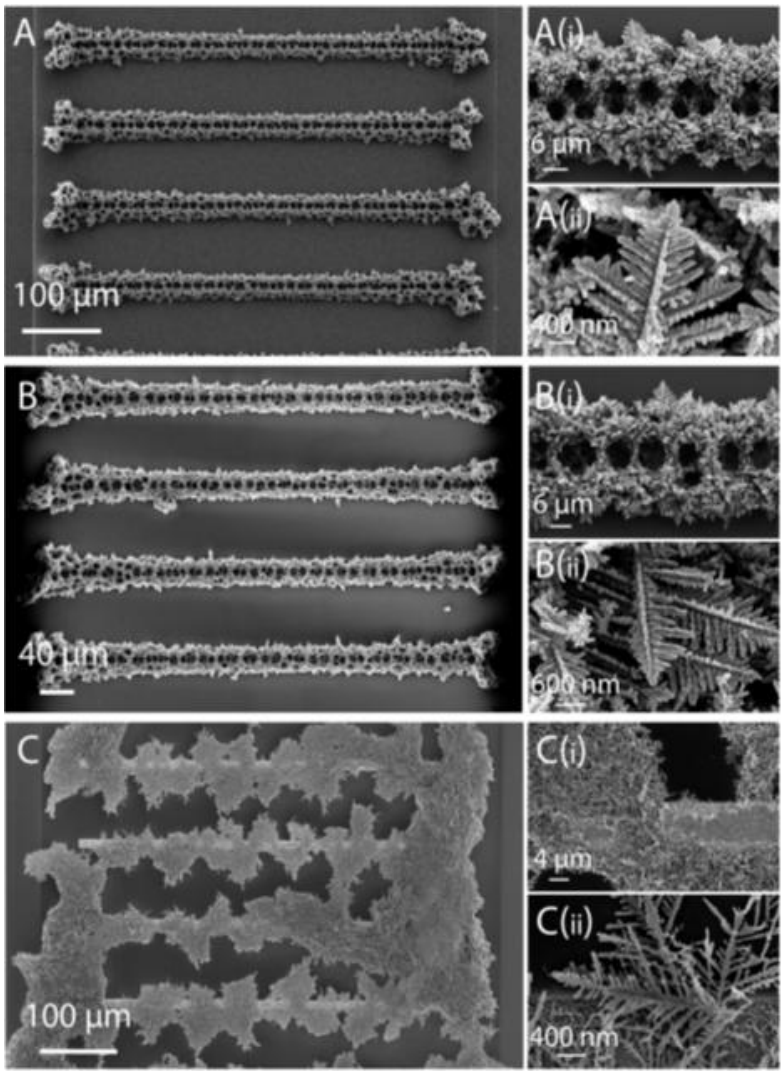


Figure 2.2. SEM images of BA10-CuFoam electrodes prepared at different H2SO4 concentrations; (A, A-i and A-ii; increased magnification), 1M H2SO4, (B, B-i and B-ii; increased magnifications) 0.5M H2SO4, (C, C-i and C-ii; increased magnifications) 0.05M H2SO4at a applied voltage of -6 V vs. Ag/AgCl in the solution containing 0.87 mg Cu2+

The determination of the optimum Cu^{2+} ion concentration (0.05, 0.20, 0.50 and 1.5 mg) in the solution was further investigated (Fig. 2.S2, Supporting Information). The solution of 0.05 mg Cu^{2+} in 2.5 M H_2SO_4 showed minimal growth of Cu nanodendrites over the band electrodes. With increased concentration of Cu^{2+}, led to an increased spread of formations. However the concentration higher than the 0.87 mg Cu^{2+} showed a very high accumulation of the foam structure which decreased the distance dramatically between the band electrodes. Due to the highly uniform formation of CuFoam across the surface of each band electrode on the array, all

electrodes were then prepared a solution of 0.87 mg Cu^{2+} in 2.5 mM H_2SO_4. As might be expected, the use of shorter deposition periods led to a decrease in the density of the CuFoam deposits over the band electrode surface. Fig.2.S3 (Supporting Information) shows the SEM micrographs of BA10-CuFoam electrodes which were prepared after 15, 20, 30 and 35 seconds of electrochemical deposition. Due to the microelectrode diffusion characteristics, we observed that the Cu deposits became denser only at the ends of the each band electrode in the array at shorter deposition times and with increased deposition time we obtained a more uniform foam distribution through the middle of the single band electrode. However, for each design of band array electrode, we obtained a denser accumulation of the Cu dendrites at the both ends of the electrodes and the diameter of the pores in the copper deposits was found to increase towards the outer surfaces of the deposits. Furthermore, the use of silicon based gold electrodes limits the deposition time since high acid concentration may damage the electrode in the long time period. Thus it is very important to determine the optimum deposition time for each design. Fig 2.3A and B shows the BA5 20 seconds and BA10 25 second depositions, respectively, as a result of determined optimum deposition times. Moreover, it was found that applied voltage also had a significant impact on the nature of the deposits along each band electrode, Fig.2.S4 (Supporting Information). While applied lower negative potentials resulted in decreased accumulation of the CuFoam deposits over the each band on the electrode surface as shown in Fig.2.S4, high negative voltage led to an increase in the density of CuFoam deposits. Therefore, in the presence of a suitable concentration of ions, using an optimized applied potential and deposition time as explained in the experimental section, Cu dendrites were grown in the interstitial spaces of the dynamic hydrogen bubble template which was generated in situ on the working electrode, the result being the formation of a microporous 3D CuFoam on the surface[27, 30], as illustrated in Scheme 2.1. The resulting optimum Cu dendrites were grown at high concentration of SO_4^{2-} and high negative overpotentials of -5.0 and -6.0 V vs. Ag/AgCl in the case of BA5 and BA10, respectively. Fig. 2.3A and B show the 3D CuFoam deposited onto BA5 and BA10, respectively. The wall of the CuFoam deposits is composed of dendritic nanostructures resulting in the increased surface area as can be seen in the higher magnification of SEM micrographs of both electrodes, Fig. 2.3C, D, and E.

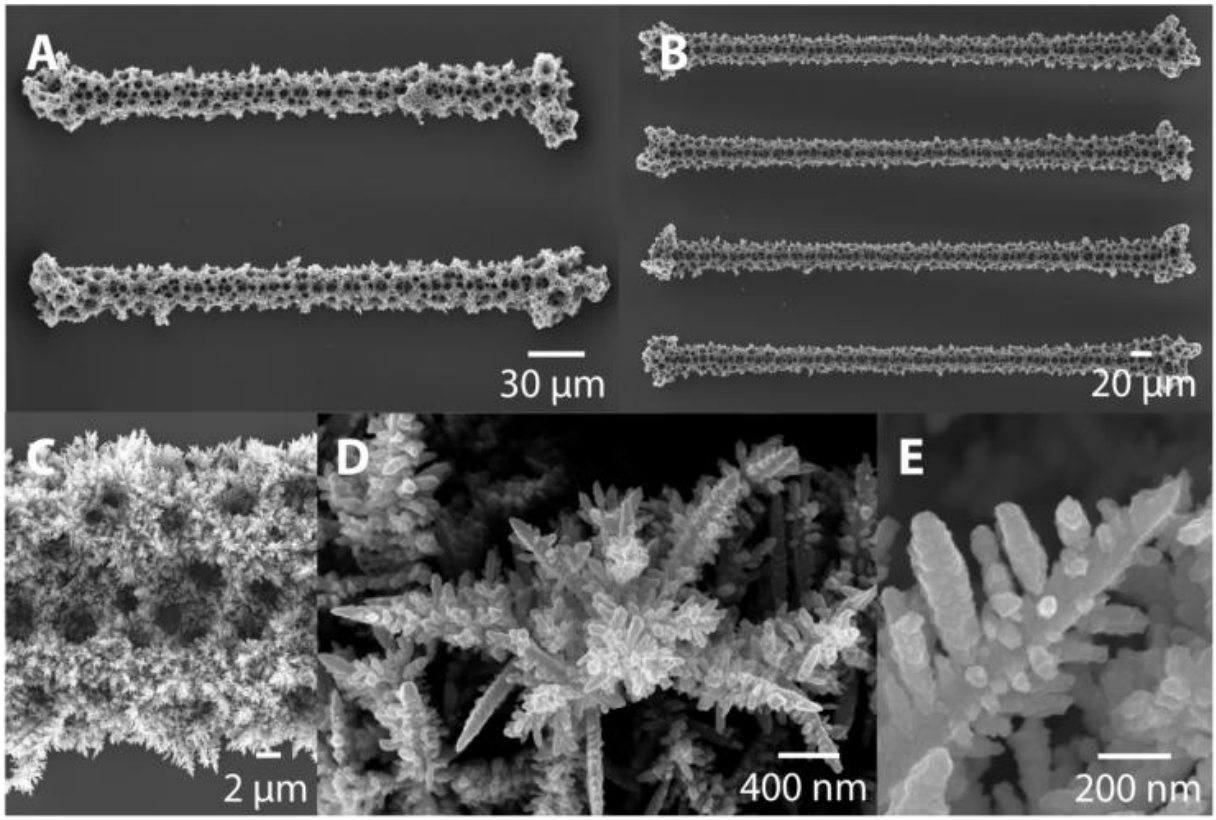


Figure 2.3. SEM images of CuFoam band array electrodes showing (A) BA5 and (B) BA10 foam structure, (C) porous foam of single band and (D and E) foam wall and Cu nanodendrites at higher magnifications.

The as-prepared CuFoam band array electrodes were used to investigate glucose electro-oxidation in alkaline environment. Fig. 2.4A shows the electrochemical behavior of the CuFoam band array electrode in an alkaline solution and Fig. 2.4B and C show the changes of the voltammograms in the absence and presence of glucose. In the anodic sweep in 0.1 M NaOH solution (Fig. 2.4A), the first multiple peaks observed at around -0.04 V vs Ag/AgCl may attributed to oxidation of Cu(0) to Cu(I) and the subsequent formation of Cu_20, according to following equation[31-33];

$$2\,Cu^0 + 2\,OH^- \rightarrow\ Cu_2O + H_2O + 2\,e^- \qquad (1)$$

The broad peak at around 0.13 V vs Ag/AgCl may be attributed to further oxidation of Cu(I) to Cu(II) and Cu(0) to Cu(II), according to following equations [32];

$$Cu_2O + 2\,OH^- \rightarrow \ 2CuO + \ H_2O + \ 2\,e^- \quad (2)$$

$$Cu_2O + 2\,OH^- + \ H_2O \rightarrow 2Cu(OH)_2 + \ 2\,e^- \quad (3)$$

In the cathodic sweep, the peak at around -0.52 V is the reduction of copper oxide species. After addition of glucose into the electrochemical cell (Fig. 2.4B and C, red lines), both electrodes give rise to voltammograms that show the electro-oxidation potential of glucose at +0.45 V vs Ag/AgCl while there are no other obvious peaks at the same potential in the absence of the glucose. The most possible explanation for the glucose-electro-oxidation in NaOH solution by Cu has been postulated as the formation of Cu(III) oxides (such as CuOOH). During the cyclic voltammetry scanning, the exterior surface of the foam is oxidized to CuO and further to Cu^{3+} which is rapidly reduced to Cu(II) at 0.64 V vs Ag/AgCl [34-36];

$$Cu(II) \rightarrow \ Cu(III) + \ e^- \quad (4)$$

$$Cu(III) + 4\,OH^- \rightarrow \ Cu(II) + \ 2H_2O + \ O_2 \quad (5)$$

$$Cu(II) - \text{glucose} \xrightarrow[-e^-]{} Cu(III) - \text{glucose} \xrightarrow[-e^-]{} \text{Gluconolactone} + Cu(II) \quad (6)$$

As the aim of the present work was to study the oxidation of the glucose, +0.45 V vs Ag/AgCl was selected as the potential for use in the subsequent analytical studies. To analyze the optimum NaOH concentration for glucose electro oxidation, BA10-CuFoam electrodes were studied in various concentrations of NaOH at an applied potential of + 0.45 V towards glucose. As is seen in Fig.2.S5 (Supporting Information), the Cu nanodendrites exhibit the higher response in the solutions of 0.1 M and 0.5 M NaOH. Thus, all electrochemical studies were then applied in 0.1 M NaOH solution.

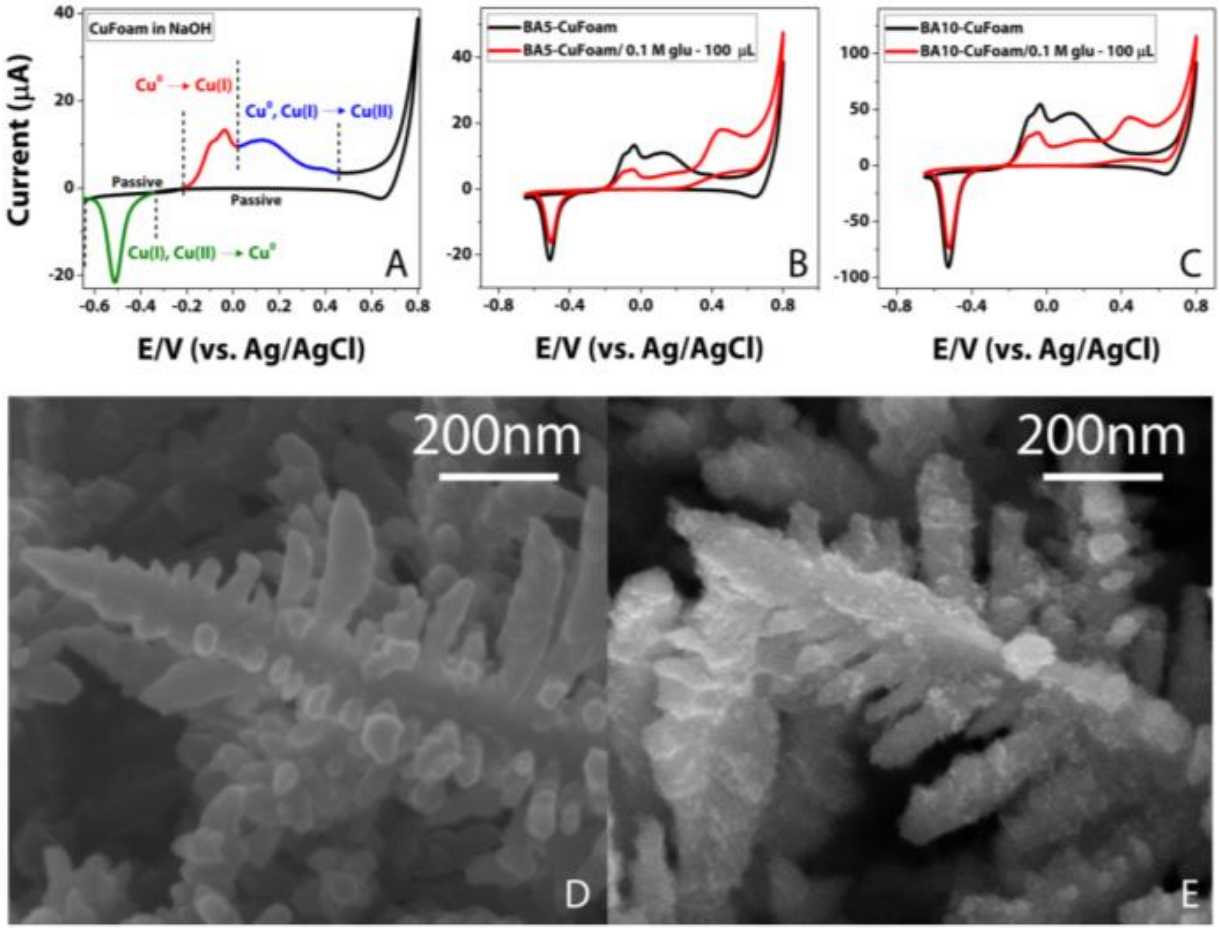


Figure 2.4. Cyclic voltammogram of CuFoam electrode in 0.1M NaOH solution (A), Cyclic voltammograms of the BA5-CuFoam (B) and BA10-CuFoam (C) microelectrodes in 0.1 M NaOH (black), and in the presence of 2 mM glucose (red), at a scan rate of 0.01 V s-1, SEM images of the deposited BA10-Cu nanodendrite before (D) and after (E) glucose electro oxidation.

Fig. 2.4D shows a high magnification SEM image of the CuFoam dendritic nanostructure. The CuFoam structure and Cu dendrites remained stable after electro-oxidation of glucose (Fig. 2.4E). However, the surface roughness changed with the appearance of the very small spike-like features over the surface of Cu dendrites (Fig. 2.4E). Those small features may be responsible for the catalytic performance of the CuFoam electrodes[27]. Nam et al. [27] observed very similar features appearing over a CuFoam surface after the electrochemical oxidation of 5-hydroxymethylfurfural. They claimed that these spike-like features covering the surface of Cu crystals were composed of similar amounts of CuO and $Cu(OH)_2$ on the surface which was demonstrated with X-ray photoelectron spectroscopy (XPS) results. Indeed, it has been reported that the electrocatalytic oxidation of glucose on copper electrodes happens via copper

oxide/hydroxide intermediates[37-39]. Therefore, the surface chemical composition of the CuFoam electrodeposits before and after glucose electro-oxidation was studied by analyzing Cu 2p peaks obtained by XPS. Fig 2.5A shows the measured and fitted curves of CuFoam deposits and Fig. 2.5C exhibits the whole survey of the surface presents all the elements detected. Due to the existence of only C (from atmosphere), O and Cu, it suggests that only copper oxides were formed on the surface. High resolution spectra of Cu 2p (Fig. 2.5A) reveals clearly that indeed a mixture of elemental copper and copper-oxide species are present on the surface. The peaks located at approximately 932.6 and 952.5 eV were attributed to Cu_2O and Cu^0. The peaks at 954.6 eV and 934.9 eV were assigned to CuO and $Cu(OH)_2$, respectively. We remark the limitation of the XPS analysis of the surface layer, because the Cu 2p peaks of Cu^+ and Cu^0 cannot be differentiated, which means that the Cu_2O peak may include the peak from the underlying elemental copper lies beneath the copper oxides surface layer[27]. After the electro-oxidation of glucose, the surface of the CuFoam electrode was reexamined with XPS. The whole survey of the used surface (Fig. 2.5D) shows clearly that the surface of the CuFoam deposits are still composed of a mixture of copper oxide species, similar with Fig. 2.5C. However, the high resolution spectra of the foam surface demonstrates the significant changes of the composition of the existing species (Fig. 2.5B). The peak at 932.6 eV attributed to Cu^+/Cu^0 decreased significantly and the Cu^{2+} at 934.9 eV increased. Similarly, the peak of Cu^{2+} (CuO) at 954.3 eV was increased, while the peak of Cu^+ at 952.5 eV decreased. The increase of the Cu^{2+} species – $Cu(OH)_2$ and CuO- is most likely due to the result of reduction of CuOOH to Cu^{2+} after the electro oxidation of glucose, Eqs. 2, 3 and 6.

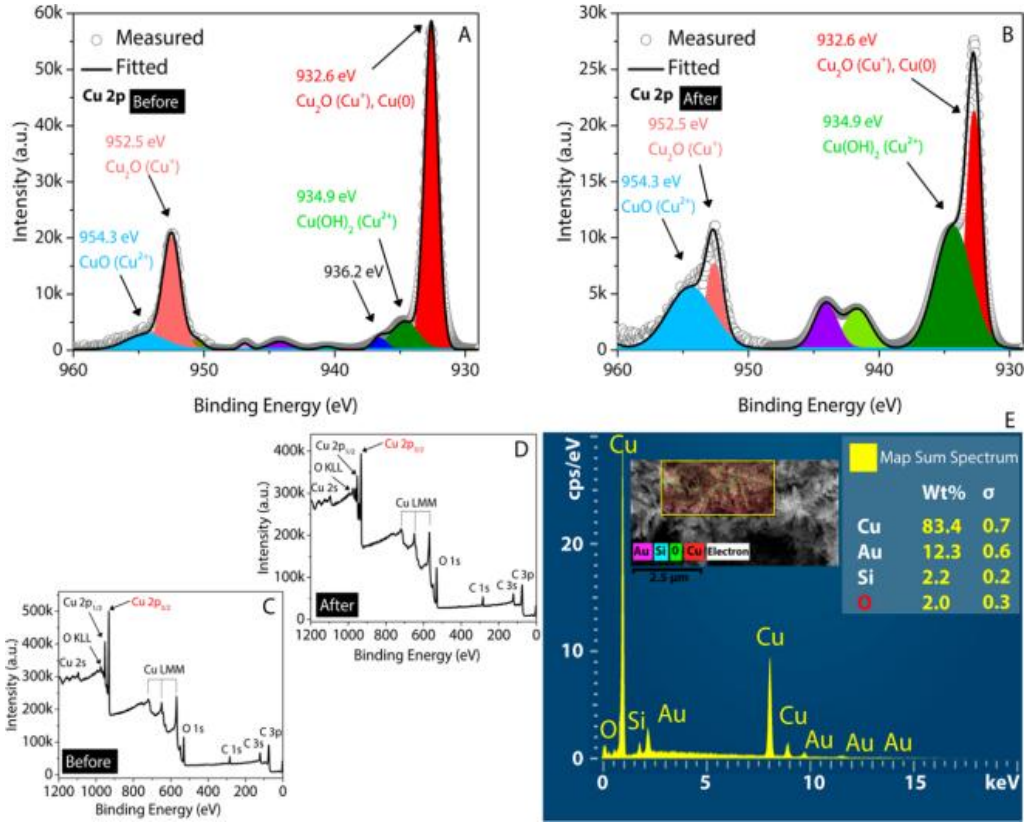


Figure 2.5. Cu 2p XPS spectra of CuFoam deposits (A) before and (B) after glucose electro-oxidation, XPS survey scans of CuFoam (C) before and (D) after glucose electro-oxidation (The quantification results of high resolution spectras are shown in Table 2.S2, supporting information) and (E) EDX spectra of CuFoam electrodeposits (insets; SEM image, EDX mapping analysis and Map Sum spectrum)

The other technique used here to analyze the chemical structure of the CuFoam electrodes is the energy-dispersive X-ray spectroscopy (EDX). Fig. 2.5E shows the EDX analysis and corresponding mapped SEM image of the analysis. The copper appears in red colour which covers the entire surface or the analysis area with the ratio of % 83.4. The result of the EDX analysis confirms the copper and copper oxides as the main constituent in the structure in the presence of gold (Au) and silicon (Si). These two elements are presented less corresponds to the existence of the electrode material based on silicon and gold.

To demonstrate the relationship between the concentration of deposited Cu crystals on surface and the sensitivity of the sensors, we measured calibration curves for the BA-CuFoam electrodes prepared using different Cu deposition times. The fittings of BA5-CuFoam with 20 seconds deposition time (■; $J(\mu A/cm^2) = 10{,}630\ [C_{glucose}](mM) + 53$, R^2=0.997), 15 seconds

deposition time (●; *J (μA/cm^2) = 7136 [C$_{glucose}$](mM) + 1284*, R^2=0.989), 10 seconds deposition time (▲ *J(μA/cm^2) = 6369 [C$_{glucose}$](mM) + 17,* R^2=0.955) and the fitting equations of BA10-CuFoam with 25 seconds deposition time (■; *J(μA/cm^2) = 4437 [C$_{glucose}$](mM) – 24*, R^2=0.999), 20 seconds deposition time (●; *J(μA/cm^2) = 3903 [C$_{glucose}$](mM) + 6*, R^2=0.996), 15 seconds deposition time (▲ *J (μA/cm^2) = 2882 [C$_{glucose}$](mM) + 41*, R^2= 0.990) are given in Fig. 2.6A and B as calibrations curves for each deposition times. As expected, lower Cu deposition times produced electrodes that showed decreased sensitivity due to a decrease in the electro-active surface area. Furthermore we observed a decreased correlation coefficient for electrodes grown with decreased Cu deposition time since the sensors' saturation levels decreased. In this regard it was found that for the BA5 electrodes growth of less than 20 seconds resulted in a marked decrease in both sensitivity and dynamic range for glucose detection, while for the BA10 electrodes this critical growth period was 25 seconds.

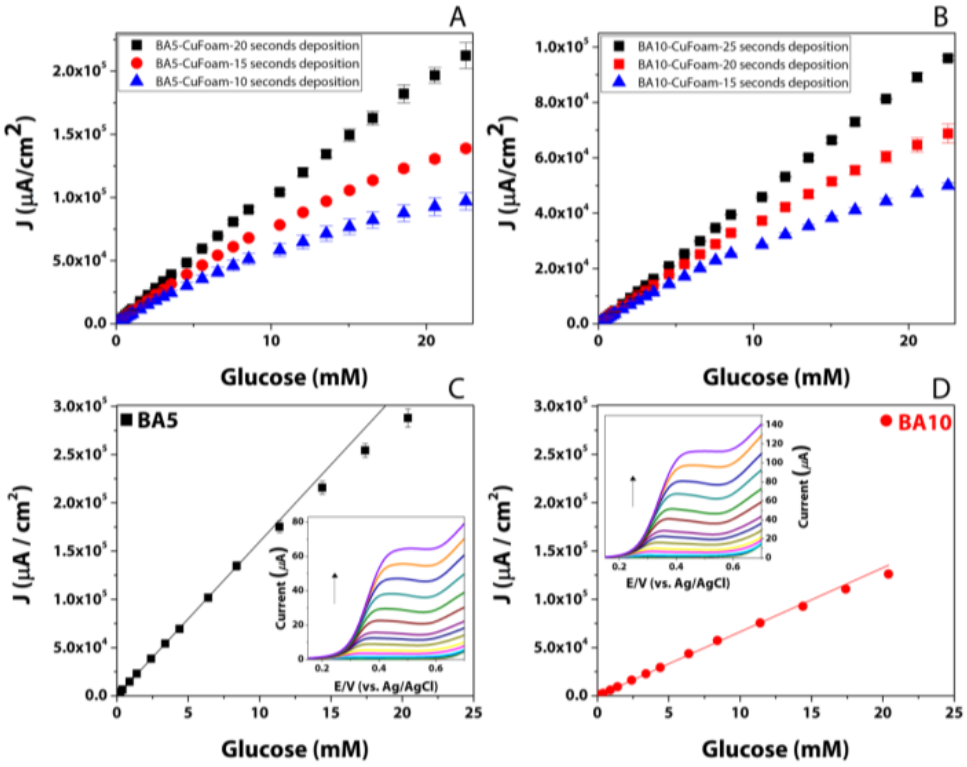


Figure 2.6. Calibration curves of BA5-CuFoam (A) with 20 seconds (■), 15 seconds (●), and 10 seconds (▲) deposition times and BA10-CuFoam (B) with 25 seconds (■), 20 seconds (●), and 15 seconds (▲), illustrating the linear relationship observed between glucose concentration and current density for BA5-CuFoam (C) and BA10-CuFoam (D) sensors with a correlation co-efficient R2=0.99 for both electrodes and linear sweep voltammograms

of BA5-CuFoam (C-inset) and BA10 (D-inset) sensors in 0.1 M NaOH towards increase concentration of glucose at a scan rate of 0.01 V s-1

The linear sweep voltammograms (LSV) obtained as a function of increasing glucose concentration over the CuFoam deposited BA5 and BA10 electrodes are shown in Fig. 2.6C and D. The anodic peak at +0.45 V increases with increasing concentration of glucose as shown in inset graphs. While the peak shape is the same for both designs, the BA10-CuFoam array electrode exhibits higher current levels than the BA5-CuFoam array electrode. Fig. 2.6C and D reveal the corresponding glucose concentration vs. current density graph for the BA5 and BA10 electrodes, respectively. These obviously linear responses towards glucose demonstrate that the CuFoam deposited band array electrodes exhibit a uniform response to glucose and show excellent electrocatalytic behavior.

2.3.3 Chronoamperometric detection of glucose and analytical parameters of the CuFoam deposited array electrodes

The as-prepared CuFoam deposited band array electrodes were studied as glucose sensing anode materials. Fig. 2.7A, B shows the chronoamperometric responses and corresponding calibration curves of both the BA5 and BA10 electrodes modified by Cu deposition. Chronoamperometry was applied as a function of increasing concentrations of glucose in 0.1 M NaOH solution at room temperature under non-stirred conditions. After each addition of glucose, the solution was stirred to obtain a homogenous distribution of glucose in the electrochemical cell and then kept stable for 15 seconds in order to reach equilibrium before the measurement. The inset graphs on Fig. 2.7A, B show the magnified images of six chronoamperograms. The current obtained at the 40^{th} second was used to prepare the calibration curves. Fig. 2.7C and D show the corresponding calibration curves of BA5 and BA10 CuFoam sensors, respectively. Both calibration curves exhibit a linear region in the range of concentrations between 0.01 mM - 22.55 mM. The fitting equation of BA5, Fig. 2.7C, is $J\ (\mu A/cm^2) = 10{,}630\ [C_{glucose}](mM) + 54$ with a correlation coefficient of 0.997 and the fitting equation of BA10, Fig. 2.7D, is $J\ (\mu A/cm^2) = 4{,}437\ [C_{glucose}](mM) - 24$ with a correlation coefficient of 0.999. The slope of the calibration curves demonstrates the sensitivities of the

BA5 and BA10 to be 10,630 µA mM^{-1} cm^{-2} and 4,437 µA mM^{-1} cm^{-2}, respectively. Both sensors showed excellent sensitivities towards glucose in comparison to many other array- based sensors reported in the literature, Table 2.2. The increased sensitivity of BA5 in comparison to the sensitivity of BA10 is due to the further miniaturization of the array and the advanced microelectrode properties arising from the diffusion profile of the miniaturized electrode. This result clearly shows the positive advantage of the miniaturized systems in terms of the analytical performance of the desired (bio)-sensors.

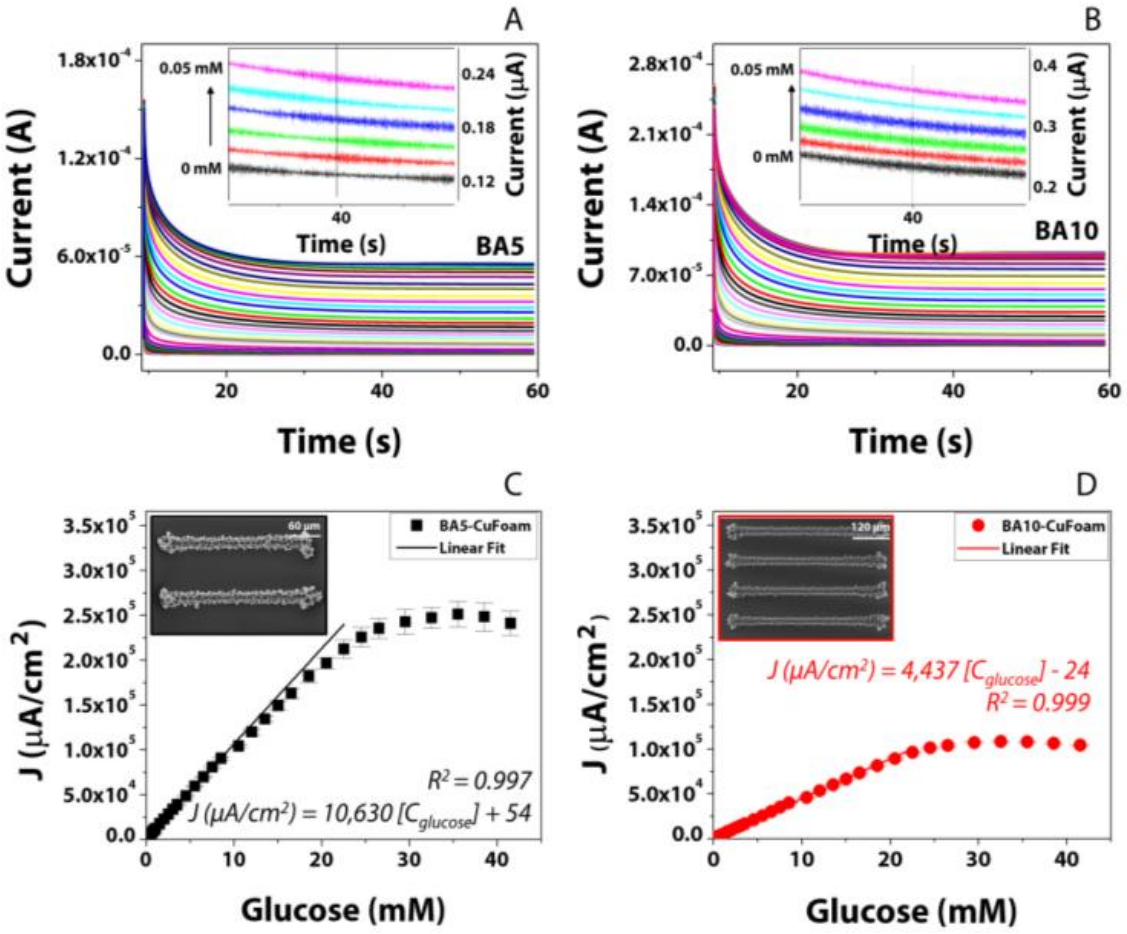


Figure 2.7. Chronoamperograms of the BA5-CuFoam (A) and BA10-CuFoam (B) sensors obtained in 0.1 M NaOH solution as a function of increasing concentration of glucose at an applied potential of + 0.45 V (inset graphs show the magnified image of first six chronoamperograms at 40th second), and corresponding calibration curves for the BA5-CuFoam (C) and BA10-CuFoam (D) sensors.

Table 2.2 presents a summary comparison of the main characteristics of the array based non-enzymatic glucose sensors reported in the literature and the BA5, BA10 CuFoam sensors

fabricated in this study. The sensors developed in this study show the widest linear range for glucose detection up to 22.55 mM among all the array based sensors reported in Table 2.2. The sensitivity of BA5 CuFoam electrode is one of the highest sensitivity among the listed sensors. These performance characteristics may be attributed to the high quality fabrication of the array electrode with the smaller surface area of 2.13×10^{-4} cm^2. Hence it is proposed that the electrochemical characteristics of the designed electrode are highly suitable for the development of sensors. The relatively easy, one-step deposition of 3-D structured porous CuFoam onto the band array electrode provides very a large electro-active surface area for glucose oxidation with superior sensitivity of 10,630 µA mM^{-1} cm^{-2}. It is therefore critical to utilize the optimized deposition process in order to achieve maximum sensor performance. This is clearly demonstrated in the results presented here, which are based on a simple, cheap and rapid method for the preparation of high performance sensors for glucose electro-oxidation.

Table 2.2. *A comparison of the performances of the BA5 and BA10-CuFoam sensors with other copper and array based non-enzymatic glucose sensors*

Electrode	Potential (V)	Linear range	Sensitivity	Ref.
CuO@Cu nanowires array	+0.65 vs. Ag/AgCl	$1.0x10^{-6}$ – $1.0x10^{-2}$ M	1250.8 µA mM^{-1} cm^{-2}	[40]
Cu(OH)2 NGA@NPC hybrid	+0.52 vs. Ag/AgCl	0.2 – 9 mM	2.09 mA cm^{-2} mM^{-1},	[41]
Cu2O/MoS2	+0.7 vs Hg/Hg_2Cl_2	0.01–4 mM	3108.08 µA mM^{-1} cm^{-2}	[42]
CuO-ZnO NRs	+ 0.62 vs. Ag/AgCl	Up to 8.45 mM	2961.7 µA mM^{-1} cm^{-2}	[43]
Cu2O PLNWs/Cu foam	+0.5 vs. SCE	0.001–1.8 mM	6.6807 mA M^{-1} cm^{-2}	[44]
Cu/graphene/NF	+0.6 vs. Ag/AgCl	Linear response range of 100 µM	7.88 mA mM^{-1} cm^{-2}	[45]
Micro-Pt/Cu NFs/nafion/GOD/PU	+0.6 vs. Ag/AgCl	0 – 20 mM	42.38 nA mM^{-1}	[46]
Co_3O_4 nanosheets	+0.5 vs Ag/AgCl	Up to 0.31 mM	12.97 mA mM^{-1} cm^{-2}	[47]
Helical Cu_2O/TiO_2 nanotubes array	+0.65 vs. SCE	3 - 9 mM	14.56 µA mM^{-1} cm^{-2}	[48]
Hierarchical Co_3O_4/Ni	+0.5 vs. SCE	0.04 – 3.6 mM	13,855 µA mM^{-1} cm^{-2}	[49]
CuFoam/BA10	+0.45 vs. Ag/AgCl	0.01 - 22.55 mM	4,437 µA mM^{-1} cm^{-2}	This work
CuFoam/BA5	+0.45 vs. Ag/AgCl	0.01 - 22.55 mM	10,630 µA mM^{-1} cm^{-2}	This work

The selectivity of the sensors was studied in the presence of ascorbic acid, uric acid and acetaminophen, which can possibly coexist with glucose in human blood. Considering that the concentration of glucose in the human blood is more than 30 times that of the interfering species, the experiments designed to test the robustness of the electrodes towards these potential interfering species interference were conducted at both BA5 and BA10-CuFoam sensors by making a series of additions of 1 mM glucose and 0.1 mM interfering species into the electrochemical cell[48]. Fig. 2.S6A and B (Supporting Information) shows the chronoamperograms of BA5 and BA10 recorded in response to each addition of glucose, ascorbic acid, uric acid, acetaminophen and glucose, respectively. The response of the glucose in the presence of interfering species showed a 5.8 % increase in the case of BA5 and a 3.1 % decrease in the case of BA10 (Fig. 2.8A). It is therefore concluded that the very small changes of the measured responses resulting from the addition of the interfering species clearly demonstrate the selectivity of the developed sensors towards glucose. Herein, the most common interfering species (ascorbic acid, uric acid and acetaminophen) were studied to demonstrate the selectivity of the developed sensors, however, we note that it is possible to include the other interfering species such as cysteine, mono- or disaccharides etc. to extend the study. The other significant effect to consider when using noble metal-based electrochemical sensors is the possible poisoning of the surface by chloride ions, which are abundant in physiological fluids. For this reason we also studied the performance of the sensors developed here in response to serial additions of 1 mM glucose into electrochemical cell in the absence and presence of 0.1 M NaCl. Fig. 2.8B shows the corresponding linear responses of both the BA5 and BA10 electrodes. The slopes of the BA5 and BA10 calibration curves in 0.1 M NaOH are 11,740 μA mM^{-1} cm^{-2} and 4,772 μA mM^{-1} cm^{-2}, respectively. Interestingly, the slope of BA5 and BA10 electrode calibration curves in a solution of 0.1 M NaOH containing 0.1 M NaCl are 12,610 μA mM^{-1} cm^{-2} and 5,016 μA mM^{-1} cm^{-2} respectively. The changes calculated are some 7.4 % for BA5 and 5.1 % for BA10 in the presence of the chloride ions. These results demonstrate that the sensors developed here not greatly perturbed by possible poisoning by chloride ions.

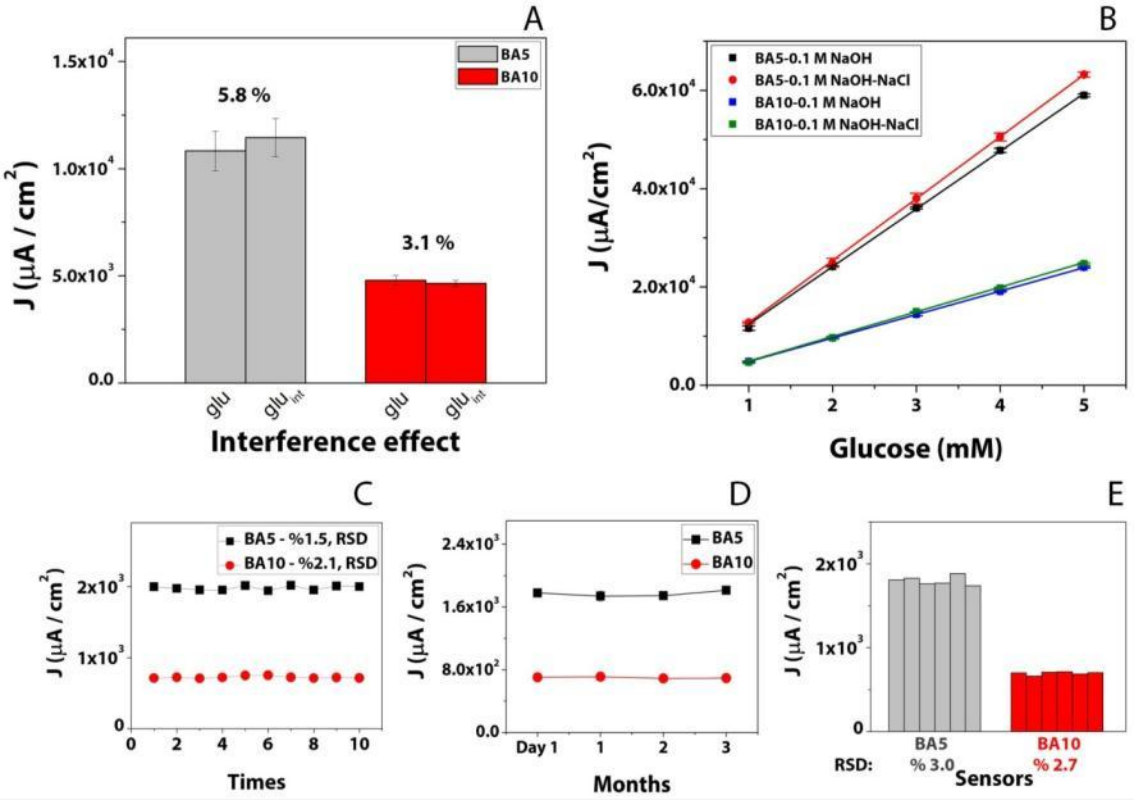


Figure 2.8. Interference effect (A), Poisoning effect (B), reusability (C), long term stability (D) and reproducibility (E) of BA5-CuFoam and BA10-CuFoam sensors

The reusability of the sensors was studied to investigate their operational stability. The sensors were examined 10 times in terms of their response towards 0.15 mM glucose and the resulting current densities are shown in Fig. 2.8C. The calculated relative standard deviations of the results from the BA5 and BA10 electrodes within 10 consecutive experiments are 1.5 % and 2.1 %, respectively. Thus it may be seen that both sensors exhibited excellent operational stability.

The long term stabilities of both sensors were also tested over a period of three months. Fig. 2.8D shows the corresponding current densities recorded towards glucose every 30 days. The sensors were then stored at room temperature in the dark when not in use. The current density of the BA5 electrode measured on the first day increased 1.9 % and the current density of the BA10 electrode decreased 1.35 % after three months. These negligible changes in the responses towards 0.15 mM glucose after three months suggest that both biosensors showed excellent long-term stabilities. The reproducibility of both the BA5 and BA10 electrodes are shown in Fig.

2.8E. Six as-prepared samples of BA5 were tested towards glucose by applying chronoamperometry and the relative standard deviation of the recorded current densities was calculated to be 3.0 % for BA5. Similarly, six BA10 biosensors were measured at the same conditions. The calculated relative standard deviation in this case was found to be 2.7 %. These statistics demonstrate the high degree of reproducibility associated with both the BA5 and BA10 sensors.

Table 2.3. Real sample analysis with spiked sterile human serum

		BA5-CuFoam biosensor		**BA10-CuFoam biosensor**	
Sample	**Spiked serum (mM)**	**Measured (mM)**	**Recovery (%)**	**Measured (mM)**	**Recovery (%)**
1	4.4	4.7 (± 0.04)	106	5.0 (± 0.07)	112
2	6.1	6.2 (± 0.06)	101	6.6 (± 0.29)	109
3	10	9.8 (± 0.35)	98	10.4 (± 0.15)	104

Finally, we have used the two sensors developed here for the detection of glucose in sterile human serum. Four different spiked sterile human serum samples were prepared; 4.4, 6.1 and 10 mM. Each spiked serum concentration was studied three times and after each addition of the prepared sample into electrochemical cell, the current responses were recorded at +0.45 V vs. Ag/AgCl. By substituting the resulting current values into the calibration curves of the sensors, the concentrations of the samples were calculated and the corresponding results are shown in Table 2.3. The recovery values of the BA5 electrode are in the range of 97.7 - 105.7 %. The recovery values of the BA10 electrode are in the range of 103.6 - 112.4 %. These results show that the developed BA5 and BA10-CuFoam biosensor electrodes can successfully determine the glucose concentrations in human serum.

2.4 Conclusions

In summary, two different band array electrodes were designed. Both designs had 17 band electrodes, 100 µm inter electrode distance and 200 nm recess depth. Silicon based micro band array electrodes, namely BA5 (with 5 µm width and 250 µm length) and BA10 (with 10 µm

width and 500 µm length) were fabricated by applying microfabrication technologies including lithography, deposition and etching. The fabrication technologies used permit the precise and reproducible fabrication of electrodes using methods which are proven to be cost-effective for the batch production of devices. Scanning electron microscopy and electrochemistry were used for characterization of the bare electrodes. The fabricated electrodes were then used as substrates for Cu dendrites deposition at high negative overpotentials in an acidic environment. We observed that the increased acidity of the electrodeposition solution gave rise to a significant improvement in terms of the morphology and adhesion of the deposits. The CuFoam deposited band array electrodes were used as high performance electro catalysts for glucose detection. Both designs showed excellent electrocatalytic activity towards glucose. While the BA10-CuFoam biosensor showed a sensitivity of 4,437 µA mM^{-1} cm^{-2}, the BA5-CuFoam biosensor in particular exhibited an outstanding sensitivity of 10,630 µA mM^{-1} cm^{-2} with a wide concentration range of 0.01 mM – 22.55 mM. This result is one of the highest sensitivity ever recorded among the non-enzymatic glucose sensors reported up to now in the literature. Furthermore, both developed sensors showed a strong resistance to the poisoning effects of chloride ions while also exhibiting excellent reproducibility, reusability, and negligible interference effects in the presence of ascorbic acid, uric acid and acetaminophen. The electrodes and sensors described in this work are suitable for further miniaturization and packaging. Moreover, this study shows the promising advantages of the foam modified array electrodes in terms of the stability, increased electroactive surface area and analytical performance.

2.5 Methods

2.5.1 Chemicals and instrumentation

Copper(II) chloride dihydrate ($CuCl_2 \cdot 2H_2O$), glucose, ascorbic acid, uric acid, acetaminophen, potassium ferrocyanide ($K_4[Fe(CN)_6]$), potassium ferricyanide ($K_3[Fe(CN)_6]$), uric acid, acetaminophen, phosphate buffer saline tablets (PBS, 0.01 M, pH7.4), sodium hydroxide (NaOH), sulfuric acid and potassium chloride were obtained from Sigma-Aldrich. All solutions

were prepared with double distilled 18.3 MΩ deionized water which was obtained by ELGAPurelab Ultra. Electrochemical measurements were performed on an Autolab electrochemical workstation (Metrohm, UK) equipped with a conventional 3-electrode setup consisting of a micro band array electrode (working electrode, see fabrication below), a spiral Pt wire counter electrode and Ag/AgCl (1 M KCl) reference electrode. The surface morphology and the nanostructure of the bare and modified electrodes was studied by scanning electron microscopy (SEM) (Zeiss Supra 40 SEM at accelerating voltages in the range of 5-10 kV). The chemical composition of the surface was characterized by using an X-ray photoemission spectrometer (XPS, Kratos AXIS ULTRA) with Al K_α at 1486.58 eV. All the XPS data were calibrated by the carbon 1s peak at 284.8 eV. The energy dispersive X-ray analyses (EDX) was studied by using SEM Quanta 650 Field Emission Gun (FEG) attached with EDX unit, with accelerating voltage of 20 kV.

2.5.2 Microfabrication of electrodes

Silicon-based gold array electrodes were fabricated by a general microfabrication flow which included lithography, deposition and etching as we reported earlier [8-9]. The masks consisted of a series of the array geometries required were designed specifically for band array fabrication. In the first step of the fabrication process, a silicon oxide layer was grown on the silicon substrate followed by spin coating of a photoresist. The metal layers - titanium first and then gold - were deposited and patterned by a lift-off process. A 200 nm thick silicon nitride layer was deposited as the passivation layer. Finally the mask was used for a passivation lithography process and the etching of the arrays and contact pad. The overall wafer was covered with a resist layer to protect the electrodes during dicing.

2.5.3 Electrochemical measurements and CuFoam electrode preparation

All electrochemical experiments were performed at room temperature, in 5mL total electrolyte volume. Prior to each electrochemical study, electrodes were treated with organic solvents and plasma cleaned to remove the resist layer. Firstly, electrodes were kept in hot acetone (56 °C; boiling point) for 3 minutes and then rapidly transferred into isopropyl alcohol and treated in an

ultrasonic bath for 3 minutes. After the organic solvent cleaning process, the electrodes were washed with deionized water and dried under nitrogen flow. Dry electrodes were placed into the plasma cleaner to increase the hydrophilicity of the surface and remove the organic residues or oxides from the surface. Electrodes were then washed with deionized water and dried under N_2 flow. The clean electrodes were then used immediately.

Cyclic voltammetry of the bare electrodes was typically performed at a scan rate of 0.01 V s^{-1}, in a stationary solution of 5 mM $[Fe(CN)_6]^{3-/4-}$ prepared in 0.01 M PBS (pH 7.4), containing 0.1 M KCl. Electrodeposition of copper was carried out by applying chronoamperometry in 6mL 2.5 M H_2SO_4 solution containing 0.87 mg Cu^{2+} with suitable applied voltage and time for each design. Prior to each electrodeposition process electrochemical cell was pre-conditioned for 2 seconds at 0 V. Band array 5 (BA5) with 5 µm width, 250 µm length was applied -5 V for 20 seconds. Band array 10 (BA10) with 10 µm width, 500 µm length was studied at -6 V for 25 seconds. Both band arrays have 17 electrodes. Both electrodes have 200 nm recess depth. After deposition, the CuFoam electrodes were rinsed with double distilled water and dried in air. Cyclic voltammetry of CuFoam deposited microelectrodes was performed in alkaline media, 0.1 M NaOH at a scan rate of 0.01 V s^{-1} in the absence and presence of glucose. Oxidation of the glucose was firstly studied by linear sweep voltammetry (LSV) at a scan rate of 0.01 V s^{-1}. Calibration of glucose sensors was prepared by measuring the chronoamperometric response at the 40^{th} second of applied potential of +0.45 V in 0.1 M NaOH solution. Firstly, electrodes were studied in the absence of glucose to determine the base current value at 40^{th} second. After addition of the glucose the current value was obtained at 40^{th} second under the same conditions used for the base study and the difference between the values was taken as an analytical signal. All sensitivities were determined by dividing the slope of the calibration curves by total geometric surface area of each array electrode.

2.6 Acknowledgments

The authors gratefully acknowledge the support of the Department of Agriculture, Food and the Marine in Ireland, via award number 14F883 .

2.7 References

1. Fekete, Z., Recent advances in silicon-based neural microelectrodes and microsystems: a review. *Sensors and Actuators B: Chemical* 2015, *215*, 300-315.

2. Seymour, J. P.; Wu, F.; Wise, K. D.; Yoon, E., State-of-the-art MEMS and microsystem tools for brain research. *Microsyst Nanoeng* 2017, *3*.

3. Pongrácz, A.; Fekete, Z.; Márton, G.; Bérces, Z.; Ulbert, I.; Fürjes, P., Deep-brain silicon multielectrodes for simultaneous in vivo neural recording and drug delivery. *Sensors and Actuators B: Chemical* 2013, *189*, 97-105.

4. Day, B. K.; Pomerleau, F.; Burmeister, J. J.; Huettl, P.; Gerhardt, G. A., Microelectrode array studies of basal and potassium-evoked release of L-glutamate in the anesthetized rat brain. *J Neurochem* 2006, *96* (6), 1626-1635.

5. Kane, S. R.; Cogan, S. F.; Ehrlich, J.; Plante, T. D.; McCreery, D. B.; Troyk, P. R., Electrical Performance of Penetrating Microelectrodes Chronically Implanted in Cat Cortex. *Ieee T Bio-Med Eng* 2013, *60* (8), 2153-2160.

6. Fekete, Z.; Németh, A.; Márton, G.; Ulbert, I.; Pongrácz, A., Experimental study on the mechanical interaction between silicon neural microprobes and rat dura mater during insertion. *Journal of Materials Science: Materials in Medicine* 2015, *26* (2), 70.

7. Wei, W.; Song, Y.; Wang, L.; Zhang, S.; Luo, J.; Xu, S.; Cai, X., An implantable microelectrode array for simultaneous L-glutamate and electrophysiological recordings in vivo. *Microsystems &Amp; Nanoengineering* 2015, *1*, 15002.

8. Buk, V.; Pemble, M. E., A highly sensitive glucose biosensor based on a micro disk array electrode design modified with carbon quantum dots and gold nanoparticles. *Electrochimica Acta* 2019, *298*, 97-105.

9. Buk, V.; Pemble, M. E.; Twomey, K., Fabrication and evaluation of a carbon quantum dot/gold nanoparticle nanohybrid material integrated onto planar micro gold electrodes for potential bioelectrochemical sensing applications. *Electrochimica Acta* 2019, *293*, 307-317.

10. Patolsky, F.; Zheng, G.; Lieber, C. M., Fabrication of silicon nanowire devices for ultrasensitive, label-free, real-time detection of biological and chemical species. *Nat Protoc* 2006, *1* (4), 1711-24.

11. Yang, N.; Uetsuka, H.; Osawa, E.; Nebel, C. E., Vertically aligned diamond nanowires for DNA sensing. *Angew Chem Int Edit* 2008, *47* (28), 5183-5185.

12. Siddiqui, S.; Arumugam, P. U.; Chen, H.; Li, J.; Meyyappan, M., Characterization of Carbon Nanofiber Electrode Arrays Using Electrochemical Impedance Spectroscopy: Effect of Scaling Down Electrode Size. *Acs Nano* 2010, *4* (2), 955-961.

13. Arumugam, P. U.; Chen, H.; Siddiqui, S.; Weinrich, J. A. P.; Jejelowo, A.; Li, J.; Meyyappan, M., Wafer-scale fabrication of patterned carbon nanofiber nanoelectrode arrays: A route for development of multiplexed, ultrasensitive disposable biosensors. *Biosensors and Bioelectronics* 2009, *24* (9), 2818-2824.

14. Lu, P.; Liu, Q.; Xiong, Y.; Wang, Q.; Lei, Y.; Lu, S.; Lu, L.; Yao, L., Nanosheets-assembled hierarchical microstructured Ni(OH)2 hollow spheres for highly sensitive enzyme-free glucose sensors. *Electrochimica Acta* 2015, *168*, 148-156.

15. Liu, A.; Ren, Q.; Xu, T.; Yuan, M.; Tang, W., Morphology-controllable gold nanostructures on phosphorus doped diamond-like carbon surfaces and their electrocatalysis for glucose oxidation. *Sensors and Actuators B: Chemical* 2012, *162* (1), 135-142.

16. Xie, L. S.; Asiri, A. M.; Sun, X. P., Monolithically integrated copper phosphide nanowire: An efficient electrocatalyst for sensitive and selective nonenzymatic glucose detection. *Sensor Actuat B-Chem* 2017, *244*, 11-16.

17. Xie, F. Y.; Cao, X. Q.; Qu, F. L.; Asiri, A. M.; Sun, X. P., Cobalt nitride nanowire array as an efficient electrochemical sensor for glucose and H2O2 detection. *Sensor Actuat B-Chem* 2018, *255*, 1254-1261.

18. Gawande, M. B.; Goswami, A.; Felpin, F. X.; Asefa, T.; Huang, X. X.; Silva, R.; Zou, X. X.; Zboril, R.; Varma, R. S., Cu and Cu-Based Nanoparticles: Synthesis and Applications in Review Catalysis. *Chemical Reviews* 2016, *116* (6), 3722-3811.

19. Koepke, S. J.; Light, K. M.; VanNatta, P. E.; Wiley, K. M.; Kieber-Emmons, M. T., Electrocatalytic Water Oxidation by a Homogeneous Copper Catalyst Disfavors Single-Site Mechanisms. *J Am Chem Soc* 2017, *139* (25), 8586-8600.

20. Bae, K. L.; Kim, J.; Lim, C. K.; Nam, K. M.; Song, H., Colloidal zinc oxide-copper(I) oxide nanocatalysts for selective aqueous photocatalytic carbon dioxide conversion into methane. *Nat Commun* 2017, *8*.

21. Buk, V.; Emregul, E.; Emregul, K. C., Alginate copper oxide nano-biocomposite as a novel material for amperometric glucose biosensing. *Mat Sci Eng C-Mater* 2017, *74*, 307-314.

22. Tian, K.; Prestgard, M.; Tiwari, A., A review of recent advances in nonenzymatic glucose sensors. *Mat Sci Eng C-Mater* 2014, *41*, 100-118.

23. Jiang, J. Y.; Zhang, P.; Liu, Y.; Luo, H. X., A novel non-enzymatic glucose sensor based on a Cu-nanoparticle-modified graphene edge nanoelectrode. *Anal Methods-Uk* 2017, *9* (14), 2205-2210.

24. Cao, F.; Gong, J., Nonenzymatic glucose sensor based on CuO microfibers composed of CuO nanoparticles. *Anal Chim Acta* 2012, *723*, 39-44.

25. Fang, L. X.; Wang, F.; Chen, Z. H.; Qiu, Y.; Zhai, T. L.; Hu, M. M.; Zhang, C. J.; Huang, K. J., Flower-like MoS2 decorated with Cu2O nanoparticles for non-enzymatic amperometric sensing of glucose. *Talanta* 2017, *167*, 593-599.

26. Zhao, Y. X.; Li, Y. P.; He, Z. Y.; Yan, Z. F., Facile preparation of Cu-Cu2O nanoporous nanoparticles as a potential catalyst for non-enzymatic glucose sensing. *Rsc Adv* 2013, *3* (7), 2178-2181.

27. Nam, D. H.; Taitt, B. J.; Choi, K. S., Copper-Based Catalytic Anodes To Produce 2,5-Furandicarboxylic Acid, a Biomass-Derived Alternative to Terephthalic Acid. *Acs Catal* 2018, *8* (2), 1197-1206.

28. Nam, D. H.; Choi, K. S., Bismuth as a New Chloride-Storage Electrode Enabling the Construction of a Practical High Capacity Desalination Battery. *J Am Chem Soc* 2017, *139* (32), 11055-11063.

29. Nikolić, N. D.; Branković, G.; Pavlović, M. G.; Popov, K. I., The effect of hydrogen co-deposition on the morphology of copper electrodeposits. II. Correlation between the properties of electrolytic solutions and the quantity of evolved hydrogen. *J Electroanal Chem* 2008, *621* (1), 13-21.

30. Cherevko, S.; Chung, C.-H., Direct electrodeposition of nanoporous gold with controlled multimodal pore size distribution. *Electrochemistry Communications* 2011, *13* (1), 16-19.

31. Caballero-Briones, F.; Artes, J. M.; Diez-Perez, I.; Gorostiza, P.; Sanz, F., Direct Observation of the Valence Band Edge by in Situ ECSTM-ECTS in p-Type Cu2O Layers Prepared by Copper Anodization. *J Phys Chem C* 2009, *113* (3), 1028-1036.

32. El Din, A. M. S.; El Wahab, F. M. A., The behaviour of the copper electrode in alkaline solutions upon alternate anodic and cathodic polarization. *Electrochimica Acta* 1964, *9* (1), 113-121.

33. Hampson, N. A.; Lee, J. B.; Macdonald, K. I., Oxidations at copper electrodes: Part 2. a study of polycrystalline copper in alkali by linear sweep voltammetry. *Journal of Electroanalytical Chemistry and Interfacial Electrochemistry* 1971, *32* (2), 165-173.

34. Deng, Y. L.; Handoko, A. D.; Du, Y. H.; Xi, S. B.; Yeo, B. S., In Situ Raman Spectroscopy of Copper and Copper Oxide Surfaces during Electrochemical Oxygen Evolution Reaction: Identification of Cu-III Oxides as Catalytically Active Species. *Acs Catal* 2016, *6* (4), 2473-2481.

35. Zheng, W. R.; Li, Y.; Tsang, C. S.; Hu, L. S.; Liu, M. J.; Huang, B. L.; Lee, L. Y. S.; Wong, K. Y., Cu-II-Mediated Ultra-efficient Electrooxidation of Glucose. *Chemelectrochem* 2017, *4* (11), 2788-2792.

36. Miller, B., Split-Ring Disk Study of Anodic Processes at a Copper Electrode in Alkaline Solution. *J Electrochem Soc* 1969, *116* (12), 1675-&.

37. Toghill, K. E.; Compton, R. G., Electrochemical Non-enzymatic Glucose Sensors: A Perspective and an Evaluation. *Int J Electrochem Sc* 2010, *5* (9), 1246-1301.

38. Kano, K.; Takagi, K.; Inoue, K.; Ikeda, T.; Ueda, T., Copper electrodes for stable subpicomole detection of carbohydrates in high-performance liquid chromatography. *J Chromatogr A* 1996, *721* (1), 53-57.

39. Kano, K.; Torimura, M.; Esaka, Y.; Goto, M.; Ueda, T., Electrocatalytic oxidation of carbohydrates at copper(II) -modified electrodes and its application to flow-through detection. *J Electroanal Chem* 1994, *372* (1), 137-143.

40. Dong, J.; Ren, L.; Zhang, Y.; Cui, X.; Hu, P.; Xu, J., Direct electrodeposition of cable-like CuO@Cu nanowires array for non-enzymatic sensing. *Talanta* 2015, *132*, 719-726.

41. Li, R.; Liu, X.; Wang, H.; Wu, Y.; Lu, Z., High-performance hybrid electrode decorated by well-aligned nanograss arrays for glucose sensing. *Biosensors and Bioelectronics* 2018, *102*, 288-295.

42. Fang, L.; Wang, F.; Chen, Z.; Qiu, Y.; Zhai, T.; Hu, M.; Zhang, C.; Huang, K., Flower-like MoS2 decorated with Cu2O nanoparticles for non-enzymatic amperometric sensing of glucose. *Talanta* 2017, *167*, 593-599.

43. Ahmad, R.; Tripathy, N.; Ahn, M. S.; Bhat, K. S.; Mahmoudi, T.; Wang, Y. S.; Yoo, J. Y.; Kwon, D. W.; Yang, H. Y.; Hahn, Y. B., Highly Efficient Non-Enzymatic Glucose Sensor Based on CuO Modified Vertically-Grown ZnO Nanorods on Electrode. *Sci Rep-Uk* 2017, *7*.

44. Lu, W.; Sun, Y.; Dai, H.; Ni, P.; Jiang, S.; Wang, Y.; Li, Z.; Li, Z., Direct growth of pod-like Cu2O nanowire arrays on copper foam: Highly sensitive and efficient nonenzymatic glucose and H2O2 biosensor. *Sensors and Actuators B: Chemical* 2016, *231*, 860-866.

45. Hussain, S.; Akbar, K.; Vikraman, D.; Choi, D. C.; Kim, S. J.; An, K. S.; Jung, S.; Jung, J., A highly sensitive enzymeless glucose sensor based on 3D graphene-Cu hybrid electrodes. *New J Chem* 2015, *39* (9), 7481-7487.

46. Fang, Y.; Wang, S.; Liu, Y.; Xu, Z.; Zhang, K.; Guo, Y., Development of Cu nanoflowers modified the flexible needle-type microelectrode and its application in continuous monitoring glucose in vivo. *Biosensors and Bioelectronics* 2018, *110*, 44-51.

47. Meng, S. J.; Wu, M. Y.; Wang, Q.; Dai, Z. Y.; Si, W. L.; Huang, W.; Dong, X. C., Cobalt oxide nanosheets wrapped onto nickel foam for non-enzymatic detection of glucose. *Nanotechnology* 2016, *27* (34).

48. Long, M.; Tan, L.; Liu, H.; He, Z.; Tang, A., Novel helical TiO2 nanotube arrays modified by Cu2O for enzyme-free glucose oxidation. *Biosensors and Bioelectronics* 2014, *59*, 243-250.

49. Xu, H.; Xia, C.; Wang, S.; Han, F.; Akbari, M. K.; Hai, Z.; Zhuiykov, S., Electrochemical non-enzymatic glucose sensor based on hierarchical 3D Co3O4/Ni heterostructure electrode for pushing sensitivity boundary to a new limit. *Sensors and Actuators B: Chemical* 2018, *267*, 93-103.

2.8 Supporting Information

Table 2.S1. Latest enzymatic sensors and their analytical performances

Electrode	Sensitivity	Linear range	Stability	Ref.
PAA-VS-PANI/GPL-FePc/GO_x-CH	18.11 µA mM^{-1} cm^{-2}	1- 20 mM	50 continuous CV scans showed similar pattern	[1]
GOx@PAVE-CNTs	High sensitivity, Linear regression equation; I(µA) = 0.0268 + 2.1971 $C_{glucose}$(mM)	1.0 µM ~ 5 mM	after 35 days, the current response to initial value still retain at 92.4%	[2]
GOx-SiO_2/Lig/CPE	0.78 µA mM^{-1}	0.5 – 9 mM	The response current was reduced to 82% and 73% of its initial value after two and three weeks, respectively	[3]
PNE/GOD/AuNPs @PNE/Au)	35.4 µA mM^{-1} cm^{-2}	0.003 – 3.43 mM	After a week, the response was approximately 99.1% of the initial value	[4]
Nafion/GOx/ZnO NRs/ITO	48.75 µA/mM	0.05 – 1 mM	The modified electrode retained 90% of its initial response after 7 days, 85% after 14 days and 57% after 35 days.	[5]
stretchable fiber-based glucose sensor	11.7 µA mM^{-1} cm^{-2}	0-500 µM	The sensor gave stable chronoamperometric responses in 6 h operation and 8 days of storage	[6]
GCE/MWCNTs-ConA/GOx	(2.22 ± 0.03) µA mM^{-1}	5 - 1200 µM	a loss of sensitivity of 20% after 44 days and 22% after the 65th day	[7]

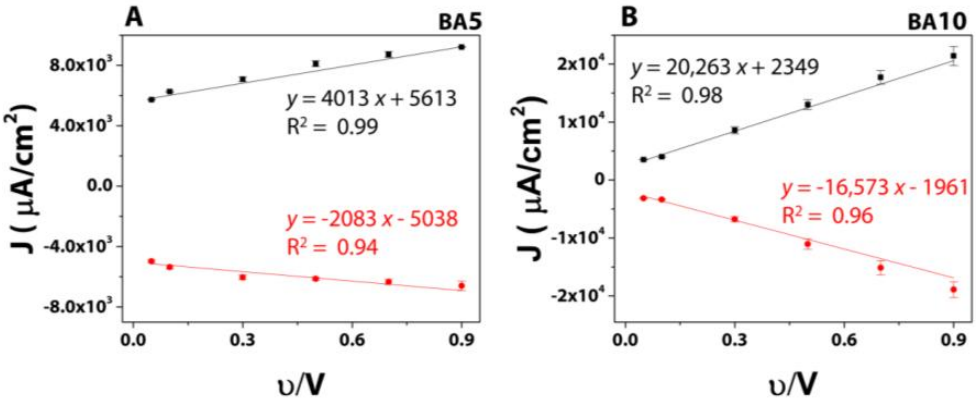


Figure 2.S1. The relationship of anodic and cathodic peak currents versus the scan rate; BA5 (A) and BA10 (B). The scan rate is 0.05, 0.1, 0.3, 0.5, 0.7 and 0.9 V s-1 in a solution of 5 mM Fe(CN)63-/4- as a redox probe in 0.01 M PBS (pH 7.4), containing 0.1 M KCl

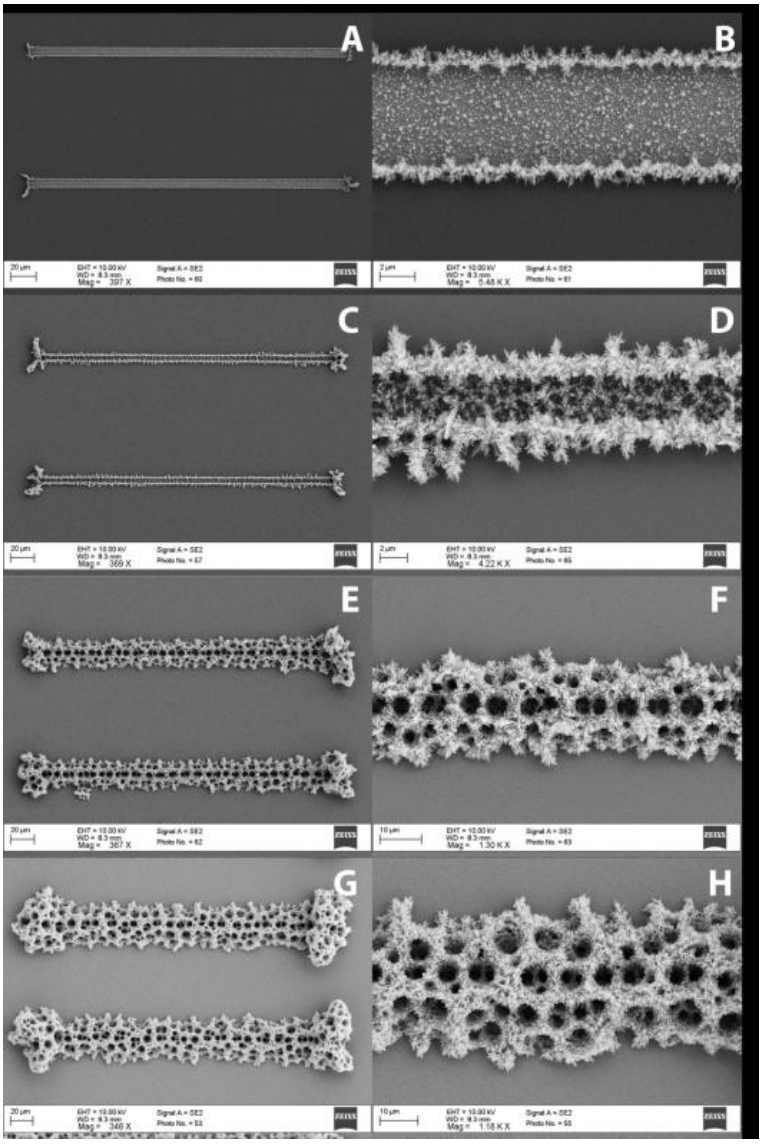


Figure 2.S2. SEM images of BA5-CuFoam electrodes prepared at different Cu2+ concentrations; (A,B) 0.05 mg Cu2+/2.5 M H2SO4, (C,D) 0.20 mg Cu2+/2.5 M H2SO4, (E,F) 0.50 mg Cu2+/2.5 M H2SO4 and (G, H) 1.5 mg Cu2+/2.5 M H2SO4 at a applied voltage of -5 V vs Ag/AgCl, deposition time is 20 seconds.

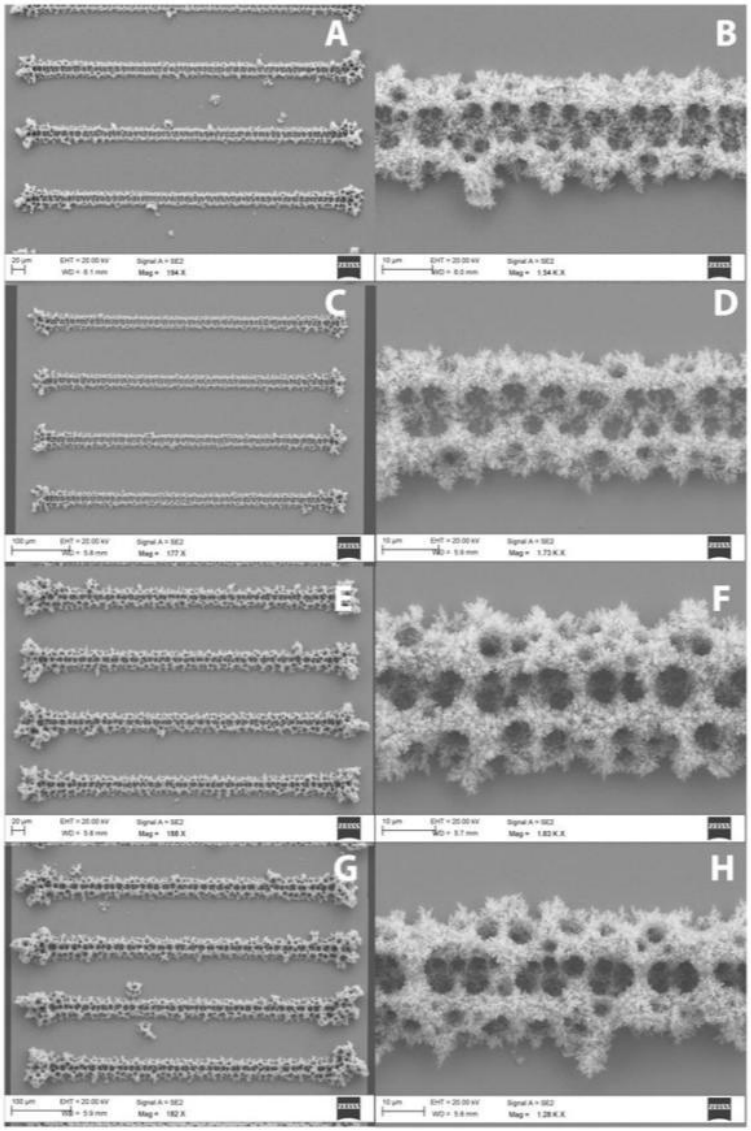


Figure 2.S3. SEM images of BA10-Cu foam electrodes prepared at different deposition times; (A-low magnification, B-high magnification) 15 seconds, (C-low magnification, D-high magnification) 20 seconds, (E-low magnification, F-high magnification) 30 seconds and (G-low magnification, H-high magnification) 35 seconds at a applied voltage of -6 V vs. Ag/AgCl in a solution of 2.5 M H2SO4 containing 0.87 mg Cu2+

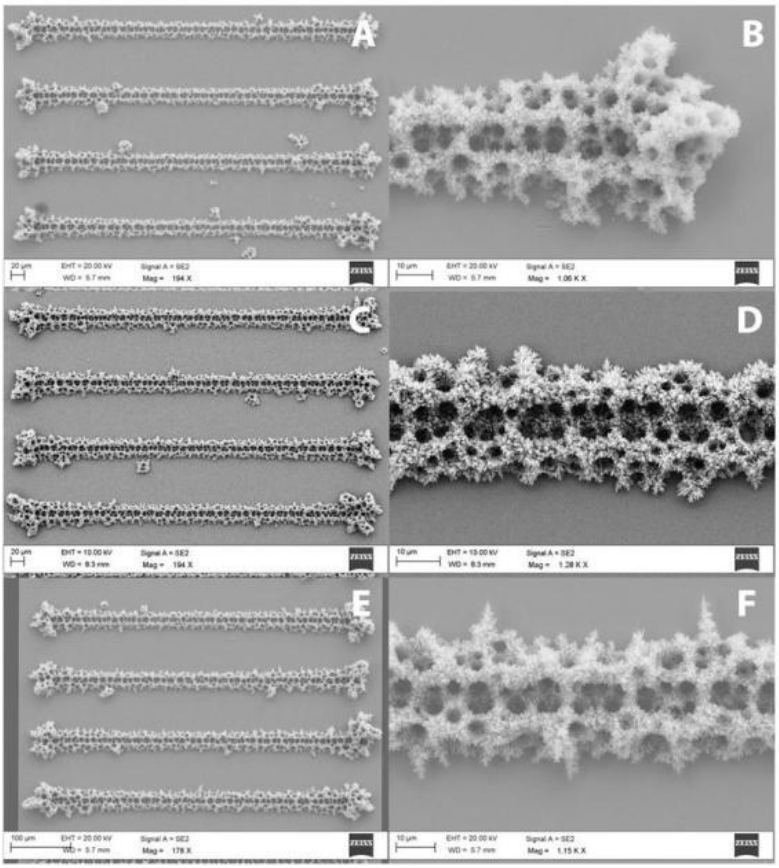


Figure 2.S4. SEM images of BA10-Cu foam electrodes prepared at different applied voltages at – 4 V (A-low magnification, B-high magnification), -5 V (C-low magnification, D-high magnification) and -7 V (E-low magnification, F-high magnification) for 30 seconds in a solution of 2.5 M H2SO4 containing 0.87 mg Cu2+

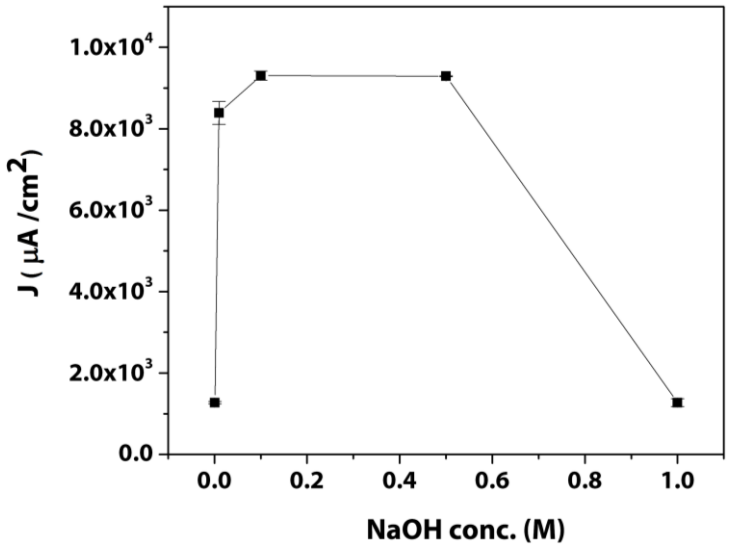


Figure 2.S5. The amperometric response of BA10-CuFoam electrode toward 2 mM glucose in various concentrations of NaOH at a applied potential of 0.45 V; 0.001 M, 0.01 M, 0.1 M, 0.5 M and 1 M NaOH

Table 2.S2. Quantification from survey scan and high resolution spectras of Cu-2p3/2 peaks

	Compound	Name	Position	FWHM	R.S.F.	% Conc.
CuFoam surface	**survey scan**	**O 1s**	**530.6**	**1.7**	**2.93**	**33.9**
		C 1s	**284.9**	**1.2**	**1**	**26.4**
		Cu 2p	**932.6**	**1.0**	**16.7**	**39.7**
	Cu2O, Cu(OH)2	O 1s_1	530.6	1.0	2.93	18.6
	O from organics	O 1s_2	531.7	1.4	2.93	14.9
	C-C,C=C	C 1s_1	284.8	1.1	1	17.1
	C-O	C 1s_2	286.1	1.5	1	4.0
	O-C=O	C 1s_3	288.2	1.0	1	2.1
	CO3	C 1s_4	289.2	1.5	1	3.0
	Cu2O, Cu(0)	**Cu 2p_1**	**932.6**	**1.0**	**16.7**	**31.8**
	Cu(OH)2	**Cu 2p_2**	**934.9**	**1.3**	**16.7**	**1.9**
		Cu 2p_3	936.3	1.8	16.7	1.1
	satellite	Cu 2p_4	940.7	2.7	16.7	1.4
	satellite	Cu 2p_5	944.1	2.5	16.7	2.8
	satellite	Cu 2p_6	946.8	1.1	16.7	0.8
After glucose electrocatalysis	**survey scan**	**O 1s**	**530.7**	**2.8**	**2.93**	**40.7**
		C 1s	**284.9**	**1.3**	**1**	**25.0**
		Cu 2p	**932.8**	**1.2**	**16.7**	**34.3**
	Cu2O	O 1s_1	530.2	1.6	2.93	22.1
	O from organics	O 1s_2	531.7	1.5	2.93	18.6
	C-C,C=C	C 1s_1	284.8	1.2	1	15.7
	C-O	C 1s_2	286.0	1.5	1	4.2
	O-C=O	C 1s_3	288.4	1.4	1	3.5
	CO3	C 1s_4	289.5	1.5	1	1.6
	Cu2O, Cu(0)	**Cu 2p_1**	**932.7**	**1.1**	**16.7**	**15.6**
	Cu(OH)2	**Cu 2p_2**	**934.6**	**2.6**	**16.7**	**11.0**
	satellite	Cu 2p_3	941.6	2.5	16.7	4.2
	satellite	Cu 2p_4	944.1	1.9	16.7	3.5

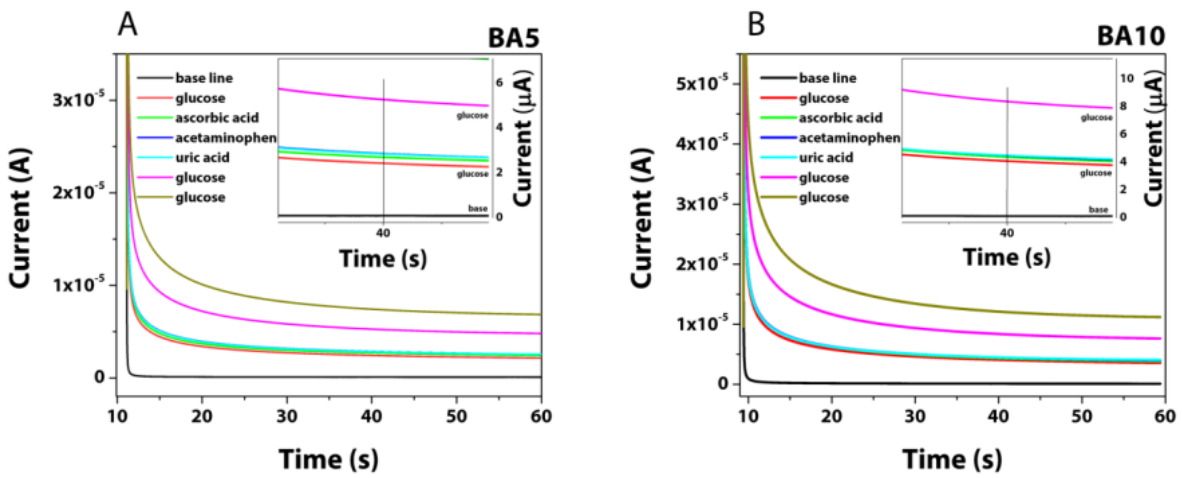


Figure 2.S6. Chronoamperograms of the BA5-Cu foam (A) and BA10-Cufoam (B) sensors obtained in 0.1 M NaOH solution towards 1 mM glucose, 0.1 mM ascorbic acid, 0.1 mM acetaminophen, 0.1 mM uric acid, 1 mM glucose and 1 mM glucose, respectively, at an applied potential of + 0.45 V (inset graphs show the magnified image of the chronoamperograms at 40th second)

References

1. Al-Sagur, H.; Shanmuga sundaram, K.; Kaya, E. N.; Durmuş, M.; Basova, T. V.; Hassan, A., Amperometric glucose biosensing performance of a novel graphene nanoplatelets-iron phthalocyanine incorporated conducting hydrogel. *Biosensors and Bioelectronics* 2019, *139*, 111323.

2. Xu, S.; Zhang, Y.; Zhu, Y.; Wu, J.; Li, K.; Lin, G.; Li, X.; Liu, R.; Liu, X.; Wong, C.-P., Facile one-step fabrication of glucose oxidase loaded polymeric nanoparticles decorating MWCNTs for constructing glucose biosensing platform: Structure matters. *Biosensors and Bioelectronics* 2019, *135*, 153-159.

3. Jędrzak, A.; Rębiś, T.; Klapiszewski, Ł.; Zdarta, J.; Milczarek, G.; Jesionowski, T., Carbon paste electrode based on functional GOx/silica-lignin system to prepare an amperometric glucose biosensor. *Sensors and Actuators B: Chemical* 2018, *256*, 176-185.

4. Liu, Y.; Nan, X.; Shi, W.; Liu, X.; He, Z.; Sun, Y. N.; Ge, D. T., A glucose biosensor based on the immobilization of glucose oxidase and Au nanocomposites with polynorepinephrine. *Rsc Adv* 2019, *9* (29), 16439-16446.

5. Ridhuan, N. S.; Razak, K. A.; Lockman, Z., Fabrication and Characterization of Glucose Biosensors by Using Hydrothermally Grown ZnO Nanorods. *Sci Rep-Uk* 2018, *8*.

6. Zhao, Y. M.; Zhai, Q. F.; Dong, D. S.; An, T. C.; Gong, S.; Shi, Q. Q.; Cheng, W. L., Highly Stretchable and Strain-Insensitive Fiber-Based Wearable Electrochemical Biosensor to Monitor Glucose in the Sweat. *Anal Chem* 2019, *91* (10), 6569-6576.

7. Ortiz, E.; Gallay, P.; Galicia, L.; Eguílaz, M.; Rivas, G., Nanoarchitectures based on multi-walled carbon nanotubes non-covalently functionalized with Concanavalin A: A new building-block with supramolecular recognition properties for the development of electrochemical biosensors. *Sensors and Actuators B: Chemical* 2019, *292*, 254-262.

CHAPTER 3

Enzymatic glucose detection at planar and micro scale

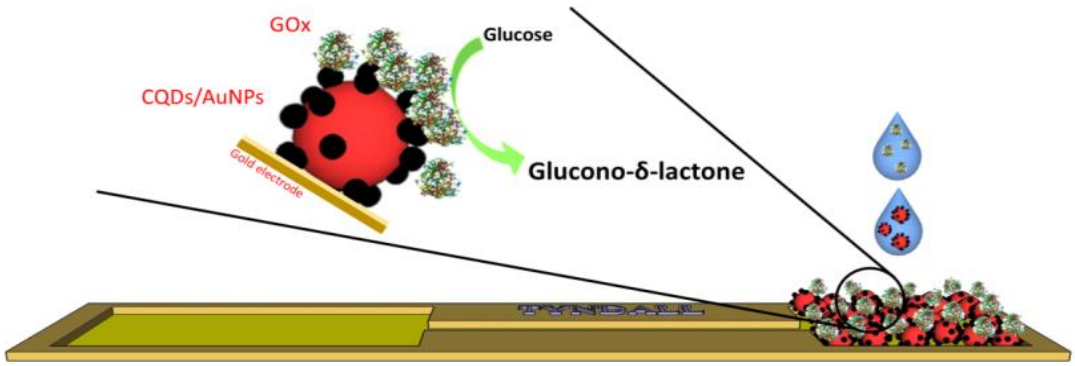
3. Fabrication and evaluation of a carbon quantum dot/gold nanoparticle nanohybrid material integrated onto planar micro gold electrodes for potential bioelectrochemical sensing applications

This work has been published in the journal of ELSEVIER Electrochimica Acta, 2019, 293, 307-317

3.1 Abstract

We have developed a hybrid nanomaterial based on both of carbon quantum dots (CQDs)/gold nanoparticles (AuNPs), such that the cheapness and versatility on the CQDs is directly combined with the inertness and electrochemical activity of the AuNPs to create a new electrochemical biosensor. Here, for the first time, we demonstrate how this interesting materials combination can be applied in the development of an enzymatic biosensor that is easily manufacturable using standard semiconductor processing methods. To demonstrate the potential and performance of the CQDs as an immobilization matrix, glucose oxidase (GOx) enzyme was chosen as a model system. The analytical performance of the developed biosensor was examined using chronoamperometry and the developed CQDs/AuNPs-GOx biosensor exhibited a sensitivity of 47.24µA mM^{-1} cm^{-2} and a detection limit of 17µM (S/N=3) with a linear response to glucose ranging from 0.05mM to 2.85mM (R=0.987). Furthermore, this new biosensor showed a high level of reproducibility and was also shown to be very selective towards glucose in the presence of the possible interference species uric acid and acetaminophen. Finally, it is demonstrated that the sensor is also capable of reliably detecting glucose levels in human serum.

Key words: *Carbon quantum dots, gold nanoparticles, nano-hybrid materials, electrochemical biosensors, semiconductor fabrication*



Graphical abstract, note that the sizes of the components shown are not drawn to scale.

3.2 Introduction

The development of enzyme-coupled electrochemical biosensors is of significant importance since they offer the possibility of high sensitivity and selectivity, and are amenable to miniaturization which opens up a wide range of application areas [1]. Additionally, the kinetics of reactions that take place at the electrochemical biosensor interface are substantially influenced by the surface characteristics [2]. Thus, various types of nanomaterials have been exploited to decrease the space between the surface and the active site of the enzyme and take advantage of the nano-size and shape. In particular, it has been found that the use of hybrid nanomaterial systems is an attractive option for such sensing platforms due to their excellent donor-acceptor behavior [3]. This study concentrates on hybrid carbon quantum dot (CQD) and gold nanoparticle (AuNP) systems, whose electrochemical properties and analytical performance when deployed on solid transducer surfaces have, to the best of our knowledge, not been extensively studied previously.

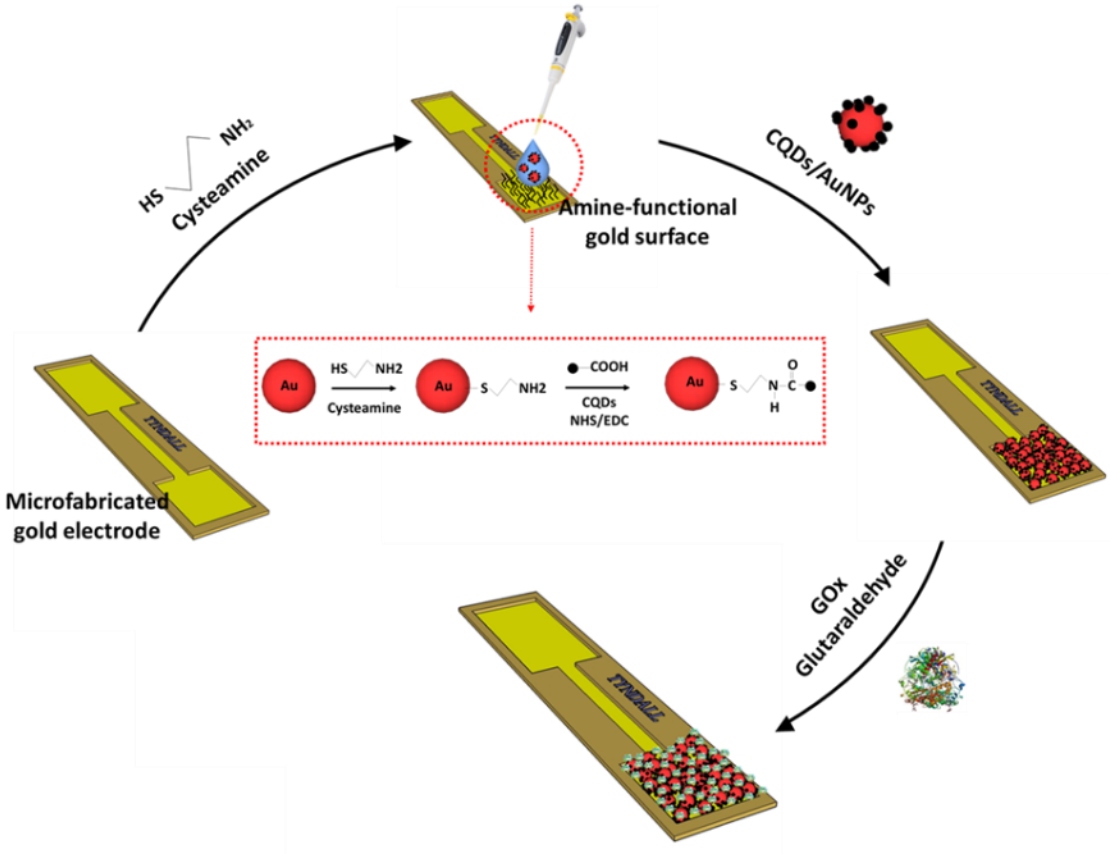
CQDs, a new class of carbon based materials, have attracted increasing interest in recent years due to their promising applications in the field of bioimaging [4], drug delivery [5] and sensors [6] and their attractive features of low cost, environmental friendliness and chemical inertness. They are very small (< 10 nm) quasi-spherical particles which consist of two main regions, namely the core and surface regions. The core regions of CQDs consist of sp^2 hybridized carbon or graphene flakes while the surface regions contain functional groups such as carboxyl or/and hydroxyl groups together with various defects in an amorphous structure.

The other part of the system studied here –AuNPs– have been well-exploited in many areas including biosensors, immunoassays, drug delivery, bioimaging etc. [7]. The ability of AuNPs to permit the fast and direct electron transfer between the redox site of the biomolecule and electrode surface has been proven [8], which facilitates the development of mediator-free electrochemical sensing. There have been many reports in the literature which demonstrate successfully the potential use of AuNPs as a Surface Enhanced Raman Spectroscopy (SERS) substrate for sensing applications since AuNPs can amplify SPR (surface plasmon resonance) signal intensity depending on their size, shape and surface properties, see for example references[9, 10].

Up to now, most research has been focused on the improvement of the fluorescence intensity of CQDs by doping [11], passivating [12] or combining with metal nanoparticles such as gold or silver [13-15]. For example, Zong et al. [3] reported the conjunction of gold nanoparticles and carbon dots via PAMAM dendrimers to provide a specific gap between materials. They demonstrated that the protected specific distance between metal and carbon dot could enhance the photoluminescence (PL) of carbon dots. However, to the best of our knowledge, there are only very limited studies which aim to study the electrochemical interface properties of CQDs in the conjunction with metal nanoparticles and biomolecules as a potential bioelectrochemical sensing device [16].

Herein, in addition to the nanomaterials themselves, the other critical component is the electrode that provides a platform to create a suitable interface for the biological reaction. In this study, we fabricated wafer-scale silicon-based gold electrodes by applying conventional microfabrication techniques including lithography, deposition and etching. We demonstrate that by combining such techniques with the assembly of the nanomaterials in question, we are able to generate patterned, functional electrodes suitable for a range of biological sensing applications [17]. The microfabricated gold devices demonstrated here are highly suitable for future miniaturization and packaging having enormous flexibility in terms of geometry and size.

In this work, our aim was to apply CQDs as an immobilization matrix as part of the development of a micro fabricated gold electrode based detection platform towards glucose. For the first time, we report the fabrication and characterization of a CQD/AuNP-GOx immobilized microfabricated gold electrode with high analytical performance towards glucose detection. Scheme 1 represents the overall immobilization process of the hybrid nanoparticles onto the biosensor. The developed biosensor showed a high sensitivity of 47.24 µA mM^{-1} cm^{-2} and selectivity towards glucose. We demonstrate that the CQDs/AuNPs matrix represents a successful proof-of-concept material for inclusion in the design of an enzymatic electrochemical biosensor based on GOx enzyme as a model system. Thus, we envision that CQDs based immobilization matrix will become an important platform for construction of other electrochemical and bioelectrochemical sensors in the future.



Scheme 3.1. The preparation of CQD/AuNP nano-hybrid materials and a schematic illustration of the immobilization process employed in the fabrication of the biosensor developed here. Note that the sizes of the components shown are not drawn to scale.

3.3 Materials and methods

3.3.1 Chemicals and instrumentation

Glucose oxidase (EC 1.1.3.4, from Aspergillus niger), glucose, potassium chloride (KCl), sodium chloride (NaCl), 1-Ethyl-3-(3-dimethylaminopropyl)carbodiimide (EDC), N-hydroxysuccinimide (NHS), potassium ferrocyanide ($K_4[Fe(CN)_6]$), potassium ferricyanide ($K_3[Fe(CN)_6]$), uric acid, acetaminophen, ascorbic acid, ethanol, cysteamine (CA), sterile human serum, phosphate buffer saline tablets (PBS, 0.01 M, pH7.4), gold(III)chloride trihydrate, sodium citrate were obtained from Sigma-Aldrich. Absolute ethanol was obtained from Ocon Chemicals-Ireland. Glucose stock solutions were prepared one day before use to allow mutarotation and kept in the fridge at +4˚C.

The gold working electrodes with 0.095 cm^2 active surface area were patterned on silicon substrates by microfabrication technology [18, 19]. Fabrication and characterization of gold electrodes are detailed in supplementary information (Fig.3.S1).

All electrochemical experiments were carried out using an Autolab electrochemical station (PGSTAT302N, Metrohm, UK) in a three-electrode cell including a gold working electrode, a platinum (Pt) wire counter electrode and Ag/AgCl (3M) reference electrode. Electrochemical impedance spectroscopy (EIS), cyclic voltammetry (CV), and chronoamperometry were used to investigate the electrochemical performance of the developed biosensor. All electrochemical results and fittings were studied by using OriginPro2016 software.

3.3.2 Preparation of CQDs/AuNPs nanohybrid material

The synthesis of carbon quantum dots (CQDs) was carried out using a previously reported method [20], with slight modifications. Briefly, a three-electrode system was used for the electrochemical carbonization process of ethanol in alkaline environment including two Pt wire electrodes and one Ag/AgCl saturated reference electrode. 15mL ethanol was mixed with saturated NaOH solution. Amperometry was applied under stirred conditions at 4V for 30 minutes. The resulting product with a white turbidity was kept in the dark overnight resulting in a color change from white to yellow. Following this the solution was evaporated at 80˚C leaving

behind a pellet of material. The pellet was dissolved in water and adjusted to neutral pH. To remove the salt and large molecules, centrifugation at 16,200 rpm was applied for 30 minutes, the supernatant was filtered for further purification and the pale-yellow CQDs solution was kept in the fridge at +4˚C. The concentration of CQDs was determined as being 10.35 (±1.53) mg/mL. To investigate the immobilization efficiency of synthesized CQDs via carbodiimide chemistry, we applied EIS and AFM for both bare and modified gold electrodes. For this purpose, clean gold electrodes were immersed in cysteamine solution and incubated overnight. Activation of carboxyl groups was employed using very well-known carbodiimide chemistry. Briefly, a mixture of NHS/EDC (molar ratio 1:4) was added to the CQDs solution and the resulting mixture was shaken for 2 hours for incubation. 5 µL of activated CQDs solution was drop-casted on each amine-functionalized gold electrode surface and allowed to dry. Then, electrodes were washed with distilled water and dried under N_2 flow. AFM and EIS were performed in order to investigate the efficacy of the immobilization process. AuNPs were prepared according to the procedure described by Turkevich et al. [21]. 25 mL % 0.02 tetrachloroauric acid solution was boiled under stirring conditions in a round bottom reaction flask with a reflux connected. % 1 trisodium citrate solution was then added rapidly to the reaction flask. The colour of solution changed from pale yellow to colorless, dark blue/black and then very bright magenta, respectively, which indicated the formation of gold nanoparticles. The solution was cooled to room temperature under stirring. The resulting colloidal gold nanoparticles solution was transferred in a brown vial and kept at +4˚C.

The CQD/AuNP hybrids were prepared by conjugating using carbodiimide chemistry (Scheme 1, red dashes). Typically, 4µL 0.01 mM cysteamine (CA) was added to 246µL of AuNPs colloidal solution and incubated by shaking for 24 hours at room temperature. The carboxyl groups of the CQDs were activated by 40µL of NHS/EDC solution (molar ratio of 1:4) which was added to the cysteamine modified AuNP solution and shaken overnight at room temperature. The preparation steps of the nanohybrid was studied by UV/VIS spectrophotometer.

3.3.3 Preparation of the CQD/AuNP-GOx modified electrodes

Gold electrodes were immersed into CA solution to obtain the amine functionalized surface and incubated overnight at room temperature. 5 µL of the prepared CQD/AuNP solution was drop-

casted and allowed to dry at room temperature. Then the electrodes were washed with distilled water and dried under a N_2 flow. Finally, 5µL of 0.04U GOx and glutaraldehyde (%1) were dropped-casted, respectively and electrodes were kept in the fridge until dried. Then electrodes were washed gently with PBS and kept in the fridge at +4˚C.

3.4 Results and discussions

3.4.1 Characterization of CQDs, AuNPs and CQDs/AuNPs nanohybrid material

The UV-Vis absorption and PL emission spectra of the CQDs at 300nm excitation is shown in Fig. 3.1A. The CQDs showed an absorption peak at 268nm and a tail extending into the visible range in the UV-Vis spectra [22]. This can be attributed to the existence of aromatic structures in the CQDs. The excitation of CQDs at 300 nm wavelength exhibited a blue fluorescent emission spectrum at 410nm. To further explore the fluorescent properties of the as-prepared CQDs, the PL intensity was studied by 20nm increments of excitation wavelengths ranging from 260 to 500nm (Fig. 3.1B). With the increase of the excitation wavelength, different energy levels were probed and as a consequence, a red shift was observed in the emission spectrum. The shift to longer wavelengths with a gradual decrease in the PL intensity may be attributed to the excitation-dependent photoluminescence phenomenon of CQDs [23]. The pre-synthesized CQDs were studied on the gold electrode surface to investigate the immobilization process as shown in Fig. 3.1C. The assembly process of the CQDs was studied by EIS. Fig. 3.1D shows Nyquist plots of the bare gold electrode, the cysteamine modified gold surface and the gold electrode with CQDs attached. This latter modified electrode exhibited a dramatic increase in Rct in comparison to the bare gold electrode, arising from the accumulation of the nanoparticles on the gold surface

AFM measurements were also applied in order to characterize the morphological changes of the electrode surface obtained after CQD immobilization. Fig. 3.1E-i and ii depicts a representative 2D AFM image of a bare gold electrode and CQDs modified surfaces, respectively. The AFM image of CQDs attached to a gold electrode surface clearly shows the formation of several clusters the diameter of which varied from 5 nm to 50 nm dispersed

homogenously over the gold electrode surface. Moreover, the CQD-modified surface was rougher than that of the bare gold electrode surface. This necessarily provided a significant increase in the effective surface area which could lead to a higher degree of immobilization of the biomolecules.

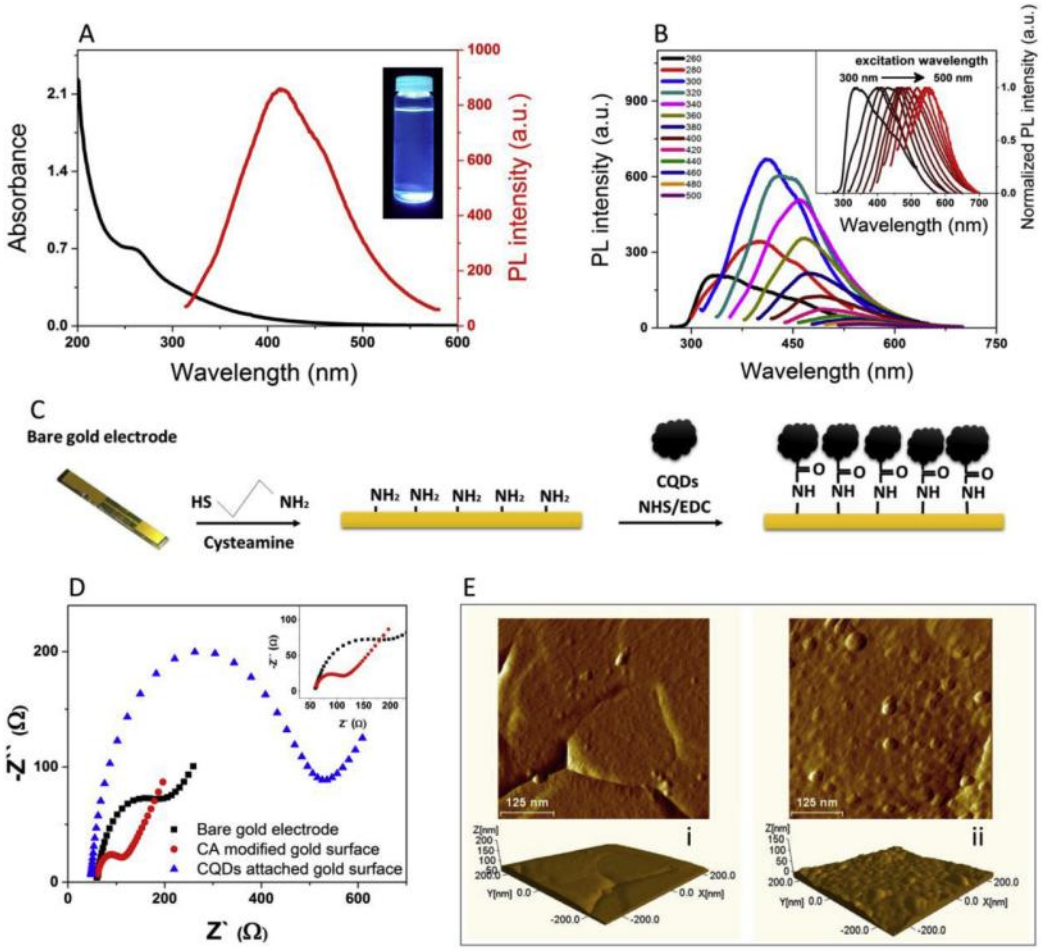


Figure 3.1. (A) absorption (black) and photoluminescence spectra (red) at 300 nm excitation(inset: the CQDs solution under UV light) and (B) emission spectra of CQDs with 20 nm increments of excitation wavelength between 260 nm and 500 nm (C) Schematic illustration of the immobilization process used for the CQDs, (D) Nyquist plots of the impedance spectra of bare gold electrode (■, black), cysteamine modified surface (●, red), and CQDs immobilized gold electrode (▲, blue) in the presence of 2.5 mM Fe(CN)63-/4- as a redox probe in 0.01 M PBS (pH 7.4) solution containing 0.1 M KCl, over the frequency range from 105 to 0.01 Hz, a bias potential of +0.24 V vs Ag/AgCl and an amplitude of 0.01 V (E) AFM images of the bare gold electrode (i), gold electrode with CQDs attached (ii).

AuNPs were synthesized by the reduction of $HAuCl_4$ with sodium citrate which exhibited a very bright magenta color and showed a characteristic surface plasmon resonance peak at 525 nm which was related to the size of the particles (Fig. 3.2A, and inset). As seen in Fig. 3.2B, the

synthesized AuNPs were spherical-shaped. The size distribution histogram of nanoparticles (Fig. 3.2C) showed an average diameter of 25.2 nm (*n*=342). The concentration and extinction coefficient (ε) of the AuNPs solution was calculated to be 1.34 x 10^{-9} M and (1.23 ± 0.058) x 10^{9} M^{-1} cm^{-1}, respectively [24].

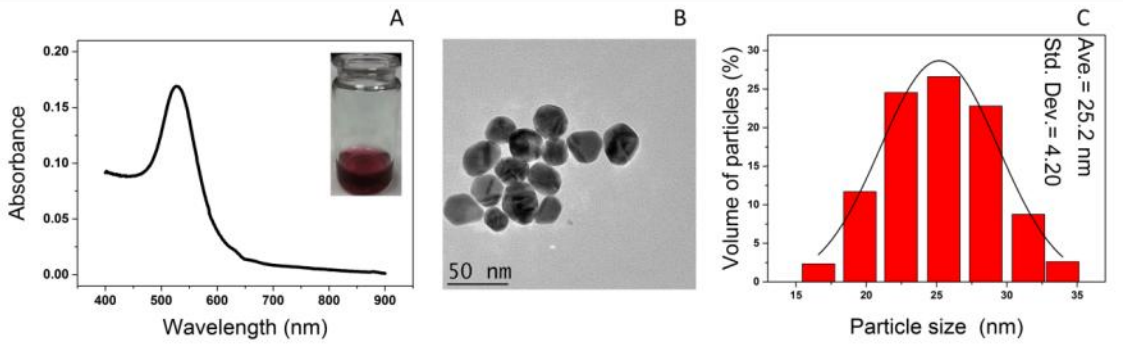


Figure 3.2. (A) UV-Vis Spectrum (inset: image of the colloidal AuNPs), (B) TEM image and (C) size distribution histogram of AuNPs

The formation of the CQD/AuNP nano-hybrid material was studied using UV/Vis spectrophotometry and TEM. Fig. 3.3A shows the UV/Vis response to the CA modification of the AuNPs. With increasing concentration of CA, a decrease of the main absorbance peak of the AuNPs was observed while at longer wavelengths, increasing CA concentration induced a linear increase of the absorbance peak after around 650 nm which could be attributed to CA induced aggregation of the AuNPs. It is known that aggregation of nanoparticles can lead to broadening together with a red shift in the position of the associated absorption band. Thus, 0.16 µM CA was chosen as the optimum concentration due to the minimum changes of the absorbance peak height and shape as compared to the spectrum of the bare AuNPs.

Fig. 3.3B illustrates the formation of the CQD/AuNP material. In Fig. 3.3B the black trace depicts the absorption spectrum of the amine-functional AuNPs. The other traces show the effects of adding increasing amounts of the treated CQDs to the AuNPs. Increasing the concentration of the CQDs causes a progressive reduction in the intensity of the plasmon absorption of the AuNPs near 525 nm. At the same time the absorption near 750 nm increases with increasing CQD concentration. In this case it is suggested that addition of the CQDs simply draws the AuNPs closer together. It is known that a process such as this could induce a rise in the levels of

absorption in this region of the spectrum [25-28]. This proposal is further supported by TEM images, Fig. 3.3D and E.

FTIR spectra were recorded in order to examine the chemical processes occurring when the amine terminated AuNPs were added to the CQDs, Fig. 3.3C. The spectrum corresponding to the CQDs only exhibits a broad feature centered around 3360cm^{-1} which would be consistent with the presence of the bonded OH groups and C-H stretching modes found on a carboxylic acid. Further evidence for the existence of carboxylic acid groups is presented via the appearance of two characteristic infrared stretching absorptions at 1631cm^{-1} and 1761cm^{-1} which corresponded to C=O symmetric coupled stretching and asymmetric coupled vibrations respectively, which form due to delocalization of the negative charge over the structure [29]. After addition of the AuNPs these particular features change significantly. The resulting feature, centered around 1631cm^{-1}, would be consistent with a C=O stretching mode of a species which is no longer delocalized, suggesting disruption to the carboxylic acid grouping. In addition, the band at 1381cm^{-1} decreases in intensity significantly upon addition of the AuNPs. This band is most likely attributed to an O-H bending mode of the carboxylic acid and again suggests disruption of the carboxylic acid grouping to some degree. Any system arising from the surface reaction of the nanoparticles employed here will inevitably be a mixed species. Some carboxylic acid and/or other carbon oxygen species will remain unreacted, while some amine species will similarly remain unreacted. However, the spectra depicted in Fig. 3.3C are not inconsistent with the formation of a species such as an amide or some other nitrogen-containing moieties.

The TEM images shown in Fig. 3.3D and E clearly reveal the AuNPs as black cores surrounded by the small grayish CQDs (highlighted by red arrows). It is important to note that AuNPs help to visualize CQDs easily in TEM since it is very difficult to collect clear images of bare CQDs. However, in places, instead of the roughly spherical CQDs, the AuNPs were surrounded by a continuous gray layer having very similar contrast to the CQDs - see the bottom of Fig. 3.3D and E. It is thought that this material could have arisen due to the possible reaction of the CQDs in the electron beam. Fig. 3.3F shows the detailed structure of an individual CQD with a lattice spacing distance of 0.24 nm, representing that the CQDs displayed a high-crystalline graphitic structure [30].

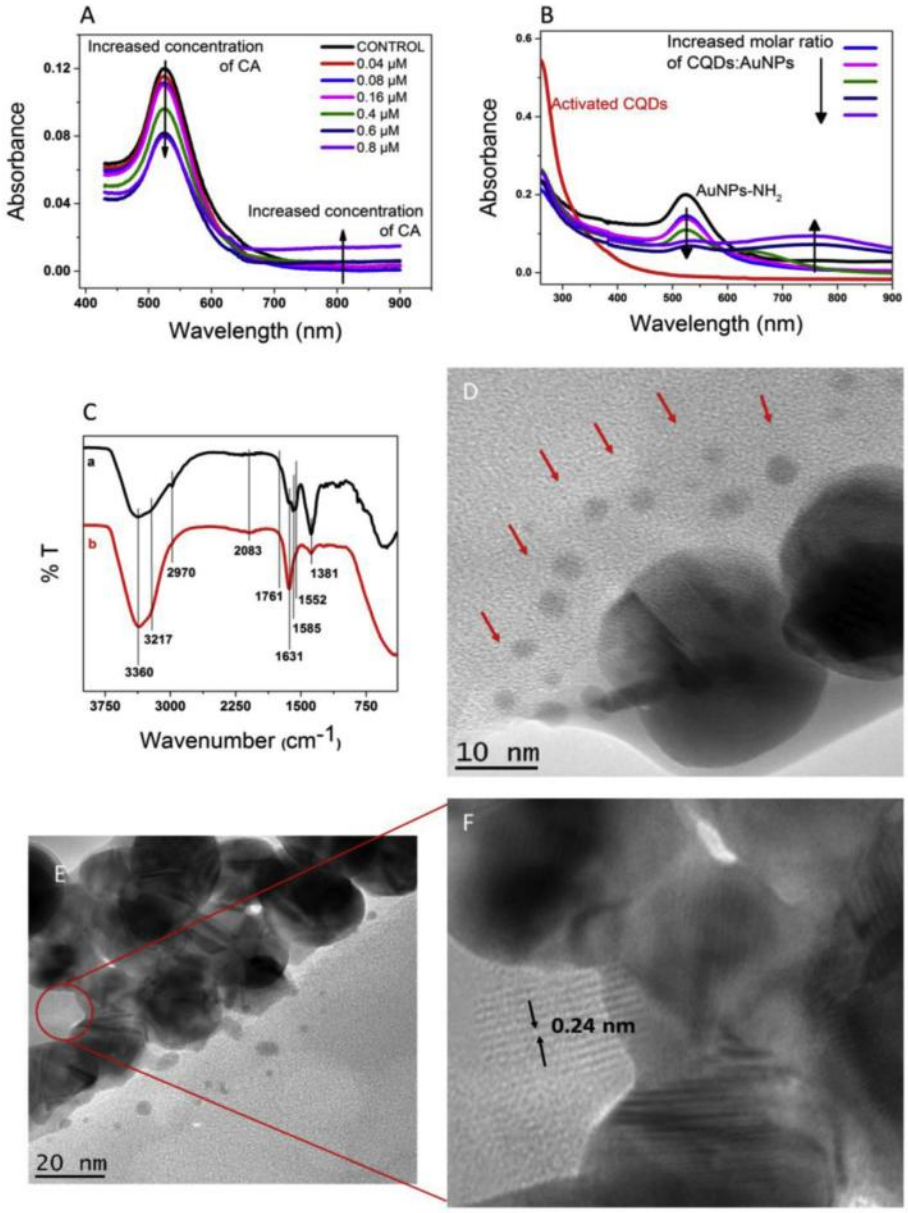


Figure 3.3. (A) UV-Vis spectrum of CA modification of AuNPs, (B) CQD/AuNP hybrids with different molar ratio, (C) FTIR spectrum of CQDs (a, black) and CQD/AuNP (b, red), (D,E) TEM images of the CQD/AuNP hybrid material with different magnifications and showing the detailed structure of the CQDs (E, F)

3.4.2 Optimization of the CQDS/AuNPs-GOx biosensor and electrochemical impedance spectroscopy

Effect of enzyme concentration and pH

Responses of the biosensors prepared using 5 different concentrations of GOx enzyme are presented in Fig. 3.4A. The optimum concentration of enzyme determined to be 0.04U.

Increased concentrations of the biomolecule on the electrode surface showed decreased amperometric responses probably due to oversaturation of the matrix and limited conformational flexibility of the enzyme which results as a catalytic activity loss [31].

The pH-dependent response of the CQD/AuNPs-GOx biosensor was also evaluated since the pH is an important factor which influences the current response of the glucose biosensors. Even though the optimum pH range for free glucose oxidase enzyme (*A. niger*) has been reported to be 3.5 - 6.5 [32], the immobilized glucose oxidase may perform well in varying pH values depending on the immobilization process and/or the nature of the immobilization matrix [31]. As shown in Fig. 3.4B, the immobilized glucose oxidase enzyme exhibited a good catalytic activity in a range from pH 5.4 to pH 7.4 which may attributed to the positive contribution of the nanohybrid material as a matrix. Therefore, the pH 7.4 was chosen as optimum condition.

Electrochemical Impedance Spectroscopy (EIS)

Fig. 3.4C illustrates the Nyquist plots of the electrodes at different modification steps, namely the bare gold electrode, the cysteamine modified electrode, the CQD/AuNP nanohybrid attached electrode and the GOx immobilized electrode in the presence of 2.5mM $Fe(CN)_6^{3-/4-}$ as a redox probe. The bare gold electrode (■) showed an obvious a straight line at lower frequencies, corresponding to a diffusion-controlled electrochemical redox process of species from the solution to the electrode interface. It also showed a semicircular plot at higher frequencies which represents the so-called kinetically controlled region and which is consistent with the magnitude of the charge transfer resistance value, Rct =177Ω which represents the opposition to the electron transfer reaction arising from the electrode. Self-assembly of cysteamine (●) on the electrode surface gave rise to electrostatic interactions between the positive amino groups of the cysteamine and negatively charged redox probe, resulting a decrease of the charge transfer resistance, R_{ct} (52.8Ω). After treatment of cysteamine modified surface with CQD/AuNP moieties (▲), the diameter of the semicircular region increased slightly in comparison to that observed for the cysteamine modified surface (R_{ct}, 80Ω). This result clearly demonstrates the conductivity of the nano-hybrid material developed here and the positive contribution to the electrochemical performance of the interface that arises via the use

of nano-sized materials. Immobilization of the GOx dramatically increased the charge transfer resistance as expected (R_{ct}, 1021Ω, ▼, which implies that the immobilization process was successful [31].

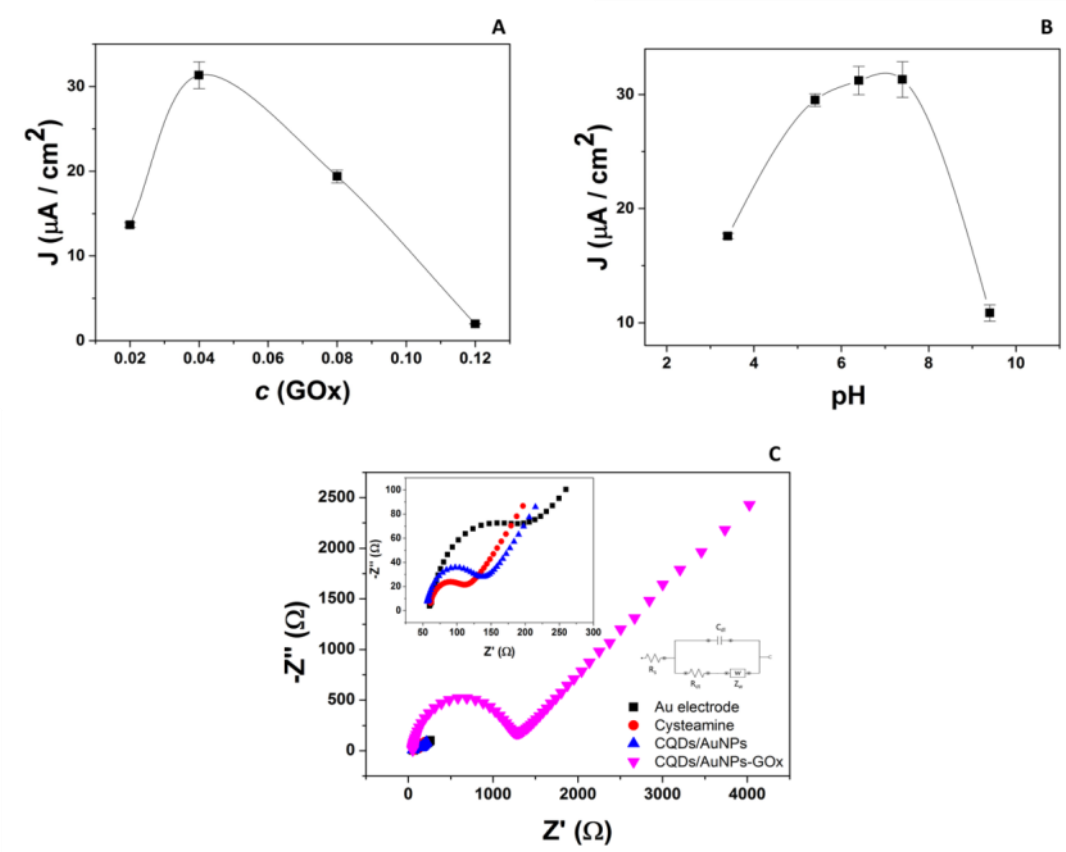


Figure 3.4. (A) GOx concentration and (B) pH optimization and (C) Nyquist plots of the impedance spectra of bare gold electrode (■, black), cysteamine modified surface (●, red), CQD/AuNP hybrid material attached to the gold electrode (▲, blue) and GOx immobilized electrode (▼, pink) in the presence of 2.5 mM Fe(CN)63-/4- as a redox probe in 0.01 M PBS (pH 7.4) solution containing 0.1 M KCl, over the frequency range from 105 to 0.01 Hz, a bias potential of +0.24 V vs Ag/AgCl and an amplitude of 0.01 V.

3.4.3 Direct electrochemistry of the CQD/AuNP-GOx modified gold surfaces

The DET between the immobilized GOx and CQD/AuNP modified gold electrode was studied by cyclic voltammetry. The biosensor created showed a pair of redox peaks at a formal potential of -0.32V (Fig. 3.5A, black). In the presence of glucose in nitrogen saturated solution an increase in the anodic peak current and a decrease in the cathodic peak current was observed. These results confirm that the CQD/AuNP-GOx biosensor developed here demonstrates DET-based biocatalytic activity towards glucose. The bioelectrocatalytic activity of GOx towards oxygen

was an important factor to consider in terms of the observed biocatalytic activity of GOx immobilized on the electrode surface. The presence of oxygen may affect the DET reaction of GOx and hence also glucose sensing at negative potentials since oxygen can oxidize the GOx ($FADH_2$). For the CQD/AuNP-GOx biosensor developed here, oxygen showed a very strong catalytic activity toward the reduction of cofactor FAD of GOx. Fig. 3.5A (blue line) shows the CV of the biosensor in oxygen saturated PBS. In comparison to the CV recorded in nitrogen saturated PBS, the CV in oxygen saturated PBS exhibited a dramatic increase of the cathodic peak current and a decrease of the anodic peak since O_2 may compete with the electrode for $FADH_2$. At the interface of the developed biosensor O_2 molecules easily and rapidly may reach to the cofactor of GOx and accelerate the oxidation reaction of $FADH_2$ by O_2 [33]. Furthermore, the CVs of the CQD/AuNP-GOx biosensor were recorded with increasing concentrations of glucose in oxygen saturated PBS. As shown in Fig. 3.5A (pink and green dash lines), an increase of the glucose concentration resulted in a significant decrease of the FAD reduction peak current. The decrease of the reduction peak current could also be attributed to the consumption of O_2 from the natural enzymatic glucose oxidation [34]. These results clearly demonstrate the bioelectrocatalytic activity of the immobilized enzyme active site.

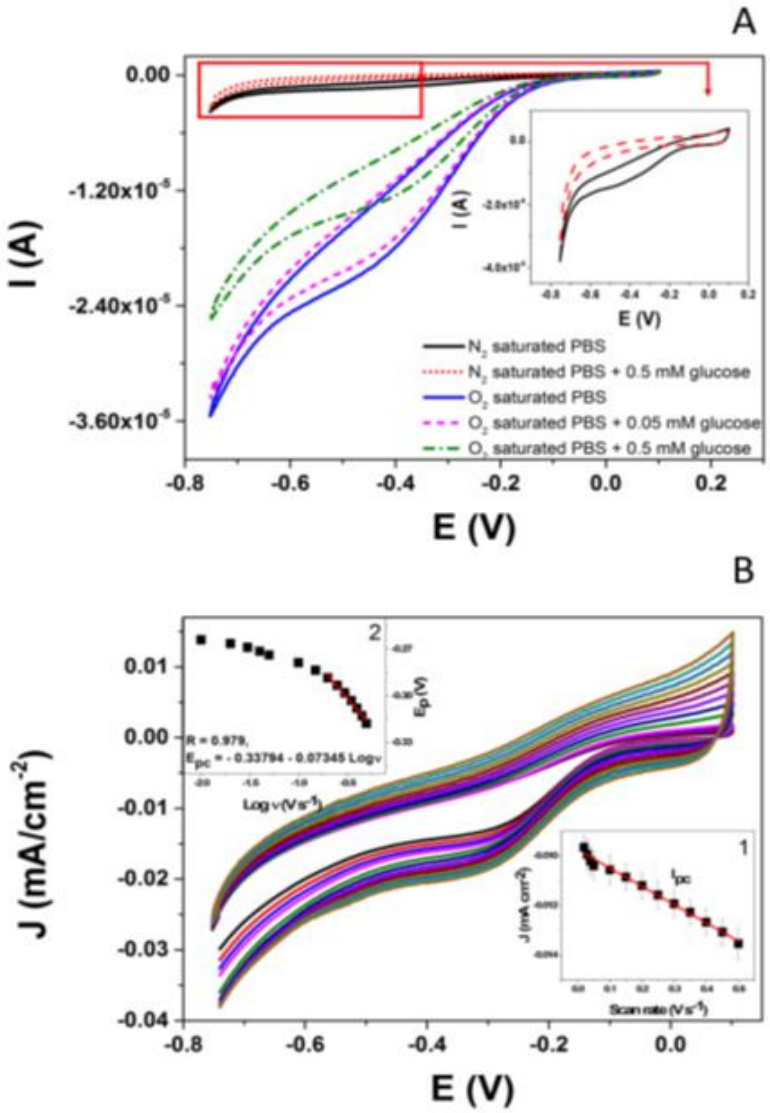


Figure 3.5. (A) Cyclic voltammograms of the CQD/AuNP-GOx biosensor in nitrogen-saturated PBS solution (black), in the presence of 0.5 mM glucose (red), in oxygen saturated PBS solution (blue), in the presence of 0.05 mM (pink) and 0.5 mM (green) glucose. Inset: enlarged graph of nitrogen-saturated PBS and in the presence of glucose. (B) Cyclic voltammograms of CQD/AuNP-GOx modified gold electrode in N2-saturated PBS at different scan rates ranging from 0.2 to 0.5V s-1. Inset 1: plots of anodic and cathodic peak currents vs. scan rate, and inset 2: plots of peak potentials vs. logarithmic scan rate.

The effect of scan rate (υ) on the DET of the immobilized GOx at the CQD/AuNP modified gold surface was also investigated. The CVs are illustrated in Fig. 3.5B. The linear increase of cathodic (I_{pc}) peak currents with increased scan rate from 0.2 to 0.5V s^{-1} in nitrogen saturated PBS, confirmed the surface-controlled electrochemical process (Fig. 3.5B-inset-1). The linear regression equations for the redox process were written as I_{pc}=-0.007υ-0.01; R^2=0.989. This

behavior can be defined by Laviron theory for the calculation of the heterogeneous electron transfer rate constant (k_s) and transfer coefficient (α), for the cases that ΔE_p are smaller than 200/n mV [35]. Fig. 3.5B-inset-2 shows the linear plots of E_{pc} versus log υ at higher scan rates. According to Laviron theory, α was calculated to be 0.40 and 0.6 from the slopes of those linear plots of E_{pc} using the equations -2.303RT/αnF. Using the equation k_s=αnFυ/RT, the calculated value for k_s was 4.66 s^{-1} which is indicative of a fast electron transfer. The k_s value obtained for the CQD/AuNP-GOx biosensor developed here is significantly higher than those reported previously for the biosensors prepared by the use of carbon based nanomaterials or gold nanoparticles such as AuNPs-activated graphite (1.90 s^{-1}) [36], graphene (2.83 s^{-1})[37], boron-doped carbon nanotubes (1.56 s^{-1})[38] and AuNPs-carbon nanotubes (2.2 s^{-1}) [39].

3.4.4 Chronoamperometric detection of glucose

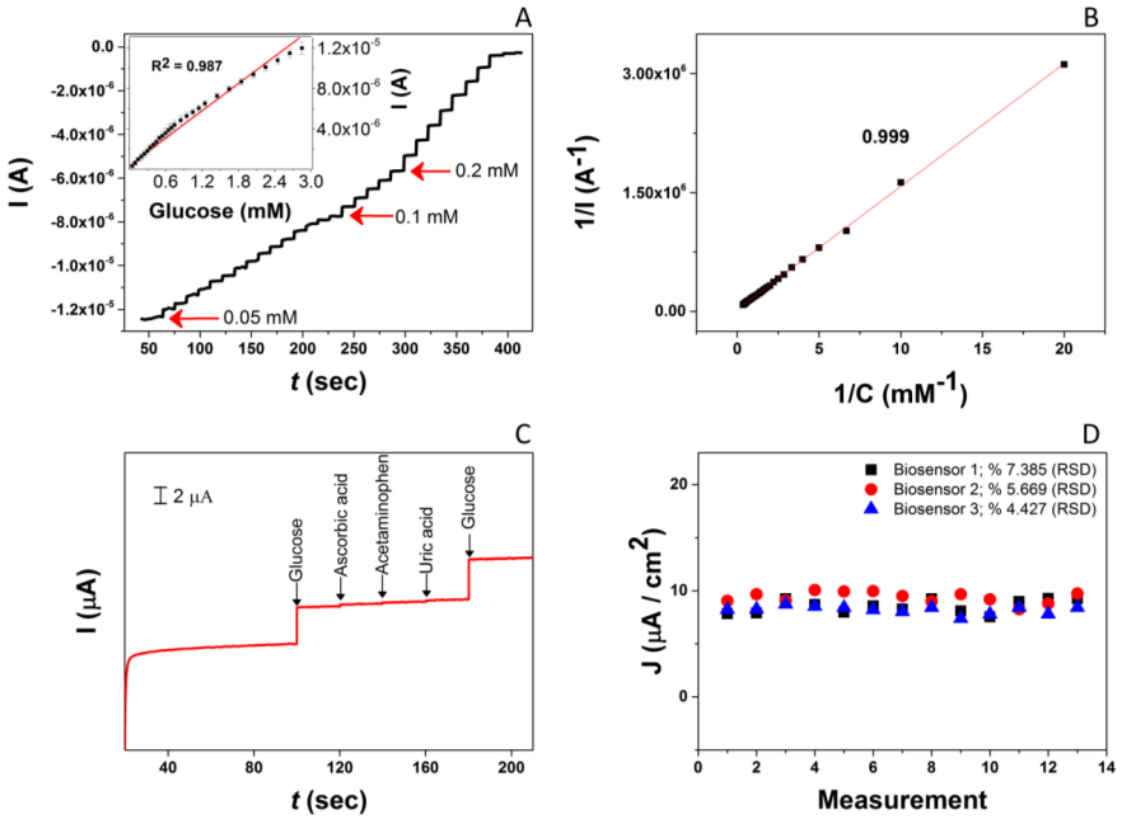


Figure 3.6. (A) The chronoamperometric response of the CQD/AuNP-GOx biosensor in response to the serial addition of glucose in O2-saturated PBS at a working potential of -0.6 V (the equilibration time for addition of each glucose step was ~ 30 s.), inset; the corresponding calibration curve, (B) The Lineweaver-Burk plot of the CQD/AuNP-GOx biosensor, (C) Chronoamperometric response of the CQD/AuNP-GOx biosensor for the addition of 1 mM glucose, 0.1mM acetaminophen, 0.1 mM uric acid and 1 mM glucose in O2 saturated PBS at an applied

potential of -0.6 V, (the equilibration time for each addition step was ~ 30 s.) and (D) reusability of CQD/AuNP-GOx biosensor.

The detection of glucose was performed by chronoamperometry at an applied potential of -0.6V in O_2-saturated PBS. Fig. 3.6A shows the effects of successive additions of glucose into the electrochemical cell with a time interval of 10s. As shown in Fig. 3.6B, the calibration curve corresponding to the chronoamperometric response exhibits two a linear response to glucose ranging from 0.05mM to 2.85mM (R=0.987) with a detection limit of 17µM (S/N=3). The detection limit was calculated using the formula, $3s_b/S$, where s_b was the standard deviation of the blank and S was the sensitivity of the biosensor [40]. In comparison to the other published glucose biosensors (Table 1), the obtained detection limit is relatively high. This drawback of the biosensor may overcome by scaling down approach of the overall biosensor. Furthermore, the equations of the linear responses of linear range was $y=4.488\cdot10^{-6} x + 3.917\cdot10^{-7}$. The sensitivity of the CQD/AuNP-GOx modified gold electrode was calculated to be 47.24µA mM^{-1} cm^{-2}, which is higher than the value of previously reported electrochemical biosensors, see Table 1. The microfabricated gold electrode surface area is 0.095 cm^2, which is a larger surface area than very common commercial 3mm diameter disk gold electrodes' surface area. In this conditions, biosensor exhibited a high sensitivity towards glucose. This result shows that the CQD/AuNP nanohybrid material provides a matrix which improves/protects the catalytic activity of the immobilized enzyme.

The apparent Michalis-Menten constant (K_m^{app}), which is an indicator of enzyme-substrate reaction kinetics, could be used to investigate the reaction kinetics of GOx on the CQD/AuNP nanohybrid modified electrodes. Fig. 3.6C shows the corresponding Lineweaver-Burk plots (1/I vs. 1/C) of the glucose biosensor developed here which has an equation of y=154978.8x + 27356.5 (R=0.999). The K_m^{app} value was estimated to be 5.66mM using the Lineweaver-Burk equation. This relatively low value of K_m^{app} is indicative of the high affinity between the enzyme and substrate. A comparison of the analytical performance of the biosensor developed here with several other enzymatic electrochemical biosensors is shown in Table 1.

Table 3.1. Comparison of the analytical performance of several carbon and/or AuNPs based enzymatic glucose biosensors

Glucose biosensor	Sensitivity	Detection Limit	Linear range	K_m	k_s	Reproducibility % RSD	Ref.
CQDs-AuNPs/GOx-Au electrode	47.24 μA mM^{-1} cm^{-2}	17 μM	0.05 - 2.85	5.66	4.66 s^{-1}	5.2 % (n=5)	This work
PPF/GOx/CNT/PPF-Au electrode	42 μA mM^{-1} cm^{-2}	6 μM	0.025 mM - 2.2 mM	11 mM	-	3 % (n=4)	[41]
AuNP-SAMs-PNT/HRP-GOx -Au electrode	0.3 mA M^{-1}	73.1 μM	0.5 mM - 2.4 mM	11 mM	-	5.74 % (n=3)	[42]
GOx/CNx-MWNTs/GCE	13.0 μA mM^{-1} cm^{-2}	0.01 mM	0.02 - 1.02	2.2 mM	4.6 s^{-1}	3.9 % (n=5)	[43]
GRA–PANI/CS–GOD	22.1 μA mM^{-1} cm^{-2}	2.769 μM	0.010-1.48 mM	1.69 m M	-	% 4.40 (n=4)	[44]
Cellulose–MWCNT–GOx	6.57 μA mM^{-1} cm^{-2}	-	0.05-1.0 mM	1.10 mM	-	acceptable	[45]
GOD-ZnO/CRG	89.84 μA m M^{-1} cm^{-2}	-	0.2- 1.6 mM	-	0.92 s^{-1}	-	[46]
Nafion/GOD/C–ZnO	35.3 μA mM^{-1} cm^{-2}	1 μM	0.01-1.6 mM	1.54 mM	4.7 s^{-1}	2.3 % (n=5)	[47]
GOx/chitosan/TiO_2 nanorod/graphite microfiber	18.6 mA M^{-1} cm^{-2}	2.2 μM	-	6.62 mM	-	3.3 % (n=10)	[48]
GOx/Pt-graphite	105 μA mM^{-1} cm^{-2}	0.010 mM	33 μM– 0.9 mM	1.2 mM	-	9 % (n= 3)	[49]
GR-MWNTs/AuNPs/GOx	(1)0.695 μA mM^{-1} cm^{-2} (2)0.238 μA mM^{-1} cm^{-2}	(1)4.1 μM (2)0.95 mM	(1)10 μM – 2 mM (2)2 mM – 5.2 mM	-	3.36 s^{-1}	2.37 % (n=7)	[50]
GCE/RGO–GOx	1.85 μA mM^{-1} cm^{-2}	-	0.1–27 mM	-	4.8 s^{-1}	4.9 % (n=4)	[51]
GCE/bMWCNTs-HBPEI/AuNPs-$B(OH)_2$/GOx	28.6 mA M^{-1} cm^{-2}	0.8 μM	2.5×10^{-4}M-5.0×10^{-3}M	8.1×10^{-3} M	-	4.5 % (n=10)	[52]
ERGO–MWCNT/GOx/Nf	7.95 μA mM^{-1} cm^{-2}	4.7 μM	0.01– 6.5 mM	-	3.02 s^{-1}	2.5 % (n=7)	[53]
RGO/HAp/GOx	16.9 μA mM^{-1} cm^{-2}	0.03 mM	0.1–11.5 mM	-	3.50 s^{-1}	-	[54]
GOD–graphene–chitosan/GCE	37.93 μA mM^{-1} cm^{-2}	0.02 mM	0.08 mM - 12 mM	4.4 mM	2.83 s^{-1}	5.3 % (n=6)	[55]
Nafion–GOx–SWCNHs/GCE	1.06 μA/mM	6 μM	0 - 6.0 mM	8.5 mM	3.0 s^{-1}	-	[56]
GOx/(AuNPs/MWCNT)5-Au electrode	19.27 μA mM^{-1} cm^{-2}	2.3 μM	0.02 μM – 10 mM	6.7 mM	-	less than 4.2% (n=6)	[57]

3.4.5 Interference effect, reproducibility and reusability of the CQD/AuNP-GOx biosensor

The selectivity of the CQD/AuNP-GOx biosensor was studied to investigate the effect of possible interferences such as acetaminophen and uric acid on the response of the biosensor toward glucose. 0.1mM glucose solution was chosen in order to evaluate the selectivity.

Chronoamperometry was performed in an O_2-saturated PBS solution at an applied voltage -0.6V and 1mM glucose, 0.1mM ascorbic acid 0.1mM acetaminophen, 0.1mM uric acid and 1mM glucose were added to the electrochemical cell every 10 seconds, respectively (Fig. 3.6C). The interference effect was calculated using the equation; $[I_{glucose}-I_{interference}]/I_{glucose}$ in order to evaluate the change of the 1mM glucose response in the presence of the ascorbic acid, acetaminophen and uric acid. The response of the glucose changed % 7.09 (±1.28), (*n*=3) in the presence of the interfering species. Thus, it may be seen that that the CQD/AuNP-GOx biosensor developed here exhibits levels of selectivity which are comparable to or better than those reported previously for some other electrode systems [58, 59].

The reproducibility of the CQD/AuNP-GOx biosensor was studied by chronoamperometry. The chronoamperometric trace was recorded in PBS (pH 7.4) at -0.6V in the presence of 0.05mM glucose addition under stirred conditions. Within a series of 5 experiments, a relative standard deviation (RSD) of 5.2% was achieved, demonstrating an acceptable level of reproducibility [43, 60] - certainly in comparison with other glucose sensors. The reusability of the developed biosensor was also studied. Three individual CQDs/AuNPs-GOx biosensors were prepared and their response to glucose was recorded by performing thirteen successive experiments, Fig. 3.6D. The RSD values of each group of electrodes were calculated to be 7.385%, 5.669% and 4.427%, respectively. These results suggest that the developed biosensor has an excellent operational stability, may attributed to the good biocompatibility and the mechanical strength of the developed biosensor to maintain the activity of the immobilized enzyme onto the CQDs/AuNPs surface.

3.4.6 Real sample analysis

Table 3.2. Determination of glucose in sterile human serum samples (n=4)

Sample	Spiked serum (mM)	CQD/AuNP-GOx biosensor (mM)	Recovery (%)
1	0.1	0.107 (±0.011)	106.9
2	0.5	0.514 (±0.030)	102.7
3	2	1.970 (±0.041)	98.5

The biosensor developed here was tested by detecting glucose concentration in sterile human serum to demonstrate the feasibility of the CQD/AuNP-GOx biosensor in real sample analysis. Sterile human serum samples were diluted to be 1:10 ratio in PBS and spiked with several concentrations of glucose. A rapid and stable response for each group of spiked serum was obtained at -0.6 V. By substituting the resulting current value into the calibration curve, the concentration of the sample was calculated. A comparison of the spiked values with the data obtained from the CQD/AuNP-GOx biosensor is shown in Table 3.2. The recovery values are in the range of 98.5 – 106.9% and based on the one sample two paired t-test with %95 confidence interval there was no statistical differences between spiked values and biosensor results (t_1 = 1.23, t_2 = 0.89 and t_3 = -1.44, p>0.05). These results show that the developed biosensor can successfully determine the glucose concentration in human serum.

3.5 Conclusions

The work presented here demonstrates the development of an electrochemical biosensor with a CQD/AuNP-GOx nano-hybrid interface for sensitive glucose detection through the reductive determination of oxygen consumption in the absence of any mediator. The gold electrodes with 0.095 cm^2 active surface area were fabricated by a typical microfabrication flow which includes lithography, deposition and etching. These gold electrodes were characterized and used to construct the biosensor. The resulting CQD/AuNP-GOx biosensor shows high electrocatalytic activity toward glucose. The high sensitivity of 47.24 μA mM^{-1} cm^{-2} and good reproducibility (5.4% RSD, n=5) and selectivity observed at such a nano-hybrid based biosensor suggests that this is likely to be an extremely promising matrix for application to the immobilization of other biorecognition elements. Moreover, the biosensor developed exhibits satisfactory relative error results when employed to determine the glucose concentrations in human serum samples, despite the presence of possible interference agents. We suggest that sensors based on the use of our CQD/AuNP nano-hybrid material as an immobilization matrix may find extensive commercial and personal use in the future, for a variety of important applications.

3.6 Acknowledgments

The authors appreciate the financial support from the Department of Agriculture, Fisheries and the Marine, 14F883. We thank Dr. Gediminas Juska for helpful discussions on carbon quantum dots. And we are also thankful to Dr. Emanuele Pelucchi for his support and providing us some of laboratory equipment.

3.7 References

[1] J.J. Gooding, R. Wibowo, J.Q. Liu, W.R. Yang, D. Losic, S. Orbons, F.J. Mearns, J.G. Shapter, D.B. Hibbert, Protein electrochemistry using aligned carbon nanotube arrays, J Am Chem Soc, 125 (2003) 9006-9007.

[2] I.M. Feigel, H. Vedala, A. Star, Biosensors based on one-dimensional nanostructures, J Mater Chem, 21 (2011) 8940-8954.

[3] J. Zong, X.L. Yang, A. Trinchi, S. Hardin, I. Cole, Y.H. Zhu, C.Z. Li, T. Muster, G. Wei, Photoluminescence enhancement of carbon dots by gold nanoparticles conjugated via PAMAM dendrimers, Nanoscale, 5 (2013) 11200-11206.

[4] L. Cao, X. Wang, M.J. Meziani, F. Lu, H. Wang, P.G. Luo, Y. Lin, B.A. Harruff, L.M. Veca, D. Murray, S.Y. Xie, Y.P. Sun, Carbon dots for multiphoton bioimaging, J Am Chem Soc, 129 (2007) 11318-11319.

[5] T. Feng, X.Z. Ai, G.H. An, P.P. Yang, Y.L. Zhao, Charge-Convertible Carbon Dots for Imaging Guided Drug Delivery with Enhanced in Vivo Cancer Therapeutic Efficiency, Acs Nano, 10 (2016) 4410-4420.

[6] X. Cui, L. Zhu, J. Wu, Y. Hou, P. Wang, Z. Wang, M. Yang, A fluorescent biosensor based on carbon dots-labeled oligodeoxyribonucleotide and graphene oxide for mercury (II) detection, Biosensors and Bioelectronics, 63 (2015) 506-512.

[7] Y.C. Yeh, B. Creran, V.M. Rotello, Gold nanoparticles: preparation, properties, and applications in bionanotechnology, Nanoscale, 4 (2012) 1871-1880.

[8] J.M. Pingarrón, P. Yáñez-Sedeño, A. González-Cortés, Gold nanoparticle-based electrochemical biosensors, Electrochimica Acta, 53 (2008) 5848-5866.

[9] G. Yang, J. Nanda, B. Wang, G. Chen, D.T. Hallinan, Jr., Self-Assembly of Large Gold Nanoparticles for Surface-Enhanced Raman Spectroscopy, ACS Appl Mater Interfaces, 9 (2017) 13457-13470.

[10] D.K. Lim, K.S. Jeon, J.H. Hwang, H. Kim, S. Kwon, Y.D. Suh, J.M. Nam, Highly uniform and reproducible surface-enhanced Raman scattering from DNA-tailorable nanoparticles with 1-nm interior gap, Nat Nanotechnol, 6 (2011) 452-460.

[11] K. Jiang, S. Sun, L. Zhang, Y.H. Wang, C.Z. Cai, H.W. Lin, Bright-Yellow-Emissive N-Doped Carbon Dots: Preparation, Cellular Imaging, and Bifunctional Sensing, Acs Appl Mater Inter, 7 (2015) 23231-23238.

[12] Z.G. Wang, P. Long, Y.Y. Feng, C.Q. Qin, W. Feng, Surface passivation of carbon dots with ethylene glycol and their high-sensitivity to Fe3+, Rsc Adv, 7 (2017) 2810-2816.

[13] Y. Shi, Y. Pan, H. Zhang, Z. Zhang, M.-J. Li, C. Yi, M. Yang, A dual-mode nanosensor based on carbon quantum dots and gold nanoparticles for discriminative detection of glutathione in human plasma, Biosensors and Bioelectronics, 56 (2014) 39-45.

[14] J.H. Deng, Q.J. Lu, Y.X. Hou, M.L. Liu, H.T. Li, Y.Y. Zhang, S.Z. Yao, Nanosensor Composed of Nitrogen-Doped Carbon Dots and Gold Nanoparticles for Highly Selective Detection of Cysteine with Multiple Signals, Anal Chem, 87 (2015) 2195-2203.

[15] R.H. Liu, H. Huang, H.T. Li, Y. Liu, J. Zhong, Y.Y. Li, S. Zhang, Z.H. Kang, Metal Nanoparticle/Carbon Quantum Dot Composite as a Photocatalyst for High-Efficiency Cyclohexane Oxidation, Acs Catal, 4 (2014) 328-336.

[16] J. Zhang, S.H. Yu, Carbon dots: large-scale synthesis, sensing and bioimaging, Mater Today, 19 (2016) 382-393.

[17] S. Sant, S.L. Tao, O.Z. Fisher, Q. Xu, N.A. Peppas, A. Khademhosseini, Microfabrication technologies for oral drug delivery, Advanced Drug Delivery Reviews, 64 (2012) 496-507.

[18] N.A.M. Said, V.I. Ogurtsov, K. Twomey, L.C. Nagle, G. Herzog, Chemically Modified Electrodes for Recessed Microelectrode Array, Procedia Chem, 20 (2016) 12-24.

[19] K. Twomey, E.A. de Eulate, J. Alderman, D.W.M. Arrigan, Fabrication and characterization of a miniaturized planar voltammetric sensor array for use in an electronic tongue, Sensor Actuat B-Chem, 140 (2009) 532-541.

[20] J.H. Deng, Q.J. Lu, N.X. Mi, H.T. Li, M.L. Liu, M.C. Xu, L. Tan, Q.J. Xie, Y.Y. Zhang, S.Z. Yao, Electrochemical Synthesis of Carbon Nanodots Directly from Alcohols, Chem-Eur J, 20 (2014) 4993-4999.

[21] J. Turkevich, P.C. Stevenson, J. Hillier, A Study of the Nucleation and Growth Processes in the Synthesis of Colloidal Gold, Discuss Faraday Soc, (1951) 55-&.

[22] H.T. Li, Z.H. Kang, Y. Liu, S.T. Lee, Carbon nanodots: synthesis, properties and applications, J Mater Chem, 22 (2012) 24230-24253.

[23] A. Sharma, T. Gadly, A. Gupta, A. Ballal, S.K. Ghosh, M. Kumbhakar, Origin of Excitation Dependent Fluorescence in Carbon Nanodots, J Phys Chem Lett, 7 (2016) 3695-3702.

[24] X. Liu, M. Atwater, J. Wang, Q. Huo, Extinction coefficient of gold nanoparticles with different sizes and different capping ligands, Colloids and Surfaces B: Biointerfaces, 58 (2007) 3-7.

[25] H. Ismaili, D.S. Geng, A.X.L. Sun, T.T. Kantzas, M.S. Workentin, Light-Activated Covalent Formation of Gold Nanoparticle Graphene and Gold Nanoparticle-Glass Composites, Langmuir, 27 (2011) 13261-13268.

[26] J. Tan, R. Liu, W. Wang, W. Liu, Y. Tian, M. Wu, Y. Huang, Controllable Aggregation and Reversible pH Sensitivity of AuNPs Regulated by Carboxymethyl Cellulose, Langmuir, 26 (2010) 2093-2098.

[27] T. Wang, X. Hu, X. Qu, S. Dong, Noncovalent Functionalization of Multiwalled Carbon Nanotubes: Application in Hybrid Nanostructures, The Journal of Physical Chemistry B, 110 (2006) 6631-6636.

[28] C. Zheng, Y. Zheng, W. Chen, L. Wei, Encapsulation of graphene oxide/metal hybrids in nanostructured sol–gel silica ORMOSIL matrices and its applications in optical limiting, Optics & Laser Technology, 68 (2015) 52-59.

[29] M. Akrami, S. Balalaie, S. Hosseinkhani, M. Alipour, F. Salehi, A. Bahador, I. Haririan, Tuning the anticancer activity of a novel pro-apoptotic peptide using gold nanoparticle platforms, Sci Rep-Uk, 6 (2016).

[30] P.F. Shen, Y.S. Xia, Synthesis-Modification Integration: One-Step Fabrication of Boronic Acid Functionalized Carbon Dots for Fluorescent Blood Sugar Sensing, Anal Chem, 86 (2014) 5323-5329.

[31] V. Buk, E. Emregul, K.C. Emregul, Alginate copper oxide nano-biocomposite as a novel material for amperometric glucose biosensing, Mat Sci Eng C-Mater, 74 (2017) 307-314.

[32] S.B. Bankar, M.V. Bule, R.S. Singhal, L. Ananthanarayan, Glucose oxidase - An overview, Biotechnol Adv, 27 (2009) 489-501.

[33] Y.F. Bai, T.B. Xu, J.H.T. Luong, H.F. Cui, Direct Electron Transfer of Glucose Oxidase-Boron Doped Diamond Interface: A New Solution for a Classical Problem, Anal Chem, 86 (2014) 4910-4918.

[34] S. Kumar-Krishnan, M.G.F. Garcia, E. Prokhorov, M. Estevez-Gonzalez, R. Perez, R. Esparza, M. Meyyappan, Synthesis of gold nanoparticles supported on functionalized nanosilica using deep eutectic solvent for an electrochemical enzymatic glucose biosensor, J Mater Chem B, 5 (2017) 7072-7081.

[35] E. Laviron, General Expression of the Linear Potential Sweep Voltammogram in the Case of Diffusionless Electrochemical Systems, J Electroanal Chem, 101 (1979) 19-28.

[36] M. Velmurugan, S. Sakthinathan, S.M. Chen, C. Karuppiah, Direct Electron Transfer of Glucose Oxidase and Electrocatalysis of Glucose Based on Gold Nanoparticles/Electroactivated Graphite Nanocomposite, Int J Electrochem Sc, 10 (2015) 6663-6671.

[37] X.H. Kang, J. Wang, H. Wu, I.A. Aksay, J. Liu, Y.H. Lin, Glucose Oxidase-graphene-chitosan modified electrode for direct electrochemistry and glucose sensing, Biosens Bioelectron, 25 (2009) 901-905.

[38] C.Y. Deng, J.H. Chen, X.L. Chen, C.H. Mao, L.H. Nie, S.Z. Yao, Direct electrochemistry of glucose oxidase and biosensing for glucose based on boron-doped carbon nanotubes modified electrode, Biosens Bioelectron, 23 (2008) 1272-1277.

[39] H.F. Zhang, Z.C. Meng, Q. Wang, J.B. Zheng, A novel glucose biosensor based on direct electrochemistry of glucose oxidase incorporated in biomediated gold nanoparticles-carbon nanotubes composite film, Sensor Actuat B-Chem, 158 (2011) 23-27.

[40] V. Mani, B. Devadas, S.-M. Chen, Direct electrochemistry of glucose oxidase at electrochemically reduced graphene oxide-multiwalled carbon nanotubes hybrid material modified electrode for glucose biosensor, Biosensors and Bioelectronics, 41 (2013) 309-315.
[41] H. Muguruma, Y. Shibayama, Y. Matsui, An amperometric biosensor based on a composite of single-walled carbon nanotubes, plasma-polymerized thin film, and an enzyme, Biosensors and Bioelectronics, 23 (2008) 827-832.
[42] B.-W. Park, R. Zheng, K.-A. Ko, B.D. Cameron, D.-Y. Yoon, D.-S. Kim, A novel glucose biosensor using bi-enzyme incorporated with peptide nanotubes, Biosensors and Bioelectronics, 38 (2012) 295-301.
[43] S. Deng, G. Jian, J. Lei, Z. Hu, H. Ju, A glucose biosensor based on direct electrochemistry of glucose oxidase immobilized on nitrogen-doped carbon nanotubes, Biosensors and Bioelectronics, 25 (2009) 373-377.
[44] X. Feng, H. Cheng, Y. Pan, H. Zheng, Development of glucose biosensors based on nanostructured graphene-conducting polyaniline composite, Biosensors and Bioelectronics, 70 (2015) 411-417.
[45] X. Wu, F. Zhao, J.R. Varcoe, A.E. Thumser, C. Avignone-Rossa, R.C.T. Slade, Direct electron transfer of glucose oxidase immobilized in an ionic liquid reconstituted cellulose–carbon nanotube matrix, Bioelectrochemistry, 77 (2009) 64-68.
[46] Y. Zhao, W. Li, L. Pan, D. Zhai, Y. Wang, L. Li, W. Cheng, W. Yin, X. Wang, J.B. Xu, Y. Shi, ZnO-nanorods/graphene heterostructure: a direct electron transfer glucose biosensor, Sci Rep, 6 (2016) 32327.
[47] J. Liu, C. Guo, C.M. Li, Y. Li, Q. Chi, X. Huang, L. Liao, T. Yu, Carbon-decorated ZnO nanowire array: A novel platform for direct electrochemistry of enzymes and biosensing applications, Electrochemistry Communications, 11 (2009) 202-205.
[48] J. Zhang, X. Yu, W.B. Guo, J.C. Qiu, X.N. Mou, A.X. Li, H. Liu, Construction of titanium dioxide nanorod/graphite microfiber hybrid electrodes for a high performance electrochemical glucose biosensor, Nanoscale, 8 (2016) 9382-9389.

[49] A. Abellán-Llobregat, I. Jeerapan, A. Bandodkar, L. Vidal, A. Canals, J. Wang, E. Morallón, A stretchable and screen-printed electrochemical sensor for glucose determination in human perspiration, Biosensors and Bioelectronics, 91 (2017) 885-891.

[50] R. Devasenathipathy, V. Mani, S.-M. Chen, S.-T. Huang, T.-T. Huang, C.-M. Lin, K.-Y. Hwa, T.-Y. Chen, B.-J. Chen, Glucose biosensor based on glucose oxidase immobilized at gold nanoparticles decorated graphene-carbon nanotubes, Enzyme Microb Tech, 78 (2015) 40-45.

[51] B. Unnikrishnan, S. Palanisamy, S.-M. Chen, A simple electrochemical approach to fabricate a glucose biosensor based on graphene–glucose oxidase biocomposite, Biosensors and Bioelectronics, 39 (2013) 70-75.

[52] M. Eguílaz, R. Villalonga, J.M. Pingarrón, N.F. Ferreyra, G.A. Rivas, Functionalization of bamboo-like carbon nanotubes with 3-mercaptophenylboronic acid-modified gold nanoparticles for the development of a hybrid glucose enzyme electrochemical biosensor, Sensors and Actuators B: Chemical, 216 (2015) 629-637.

[53] V. Mani, B. Devadas, S.-M. Chen, Direct electrochemistry of glucose oxidase at electrochemically reduced graphene oxide-multiwalled carbon nanotubes hybrid material modified electrode for glucose biosensor, Biosensors and Bioelectronics, 41 (2013) 309-315.

[54] G. Bharath, R. Madhu, S.M. Chen, V. Veeramani, A. Balamurugan, D. Mangalaraj, C. Viswanathan, N. Ponpandian, Enzymatic electrochemical glucose biosensors by mesoporous 1D hydroxyapatite-on-2D reduced graphene oxide, J Mater Chem B, 3 (2015) 1360-1370.

[55] X. Kang, J. Wang, H. Wu, I.A. Aksay, J. Liu, Y. Lin, Glucose Oxidase–graphene–chitosan modified electrode for direct electrochemistry and glucose sensing, Biosensors and Bioelectronics, 25 (2009) 901-905.

[56] X. Liu, L. Shi, W. Niu, H. Li, G. Xu, Amperometric glucose biosensor based on single-walled carbon nanohorns, Biosensors and Bioelectronics, 23 (2008) 1887-1890.

[57] P. Si, P. Kannan, L. Guo, H. Son, D.-H. Kim, Highly stable and sensitive glucose biosensor based on covalently assembled high density Au nanostructures, Biosensors and Bioelectronics, 26 (2011) 3845-3851.

[58] X. Chen, J. Chen, C. Deng, C. Xiao, Y. Yang, Z. Nie, S. Yao, Amperometric glucose biosensor based on boron-doped carbon nanotubes modified electrode, Talanta, 76 (2008) 763-767.

[59] X. Chu, D. Duan, G. Shen, R. Yu, Amperometric glucose biosensor based on electrodeposition of platinum nanoparticles onto covalently immobilized carbon nanotube electrode, Talanta, 71 (2007) 2040-2047.
[60] M. Baghayeri, H. Veisi, M. Ghanei-Motlagh, Amperometric glucose biosensor based on immobilization of glucose oxidase on a magnetic glassy carbon electrode modified with a novel magnetic nanocomposite, Sensors and Actuators B: Chemical, 249 (2017) 321-330.

3.8 Supporting Information

Microfabrication and characterization of gold electrodes

Gold working electrodes were fabricated using microfabrication technology. Silicon was chosen as substrate. Briefly, a silicon oxide layer was growth on the silicon wafer. Prior to metal deposition substrates were treated with an Ar plasma which improved the metal adhesion to the substrate. After this titanium and gold were deposited using e-beam evaporation and the metal layers were patterned using a lift off procedure. A passivation layer of silicon nitride (S_3N_4) of 500 nm thickness was deposited by plasma-enhanced chemical vapour deposition. This was followed by a passivation lithography process and passivation etching. The Si_3N_4 passivation layer was etched in an inductively coupled plasma etch system (ICP) and the remaining resist was removed. Finally, the substrate was covered a plasma layer to protect the wafer surface during dicing. Fig. 3.S1A and B depict the microfabrication process and show a schematic representation of the wafer after fabrication.

Prior to the experiments, gold electrodes were pre-treated carefully to remove the protection layer. Firstly, electrodes were immersed in boiling acetone, then they were sonicated in isopropyl alcohol, washed with distilled water and dried with N_2 flow. Dry electrodes were placed in a plasma cleaner for 10 minutes to remove the organic residues and increase the hydrophilicity of the surface. Electrochemical characterization of the bare gold surface was studied by running a CV in 0.5 M H_2SO_4 solution between -0.1 V and +1.5 V electrode potential with a scan rate of 0.1 V s^{-1}. As can be seen in Fig. 3.S1.C, a sharp peak corresponding to gold

oxide reduction was observed at about +0.9 V and a broad peak corresponding to gold oxidation was observed in the range of +1.1 to +1.35 V, for the microfabricated gold electrode [1, 2]. After this cyclic voltammetry (CV) experiments were performed between potentials of -0.2 V and +0.6 V on both the micro array electrodes and the planar electrodes in a 2.5 mM $Fe(CN_6)^{3-/4-}$ solution containing 0.1 M KCl with a scan rate of 0.01 V s^{-1}. The microfabricated gold electrode with a surface area of 0.095 cm^2 showed a typical peak-shaped voltammogram (Fig. 3.S1. D) arising due to the diffusion characteristics of the electrodes[3].

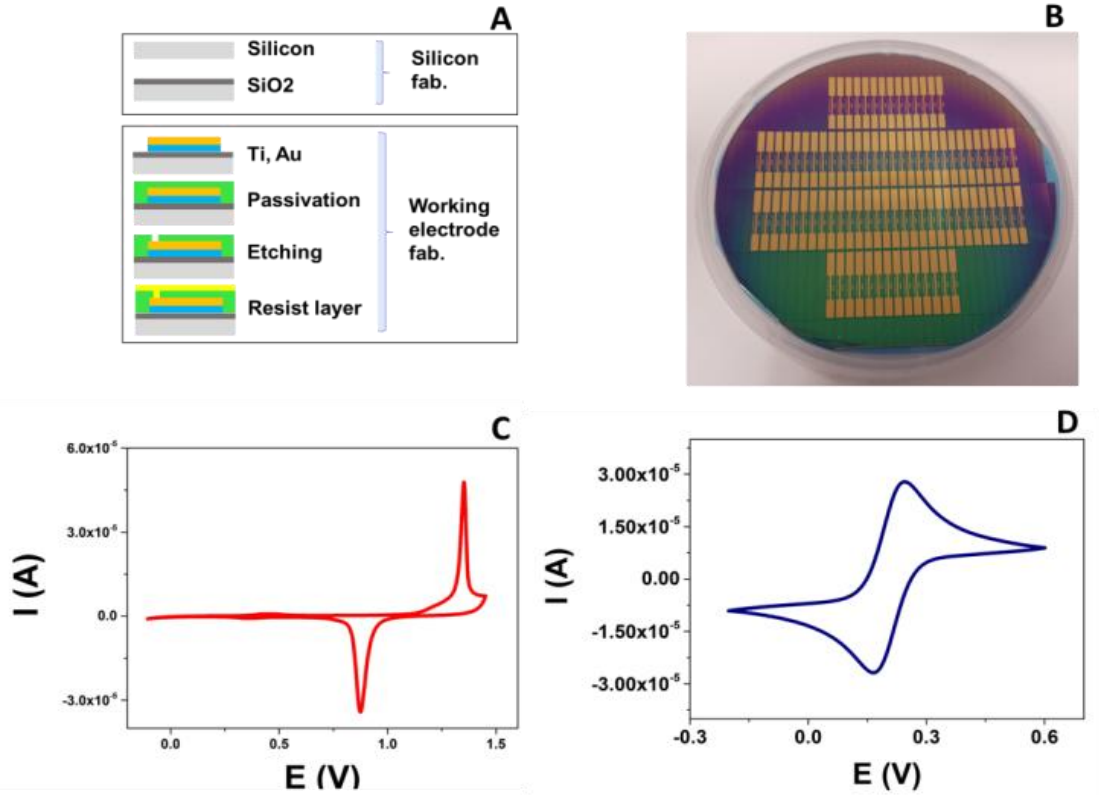


Figure 3.S1. A cross-sectional schematic of the microfabrication process (A), a picture of microfabricated gold working electrodes (B), cyclic voltammogram for the clean gold electrodes in 0.5 M H2SO4 solution (C) and voltammetric response of gold electrode in a 2.5 mM Fe(CN6)3-/4- solution containing 0.1 M KCl, scan rate: 0.01 V s-1 (D).

References

[1] M.D. Scanlon, U. Salaj-Kosla, S. Belochapkine, D. MacAodha, D. Leech, Y. Ding, E. Magner, Characterization of Nanoporous Gold Electrodes for Bioelectrochemical Applications, Langmuir, 28 (2012) 2251-2261.

[2] L.D. Burke, P.F. Nugent, The Electrochemistry of Gold: I The Redox Behaviour of the Metal in Aqueous Media, Gold Bull, 30 (1997) 43-53.

[3] A.J. Bard, J.A. Crayston, G.P. Kittlesen, T.V. Shea, M.S. Wrighton, Digital-Simulation of the Measured Electrochemical Response of Reversible Redox Couples at Microelectrode Arrays - Consequences Arising from Closely Spaced Ultramicroelectrodes, Anal Chem, 58 (1986) 2321-2331.

CHAPTER 4

Enzymatic glucose detection at planar and micro scale

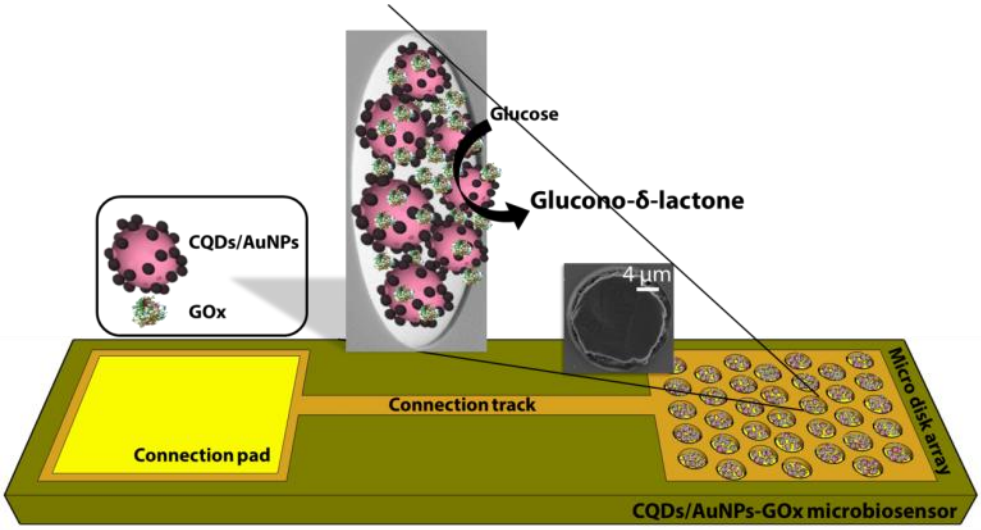
4. A highly sensitive glucose biosensor based on a micro disk array electrode design modified with carbon quantum dots and gold nanoparticles

This work has been published in the journal of ELSEVIER Electrochimica Acta, 2019, 298, 97-105

4.1 Abstract

A miniaturized biosensor for glucose was prepared by immobilizing glucose oxidase (GOx) onto a carbon quantum dots (CQDs)-gold nanoparticles (AuNPs) nanohybrid material which was in turn attached to gold micro disk array electrodes. The gold micro disk array electrodes (GDAE) were microfabricated on Si substrate using electronics-standard lithography, deposition and etching techniques. Each microelectrode consisted of 85 gold disk electrodes with 20 μm diameter and 200 μm inter-electrode distance and were located hexagonally. The electrodes were studied by scanning electron microscopy (SEM), atomic force microscopy (AFM) and cyclic voltammetry (CV). CV of the bare electrodes showed a symmetrical sigmoidal voltammogram arising from their radial diffusion profile. The electrodes developed were used to fabricate a miniaturised glucose biosensor. The resulting biosensor exhibited a high sensitivity of 626.06 μA mM^{-1} cm^{-2} towards glucose detection with excellent reproducibility and reusability. The superior performance of the biosensor is discussed in relation to the use of the micron-sized low density disk array electrodes.

Key words: Glucose microbiosensor, micro disk array electrodes, carbon quantum dots, gold nanoparticles, microfabrication



Graphical abstract, note that the sizes of the components shown are not drawn to scale.

4.2 Introduction:

There is currently increasing interest in the miniaturisation of electrodes from the planar scale to the micron or even the nano scale for the development of next-generation biosensors since the consequent reduction in electrode surface area is expected to result in enhanced sensitivities, increased signal-to-noise ratios and decreased detection limits [1, 2]. In addition such miniaturised electrodes are found to reach steady-state currents very rapidly due to their radial diffusion properties [3, 4]. In this regard, micro disk array electrodes are currently the most commonly studied microelectrode geometry since they are easily able to attain true steady-state current levels. The other advantage of such devices are the decreased volume of the sample and batch production of the electrodes which both may decrease the cost per device at industrial scale [5]. The use of microfabrication methods in the silicon technologies including lithography, deposition and etching to fabricate array electrodes offer excellent precision and high resolution for nano-scale features. Furthermore, the biocompatibility of silicon and the flexibility of the arrangement of the arrays with various shape, size and dimensions make them promising components for various bio-application such as biosensors [6, 7], implantable sensors [8], microfluidics [5], drug delivery [9] and neural probes [10].

Arguably the most crucial aspect of the development of a biosensor is the immobilisation of the biorecognition element onto a suitable matrix. Modification of the surface with metal

nanoparticles, carbon based nanomaterials or biocompatible polymers are among the most common ways to create selectively advantageous surfaces for biomolecules [11-14]. Thus, in this present work we have modified gold electrode surfaces with a hybrid nano-material that consists of two different types of nanoparticles, namely gold nanoparticles (AuNPs) and carbon quantum dots (CQDs). Both materials have a large number of advantages regarding to their chemical and physical characteristics. As a new class of nanocrystalline carbon materials, CQDs, have been gaining great attention in multiple research fields, particularly in biological applications due to their small size, surface functional groups, cheapness and non-toxicity [15, 16]. The other component, AuNPs, have been used extensively in bio-imaging controlled drug release systems and biosensors [17, 18]. They are able to rapidly transfer electrons between the transducer and a wide range of biorecognition element such as enzymes, which greatly improves the signal to noise ratios resulting from electrochemical biosensors [11].

In our previous work, we reported the CQDs/AuNPs nanohybrid material as an immobilisation matrix for a large surface area microfabricated gold electrode in order to develop a glucose oxidase biosensor [6]. The planar biosensor developed, with a 0.095 cm^2 surface area, exhibited very good analytical performance which may attributed to the positive contribution of the CQDs/AuNPs nanohybrid system. Such nanomaterials increase the surface area of the electrode and provide suitable immobilisation matrix to maintain the activity of the enzyme [6, 19]. Thus, the present study therefore explores the development of an electrochemical biosensor which combines the use of the CQDs/AuNPs nanohybrid materials and miniaturized electrode technologies in order to take advantage of both systems for the improved analytical performance of the desired biosensor. Gold micro disk array electrodes, with 20 µm diameter and 85 disk electrodes, were microfabricated using electronics industry-standard lithography, deposition and etching technologies. Fabricated electrodes were characterised electrochemically to investigate the efficacy of the microfabrication route and the morphology of gold arrays was studied with SEM and AFM. Then, CQDs/AuNPs-GOx micro disk array electrodes were prepared by applying several immobilisation methods as described in the experimental section. The micro disk array based glucose biosensor was studied by chronoamperometry to investigate its analytical performance. The resulting CQDs/AuNPs-GOx

modified gold micro disk array electrodes showed a 13-fold increase in sensitivity in comparison to the counterpart planar biosensor which was reported in our previous study [6].

4.3 Materials and Methods

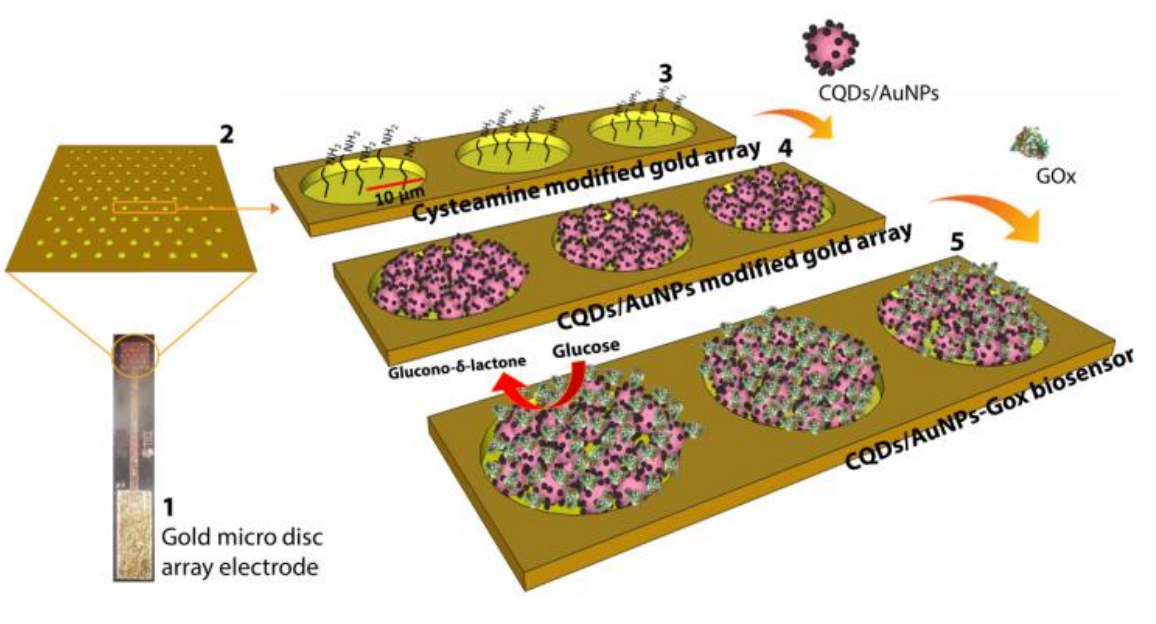
4.3.1 Materials

Glucose oxidase (EC 1.1.3.4, from Aspergillus niger), glucose, potassium chloride (KCl), sodium chloride (NaCl), 1-Ethyl-3-(3-dimethylaminopropyl)carbodiimide (EDC), N-hydroxysuccinimide (NHS), sulfuric acid, potassium ferrocyanide ($K_4[Fe(CN)_6]$), potassium ferricyanide ($K_3[Fe(CN)_6]$), cysteamine, acetaminophen, uric acid, phosphate buffer saline tablets (PBS, 0.01 M, pH 7.4) were obtained from Sigma-Aldrich. D-Glucose, UV-method commercial kit was obtained by Fannin. All aqueous solutions were prepared with doubly distilled water. Glucose stock solutions were prepared one day before use to allow mutarotation, kept in the fridge at + 4˚C overnight. Nanomaterials preparation methods and the gold micro disk array electrode fabrication process are included in the **supplementary data**.

4.3.2 Instrumentation and Methods

Micro disk array electrode characterization was studied with electrochemistry, scanning electron microscopy (SEM) and atomic force microscopy (AFM). Electrochemical studies were carried out using an AUTOLAB electrochemical workstation (METROHM, UK) in a standard three-electrode cell including a gold micro disk array working electrode, a platinum (Pt) wire counter electrode and an Ag/AgCl (1 M) reference electrode. Electrochemical impedance spectroscopy (EIS), cyclic voltammetry (CV), and chronoamperometry were applied to investigate the electroanalytical performance of the fabricated disk array electrodes and the biosensor developed. The Nyquist plots were obtained in a solution of 5 mM $Fe(CN)_6^{3-/4-}$ as a redox probe in the frequency range from 0.01 to 10^5 Hz at an amplitude of 0.01 V at open circuit potential. The used equivalent electrical circuit was [R(RQ)([RW]Q)]. The analytical performance of the biosensor was studied by chronoamperometry, in O_2 saturated 0.01 M PBS (pH 7.4) at an applied potential of -0.6 V. The calibration curve was studied to obtain the

current (I)-concentration (mM) graph of the biosensor. The sensitivity of the biosensor was obtained by dividing the slope of the calibration curve to surface area of the array. The detection limit was determined using the formula, $3s_b/S$, where s_b was the standard deviation of the blank and S was the sensitivity of the biosensor.



Scheme 4.1 Schematic diagram of the biosensor preparation process; (1) the bare individual disk array electrode, (2) magnified surface of array, (3) amine functionalised gold surface after cysteamine modification, (4) CQDs/AuNPs attached surface, (5) GOx enzyme immobilized overall CQDs/AuNPs-GOx biosensor. Note that the size of the electrodes, nanomaterials and biomolecule shown are not drawn to scale.

4.3.3 Preparation of CQDs/AuNPs-GOx biosensor

Scheme 1 depicts the steps involved in biosensor preparation. Disk array electrodes were modified with slight changes as we described previously [6]. Firstly, gold disk array working electrodes were cleaned using organic solvents and a plasma cleaner. The clean electrodes were then immersed into a cysteamine solution to obtain the amine functionalized surface and incubated overnight in the fridge, at +4°C. 5 µL of CQDs-AuNPs nano-hybrids solution was then drop-casted onto the amine-functionalized gold electrode surfaces and allowed to incubate in the fridge, at +4°C for 48 hours. Finally, 0.04 U GOx and 5 µL of gluteraldehyde (%1) were drop-casted to the electrode surface, respectively and the electrodes prepared kept in the fridge, at +4°C until dry. The electrodes were washed with PBS and kept in the fridge, at +4°C until used.

4.4 Results and discussion

4.4.1 Characterisation of fabricated micro disk array electrodes

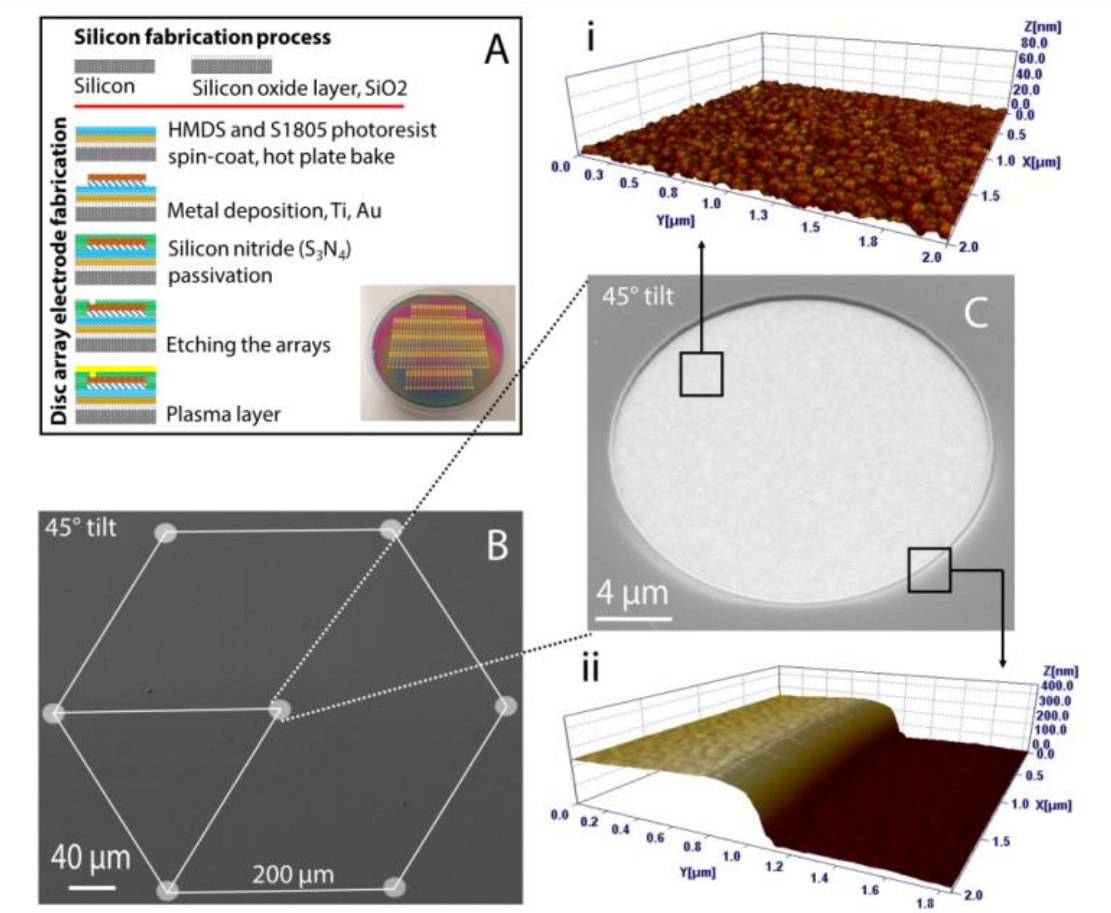


Figure 4.1. (A) Microfabrication process flow of the gold microelectrodes (inset: whole wafer picture of electrodes after fabrication process), (B) SEM image of the bare gold micro disk array electrode hexagonal structure with 200 µm inter-electrode distance and (C) an individual bare gold disk electrode with 10 µm radius, (i) AFM image of gold electrode surface and (ii) recess depth of the edge of the disk array.

SEM and AFM are very powerful tools for the study of the morphology and surface topography of microfabricated electrodes. Here, we applied both techniques to demonstrate the shape and dimensions of the array electrodes, the recess depth and the success of the modification process. An SEM image of the bare gold micro disk array electrode taken at low magnification and 45 º tilt, Fig. 4.1B, clearly reveals a series of well-situated disk electrodes arranged in a hexagonal pattern. The hexagonally arranged micro disk electrodes have an inter-electrode

distance of 200 µm. Fig. 4.1C shows the SEM image of an individual disk with a diameter 20 µm. This image demonstrates a well-defined shape of the disk electrode with a 45º tilt and a very clean surface of the gold electrode without any obvious residue from the microfabrication process materials such as photoresist or passivation. Fig. 4.1-(i) shows the resulting AFM image of an interior gold surface of the array electrode, which exhibits a nonporous morphology with a granular structure typical of evaporated gold. Fig. 4.1 (ii) shows an AFM image of the edge study of the individual disk electrode. As can be seen, the recess depth of the fabricated array is around 200 nm which was the expected result of the carefully applied microfabrication process. As noted earlier, the fabrication of the electrodes was performed using standard Si/SiO_2/metal microfabrication technology. In this technology, the patterning process for the disk arrays requires the etching of a passivation layer deposited on top of the metal layer as described in the supplementary data. As a result it was important to consider the possibility that a small fraction of the substrate remained passivated since this may decrease the analytical performance of the fabricated electrodes. Thus, it was very important to apply electrochemistry in order to investigate the success of the fabrication process [20]. Cyclic voltammetry in sulphuric acid is generally used for the characterisation of various different metal electrodes, especially platinum and gold, where the voltammograms reveal the formation of surface oxides during the positive sweep and their subsequent reduction [21]. The CVs recorded in this acid environment can also be used as a surface cleaning or activation method since electrodes fabricated in this study cannot be cleaned mechanically. Cyclic voltammetry in sulphuric acid was studied as a preliminary test in order to investigate if the microelectrode arrays were active. Typical voltammograms of gold planar (red) and micro (black) electrode in 0.5 M H_2SO_4 are shown in Fig. 4.2A. A broad peak between 1.1 – 1.4 V *vs*. Ag/AgCl was observed during the forward sweep, which can be attributed to the formation of monolayer oxides of gold (Au_2O_3), and during the backward sweep, a sharp reduction peak at 0.95 V *vs*. Ag/AgCl is due to the subsequent removal of oxides [22, 23]. The reduction of the current of the micro disk array electrode in comparison to the large surface area gold disk electrode is due to the decreased surface area of the electrode.

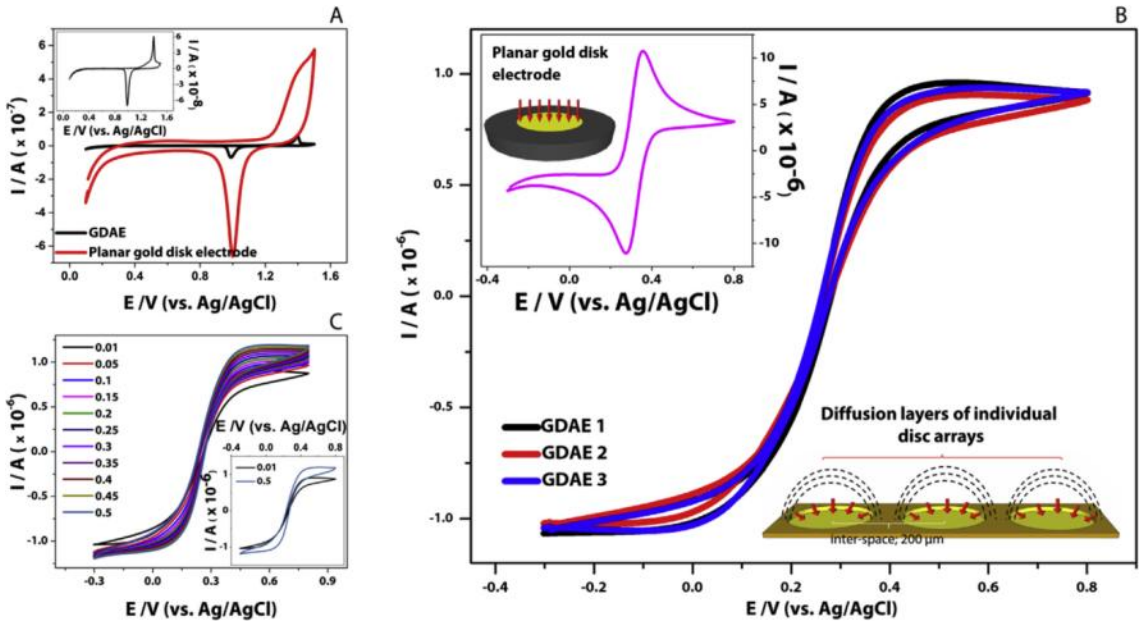


Figure 4.2. (A) Cyclic voltammograms recorded for gold disk planar, 1 mm diameter (red) and gold micro disk array (black) electrodes in 0.5 M H2SO4 at a scan rate of 0.01 V s-1, (B) cyclic voltammogram of three gold micro disk array electrodes and schematic representation of radial diffusion profile (inset: CV of planar gold electrode), and (C) cyclic voltammograms of gold micro disk array electrode at different scan rates ranging from 0.01 to 0.5 V s-1, in a solution of 5 mM Fe(CN)63-/4- as a redox probe containing 0.1 M KCl, 0.01 M PBS (pH 7.4).

One of the most important advantages of the use of microelectrodes is the radial diffusion profile which improves their performance due to enhanced mass transport to and from the microelectrode [24]. This behaviour can be investigated by cyclic voltammetry in the presence of an electroactive species since the diffusion zones associated with these electrodes influence the electrochemistry observed. A symmetrical sigmoidal cyclic voltammogram is expected from the microelectrodes in the absence of any shielding effect which may arise from the adjacent microelectrodes in the array. Moreover, the diffusion behaviour at the electrodes produces varying voltammetric responses ranging from sigmoidal to a 'peak shape' depending on the diameter and space between the electrodes in the array [25, 26]. As it can be seen in Fig. 4.2B-inset, the planar gold electrode shows a peak shaped cyclic voltammogram which arises from the planar diffusion profile concomitant with the relatively large surface area. In this work, the fabricated micro disk array electrodes consisted of an array of 20 µm diameter disk electrodes with a 200 µm spacing distance. Fig. 4.2B shows a schematic illustration of the diffusion profile of the microelectrode. In this case, the microelectrodes show a sigmoidal response using cyclic

voltammetry due to there being sufficient distance between the adjacent electrodes in the array. Thus, the diffusion layers do not interact and the voltammogram obtained represents the steady-state characteristics of an individual disk multiplied by the number of the electrodes in the array [27]. The CVs of the three-bare gold micro disk array electrodes in 5 mM $Fe(CN)_6^{3-/4-}$ solution at a slow scan rate of 0.01 V s^{-1} are shown in Fig. 4.2B. These data demonstrates the symmetrical and sigmoidal shape response of the fabricated gold microelectrodes. As can clearly be seen, the oxidation and reduction peak current densities are almost equal and reversible. The effect of increased scan rate on the electrochemical response of the micro disk electrodes was also studied and Fig. 4.2C shows the CVs of the disk electrode with increasing scan rate in a range of 0.01 to 0.5 V s^{-1}, in the presence of 5 mM $Fe(CN)_6^{3-/4-}$ as a redox probe. Even though a slight increase of the current density is observed with increased scan rate, the most significant result is the consistent appearance of the sigmoidal feature of the CVs at high scan rates which suggests that the every single disk remains isolated within the range of scan rates and that mass transport is dominated by radial diffusion. These results confirm the satisfactory electrochemical performance of the fabricated micro disk array electrodes developed in this work.

4.4.2 Fabrication process of the biosensor

Electrochemical impedance spectroscopy (EIS) and Cyclic Voltammetry (CV)

Electrochemical impedance spectroscopy (EIS) was employed in order to provide further understanding as to the changes of the surface properties during the biosensor development process [28]. Figure 4.3A shows the Nyquist plots corresponding to each step in the modification process including the bare gold electrode, the cysteamine modified gold surface, this surface with CQDs-AuNPs attached and finally, the GOx immobilised surface. These plots were obtained by applying EIS in a solution of 5 mM $Fe(CN)_6^{3-/4-}$ as a redox probe. The impedance data were studied by fitting the equivalent electrical circuit, [R(RQ)([RW]Q)] shown in Fig. 4.3B, where R_1, R_2 and R_3 represent electrolyte resistance (R_s), array surface film resistance (R_f) and charge transfer resistance (R_{ct}), respectively while W represents the Warburg impedance. The values of these parameters are listed in Table S1. In this analysis, the

circuit includes CPE (Constant phase element) due to the presence of the microfabrication-induced surface heterogeneities [29]. All Nyquist plots have a similar structure consisting of a high-frequency semicircle, a medium-frequency semicircle and a following short low-frequency line. Rs values of the circuits which are mainly related with the electrolyte, did not vary much for the microelectrode modification steps. The R_{ct} of the bare GDAE was calculated to be 71.4 kΩ (Fig. 4.3A, ■), which is larger than that of the cysteamine modified surface (R_{ct}; 1.3 kΩ) indicating the electrostatic interaction between the amine functional groups of cysteamine and the redox probe (Fig. 4. 3A, ●). Attachment of the nanohybrid material onto the electrode surface then increased the R_{ct} and R_f (111 kΩ and 36.1 kΩ) values since the accumulation of the nanomaterials may affect the transfer of redox species (Fig. 4.3A, ♦). In the last step, immobilisation of the enzyme onto surface resulted in a dramatic increase of R_{ct} and R_f (239 kΩ and 282 kΩ, Fig. 4.3A, ▼). This is due to the successful immobilisation of GOx on the electrode and the corresponding increase in the thickness of the modifying layer.

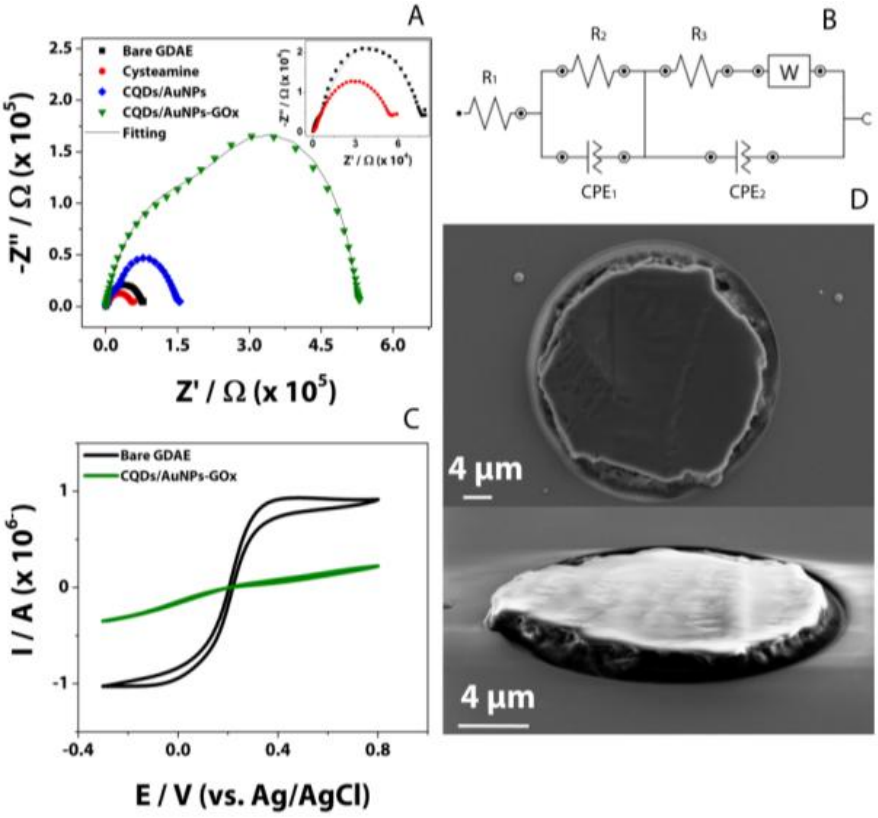


Figure 4.3. (A) Nyquist plots of the impedance spectra of bare gold micro disk array electrode (■), after cysteamine modification (●), CQD/AuNP hybrid material attached surface (♦) and GOx immobilized (▼) biosensor, (B)

equivalent electrical circuit model of [R(RQ)([RW]Q)], (C) cyclic voltammograms of bare gold micro disk array electrode and CQD/AuNPs-GOx bioelectrode and (D) SEM images of the CQDs/AuNPs-GOx modified single disk of the array. (The solution for EIS and CV is 5 mM Fe(CN)63-/4- as a redox probe in 0.01 M PBS (pH 7.4) solution containing 0.1 M KCl.)

Cyclic voltammetry was applied to probe the changes of the bare gold disk array electrode after CQDs/AuNPs-GOx layer formation at a scan rate of 0.01 V/s. As can be seen from Fig. 4.3C, in comparison to the bare gold surface, the overall surface modification decreased the current density at the electrode due to the accumulation of molecules/nanoparticles on the surface in a manner so as to block the electronic transfer to the electrode. Moreover, Fig. 4.3 D represents the SEM images of CQDs-AuNPs/GOx modified surface. The successful immobilisation of the bio-matrix onto the gold disk array surface can be clearly seen in the images of top and 70° tilt. The SEM images of the CQDs-AuNPs/GOx surface shown in here are in good agreement with the above interpretation of the EIS and CV data.

4.4.3 Chronoamperometric detection of glucose

The chronoamperometric detection of glucose was studied based on oxygen-consumption induced by the enzyme-catalyzed reaction of GOx as shown in the equations (1) and (2) [30]

$GOx(FAD) + glucose \rightarrow GOx(FADH_2) + gluconolactone$ (1)

$GOx(FADH_2) + O_2 \rightarrow GOx(FAD) + H_2O_2$ (2)

Chronoamperometric techniques was applied at an applied potential of -0.6 V in 0.01 M PBS (pH 7.4) O_2 saturated solution. Fig. 4.4A displays the chronoamperometric responses of the biosensor towards the serial additions of 0.16 mM glucose at 10 second intervals. As it can be seen from Fig. 4.4A(i), after each addition of the glucose, the biosensor reaches the steady state current rapidly and exhibits a well-defined response. As shown in Fig. 4.4B, the response time for the CQDs/AuNPs-GOx microbiosensor is about 0.5 sec which is defined as the time that current reaches 95% of the steady-state value. Fig. 4.4A(ii) and B show the corresponding calibration curve and the linear range of the biosensor, respectively. The linear response of the microbiosensor to glucose concentration is in the range from 0.16 mM – 4.32 mM with the linear regression equation of $y = 1.67 \cdot 10^{-7} x + 5.29 \cdot 10^{-8}$ ($R^2 = 0.99$). The sensitivity of the microbiosensor which was calculated from the slope of the plot, was determined to be 626.06

µA mM^{-1} cm^{-2}. The obtained excellent sensitivity of the array biosensor is some 13-times higher than that of a CQDs/AuNPs-GOx micro planar gold electrode based biosensor. This result may be attributed to the superior advantages of the micron-sized electrode array discussed earlier. The detection limit was calculated to be 13.6 µM which is comparable to that of other previously described array-based glucose biosensors [31-33]. Furthermore, we obtained a decrease of the limit of detection in comparison to planar counterpart of the biosensor (17 µM) [6]. Fig. 4.4D shows the Lineweaver-Burk plot from the micro disk array biosensor with a linear regression equation of $y = 3.03 \cdot 10^6 x + 1.035 \cdot 10^6$ ($R^2 = 0.98$). The apparent Michaelis-Menten constant (K_m^{app}), was calculated to be 2.93 mM. This quite low concentration value of the constant is indicative of the high affinity between the immobilised glucose oxidase and glucose. The constant value determined here is considerably smaller than previously reported values, e.g. 27 mM for free glucose oxidase [34] and 6.5 mM for a gold nanowire array–GLA–BSA–GO_x glucose biosensor [35]. This reduction in K_m^{app} is illustrated in more detail in a comparison between this work and other work presented in the literature, shown in Table S2.

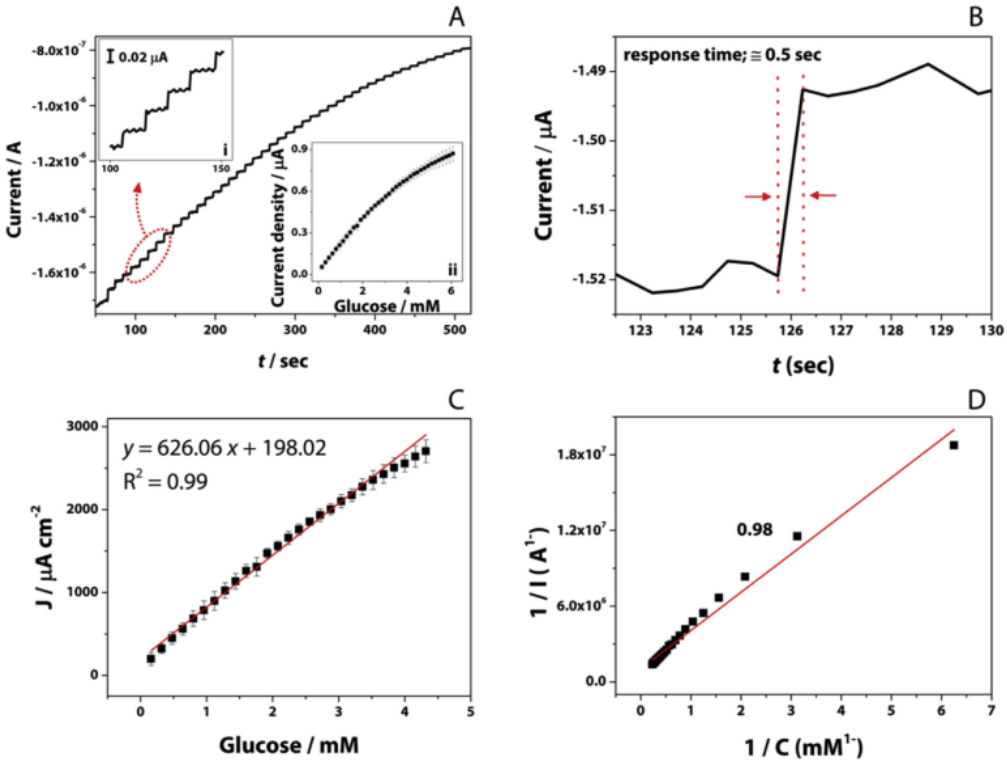


Figure 4.4. (A) Chronoamperometric response of the CQDs/AuNPs-GOx micro disk array biosensor to the serial addition of 20 µL of 40 mM glucose in O2-saturated 0.01 M PBS (pH 7.4) at a working potential of -0.6 V (inset i;

detailed presentation of serial addition steps and inset ii; corresponding calibration curve of the biosensor), (B) the response time for the biosensor to reach the steady-state current, (C) corresponding linear range of the biosensor and (D) The Lineweaver-Burk plot of the micro disk array biosensor.

The analytical performance of the developed biosensor may be attributed to the use of a combination of the micro array electrodes and the chosen nanomaterials. It has been reported that electrodes that are based on the use of nano materials provide several beneficial characteristics including their large surface area, high surface activity, high catalytic efficiency and strong adsorption capacity [7, 19]. Moreover, it is very well known that micro array electrodes offer a number of advantages over planar electrodes due to their radial diffusion profile and improved mass transport [1, 24]. Table S2 clearly reveals the advantages associated with miniaturization of the devices and the use of the nanomaterials selected here, as may clearly be seen from the measured analytical parameters. Specifically the approach leads to improvements in sensitivity and reductions in both detection limits and Michaelis-Menten constant values.

3.2.3 Studies of selectivity, reproducibility, reusability, stability and real samples

To evaluate the possible analytical application of the microbiosensor developed, the effects of common interfering species have been examined. Fig. 4.5A displays the responses of the microbiosensor towards 2 mM glucose and 0.16 mM of the most common interfering species namely, ascorbic acid (AA), uric acid (UA) and acetaminophen (AC). In the presence of ascorbic acid, uric acid and acetaminophen, the response of the biosensor towards 2 mM glucose changed % 8.21, % 7.9 and % 7.54, respectively. These results demonstrate that the microbiosensor developed is highly selective for glucose detection even in the presence of electroactive substances known to endogenously coexist.

Five individual CQDs/AuNPs-GOx micro disk array biosensors were prepared and their responses to glucose in O_2 saturated PBS were measured by chronoamperometry under the same conditions in order to investigate the biosensor reproducibility, Fig. 4.5B. The relative standard deviation (RSD) towards detection of a 0.16 mM glucose was determined to be 4.20% which demonstrates quite a reasonable good level of reproducibility. Moreover, the reusability

of the biosensor was studied by performing seven successive experiments each with three individual electrodes. The RSD values of the fabricated biosensors were calculated to be 4.85%, 4.31% and 6.64%, suggesting good operational stability of the CQDs/AuNPs-GOx micro disk array biosensor, Fig. 4.5C. After storing the biosensor at +4C for one month, its current density decreased by approximately 5.53%. This impressive long term stability (shelf-life) can be attributed to the biocompatibility of the CQDs/AuNPs nanohybrid matrix which can provide a 'friendly' microenvironment for the 'active' component- the GOx enzyme.

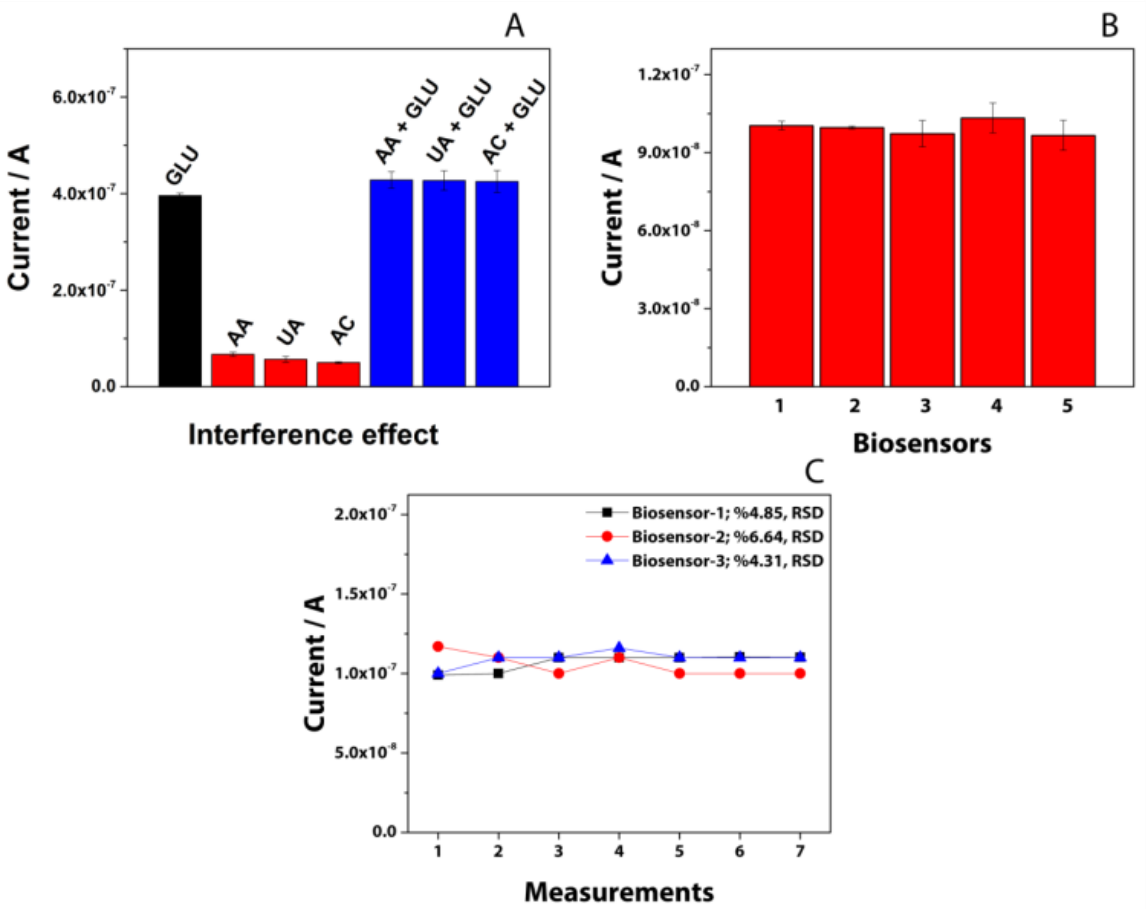


Figure 4.5. (A) Response of the CQDs/AuNPs-GOx-GDAE microbiosensor to glucose, ascorbic acid (AA) , uric acid (UA) and acetaminophen (AC) , (B) reproducibility (n=5) and (C) reusability of the CQDs/AuNPs-GOx-GDAE microbiosensor in O2 saturated 0.01 M PBS (pH 7.4) at an applied potential of -0.6V.

By way of a practical application, the CQDs/AuNPs-GOx biosensor developed here was deployed to measure the glucose content of two different commercial sweet wines. The

concentration of glucose in those wines was firstly determined by using a commercial glucose kit based on the (spectrophotometric) enzymatic reaction. For this purpose, wine samples were diluted as a ratio of 1:100 and their pH was adjusted to approximately pH 8 by adding 1M NaOH solution and incubated for 15 minutes at room temperature. After sample preparation, each sample was measured 3 times by the spectrophotometric method to determine the concentration. To study the target wines using the biosensor developed here, wine samples were simply diluted with deionised water to keep the concentration in the linear range of the calibration curve. Briefly each wine sample was prepared to be 40 mM and added into electrochemical cell 20 µL for each measurement. No further preparation process was required. The concentration of glucose was calculated based on the calibration curve. The comparison of the results obtained from both the spectrophotometric enzymatic method and CQDs/AuNPs-GOx electrochemical biosensor are shown in Table 4.1. The results displayed in Table 1 reveal that the biosensor developed can be easily applied for glucose detection in alcoholic beverages without any special sample pre-treatment. Moreover, the biosensor developed is highly suitable for further miniaturisation and packaging for on-site and in-line applications.

Table 4.1. Real samples analysis

	Glucose concentration (g/L)			
	Spectrophotometric commercial method	CQDs/AuNPs-GOx micro-biosensor	Relative standard deviation (%)	
			spectrophotometric	micro-biosensor
Moscato wine 1	20.10 (± 0.18)	22.47 (± 3.80)	0.9	17
Moscato wine 2	20.984 (± 0.31)	26.14 (± 2.51)	1.5	9.6

4. Conclusions

In this present study we describe the fabrication of a highly promising biosensor most suitable for further miniaturisation and packaging. A general microfabrication process based on lift-off technology was applied for device fabrication and two specific masks were designed and fabricated for the etching process used to define the array. Fabricated gold micro electrodes

were characterised electrochemically to investigate the success of the microfabrication. The micro-scale array device showed a very specific symmetric sigmoidal cyclic voltammogram which is characteristic of a radial diffusion profile. Furthermore, bare electrodes were studied by SEM and AFM. These results demonstrate that the device fabrication process employed here was successful in terms of making electrochemically-viable electrodes.

The subsequent modification of the electrodes with CQDs/AuNPs nanohybrid and GOx to create the biosensor was then successfully demonstrated. The CQDs/AuNPs-GOx-GDAE microbiosensor developed showed a sensitivity of 626.06 μA mM^{-1} cm^{-2} with a linear range from 0.16 mM to 4.32 mM. Developed biosensor reached to a stable steady-state currents within ~ 0.5 sec. Furthermore, the apparent Michalis-Menten constant (K_m^{app}), which is an indicator of enzyme-substrate reaction kinetics, was calculated to be 2.93 mM.

Finally, we note that the methods deployed to fabricate the biosensor described in this paper are particularly suitable for further development towards a completely on-chip system, with possible further miniaturization, which would reduce the unit costs associated with biosensor production making it particularly attractive for various applications yet still highly reliable and reproducible.

4.5 Acknowledgments

The authors appreciate the financial support from the Department of Agriculture, Food and the Marine, 14F883, Ireland. We would like to thank Dr. Gediminas Juska for helpful discussions on carbon quantum dots. And we are also thankful to Dr. Emanuele Pelucchi for providing us some of laboratory equipment.

4.6 References

[1] X.J. Huang, A.M. O'Mahony, R.G. Compton, Microelectrode arrays for electrochemistry: approaches to fabrication, Small, 5 (2009) 776-788.

[2] J. Li, J.E. Koehne, A.M. Cassell, H. Chen, H.T. Ng, Q. Ye, W. Fan, J. Han, M. Meyyappan, Inlaid multi-walled carbon nanotube nanoelectrode arrays for electroanalysis, Electroanal, 17 (2005) 15-27.

[3] T. Noda, M. Wanibuchi, Y. Kitazumi, S. Tsujimura, O. Shirai, M. Yamamoto, K. Kano, Diffusion-controlled detection of glucose with microelectrodes in mediated bioelectrocatalytic oxidation, Anal Sci, 29 (2013) 279-281.

[4] D.W.M. Arrigan, Nanoelectrodes, nanoelectrode arrays and their applications, Analyst, 129 (2004) 1157-1165.

[5] Y. Temiz, A. Ferretti, Y. Leblebici, C. Guiducci, A comparative study on fabrication techniques for on-chip microelectrodes, Lab Chip, 12 (2012) 4920-4928.

[6] V. Buk, M.E. Pemble, K. Twomey, Fabrication and evaluation of a carbon quantum dot/gold nanoparticle nanohybrid material integrated onto planar micro gold electrodes for potential bioelectrochemical sensing applications, Electrochimica Acta, 293 (2019) 307-317.

[7] C.-W. Hsu, F.-C. Su, P.-Y. Peng, H.-T. Young, S. Liao, G.-J. Wang, Highly sensitive non-enzymatic electrochemical glucose biosensor using a photolithography fabricated micro/nano hybrid structured electrode, Sensors and Actuators B: Chemical, 230 (2016) 559-565.

[8] S. Zhang, Y. Song, M. Wang, Z. Zhang, X. Fan, X. Song, P. Zhuang, F. Yue, P. Chan, X. Cai, A silicon based implantable microelectrode array for electrophysiological and dopamine recording from cortex to striatum in the non-human primate brain, Biosensors and Bioelectronics, 85 (2016) 53-61.

[9] J.-H. Park, M.G. Allen, M.R. Prausnitz, Biodegradable polymer microneedles: Fabrication, mechanics and transdermal drug delivery, Journal of Controlled Release, 104 (2005) 51-66.

[10] G. Marton, P. Baracskay, B. Cseri, B. Plosz, G. Juhasz, Z. Fekete, A. Pongracz, A silicon-based microelectrode array with a microdrive for monitoring brainstem regions of freely moving rats, J Neural Eng, 13 (2016).

[11] M. Holzinger, A. Le Goff, S. Cosnier, Nanomaterials for biosensing applications: a review, Front Chem, 2 (2014) 63.

[12] V. Buk, E. Emregul, K.C. Emregul, Alginate copper oxide nano-biocomposite as a novel material for amperometric glucose biosensing, Mat Sci Eng C-Mater, 74 (2017) 307-314.

[13] B. Derkus, K.C. Emregul, E. Emregul, Evaluation of protein immobilization capacity on various carbon nanotube embedded hydrogel biomaterials, Materials Science and Engineering: C, 56 (2015) 132-140.

[14] B. Derkus, E. Emregul, K.C. Emregul, C. Yucesan, Alginate and alginate-titanium dioxide nanocomposite as electrode materials for anti-myelin basic protein immunosensing, Sensors and Actuators B: Chemical, 192 (2014) 294-302.

[15] M. Roy, 17 - Nanocrystalline and Disordered Carbon Materials, in: S. Banerjee, A.K. Tyagi (Eds.) Functional Materials, Elsevier, London, 2012, pp. 675-706.

[16] R. Das, R. Bandyopadhyay, P. Pramanik, Carbon quantum dots from natural resource: A review, Materials Today Chemistry, 8 (2018) 96-109.

[17] Y. Li, H.J. Schluesener, S. Xu, Gold nanoparticle-based biosensors, Gold Bull, 43 (2010) 29-41.

[18] R. Popovtzer, A. Agrawal, N.A. Kotov, A. Popovtzer, J. Balter, T.E. Carey, R. Kopelman, Targeted gold nanoparticles enable molecular CT imaging of cancer, Nano Lett, 8 (2008) 4593-4596.

[19] A. Walcarius, S.D. Minteer, J. Wang, Y.H. Lin, A. Merkoci, Nanomaterials for bio-functionalized electrodes: recent trends, J Mater Chem B, 1 (2013) 4878-4908.

[20] J. Orozco, C. Fernandez-Sanchez, C. Jimenez-Jorquera, Ultramicroelectrode Array Based Sensors: A Promising Analytical Tool for Environmental Monitoring, Sensors, 10 (2010) 475-490.

[21] Y.Y. Zhang, S. Xu, Y.Y. Qian, X.S. Yang, Y.X. Li, Preparation, electrochemical responses and sensing application of Au disk nanoelectrodes down to 5 nm, Rsc Adv, 5 (2015) 77248-77254.

[22] M.D. Scanlon, U. Salaj-Kosla, S. Belochapkine, D. MacAodha, D. Leech, Y. Ding, E. Magner, Characterization of Nanoporous Gold Electrodes for Bioelectrochemical Applications, Langmuir, 28 (2012) 2251-2261.

[23] L.D. Burke, P.F. Nugent, The Electrochemistry of Gold: I The Redox Behaviour of the Metal in Aqueous Media, Gold Bull, 30 (1997) 43-53.

[24] F. Davis, S.P. Higson, Arrays of microelectrodes: technologies for environmental investigations, Environ Sci Process Impacts, 15 (2013) 1477-1489.

[25] R.S. Chen, Y. Li, K.F. Huo, P.K. Chu, Microelectrode arrays based on carbon nanomaterials: emerging electrochemical sensors for biological and environmental applications, Rsc Adv, 3 (2013) 18698-18715.

[26] M. Ikegami, Y. Hirano, Y. Mie, Y. Komatsu, Fabrication and characterization of nanoporous gold on microelectrode, J Electroanal Chem, 783 (2016) 188-191.
[27] Y. Tu, Y.H. Lin, Z.F. Ren, Nanoelectrode arrays based on low site density aligned carbon nanotubes, Nano Letters, 3 (2003) 107-109.
[28] E.P. Randviir, C.E. Banks, Electrochemical impedance spectroscopy: an overview of bioanalytical applications, Anal Methods-Uk, 5 (2013) 1098-1115.
[29] G. Dutta, S. Siddiqui, H. Zeng, J.A. Carlisle, P.U. Arumugam, The effect of electrode size and surface heterogeneity on electrochemical properties of ultrananocrystalline diamond microelectrode, J Electroanal Chem, 756 (2015) 61-68.
[30] J. Wang, Electrochemical glucose biosensors, Chem Rev, 108 (2008) 814-825.
[31] S. Liébana, L.J. Jones, G.A. Drago, R.W. Pittson, D. Liu, W. Perrie, J.P. Hart, Design and development of novel screen-printed microelectrode and microbiosensor arrays fabricated using ultrafast pulsed laser ablation, Sensors and Actuators B: Chemical, 231 (2016) 384-392.
[32] Y.H. Lin, F. Lu, Y. Tu, Z.F. Ren, Glucose biosensors based on carbon nanotube nanoelectrode ensembles, Nano Letters, 4 (2004) 191-195.
[33] H.B. Habtamu, P. Ugo, Miniaturized Enzymatic Biosensor via Biofunctionalization of the Insulator of Nanoelectrode Ensembles, Electroanal, 27 (2015) 2187-2193.
[34] M.J. Rogers, K.G. Brandt, Interaction of D-Glucal with Aspergillus-Niger Glucose Oxidase, Biochemistry-Us, 10 (1971) 4624-&.
[35] J. Cui, S.B. Adeloju, Y. Wu, Integration of a highly ordered gold nanowires array with glucose oxidase for ultra-sensitive glucose detection, Anal Chim Acta, 809 (2014) 134-140.

4.7 Supporting information

Nanomaterials preparation and gold micro disk array fabrication

CQDs were synthesised from ethanol in an alkaline environment at a constant potential using the method reported by Deng et al. [1], with slight changes, and combined together with gold nanoparticles as described in our previous study to obtain a CQDs decorated AuNPs nano-hybrid material [2]. Briefly, 15 mL ethanol was mixed with saturated NaOH and stirred for 30

minutes at an applied potential of 4V. The product was kept in the dark overnight. The resulting yellow coloured solution was evaporated at 80°C. The pellet was dissolved in the double distilled water and pH was adjusted to pH 7.0. For further purification, solution was filtered and stored at +4 °C. AuNPs were prepared by following the procedure reported by Turkevich et al. [3]. Tetrachloroauric acid, % 0.02 was boiled in a round bottom reaction flask under stirring conditions, and then %1 trisodium citrate was added into flask rapidly. The colour of the solution changed from yellow to magenta, and the solution was cooled to room temperature under stirring conditions. The resulting gold nanoparticles were kept at +4°C. To form the CQDs/AuNPs nanohybrid system, AuNPs were modified by adding 0.01 mM cysteamine which forms amine terminated self-assembly monolayers on the surface. The mixture were incubated for 24 hours at room temperature by shaking. Carboxyl groups of CQDs were treated by 40 µL of NHS/EDC solution (1:4). Finally the activated-CQDs were added to the amine functional AuNPs and shaken overnight. The characterisation of the nanomaterials were studied in detail in our previous work, please see reference [2]. Moreover, in here we studied the Raman spectrum of the nanomaterials (Fig. **4.**S1). The spectrum of CQDs does not show any Raman signal due to their strong fluorescence properties (Fig. **4.**S1- B) while the spectrum of AuNPs (Fig. **4.**S1- A) exhibits a band at ca. 1600 cm^{-1} (G band) [4]. When combined to form the hybrid material the spectrum (Fig. **4.**S1- C) showed a decrease in the peak counts originating from the AuNPs most likely because addition of the CQDs obscures or dampens part of the Raman signal.

The gold micro disk array working electrodes (GDAE) were fabricated using a classical microfabrication process flow which is shown in Fig. **4.**1A. Briefly, silicon was chosen as the substrate and a silicon oxide layer was growth on the silicon substrate. The substrates were treated with an argon plasma to improve the metal adhesion to the substrate. The wafer was then spin-coated at 3000 rpm for 50 seconds with a layer of photoresist. This was followed by the titanium and gold deposition using e-beam evaporation and patterning using a lift off procedure, respectively. Silicon nitride (S_3N_4) with 200 nm thickness was deposited as the passivation layer by plasma-enhanced chemical vapor deposition. Then, the mask which was designed for disk arrays was applied by a passivation lithography process and passivation

etching. For this purpose an inductively coupled plasma etch system (ICP) was used to etch the Si_3N_4 passivation layer and the remaining resist was removed. Last step involved covering the substrate with a resist layer to protect the electrodes during the dicing process. Fig. **4.**1A-inset shows a photograph of the whole wafer after fabrication. The resulting individual electrodes consisted of 85 disk arrays with 20 µm diameter, 200 µm inter-electrode distance and 200 nm recess depth. The overall surface area of the array is 2.67 x 10^{-4} cm^2.

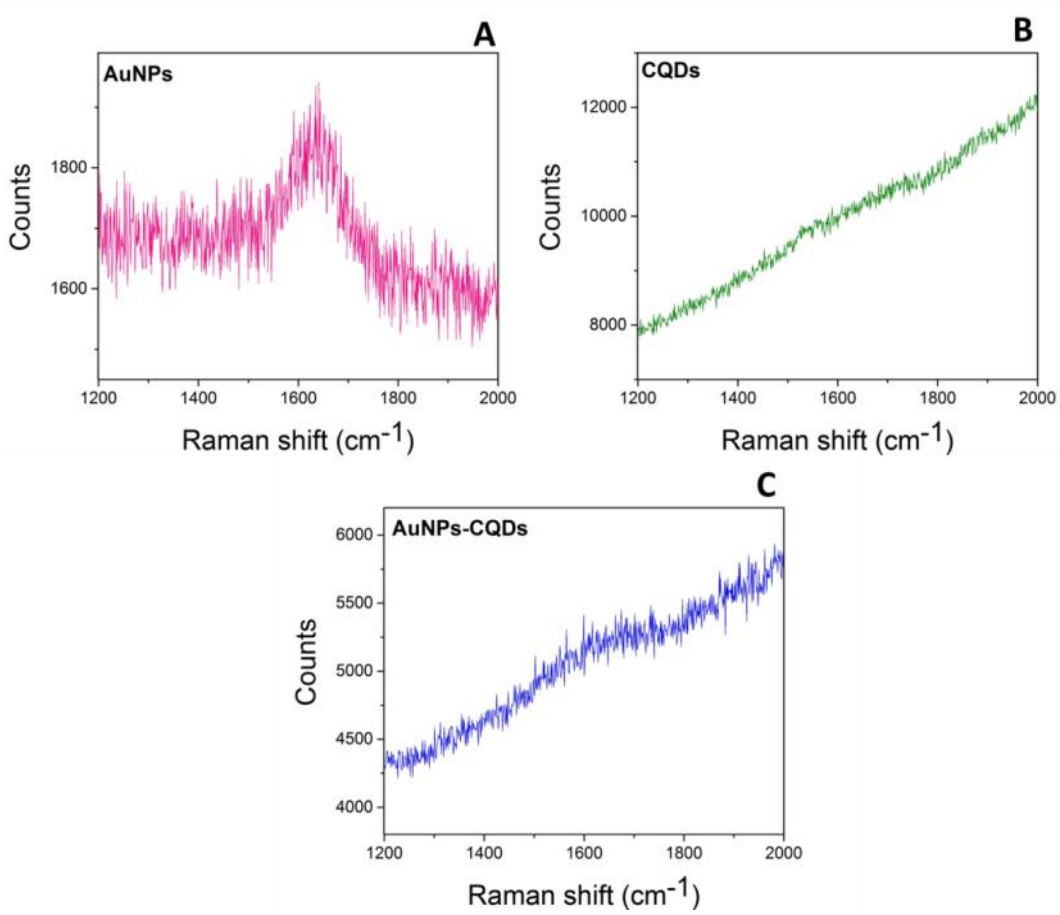


Figure 4.S1. Raman Spectrum of AuNPs (A), CQDs (B) and AuNPs-CQDs nanohybrid material (C)

Table 4.S1. Typical values of interfacial parameters of CQDs/AuNPs-GOx micro disk array biosensor surface modifications steps obtained by fitting the [R(RQ)([RW]Q)] circuit to the experimental data

	R_1	R_2	R_3	CPE_1	CPE_2
Surface layers	Ω	kΩ	kΩ	nMho	nMho
bare GDME	120	4.39	71.4	192	2310
Cysteamine	51.4	54.6	1.30	4200	23.8
CQDs/AuNPs	120	36.1	111	561	873
CQDs/AuNPs-GOx	126	282	239	258	75.3

Table S2. Comparison of the analytical performance of the array based glucose oxidase biosensors

Glucose biosensor	Sensitivity	Detection Limit	Linear range	K_m	Reproducibility	Reusability	Long term stability	Ref.
CQDs/AuNPs-GOx-GDAE	626.06 μA mM^{-1} cm^{-2}	13.6 μM	0.16–4.32 mM	2.93 mM	RSD 4.2% (n=5)	RSD 4.85%, 4.31% and 6.64% (3 biosensors, 7 successive measurements)	Dry storage at 4°C, one month	This work
AuNWA–BSA–GLA–GOx	298.2 μA mM^{-1} cm^{-2}	0.1 μM	0.005-6 mM	6.5 mM	-	-	four weeks	[5]
GOx-modified porous gold nanowire-array electrode	15.6 μA mM^{-1} cm^{-2}	$4.6x10^{-5}$ M	0.05-2 mM	0.046 mM	-	-	-	[6]
GOx-PEGDE-microelectrode	147 μA mM^{-1} cm^{-2}	~ 1 nM	0-400 μM	1.4 mM	At the optimal PEGDE concentration, enzyme immobilization was reproducible (app. 12% in the sensitivity ratio)	4-5 hours repeatedly for vivo and in vitro	during dry storage at 4°C over 3 mos.	[7]
MEA100-Gox	1.73 μA mM^{-1}	1.7 μM	0.1-1 mM		-	-	-	[8]
PPy-GOx-Gel–Pt	281nA/mM/cm^2	0.033 mM	1-15 mM	33 mM	-	-	A temporal increase in sensitivity with storage over a 17 days period.	[9]

Abbreviations; AuNWA: gold nanowires array, BSA: bovine serum albumin, GLA: glutaraldehyde, PEGDE: poly(ethylene glycol) diglycidyl ether, MAE: silver microelectrode arrays, Ppy: polypyrrole

References

[1] J.H. Deng, Q.J. Lu, N.X. Mi, H.T. Li, M.L. Liu, M.C. Xu, L. Tan, Q.J. Xie, Y.Y. Zhang, S.Z. Yao, Electrochemical Synthesis of Carbon Nanodots Directly from Alcohols, Chem-Eur J, 20 (2014) 4993-4999.

[2] V. Buk, M.E. Pemble, K. Twomey, Fabrication and evaluation of a carbon quantum dot/gold nanoparticle nanohybrid material integrated onto planar micro gold electrodes for potential bioelectrochemical sensing applications, Electrochimica Acta, 293 (2019) 307-317.

[3] J. Turkevich, P.C. Stevenson, J. Hillier, A Study of the Nucleation and Growth Processes in the Synthesis of Colloidal Gold, Discuss Faraday Soc, (1951) 55-&.

[4] P.H. Luo, C. Li, G.Q. Shi, Synthesis of gold@carbon dots composite nanoparticles for surface enhanced Raman scattering, Phys Chem Chem Phys, 14 (2012) 7360-7366.
[5] J. Cui, S.B. Adeloju, Y. Wu, Integration of a highly ordered gold nanowires array with glucose oxidase for ultra-sensitive glucose detection, Anal Chim Acta, 809 (2014) 134-140.
[6] X.Y. Zhang, D. Li, L. Bourgeois, H.T. Wang, P.A. Webley, Direct Electrodeposition of Porous Gold Nanowire Arrays for Biosensing Applications, Chemphyschem, 10 (2009) 436-441.
[7] N. Vasylieva, B. Barnych, A. Meiller, C. Maucler, L. Pollegioni, J.-S. Lin, D. Barbier, S. Marinesco, Covalent enzyme immobilization by poly(ethylene glycol) diglycidyl ether (PEGDE) for microelectrode biosensor preparation, Biosensors and Bioelectronics, 26 (2011) 3993-4000.
[8] H.-M. Huang, P.-K. Huang, W.-H. Kuo, Y.-H. Ju, M.-J. Wang, Sol–gel immobilized enzymatic glucose biosensor on gold interdigitated array (IDA) microelectrode, J Sol-Gel Sci Techn, 67 (2013) 492-500.
[9] C.N. Kotanen, C. Tlili, A. Guiseppi-Elie, Amperometric glucose biosensor based on electroconductive hydrogels, Talanta, 103 (2013) 228-235.

CHAPTER 5

Dual-enzyme based glucose detection

5. A dual-enzyme, micro-band array biosensor based on the electrodeposition of carbon nanotubes embedded in chitosan and nanostructured Au-foams on microfabricated gold band electrodes

This work has been published in the journal of RSC Analyst, 2020 (DOI: 10.1039/C9AN01664C)

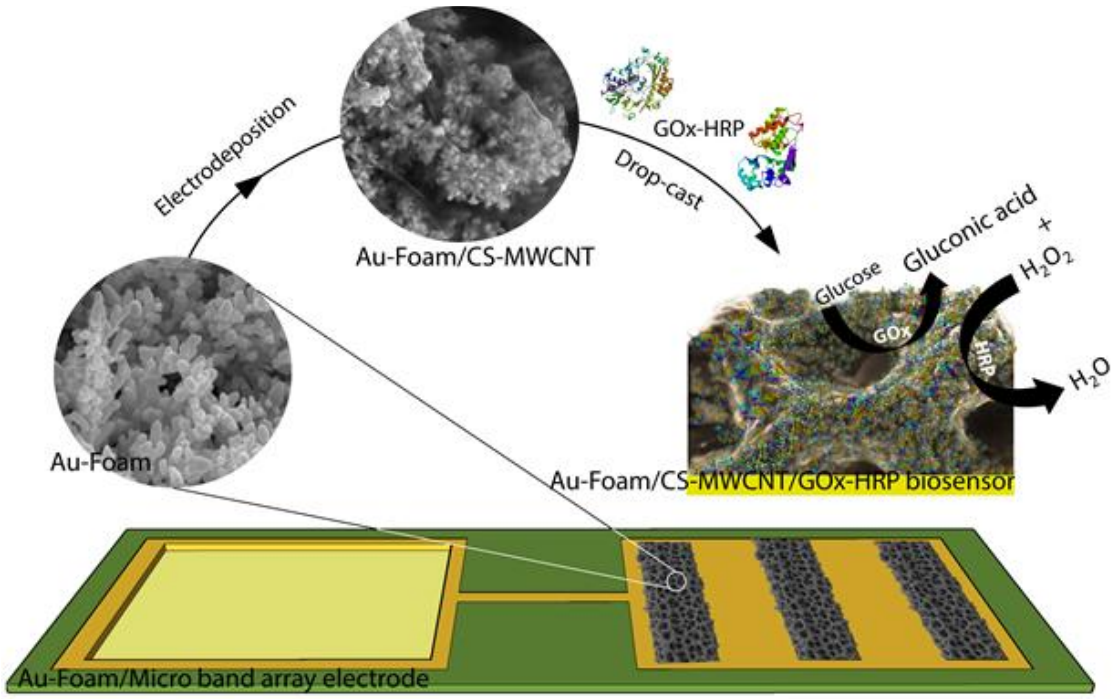
5.1 Abstract

We report the development of a dual-enzyme electrochemical biosensor based on microfabricated gold band array electrodes which were first modified by gold foam (Au-foam) in order to dramatically increase the active surface area. The resulting nanostructured Au-foam deposits then served as a highly porous 3D matrix for the electrodeposition of a nanocomposite film consisting of multi walled carbon nanotubes embedded in a chitosan matrix (CS:MWCNT) designed to provide a conducting, biocompatible and chemically versatile surface suitable for the attachment of a wide range of chemically or biologically active agents. Finally, a dual enzyme mixture of glucose oxidase (GOx) and horseradish peroxidise (HRP) was immobilised onto the CS:MWCNT nanocomposite film surface.

It is shown that the resulting sensing platform developed demonstrates excellent analytical performance in terms of glucose detection with a sensitivity of 261.8 µA mM^{-1} cm^{-2} and a reproducibility standard deviation (RSD) of 3.30% as determined over 7 measurements. Furthermore, long term stability studies showed that the electrodes exhibited an effectively unchanged response to glucose detection after some 45 days.

The example of glucose detection presented here illustrates the fact that the particular combination of nanostructured materials employed represents a very flexible platform for the attachment of enzymes or indeed any other bioactive agent and as such may form the basis of the fabrication of a wide range of biosensors. Finally, since the platform used is based on lithographically-deposited gold electrodes on silicon, we note that it is also very suitable for further miniaturisation, mass production and packaging- all of which would serve to reduce production costs.

Keywords: *Enzymatic sensor, biosensor, microelectrode, electrodeposition, microfabrication, chitosan, carbon nanotubes, gold foam*



Graphical abstract, note that the sizes of the components shown are not drawn to scale.

5.2 Introduction:

Electrochemical biosensors recognize the corresponding analyte through a catalytic or binding event occurring at the surface of the electrode and as a result of the high-sensitivities that have been achieved they have been extensively studied in various clinical, environmental, industrial and agricultural applications [1-3]. The close relationship between analytical performance and the characteristics of the electrode has stimulated considerable efforts devoted to the design and fabrication of miniaturised electrodes. Silicon-based microfabricated electrodes, in particular those based on lithography, etching and deposition show considerable promise for the relatively low-cost batch fabrication of a range of highly-reproducible microelectrodes or arrays of microelectrodes whose precise dimensions and shapes may be directly controlled via

the choice of a suitable mask [4, 5]. Microelectrodes are commonly used for electrochemical analysis [6, 7] and biosensing [4] due to several well-established advantages of such electrodes including small size, fast response time, high signal-to-noise ratio and the rapid generation of a steady state response [6, 8, 9].

In our previous work we demonstrated how the combination of microfabricated electrodes with nanostructured overlayers can be used most effectively for the sensitive, rapid and reliable detection of glucose via both enzymatic and non-enzymatic electrochemical processes [4, 5, 10]. In those studies the advantages of increased active surface area achieved via either metal nanoparticle (Au) attachment or metal (Cu) foam electrodeposition was clearly demonstrated. Especially, the use of the metal foams for the creation of a high active surface area sensor is a particularly attractive approach since such foams may be readily formed in-situ via an electrodeposition process that utilises the so-called dynamic hydrogen bubble template method [10-13].

In this present work we continue with this approach, utilising gold foam (Au-foam) electrodeposition onto micro band array electrodes in acidic solution at high negative overpotentials to form a very elegant, highly porous foam nanocrystal deposits along each single band of the array electrode. We then subsequently modify the Au-Foam surface using the electrodeposition of an organic functional layer (OFL) consisting of a chitosan (CS) / carbon nanotube (CNT) composite material. CS was chosen as the major component of the OFL since it possesses excellent characteristics in terms of biocompatibility, nontoxicity, good water permeability low-cost, non-antigenic, abundant functional groups and biodegradability [14-17]. From the point of view of functionalisation, the amine ($-NH_2$) groups present in CS make it a superb candidate for surface modification and the immobilisation of a wide variety of biomolecules. In addition, it is known that combining CS with CNTs not only increases the mechanical stability and robustness of the layer but also greatly enhances its conductivity/rate of electron transfer and electrocatalytic properties [18-21]. After the anodic electrodeposition of the Au-foam and the subsequent cathodic electrodeposition of CS in the presence of the CNTs resulting in the formation of the CNT-embedded composite OFL, the enzymes glucose

oxidase and horseradish peroxidase were immobilised onto the functionalised surface by drop casting so as to create a dual-enzyme sensing platform. We show here that the resulting dual-enzyme microbiosensor exhibited a sensitivity of 261.8 μA mM^{-1} cm^{-2} towards glucose detection while also being reproducible (RSD, 3.30%) and relatively unaffected by the common interferences found in human blood serum. These data serve to illustrate the enormous potential that this microfabricated electrode/porous metal/OFL approach possesses in terms of the reliable, reproducible and cheap fabrication of a wide range of sensors.

5.3 Materials and methods

5.3.1 Chemicals and Instrumentation

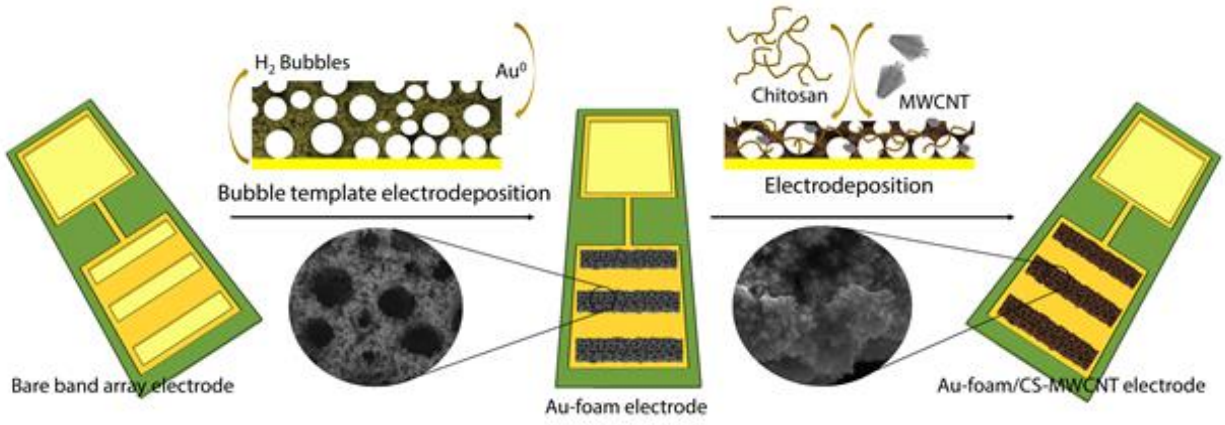
Glucose oxidase (EC 1.1.3.4, from Aspergillus niger; GOx), Horseradish peroxidase (EC 1.11.1.7; HRP), gold (III) chloride trihydrate ($HAuCl_4 \cdot 3H_20$), multi-walled carbon nanotube (-COOH), chitosan, glucose, ascorbic acid, uric acid, acetaminophen, acetone, potassium ferrocyanide ($K_4[Fe(CN)_6]$), potassium ferricyanide($K_3[Fe(CN)_6]$), phosphate buffer saline tablets (PBS, 0.01 M, pH7.4), potassium chloride (KCl), sulfuric acid (H_2SO_4), sulfuric acid, 1-Ethyl-3-(3-dimethylaminopropyl) carbodiimide (EDC), and N-hydroxysuccinimide (NHS) were obtained from Sigma-Aldrich. Acetic acid was obtained from Riedel-de Haen. All solutions were prepared with deionized water (18.3 MΩ, ELGAPurelab Ultra).

Scanning electron microscopy (SEM) (Zeiss Supra 40 SEM at accelerating voltages in the range of 5-10 kV) was used to study of the surface morphology of bare and modified band array electrodes. Energy dispersive X-ray analysis (EDX) was performed using a Quanta 650 Field Emission Gun (FEG) attached with an EDX unit, with an accelerating voltage of 20 kV. The chemical composition of the surfaces was studied by using X-ray photoemission spectroscopy (XPS, Kratos AXIS ULTRA) with Al K_α at 1486.58 eV. The analysis area was approximately 1 mm^2 and the depth of analysis was approximately 10 nm. All the XPS data were calibrated by the carbon 1s peak at 284.8 eV.

5.3.2 Au-foam/CS-MWCNT/GOx-HRP micro band array biosensor preparation

Gold band array electrodes on silicon were fabricated by a microfabrication process which includes lithography, deposition and etching as we reported earlier [4, 5, 10]. Firstly the thermal growth of an oxide layer on the silicon substrate was achieved after a series of cleaning steps of the substrate and treated with argon plasma. This was followed by the spin-coating process of a photoresist layer. Then metal deposition of titanium and gold was applied by using e-beam evaporation and wafer was patterned by using a lift off procedure. Silicon nitride with 200 nm thickness was deposited by plasma-enhanced chemical vapour deposition and the mask designed for band array was applied by passivation lithography and etching to obtain electroactive surface areas of the band electrodes on the array and connection pad. Finally, wafer was covered by a resist layer to protect electrodes during the dicing process. The microfabricated band array electrode has a 200 nm recess depth which is the thickness of the Si_3N_4 passivation layer on the silicon wafer. A typical system consisted of three individual gold band electrodes of length 2000 µm and width 40 µm. Prior to the use of the electrodes, they were cleaned with organic solvents and a plasma cleaner to remove the resist as we have described in detail previously [4, 5, 10]. All electrochemical measurements were performed on an Autolab workstation (Metrohm, UK) at room temperature. The electrochemical setup consisted of a micro band array electrode as a working electrode, a spiral PT wire electrode as a counter electrode and an Ag/AgCl (1 M KCl) electrode as reference electrode. Electrodeposition of Au-foam was carried out by applying a chronoamperometric method in a solution of 1.2 mM $HAuCl_4 \cdot 3H_20/H_2SO_4$ (2.4 M) at a potential of -7 V for 60 seconds. The Au-foam electrodes prepared were covered with a layer of CS-MWCNT nanocomposite by applying another chronoamperometric deposition process in which a potential of -3 V was applied for 25 seconds in 2 mL electrolyte consisting MWCNT and CS. To prepare the stock solution of the CS-MWCNT, 0.1 g CS was solved in 20 mL of 0.1 M acetic acid solution and mixed overnight. Then 5.2 mg MWCNT was added into CS solution and kept in ultrasonicator until to obtain a homogeneous distribution of MWCNTs. 200 µL of the deposition solution of CS-MWCNT was added into 1800 µL double distilled water and used immediately for CS-MWCNT layer deposition. Following completion of this process the electrodes were washed with double distilled water and dried at

room temperature. **Scheme 1** illustrates the 2-step electrodeposition process used to fabricate the Au-foam/CS-MWCNT band array electrode. After the matrix preparation by the electrochemical approaches, the GOx-HRP enzyme mixture was immobilised onto the surface. For this purpose, an immobilisation solution was prepared which contained 0.16U GOx and 8U HRP, mixed with 2 µL of NHS/EDC (molar ratio of 1:4). The immobilization mixture was drop-cast onto the surface and the electrodes were kept in the fridge at +4 °C for overnight. Finally, the electrodes were washed gently to remove the unbounded enzyme molecules and stored in the fridge when not in use. Cyclic voltammetry was applied to investigate the changes of the surface characteristics after each electrodeposition and modification step in a solution of 5 mM $Fe(CN)_6^{3-/4-}$ as a redox probe containing 0.1 M KCl, 0.01 M PBS (pH 7.4).



Scheme 5.1. Illustration of the 2-step electrochemical deposition process used to fabricate the Au-foam/CS-MWCNT electrode

5.4 Results and Discussions

5.4.1 Micro band array electrode characterisation

Micro band array electrodes consisting of three gold band individual electrodes with 40 µm width, 2000 µm length were designed and fabricated by standard lithography. Fig.5.1A, B and inset show the SEM images of the bare band array electrodes after the fabrication process at both low and high magnification. As can be seen in Fig. 5.1A, the SEM micrograph shows the three well-arranged individual band electrodes of length 2000 µm on the insulation layer with

an 800 µm inter-electrode-distance between them. Fig. 5.1B shows a higher magnification image of the end of one of the electrodes which clearly displays the well-defined shape of the band electrode of width 40 µm. An SEM image of the edge of the corner of a single band electrode is then displayed in Fig. 5.1B-inset where the higher magnification clearly shows the ability of the microfabrication process to produce highly smooth gold surfaces [4]. Fig. 5.1C is a schematic representation of the whole electrode showing the three band array electrodes, the connection track and the connection pad. The elemental composition of the gold surface and the passivated surface were studied using EDX. The SEM-EDX spectral analysis results are shown in Fig. 5.S1 (supporting information). The elements of Au (83.9 %), Si (15.3 %) and Ti (0.7 %) were detected on the electrode active surface area (Fig. 5.S1A, supporting information), where the silicon was the substrate material and the titanium was used as an adhesion layer. On the passivation area, Si (63.4 %), O (20.3 %, presumably from the atmosphere) and N (16.2 %) were detected, indicating the silicon nitride (Si_3N_4) passivation layer Fig. 5.S1B. (Supporting information). These results indicate the success of the microfabrication steps including deposition, lithography and etching. Cyclic voltammetry (CV) was used to study the characteristics of the bare micro band array electrodes. Fig. 5.1D shows cyclic voltammograms recorded from the three individual band array electrodes in a solution of 5 mM $Fe(CN)_6^{3-/4-}$ as a redox probe in 0.01 M PBS (pH 7.4), containing 0.1 M KCl. As shown in the Fig. 5.1D, the micro band array electrodes all exhibit highly reproducible voltammograms. However, the designed electrode tended towards a slightly peak-shaped voltammogram presumably due to the partially overlapping or close diffusion hemispheres of each band on the array. The voltammetry is intermediate between the diffusionally independent profile (category 2) and linear diffusion (category 4) [22]. The effect of scan rate on the voltammetric response was also investigated, Fig. 5.S2. At high scan rate a peak-shaped voltammogram was observed due to the increased contribution from linear diffusion profile, Fig. 5.S2 (inset).

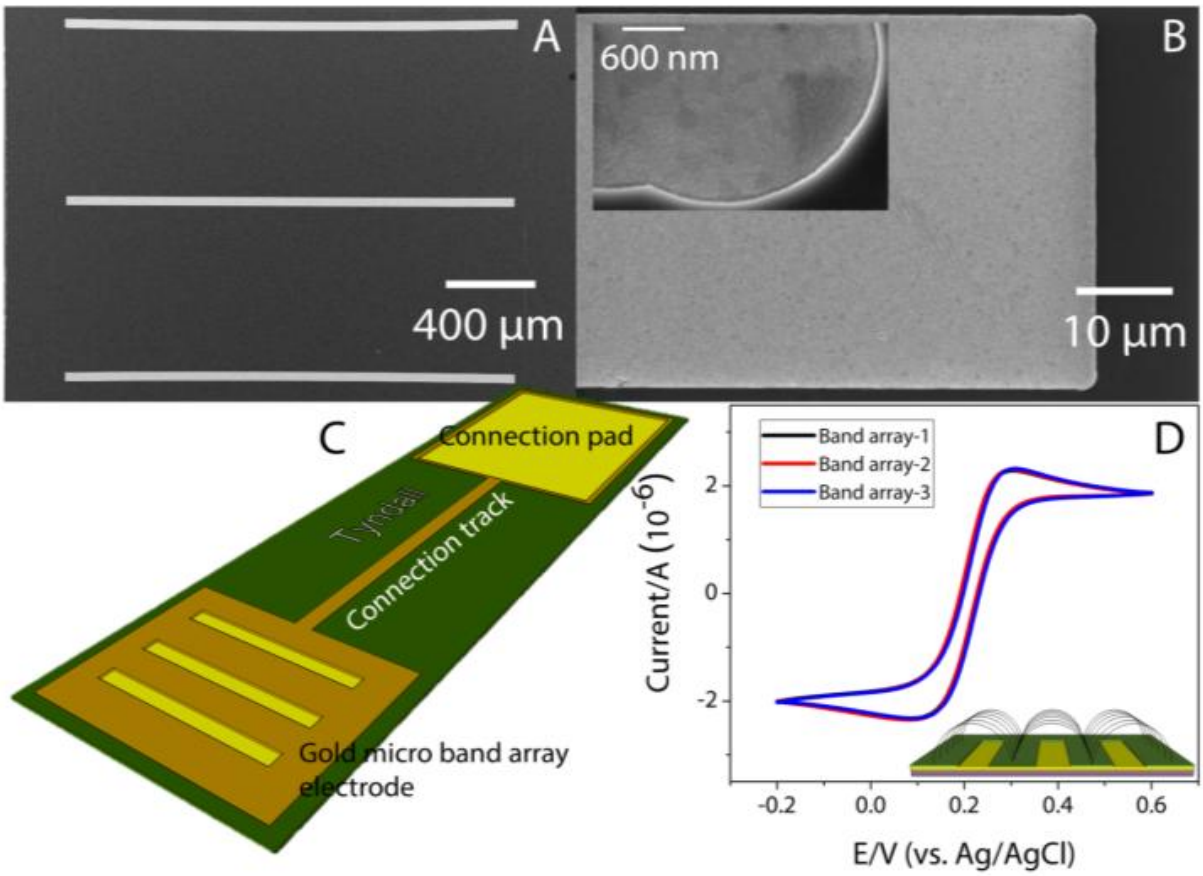


Figure 5.1. SEM images of the bare micro band array electrode; (A) all three bands (low magnification), (B) the edge of the single band electrode (INSET: single band electrode corner-high magnification); (C) schematic illustration of microfabricated band array electrode; (D) overlay cyclic voltammograms of individual three band array electrodes at a scan rate of 5 mV s-1 in a solution of 5 mM Fe(CN)63-/4- as a redox probe in 0.01 M PBS (pH 7.4), containing 0.1 M KCl and the associated diffusion zones

5.4.2 Au-foam and CS-MWCNT electrodeposition, characterisation and the construction of the biosensor

SEM was used to explore the morphological characteristics of the electrodeposits of Au foam and the CS-MWCNT composite. Fig. 5.2A presents an image of the Au foam band array electrode. As can be seen, the highly homogenous distribution of Au foam was achieved as a result of the controlled electrodeposition process. Fig. 5.2B shows an SEM image of a small portion of a single band electrode at higher magnification. From these images it is clear that the Au foam deposits are three-dimensional and highly porous (Fig. 5.2C). Fig. 5.2D demonstrates the nanostructured nature of the gold foam wall.

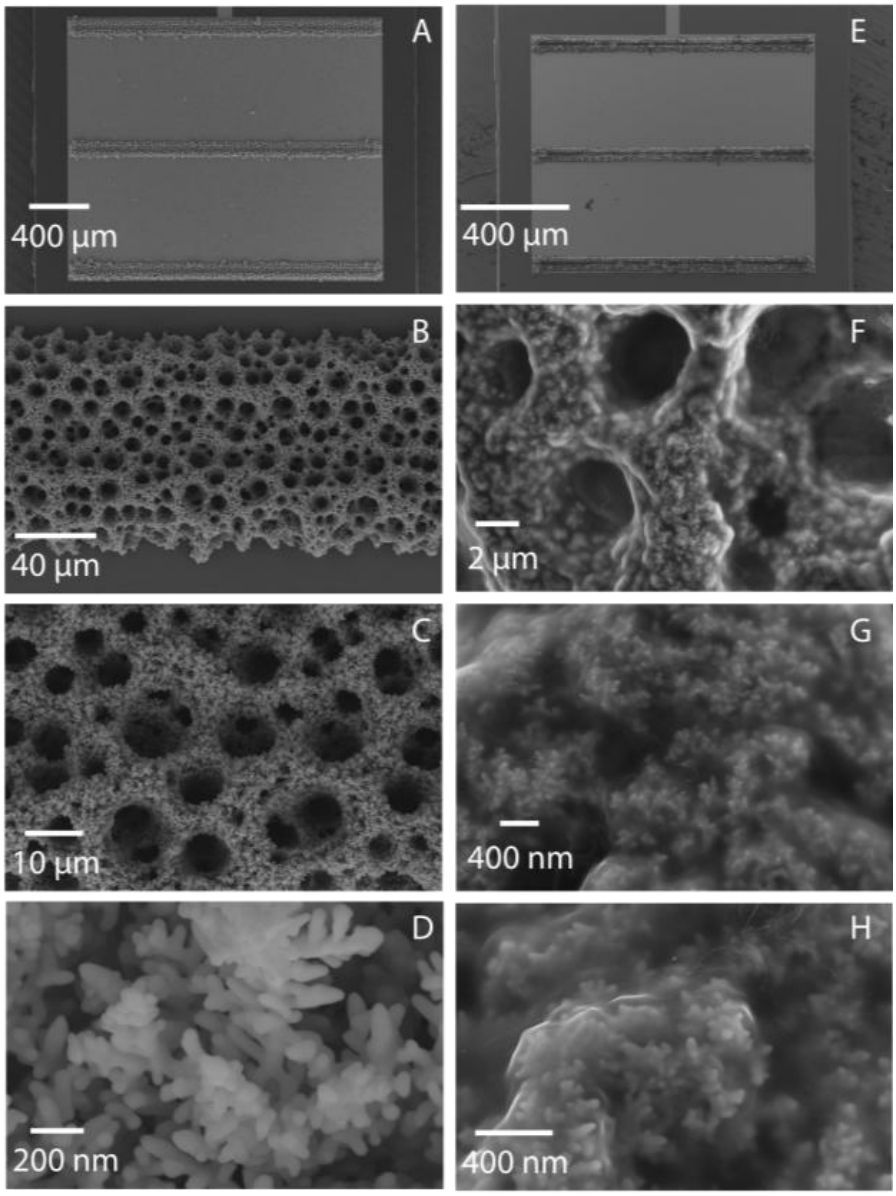


Figure 5.2. SEM images of (A), the Au-foam deposited band array electrode, (B), an Au-foam single band electrode, (C), showing the pore structure of the deposits, (D), showing nanocrystals of the Au-foam wall at higher magnification, (E), the Au-foam band array after CS-MWCNT electrodeposition, (F), the Au-foam/CS-MWCNT pores, and (G and H) SEM images of the CS-MWCNT nanocomposite film electrodeposited nanocrystals with higher magnification

After the electrodeposition of the gold foam, the wall of the foam was covered by a thin film of the chitosan gel by applying -3 V for 25 seconds in the presence of MWCNTs. This process results in the formation of an insoluble chitosan layer on the surface due to the pH changes that occur near to the electrode surface. Furthermore, while the chitosan monomers are accumulating at the electrode surface, the MWCNTs may become trapped in the thin film of

chitosan gel as it forms. Fig. 5.2E shows the whole array electrode after CS-MWCNT electrodeposition. The changes in contrast that are seen following CS-MWCNT electrodeposition are due to the addition of this organic functional layer (OFL) with a darker appearance being associated to a thicker OFL. As it can be seen in Fig. 5.2F, OFL encapsulates the walls of the gold foam. This is more apparent from the higher magnification images presented in Fig. 5.2G and H. Following the drop casting of the enzymes onto the electrode, the effect of the electrodeposition time and hence thickness of the OFL on the current responses of the completed biosensor was studied, Fig. 5.S3A (Supporting Information). From this figure it may be seen that the optimum current value was obtained for an electrode prepared using 25 seconds deposition time to deposit the OFL. Lower deposition times (20 seconds) showed a decreased current level which we suggest may be due to insufficient amounts of the polymer deposits which in turn results in an insufficient number of the functional groups used to attach the enzyme molecules onto surface, leading to a reduction in the amount of immobilised enzymes. However, the figure also reveals that higher deposition times for the OFL also resulted in a decrease in the current response of the sensor. We suggest that this may be due to the presence of a thicker, polymeric OFL which may act as an insulation layer due to the poor conductivity of the polymer. In addition, over deposition of the OFL may lead the formation of a more compact film which may hinder electron transfer and solution diffusion [23, 24]. Thus it is apparent that the thickness of the particular OFL used in this study is a factor which requires some optimisation.

The electrodeposited materials were studied further using XPS and EDX. Fig. 5.3 displays the spectra obtained for each analysis. The XPS survey spectrum confirms the presence of Au, O and C (mostly from atmosphere). Fig. 5.3B shows the high resolution Au 4f XPS spectra of the Au-foam. The Au 4 $f_{7/2}$ and Au $4f_{5/2}$ peaks were centred at 85.0 and 88.7 eV binding energy, respectively, which indicate the presence of metallic gold. The spectrum also shows a peak at ~84.0 eV (4 $f_{7/2}$). This peak is also believed to arise from the bulk gold where the observed shift in energy may be attributed to possible size-related changes in the electronic structure of the material resulting from its nanostructured nature, to the possible presence of oxides or to the

influence of the underlying support materials (Au/ TiO_2/ SiO_2/ Si) and treatment conditions [25, 26]. However, the Au 4f doublet peaks are sufficiently narrow, with a FWHM of 0.68 eV, to be a good indicator of metallic Au [refs]. The 'peaks' at 88.2 and 89.4 eV binding energies which are suggested by the line fitting analysis as shown are possibly related to the presence of Au(III) and similarly the peak at 85.8 eV binding energy may be related to a species that is labelled as $Au^{\delta+}$, which is essentially non-metallic gold but not in the +3 oxidation state. It is suggested that these weaker features most likely result from the presence of some oxide material.

EDX also reveals the presence of the gold, as expected, Fig. 5.3C. In addition, EDX reveals that following electrodeposition of the OFL the elemental composition of the material changes, also as expected, figure 3D. From Fig. 5.3D it can be seen that following deposition of the OFL the surface is composed of Au (52.8%), C (36.8%) and O (10.4%).

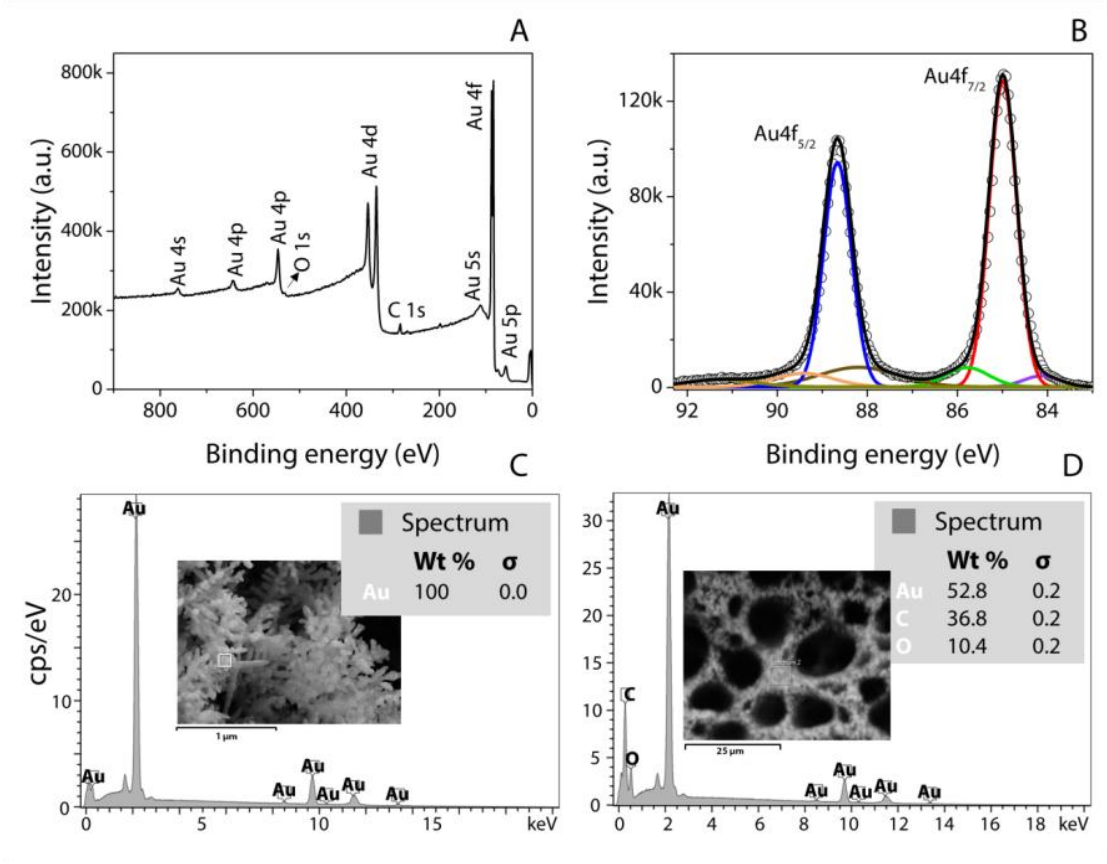


Figure 5.3. (A), an XPS survey spectrum of the Au-foam, (B), a high resolution XPS spectrum of the Au 4f region, (C), an EDX spectrum recorded from the Au-foam and (D), an EDX spectrum recorded from the Au-foam/CS-MWCNT.

The ratio of enzyme loading onto Au-foam/CS-MWCNT surface was also studied, Fig. 5.S3B (supporting information). A series of different molar ratio of GOx: HRP (0.01, 0.015, 0.02 and 0.025) was immobilised onto the Au-foam/CS-MWCNT OFL band array electrode surface. As may be seen from this figure a molar ratio of 0.02 GOx to HRP exhibited the maximum biosensor response. At lower ratios a gradual decrease in current is observed due to the decreasing concentration of the GOx enzyme on the surface. However, a decrease in current is also observed at higher ratios. Although these are preliminary data we may suggest that it is not unreasonable to expect there to be an optimum ratio for the operation of the dual enzyme mechanism based on orientation and conformation factors for the immobilised species and the ease with which the glucose may approach the active sites on the enzymes [23]. As a result of this study a molar ratio, GOx: HRP of 0.02 was adopted in the development of the biosensor.

Fig. 5.4A shows typical cyclic voltammograms recorded from the bare gold band array electrodes and gold foam deposited array electrodes in 0.5 M H_2SO_4. Both surfaces showed a similar electrochemical response, but the current values recorded are very different, with the current observed from the foam electrode being much larger. The foam structured metals are very well-known to be highly porous, possessing very large surface areas. Thus, it is to be expected that in comparison with the bare gold band electrodes the Au foam electrodes would show a much higher response, as shown. Fig. 5.4B represents the voltammograms recorded after the various surface modifications. Clearly, the very large active surface area of the Au-foam deposits resulted in a significant increase in the peak current in comparison to that observed for the bare band array electrode. However, Fig. 5.4B also reveals that following the electrodeposition of the Au foam the shape of the voltammogram changes, adopting the typical shape associated with a voltammogram which arises from a mixture of both planar and radial diffusion. This is most likely due to the increased width of the each band of the array after deposition of foam structures, which may cause overlapping diffusion zones to arise between the adjacent Au-foam band electrodes. It might be expected that if we cover a conductive surface like the Au/Au foam with a non-conductive polymer that a decrease in the peak current of the electrode should result. However, we find that the presence of the MWCNTs appears to improve the conductivity of the OFL resulting in higher current. Moreover, the immobilisation

of the enzymes on the surface results in a decrease of the peak current due to the blocking action of the enzymes towards the test redox couple, as can be seen in Fig. 5.4B.

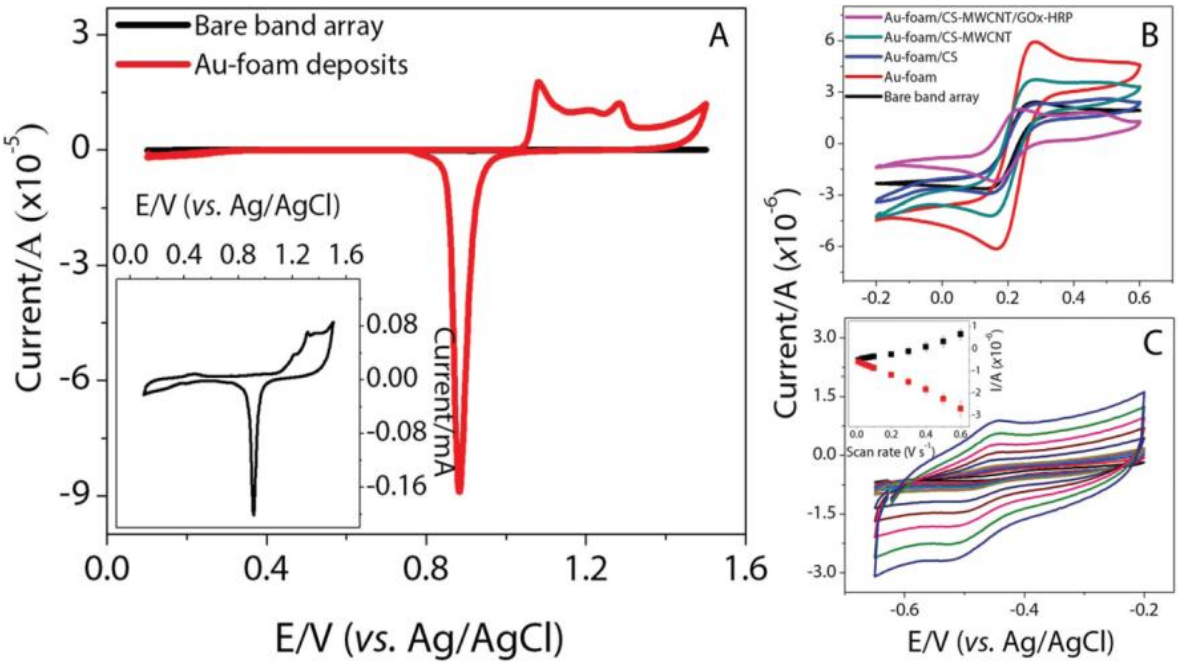


Figure 5.4 (A), CVs recorded from the bare and Au-foam deposited band array electrodes in in 0.5 M H2SO4, (B), CVs recorded from the bare, Au-foam, Au-foam/CS, Au-foam/CS-MWCNT and Au-foam/CS-MWCNT/GOx-HRP modified band array electrodes in 5 mM Fe(CN)63-/4- as a redox probe containing 0.1 M KCl, 0.01 M PBS (pH 7.4), (C), CVs recorded from the complete biosensor at the scan rates of 0.01, 0.03, 0.05, 0.07, 0.09, 0.1, 0.2, 0.3, 0.4, 0.5, 0.6, 0.7 V s-1 in 0.01 M PBS (pH 7.4)

The effect of the scan rate on the voltammetric response was also studied in 0.01 M PBS (pH 7.4). High scan rates lead a decrease in the size of diffusion layer which causes the appearance of increased current levels. As shown in Fig. 5.4C, both anodic and cathodic peak currents increase linearly with increased scan rates from 0.01 to 0.7 V s^{-1}, suggesting a surface-controlled process [27, 28].

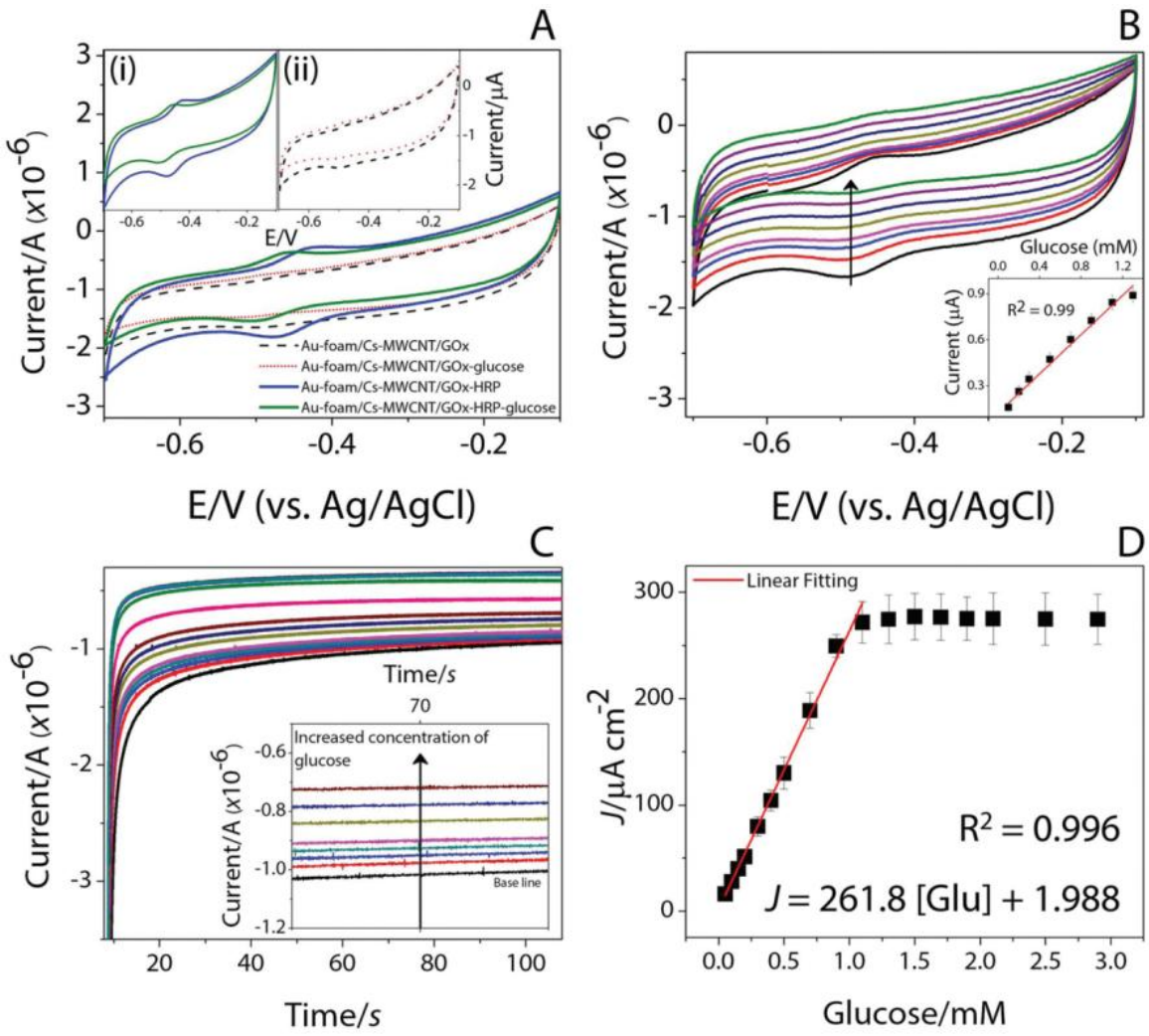


Figure 5.5 (A), CVs recorded from Au-foam/CS-MWCNT/GOx and Au-foam/CS-MWCNT/GOx-HRP modified band array electrodes in the absence of presence of 0.1 mM glucose in 0.01 M PBS (pH 7.4) at a scan rate of 0.05 V s-1 (inset; individual graphs of (i)Au-foam/CS-MWCNT/GOx-HRP and (ii) Au-foam/CS-MWCNT/GOx (B), CVs recorded from the Au-foam/CS-MWCNT/GOx-HRP microbiosensor with increasing concentrations of glucose in 0.01 M PBS (pH 7.4) (inset: corresponding linear range), (C), the chronoamperometric response of the biosensor towards glucose with increasing concentration of glucose at a applied potential of -0.45 V (inset: the magnified graph of 60th second of amperograms of the base and first seven additions), and (D), the corresponding calibration curve obtained from the amperograms recorded from the biosensor.

GOx-HRP dual enzyme system is that cascade scheme where HRP is catalytically linked to GOx, may provide several advantages including signal amplification of the biosensor response and decreased peroxide-induced degradation of immobilised GOx as a result of removal of H_2O_2 [29]. Such systems were developed for glucose detection commonly in the presence of an oxidized mediator for the regeneration of the oxidase [30-32]. Here, we developed a dual-enzyme system without redox mediators. Fig. 5.5 exhibits the CVs obtained from dual enzyme

electrode (i: Au-foam/CS-MWCNT/GOx-HRP) and single enzyme electrode (ii: Au-foam/CS-MWCNT/GOx) in the absence and presence of glucose in PBS. A weak reduction peak was observed at Au-foam/CS-MWCNT/GOx biosensor in the absence of glucose and a decrease of the reduction peak current after glucose addition due to the consumption of the dissolved oxygen by the following enzyme catalyzed reactions (1) and (2) [5, 33, 34] ;

$$GOx\ (FAD) + glucose \longrightarrow GOx\ (FADH_2) + Gluconic\ acid \quad (1)$$

$$GOx\ (FADH_2) + O_2 \longrightarrow GOx\ (FAD) + H_2O_2 \quad (2)$$

However, Au-foam/CS-MWCNT/GOx-HRP biosensor showed greater response towards glucose at -0.45 V without any redox mediator in comparison to single enzyme sensor **(Fig. 5.5i).** This reflects the great cascade scheme of the developed biosensor which based on the current decrease of the dissolved oxygen. The mechanism can be explained as below. HRP contains the heme as prosthetic group, which is also the active site of the protein (with resting state of the heme-iron: Fe (III)). HRP reacts with H_2O_2 to form compound I which is a two-equivalent oxidized form containing oxyferryl heme ($Fe^{4+} = O$) and H_2O (Eq. 3) [33]. In turn, compound I is further reduced (Eq. 4) or it also may produce HRP (Fe^{3+}), O_2 and H_2O if it reacts with the H_2O_2 as proton and electron donor (Eq. 5) [35-37].

$$HRP\ (Fe^{3+}) + H_2O_2 \longrightarrow Compound\ I\ [HRP\ (Fe^{4+} = O)] + H_2O \quad (3)$$

$$Compound\ I\ [HRP\ (Fe^{4+} = O)] + 2e^- + 2H^+ \longrightarrow HRP\ (Fe^{3+}) + H_2O \quad (4)$$

$$Compound\ I\ [HRP\ (Fe^{4+} = O)] + H_2O_2 \longrightarrow HRP\ (Fe^{3+}) + O_2 + H_2O \quad (5)$$

Furthermore the biosensor was studied by applying cyclic voltammetry in a series of standard glucose solutions in 0.01 M PBS (pH 7.4). Fig. 5.5B shows the corresponding CVs recorded after each addition of glucose into electrochemical cell. With increasing concentration of glucose, a decrease of the reduction current and an increase of the oxidation current is observed due to the consecutive catalytic reactions induced by both enzymes with firstly the glucose and secondly the hydrogen peroxide. The inset graphs (Fig. 5.5B) demonstrate the linear

relationship between the glucose concentration and the reduction current density with a correlation coefficient (R^2) of 0.99. This result reveals that the dual-enzyme biosensor developed has some considerable potential for the detection of glucose via these enzymatic processes.

5.4.3 Chronoamperometric detection of glucose by Au-foam/CS-MWCNT/GOx-HRP micro band array biosensor

Fig.5C displays the chronoamperograms obtained by using the Au-foam/CS-MWCNT/GOx-HRP micro band array biosensor at an applied potential of -0.45 V. The inset graph (Fig. 5.5C) shows the 70^{th} second of amperograms belong to the base line and first 7 subsequent additions of glucose. Fig. 5.5D demonstrates the corresponding calibration curve of the biosensor, obtained by subtraction of the current values at 70^{th} second from the base line current value at the same second. As it can be seen in the Fig. 5.5C and the inset, each amperogram reaches steady-state current level very quickly, which is one of the most important advantages of the miniaturised systems that form the basis of our work [4, 10]. The biosensor developed exhibited a linear range from 0.05 mM to 1.1 mM with the linear regression equation of $J\ (\mu A\ cm^{-2}) = 261.8\ [Glu]\ (mM) + 1.988$ (R^2= 0.996). The sensitivity of the biosensor was calculated to be 261.8 µA mM^{-1} cm^{-2}. This high value of sensitivity may be attributed to the advantages of the electrode/ OFL matrix developed for enzyme immobilisation, being a combination of the gold foam-chitosan–multi walled carbon nanotubes, the use of a dual-enzyme system and the use of micron-scale, band array electrodes. The limit of detection (LOD) was calculated to be 0.025 mM by using the formula, $3s_b/S$ (s_b, standard deviation of the blank; S, sensitivity). A performance comparison of the biosensor developed with the other dual-enzyme biosensors described in the literature is given in Table 5.1.

Table 5.1. The analytical performance comparison list of dual-enzyme biosensors available in literature

	Sensitivity	**Linear range**	**Detection limit**	**Reproducibility**	**Reusability, repeatability, or operational stability**	**Long term stability**	**Ref.**
Polymerized-multiporous SnO_2 nanofibers/HRP/GOx	-	5 - 100 µM	1.8 µM	-	3.5% (RSD), n=10	94%, after 60 days	[38]
Au/SWNT/GOD-HRP/PPy	7.01 ± 0.18 µA mM^{-1} cm^{-2}	0.030 - 2.43 mM	0.03 ± 0.009 mM	5.4% (RSD), n=8	A decrease of 35% within 10hours, good operational stability	82% and 67% of after 1 and 2 weeks	[39]
Au/MPS/TH/$(SCGNPs/TH)_6$ /GOx/HRP	3.8 µA mM^{-1} cm^{-2}	up to at least 3.0 mM	3.5×10^{-5} M	-	-	80%, 3 weeks	[40]
GC/[TMOS−HRP−graphite] −[TMOS−GOD]	2.95 mA M^{-1} cm^{-2}	Up to 0.70 mM	-	-	-	74%, one week	[41]
(GOD/PPy) membrane on the surface of (FCA)-mediated (HRP)-modified CCE	1.11 µA mM^{-1}	8.0×10^{-5} - 1.3×10^{-3} M	1.0×10^{-5} M	-	-	68%, 3 weeks	[42]
GC/CNT/GOx + HRP/PTBO	113 mA M^{-1} cm^{-2}	0.1-1.2mM	0.03 mM	4.3% (RSD), n=8	-	75%, 25 days	[43]
fMWCNT–TB–GOx–HRP–Nf	8.3 µA mM^{-1} cm^{-2}	1.5×10^{-8} - 1.8×10^{-3} M	3×10^{-9} M	2.5%(RSD), n=10	1.9% (RSD), n=8	95%, 4 months	[44]
GOD–HRP–Cys–SG/GNP/ITO	131.7 nA $mmol^{-1}$ L^{-1}	0.02-3.2 mmol L^{-1}	0.01 mmol L^{-1}	6.7%(RSD), n=5	3.1%(RSD), n=9	80%, 2 months	[29]
GOx–CS–HRP/AgNCs–CS	-	10 µM - 1.5 mM	0.6977 µM	1.27%(RSD), n=6	2.14%(RSD), n=4	93%, 9days; 70%, 2 weeks	[45]
Nf–GOD–HRP/Au–Fe3O4@SiO2/ITO	(1) 92.14, (2) 15.00 µA mM^{-1} cm^{-2}	(1) 0.05 - 1.0mM, (2) 1.0 - 8.0mM	0.01 mM	5.2% (RSD), n=6	3.7% (RSD), n=5	97.2%, 25 days; 94.8%, 30 days; 50% 60 days	[46]
HRP–GOD/Con A/CS	1.18 µA mM^{-1}	0.001 – 0.22 mM	6.7×10^{-7} M	3.8%(RSD), n=6	2.9% (RSD), n=7	89%, 5 weeks	[47]
PANI|HRP–GOD|MWNTs	0.94 µA mM^{-1}	0.05-12 mM	0.02 mM	9.5%(RSD), n=8	-	-	[48]
MWNT/TH/GOD/HRP/Nf	-	10 nM – 10 mM	3 nM	-	2.3% (RSD), n=9	>90%, 90 days	[49]
Au-foam/Cs-MWCNT/GOx-HRP micro band array biosensor	261.8 µA mM^{-1} cm^{-2}	0.05 – 1.3 mM	25 µM	3.30% (RSD), n=7	4.41%, 3.93% and 4.99% (RSD), n=10 for each biosensor	No significant change after 45 days	This study

Abbreviations; Au: gold, SWNT: single-walled carbon nanotube, Ppy: electropolymerized pyrrole, MPS: 3-mercapto-1-propanesulfonic acid sodium salt, SCGNPs: sulfonate-capped gold nanoparticles, TH: thionine, TMOS: Tetramethoxysilane , GC: glassy carbon electrode, FCA: Ferrocenecarboxylic acid, CCE: sol-gel derived composite carbon electrode, PTBO: poly(toluidine blue O), CNT: Carbon nanotube, fMWCNT: functionalized multiwalled carbon nanotubes, TB: Toluidine blue, Nf: Nafion, Cys: Cysteine, SG: silica sol-gel, GNP: gold nanoparticles, ITO: indium tin

oxide, AgNCs: Silver nanocubes, CS: Chitosan, Con A: Concanavalin A, PANI: polyaniline, MWCNTs: multiwalled carbon nanotubes

5.4.4 Interference effect, Stability and Reproducibility

To evaluate the selectivity of the biosensor towards glucose in the presence of the common interfering species, three individual biosensors were prepared and studied with glucose, ascorbic acid, acetaminophen and uric acid. Fig. 5.S4 (supporting information) shows chronoamperograms recorded after each addition of the interfering species. Briefly, the prepared biosensors were studied with blank PBS (0.01 M, pH 7.4), and then a 0.4 mM glucose solution was measured. This was followed by the serial additions of 0.1 mM ascorbic acid, acetaminophen and uric acid, respectively. 0.4 mM glucose was studied at the end in the presence of those interfering molecules. Fig. 5.6A shows a comparison of current densities obtained from the first (glu) and last (glu_{int}) glucose measurements. The calculated changes of the biosensor responses are 11.45 %, 10.75 % and 9.89 %. The operational stability of the developed biosensor was studied by 10 subsequent chronoamperometric measurements of three individual biosensors. Fig. 5.6B displays the current densities obtained from each experiment, for each biosensor. The calculated standard deviations for each biosensor in regard to operational stability are 4.41 %, 3.93 % and 4.99 %. After storing the biosensor in 0.01 M PBS (pH 7.4) at 4°C for 45 days, there was no significant change of the response of the biosensor. Seven individual biosensors were prepared and their responses to glucose in 0.01 M PBS (pH 7.4) were measured under the same conditions in order to evaluate the biosensor reproducibility, Fig. 5.6C. The relative standard deviation towards glucose detection was determined to be 3.30%.

These noteworthy performance results obtained for the biosensor developed indicate the success of the biosensor as an analytical device. While the band array electrode provides a micro-scaled environment, the Au-foam deposit offers a highly porous 3D surface which was optimised to the borders of each band of the array. After the one step electrochemical deposition of chitosan-multiwalled carbon nanotube nanocomposite OFL, the overall matrix becomes a biocompatible microenvironment for biomolecule immobilisation which contributes to maintaining and improving the catalytic activity of the attached enzymes. Furthermore, the

developed matrix is highly suitable for high concentration biomolecule immobilisation due to its high surface.

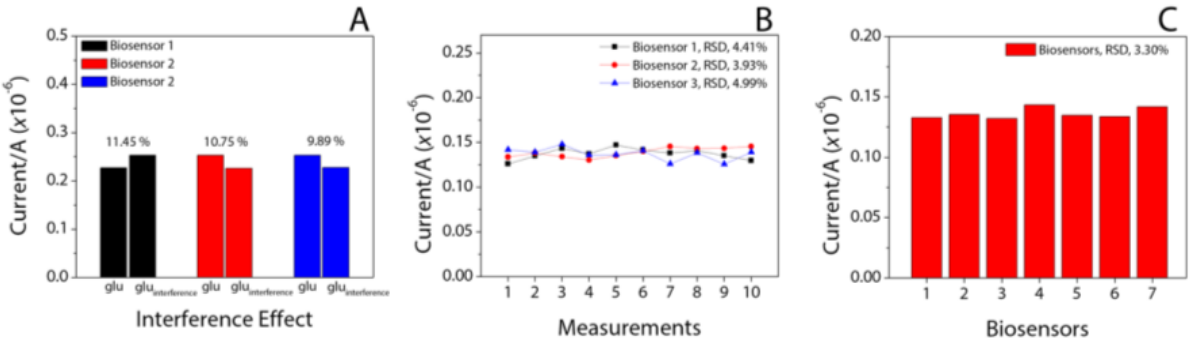


Figure 5.6 (A), Interference effects recorded for three individual biosensors , (B), the operational stability of the three individual biosensors, and (C), the reproducibility of the biosensor (n=7)

5.4.5 A real-world application

To demonstrate a possible real world application of our biosensor, sterile human serum samples were used. A sterile serum sample was diluted to 1:10 in 0.01 M PBS (pH 7.4) and spiked with two different concentrations of glucose to obtain 0.5 mM and 1 mM glucose concentrations in the electrochemical cell. The biosensor was used to determine the glucose level in both spiked samples, respectively. Firstly, prepared electrodes were studied with chronoamperometry in 0.01 M PBS (pH 7.4) to be used as a baseline. Then spiked serum samples were added into electrochemical cell using standard addition method, mixed very well and measured by applying chronoamperometry at – 0.45 V. The obtained value at 70th second from spiked serum was subtracted from the baseline value obtained at 70th second to determine the concentration from the calibration curve equation. The results obtained for both spiked samples are shown in Table 5.2. The obtained concentration of non-spiked sterile serum in the electrochemical cell (0.002 mM < LOD) is neglected due to the lower value than the limit of detection of the developed biosensor.

Table 5.2. Determination of glucose in sterile serum samples

Sample	Spiked serum glucose concentration (mM)	Au-foam/CS-MWCNT/GOx-HRP micro band array biosensor measured glucose concentration	Recovery (%)
1	0.5	0.54 (±0.01)	108
2	1	0.99 (±0.01)	99

Conclusion

This paper reports the development of a dual-enzyme micro band array biosensor for the detection of glucose. The in-house microfabricated electrode is a silicon-based highly reproducible micro band array electrode consisting of three bands on the array with 40 µm band-width and 2000 µm band-length. The band array electrode is then modified with 3D gold foam by controlled electrodeposition. The gold foam, being a highly porous material, serves to dramatically increase the active surface area. An OFL in the form of an electrodeposited chitosan-multiwalled carbon nanotubes nanocomposite film is then added as the main immobilisation matrix for glucose oxidase and horseradish peroxidase.

The resulting biosensor showed a sensitivity of 261.8 µA mM^{-1} cm^{-2} and reproducibility (RSD 3.30%, n=7). Furthermore, it demonstrated a lifetime of up to 45 days (stored at +4 °C, in 0.01 M PBS, pH 7.4). The operational stability of the biosensor demonstrates a very good level of reusability with low RSD values of 4.41%, 3.93% and 4.99%. The biosensor showed corresponding values towards the spiked serum samples with 108% and 99% recovery levels.

The principle benefits of the sensing platform developed here arise from a combination of the micro-scaled matrix architecture used combined with the nanoscale deposits and the highly flexible, biocompatible, easily functionalised OFL material. We suggest there that this platform may be highly suitable for the detection of other biomolecules and further miniaturisation and/or packaging.

5.5 Acknowledgements

The authors appreciate the financial support from the Department of Agriculture, Food and the Marine, 14F883, Ireland.

5.6 References

[1] X.Y. Lang, H.Y. Fu, C. Hou, G.F. Han, P. Yang, Y.B. Liu, Q. Jiang, Nanoporous gold supported cobalt oxide microelectrodes as high-performance electrochemical biosensors, Nat Commun, 4 (2013).

[2] J. Wang, Electrochemical glucose biosensors, Chemical Reviews, 108 (2008) 814-825.

[3] A.P.F. Turner, Biosensors: Fundamentals and applications – Historic book now open access, Biosensors and Bioelectronics, 65 (2015) A1.

[4] V. Buk, M.E. Pemble, A highly sensitive glucose biosensor based on a micro disk array electrode design modified with carbon quantum dots and gold nanoparticles, Electrochim Acta, 298 (2019) 97-105.

[5] V. Buk, M.E. Pemble, K. Twomey, Fabrication and evaluation of a carbon quantum dot/gold nanoparticle nanohybrid material integrated onto planar micro gold electrodes for potential bioelectrochemical sensing applications, Electrochimica Acta, 293 (2019) 307-317.

[6] I. Streeter, N. Fietkau, J. Del Campo, R. Mas, F.X. Munoz, R.G. Compton, Voltammetry at regular microband electrode arrays: Theory and experiment, J Phys Chem C, 111 (2007) 12058-12066.

[7] J. Okuno, K. Maehashi, K. Matsumoto, K. Kerman, Y. Takamura, E. Tamiya, Single-walled carbon nanotube-arrayed microelectrode chip for electrochemical analysis, Electrochemistry Communications, 9 (2007) 13-18.

[8] C.X. Ma, N.M. Contento, L.R. Gibson, P.W. Bohn, Redox Cycling in Nanoscale-Recessed Ring-Disk Electrode Arrays for Enhanced Electrochemical Sensitivity, Acs Nano, 7 (2013) 5483-5490.

[9] D. Li, C. Lin, C. Batchelor-McAuley, L. Chen, R.G. Compton, Electrochemical measurement of the size of microband electrodes: A theoretical study, J Electroanal Chem, 840 (2019) 279-284.

[10] V.B. Juska, A. Walcarius, M.E. Pemble, Cu Nanodendrite Foams on Integrated Band Array Electrodes for the Nonenzymatic Detection of Glucose, ACS Applied Nano Materials, (2019).

[11] D.H. Nam, B.J. Taitt, K.S. Choi, Copper-Based Catalytic Anodes To Produce 2,5-Furandicarboxylic Acid, a Biomass-Derived Alternative to Terephthalic Acid, Acs Catal, 8 (2018) 1197-1206.

[12] W. Lu, Y. Sun, H. Dai, P. Ni, S. Jiang, Y. Wang, Z. Li, Z. Li, Direct growth of pod-like Cu2O nanowire arrays on copper foam: Highly sensitive and efficient nonenzymatic glucose and H2O2 biosensor, Sensors and Actuators B: Chemical, 231 (2016) 860-866.

[13] X. Niu, Y. Li, J. Tang, Y. Hu, H. Zhao, M. Lan, Electrochemical sensing interfaces with tunable porosity for nonenzymatic glucose detection: A Cu foam case, Biosensors and Bioelectronics, 51 (2014) 22-28.

[14] E. Zhang, R. Xing, S. Liu, Y. Qin, K. Li, P. Li, Advances in chitosan-based nanoparticles for oncotherapy, Carbohyd Polym, 222 (2019) 115004.

[15] R. Shanmuganathan, T.N.J.I. Edison, F. LewisOscar, P. Kumar, S. Shanmugam, A. Pugazhendhi, Chitosan nanopolymers: An overview of drug delivery against cancer, Int J Biol Macromol, 130 (2019) 727-736.

[16] J. Cui, S.B. Adeloju, Y. Wu, Integration of a highly ordered gold nanowires array with glucose oxidase for ultra-sensitive glucose detection, Anal Chim Acta, 809 (2014) 134-140.

[17] C.C. Ryan, M. Bardosova, M.E. Pemble, Structural and mechanical properties of a range of chitosan-based hybrid networks loaded with colloidal silica and polystyrene particles, J Mater Sci, 52 (2017) 8338-8347.

[18] Y.H. Lin, F. Lu, Y. Tu, Z.F. Ren, Glucose biosensors based on carbon nanotube nanoelectrode ensembles, Nano Letters, 4 (2004) 191-195.

[19] W. Sun, P. Qin, H. Gao, G. Li, K. Jiao, Electrochemical DNA biosensor based on chitosan/nano-V2O5/MWCNTs composite film modified carbon ionic liquid electrode and its application to the LAMP product of Yersinia enterocolitica gene sequence, Biosensors and Bioelectronics, 25 (2010) 1264-1270.

[20] Q. Wang, B. Zhang, X. Lin, W. Weng, Hybridization biosensor based on the covalent immobilization of probe DNA on chitosan–mutiwalled carbon nanotubes nanocomposite by using glutaraldehyde as an arm linker, Sensors and Actuators B: Chemical, 156 (2011) 599-605.

[21] Y. Liu, M. Wang, F. Zhao, Z. Xu, S. Dong, The direct electron transfer of glucose oxidase and glucose biosensor based on carbon nanotubes/chitosan matrix, Biosensors and Bioelectronics, 21 (2005) 984-988.

[22] K.R. Ward, N.S. Lawrence, R.S. Hartshorne, R.G. Compton, The theory of cyclic voltammetry of electrochemically heterogeneous surfaces: comparison of different models for surface geometry and applications to highly ordered pyrolytic graphite, Phys Chem Chem Phys, 14 (2012) 7264-7275.

[23] V. Buk, E. Emregul, K.C. Emregul, Alginate copper oxide nano-biocomposite as a novel material for amperometric glucose biosensing, Mat Sci Eng C-Mater, 74 (2017) 307-314.

[24] Q. Zhu, B. Liang, Y. Cai, Q. Cao, T. Tu, B. Huang, L. Fang, X. Ye, Layer-by-layer chitosan-decorated pristine graphene on screen-printed electrodes by one-step electrodeposition for non-enzymatic hydrogen peroxide sensor, Talanta, 190 (2018) 70-77.

[25] M. Sankar, Q. He, M. Morad, J. Pritchard, S.J. Freakley, J.K. Edwards, S.H. Taylor, D.J. Morgan, A.F. Carley, D.W. Knight, C.J. Kiely, G.J. Hutchings, Synthesis of Stable Ligand-free Gold-Palladium Nanoparticles Using a Simple Excess Anion Method, Acs Nano, 6 (2012) 6600-6613.

[26] F.-W. Chang, H.-Y. Yu, L. Selva Roselin, H.-C. Yang, Production of hydrogen via partial oxidation of methanol over Au/TiO2 catalysts, Applied Catalysis A: General, 290 (2005) 138-147.

[27] J.R. Anusha, C.J. Raj, B.-B. Cho, A.T. Fleming, K.-H. Yu, B.C. Kim, Amperometric glucose biosensor based on glucose oxidase immobilized over chitosan nanoparticles from gladius of Uroteuthis duvauceli, Sensors and Actuators B: Chemical, 215 (2015) 536-543.

[28] S. Deng, G. Jian, J. Lei, Z. Hu, H. Ju, A glucose biosensor based on direct electrochemistry of glucose oxidase immobilized on nitrogen-doped carbon nanotubes, Biosensors and Bioelectronics, 25 (2009) 373-377.

[29] M. Gu, J. Wang, Y. Tu, J. Di, Fabrication of reagentless glucose biosensors: A comparison of mono-enzyme GOD and bienzyme GOD–HRP systems, Sensors and Actuators B: Chemical, 148 (2010) 486-491.

[30] M. Delvaux, A. Walcarius, S. Demoustier-Champagne, Bienzyme HRP–GOx-modified gold nanoelectrodes for the sensitive amperometric detection of glucose at low overpotentials, Biosensors and Bioelectronics, 20 (2005) 1587-1594.

[31] X. Chen, J. Zhu, R. Tian, C. Yao, Bienzymatic glucose biosensor based on three dimensional macroporous ionic liquid doped sol–gel organic–inorganic composite, Sensors and Actuators B: Chemical, 163 (2012) 272-280.

[32] C.C. Gong, J.Y. Chen, Y.H. Song, M. Sun, Y.G. Song, Q.H. Guo, L. Wang, A glucose biosensor based on the polymerization of aniline induced by a bio-interphase of glucose oxidase and horseradish peroxidase, Anal Methods-Uk, 8 (2016) 1513-1519.

[33] Z. Dai, J. Bao, X. Yang, H. Ju, A bienzyme channeling glucose sensor with a wide concentration range based on co-entrapment of enzymes in SBA-15 mesopores, Biosensors and Bioelectronics, 23 (2008) 1070-1076.

[34] R. Madhu, B. Devadas, S.M. Chen, M. Rajkumar, An enhanced direct electrochemistry of glucose oxidase at poly(taurine) modified glassy carbon electrode for glucose biosensor, Anal Methods-Uk, 6 (2014) 9053-9058.

[35] M. Christwardana, Y. Chung, D.-H. Kim, Y. Kwon, Glucose biofuel cells using the two-step reduction reaction of bienzyme structure as cathodic catalyst, J Ind Eng Chem, 71 (2019) 435-444.

[36] J. Vlasits, C. Jakopitsch, M. Schwanninger, P. Holubar, C. Obinger, Hydrogen peroxide oxidation by catalase-peroxidase follows a non-scrambling mechanism, Febs Lett, 581 (2007) 320-324.

[37] C.J. Baker, K. Deahl, J. Domek, E.W. Orlandi, Scavenging of H2O2 and Production of Oxygen by Horseradish Peroxidase, Archives of Biochemistry and Biophysics, 382 (2000) 232-237.

[38] S. Alim, A.K.M. Kafi, J. Rajan, M.M. Yusoff, Application of polymerized multiporous nanofiber of SnO2 for designing a bienzyme glucose biosensor based on HRP/GOx, Int J Biol Macromol, 123 (2019) 1028-1034.

[39] L.D. Zhu, R.L. Yang, J.G. Zhai, C.Y. Tian, Bienzymatic glucose biosensor based on co-immobilization of peroxidase and glucose oxidase on a carbon nanotubes electrode, Biosens Bioelectron, 23 (2007) 528-535.

[40] Y.Y. Sun, Y. Bai, W.W. Yang, C.Q. Sun, Controlled multilayer films of sulfonate-capped gold nanoparticles/thionine used for construction of a reagentless bienzymatic glucose biosensor, Electrochimica Acta, 52 (2007) 7352-7361.

[41] L. Coche-Guérente, S. Cosnier, P. Labbé, Sol−Gel Derived Composite Materials for the Construction of Oxidase/Peroxidase Mediatorless Biosensors, Chem Mater, 9 (1997) 1348-1352.

[42] F. Tian, G. Zhu, Bienzymatic amperometric biosensor for glucose based on polypyrrole/ceramic carbon as electrode material, Anal Chim Acta, 451 (2002) 251-258.
[43] W.J. Wang, F. Wang, Y.L. Yao, S.S. Hu, K.K. Shiu, Amperometric bienzyme glucose biosensor based on carbon nanotube modified electrode with electropolymerized poly(toluidine blue O) film, Electrochimica Acta, 55 (2010) 7055-7060.
[44] D.R.S. Jeykumari, S.S. Narayanan, Functionalized carbon nanotube-bienzyme biocomposite for amperometric sensing, Carbon, 47 (2009) 957-966.
[45] P. Yang, L. Wang, Q. Wu, Z. Chen, X. Lin, A method for determination of glucose by an amperometric bienzyme biosensor based on silver nanocubes modified Au electrode, Sensors and Actuators B: Chemical, 194 (2014) 71-78.
[46] X. Chen, J. Zhu, Z. Chen, C. Xu, Y. Wang, C. Yao, A novel bienzyme glucose biosensor based on three-layer Au–Fe3O4@SiO2 magnetic nanocomposite, Sensors and Actuators B: Chemical, 159 (2011) 220-228.
[47] F. Li, Z. Wang, W. Chen, S. Zhang, A simple strategy for one-step construction of bienzyme biosensor by in-situ formation of biocomposite film through electrodeposition, Biosensors and Bioelectronics, 24 (2009) 3030-3035.
[48] Q.L. Sheng, J.B. Zheng, Bienzyme system for the biocatalyzed deposition of polyaniline templated by multiwalled carbon nanotubes: A biosensor design, Biosens Bioelectron, 24 (2009) 1621-1628.
[49] D.R.S. Jeykumari, S.S. Narayanan, Fabrication of bienzyme nanobiocomposite electrode using functionalized carbon nanotubes for biosensing applications, Biosens Bioelectron, 23 (2008) 1686-1693.

5.7 Supporting Information

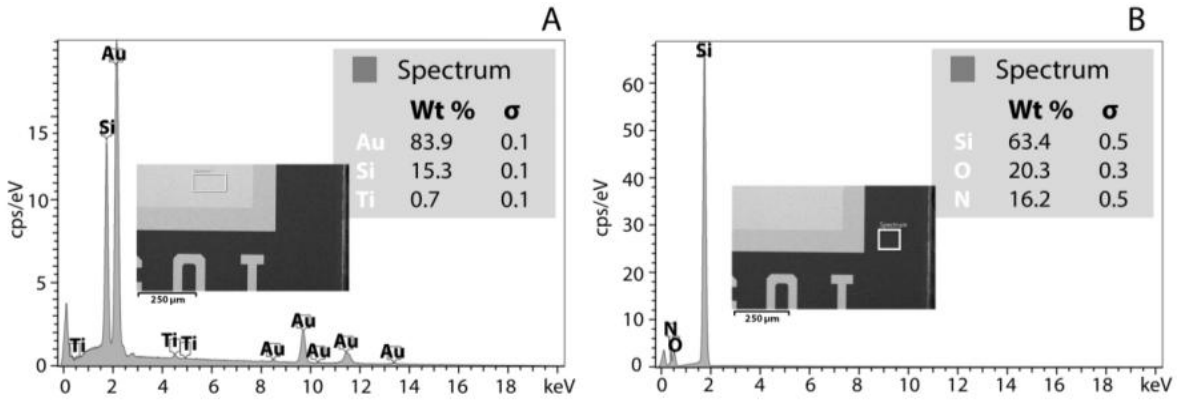


Fig 5.S1. EDX spectrum analysis of (A) gold surface of the connection pad and (B) passivated outer layer.

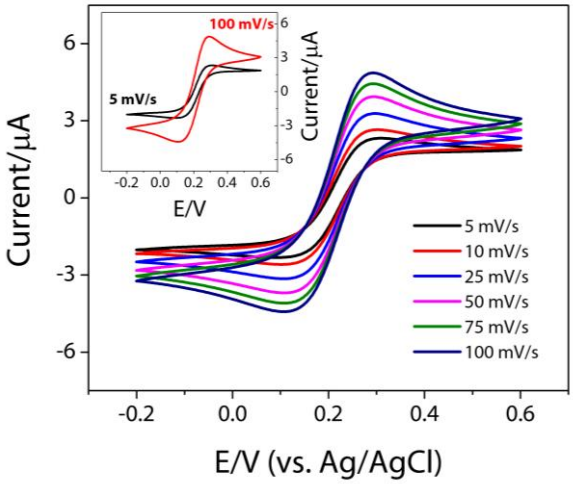


Fig 5.S2. CVs of bare band array electrode recorded at different scan rates; 5, 10, 25, 50, 75 and 100 mV s-1, (inset: CVs recorded at scan rates of 5 and 100 mV s-1) in a solution of 5 mM Fe(CN)63-/4- as a redox probe in 0.01 M PBS (pH 7.4), containing 0.1 M KCl

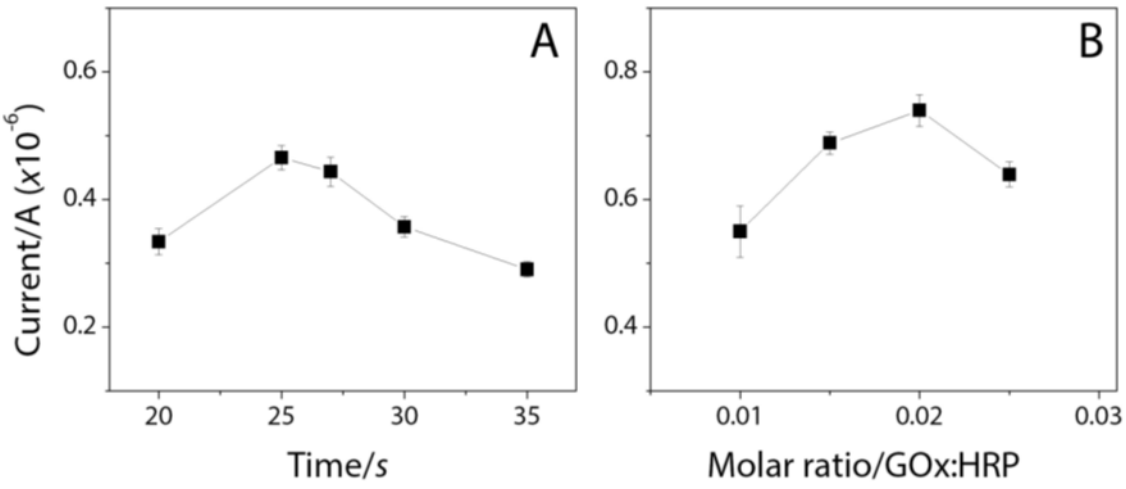


Figure 5.S3. (A) Effect of the CS-MWCNT electrodeposition time in 0.01 M PBS (pH 7.4) containing 1 mM glucose, and (B) Effect of the molar ratio of GOx and HRP in 0.01 M PBS (pH 7.4) containing 5 mM glucose

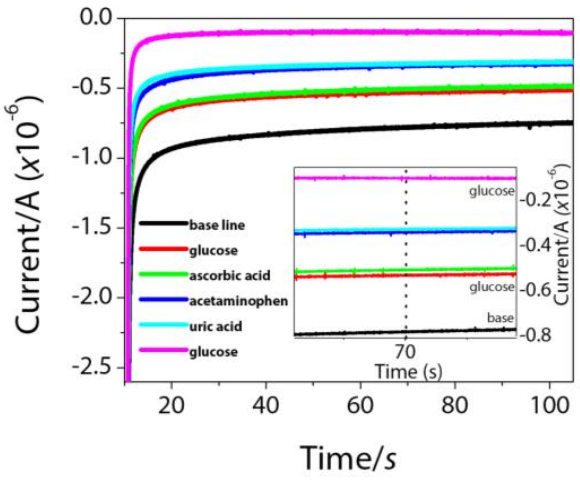


Figure 5.S4. Chronoamperometric response of the biosensor towards glucose, ascorbic acid, acetaminophen and uric acid

CHAPTER 6

Summary and future perspectives

6. Summary and future perspectives

While comprehensive conclusions were given at the end of each chapter outlining the main results and impact of the particular studies in question, this section aims to draw the work presented in this thesis to a conclusion and to provide suggestions as to the future perspectives for work of the type described in this thesis, namely the 'Design, Development and Characterization of Nanostructured Electrochemical Sensors'.

In Chapter 1 a comprehensive review of the development of electrochemical biosensors was presented with a brief history of biosensors and commercialisation of glucometers. This Chapter explains the progress of electrochemical biosensors as first, second and third generation biosensors respectively by using game-changing literature examples from leading researchers who opened up new directions for the field. Moreover, it provides an insight of the use of miniaturisation for the construction of various types of electrochemical sensing platforms. This is particularly significant because of the increasing trend towards the use of semiconductor microfabrication methods to make reliable, reproducible and highly efficient sensors of all types, including those that operate via a bioelectrochemical mechanism. The Chapter demonstrates that recent advancements in several research areas, such as biochemistry, bioengineering, microtechnologies, materials, microfluidics and packaging technologies, have all greatly contributed to the expansion of the field of electrochemical biosensors.

As a part of these contributions, via Chapters 2-5, this thesis has demonstrated the use of microtechnologies and advanced nanostructures by using glucose as a model analyte. The systems developed have proven to be capable of detecting the target analyte with high sensitivities (for instance a sensitivity of $10{,}630\ \mu A\ mM^{-1}\ cm^{-2})$[24] and furthermore they have shown excellent stability, reproducibility and resistance to potential interfering species, – clearly demonstrating the high potential for their use in practical applications. It is hoped that the work presented in Chapter 2-5 will set the scene for the development of a wide range of new or improved sensors that can address particular medical issues but also issues in the environment and in food production.

With this in mind it is possible to speculate as to the direction in which this work should now proceed:

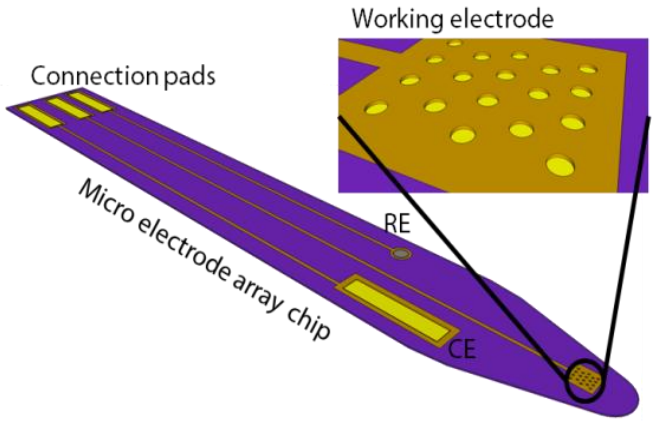


Figure 6.1.Schematic image of the possible design of micro electrode array chip

One of the first potential topics for future study is the further miniaturisation of the overall system. For example a "3-electrode-on-a-chip" device may be developed by applying microfabrication technologies, such as lithography, deposition and etching. A proposed design of such a chip is presented above, Figure 6.1.

Such a device would be highly suitable for surface modification processes, such as dip-coating, drop-casting and electrodeposition, even in harsh conditions due to the specific distance between the working electrode and the others (counter and reference electrodes). Fig. 6.1 shows a schematic image of a disk array electrode-based chip design in the presence of working electrode and counter electrode.

Such chips could be easily adapted to achieve the immobilisation of different types of enzymes, antibodies, DNA or aptamers in the presence of the nanostructures applied in this thesis for the development of electrochemical biosensors for application in the health, agriculture, food and many other industries. Furthermore, the design of the chip may be adjusted so as to facilitate the integration of the device with a microfluidic system such as may be required for the development of a highly advanced sensing platform.

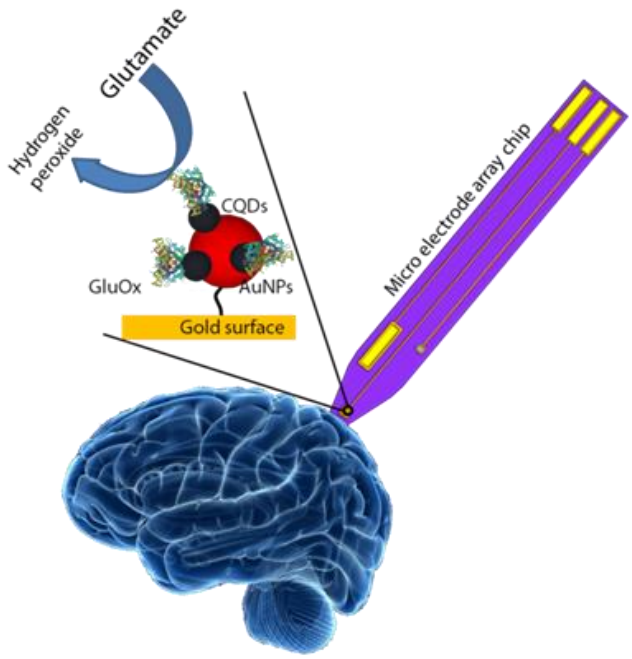


Figure 6.2.Glutamate biosensor probe modified with gold nanoparticles and carbon quantum dots for neural applications

One particular future perspective is the application of the micro array chips developed here in the field of the neuroscience either for neural recordings or neurotransmitter detection. Neurotechnology requires highly sensitive (bio)-sensor probes with high stability. Thus it will be crucial to develop such probes for detection of critical marker neurotransmitters of a variety of degenerative brain diseases. Fig. 6.2 represents a possible example biosensor probe towards glutamate which is one of the most abundant free amino acid in the brain. Such a biosensor probe in the presence of specific nano structures may provide excellent performance towards glutamate and may also be used in neuroscience applications.

Another approach is to use array chips for immunosensor development. Electrochemical biosensors constructed on such small chips could provide several advantages over conventional devices in terms of analytical performance; however, most importantly they would allow for the use of small volumes of biomolecules and small volumes of sample which could be a critical issue. . Fig. 6.3 represents a schematic image of a possible antibody, DNA and aptamers-based biosensor surfaces in the presence of gold nanoparticles and carbon quantum dots deposited onto micro band electrode array chips. Furthermore, miniaturisation of the 3-electrode system on a chip provides an easy-to-use platform with a dedicated custom made connector. The biosensor platforms described in this thesis are highly suitable

to be used as matrixes for the (bio)-molecule immobilisation such as antibodies or their fragments, affimers, DNA, aptamers, etc.

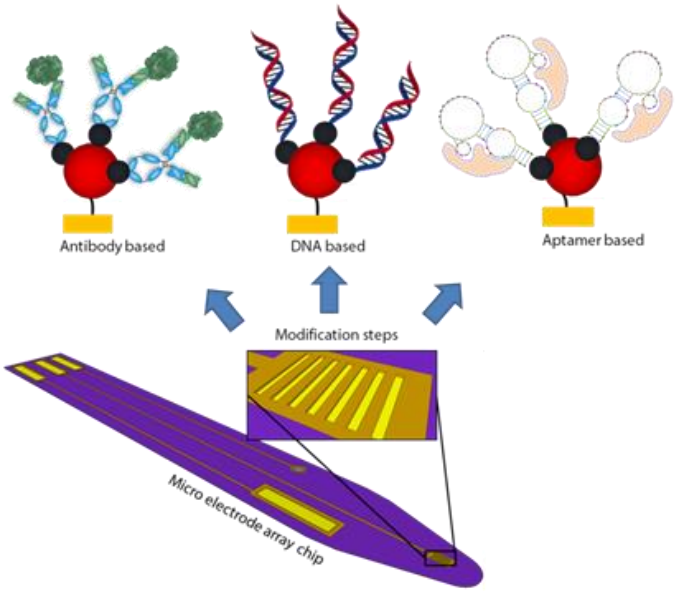


Figure 3.Representative image of a band array based micro electrode array chip as antibody, DNA and aptamer based biosensor

7. APPENDIX

7.1 GRANTS

1. **Catalyst Grant**, Tyndall National Institute, 25K Euro, LABEL-FREE MICRO IMMUNOSENSOR DEVELOPMENT FOR MULTIPLE SCLEROSIS DETECTION (MISMS), 2019/2020

7.2 PUBLICATIONS

1. Buk V., *Pemble M. E., Twomey K., Fabrication and evaluation of a carbon quantum dot/gold nanoparticle nanohybrid material integrated onto planar micro gold electrodes for potential bioelectrochemical sensing applications, Electrochimica Acta 293 (2019) 307-317, https://doi.org/10.1016/j.electacta.2018.10.038

2. *Buk V., Pemble M. E., A highly sensitive glucose biosensor based on a micro disk array electrode design modified with carbon quantum dots and gold nanoparticles, Electrochimica Acta 298 (2019) 97-105, https://doi.org/10.1016/j.electacta.2018.12.068

3. *Juska V. B., Walcarius A., Pemble M. E., Cu Nanodendrite Foams on Integrated Band Array Electrodes for the Non-Enzymatic Detection of Glucose, ACS Appl. Nano Mater. 2019, 2, 5878-5889, DOI: 10.1021/acsanm.9b01325

4. *Juska V. B., Pemble M. E., A dual-enzyme, micro-band array biosensor based on the electrodeposition of carbon nanotubes embedded in chitosan and nanostructured Au-foams on microfabricated gold band electrodes, RSC, Analyst, DOI: 10.1039/c9an01664c

7.3 ACADEMIC HONORS AND AWARDS

1. Nomination of best poster award, 5th International Conference on Bio-Sensing Technology, Italy, 7-10 May 2017

2. Best poster award, 69th Irish Universities Colloquium, DCU, Ireland, 22-23 June 2017

3. Travel grant, NanoBioSensors, Germany, 4-5 September 2017

4. RSC registration fee waiver, 7th Baltic Electrochemistry Conference: Finding New Inspiration (BEChem 2018), Estonia, 4-7 November 2018

5. Best scientific image competition winner, Tyndall National Institute, 2018

6. Postgraduate Research Publication of the year winner, https://www.tyndall.ie/news/postgraduate-research-publication-of-the-year//, 2018, Tyndall National Institute, sponsored by Pilot Photonics, Ireland. Research article; Vuslat Buk, Martyn E. Pemble, Karen Twomey; Fabrication and evaluation of a carbon quantum dot/gold nanoparticles nanohybrid material integrated onto planar micro gold electrodes for potential bioelectrochemical sensing applications, Electrochimica Acta 293 (2019) 307-317; https://doi.org/10.1016/j.electacta.2018.10.038

7. Runner-up award, UCC-SEFS-Research publication of the year competition 2018, University College Cork, Ireland

8. Research article; Vuslat Buk, Martyn E. Pemble, Karen Twomey; Fabrication and evaluation of a carbon quantum dot/gold nanoparticles nanohybrid material integrated onto planar micro gold electrodes for potential bioelectrochemical sensing applications, Electrochimica Acta 293 (2019) 307-317; https://doi.org/10.1016/j.electacta.2018.10.038

9. Best scientific image competition winner, Tyndall National Institute, 2019

10. ELSEVIER Young Scientist Oral Presentation Award, 1st Place, XX Euroanalysis Conference, Istanbul, Turkey, 1-5 September 2019

7.4 CONFERENCES, SEMINARS

Oral presentations

1. 8th Conference on Analytical Science Ireland (CASI), Ireland, 14th-15th April 2016, A novel miniaturized biosensor for hydrogen peroxide sensing for use in agri-food applications
   Buk, V.; Kelly, P.; Pemble, M.; Twomey, K.

2. 68th Irish Universities Chemistry Research Colloquium, UCC, Ireland 23rd & 24th June 2016, Novel miniaturized gold microelectrodes for electrochemical detection of hydrogen peroxide
   Buk, V.; Kelly, P.; Pemble, M.; Twomey, K.

3. 69th Irish Universities Colloquium, DCU, Ireland, 22-23 June 2017, A study of "carbon quantum dots-gold nanoparticles" nanohybrid material for enhanced enzyme immobilization in biosensor development
   Buk, V.; Pemble, M.; Twomey, K.

4. NanoBioSensors, Germany, 4-5 September 2017, Carbon quantum dots decorated microfabricated gold electrodes for sensitive glucose detection
   Buk, V.; Pemble, M.; Twomey, K.

5. 8th Meeting of Electrochemistry in Nanoscience, France, 29-31 May 2018, Integration of micro gold electrodes with advanced nanomaterials for electrochemical biosensing applications
   Buk, V.; Pemble, M.

6. 7th Baltic Electrochemistry Conference: Finding New Inspiration (BEChem 2018), Estonia, 4-7 November 2018, New Nanomaterial-Based, Microfabricated, Miniaturized Electrochemical Sensors for the Detection of Glucose
   Buk, V.; Pemble, M.

7. RSC 6th Analytical Biosciences Early Career Researcher Meeting (ECRM2019), Cambridge, UK, 28-29 March 2019, Nanomaterials-based miniaturized systems for electrochemical applications
   Buk, V.; Pemble, M.

8. XX Euroanalysis Conference, Istanbul, Turkey, 1-5 September 2019, Microfabricated gold array electrodes modified by nanomaterials for highly sensitive electrochemical application
   Buk, V.; Pemble, M.

Poster presentations and demonstration

1. Tyndall Technology Days, 14th-15th October 2015, demonstrator

2. Annual Research Days, IADR (International Association for Dental Research), 3rd-4th March 2016

3. Use of semiconductor processing technology for development of miniaturized devices for oral health monitoring
   Buk V., O`Mara P., O`Callaghan S., McKenna G., Twomey K.

4. Tyndall National Institute, Ireland, Poster Competition, 29th July 2016, A New Approach to the Sensing of Hydrogen Peroxide for Application in the Food Industry
   Buk, V.; Kelly, P.; Pemble, M.; Twomey, K.

5. 5th International Conference on Bio-Sensing Technology, Italy, 7-10 May 2017, Development of carbon quantum dot-based nano-hybrid materials and their application as electrochemical biosensors
   Buk, V.; Pemble, M.; Twomey, K.

6. 69th Irish Universities Colloquium, DCU, Ireland, 22-23 June 2017, A study of “carbon quantum dots-gold nanoparticles” nanohybrid material for enhanced enzyme immobilization in biosensor development
   Buk, V.; Pemble, M.; Twomey, K.

7. Postgraduate research day, UCC, Ireland, 21 August 2017, A study of “carbon quantum dots-gold nanoparticles” nanohybrid material for enhanced enzyme immobilization in biosensor development
   Buk, V.; Pemble, M.; Twomey, K.

8. Tyndall National Institute, Ireland, Poster Competition, 14th December 2017, Integration of Microelectrodes with Carbon Quantum Dots - Gold Nanoparticles for Biosensing
   Buk, V.; Twomey, K.; Pemble, M.

9. RSC 6th Analytical Biosciences Early Career Researcher Meeting (ECRM2019), Cambridge, UK, 28-29 March 2019, Nanomaterials-based miniaturized systems for electrochemical applications
   Buk, V.; Pemble, M.